Division of Biomedical Engineering

Department of Human Biology

University of Cape Town

Characterising the structural brain connectome in Alzheimer's disease and its relation to cognitive intra-individual variability.

Thesis write-up

In fulfilment of the requirements for the degree:

MSc (Med) in Neuroscience

Stephanie Shao-Hsuan Lee (LXXSHA009)

Supervisor: Dr Marcin Jankiewicz

Co-supervisors: Dr Frances Robertson, Dr Björn Christ

Date: 14/02/22

"The financial assistance of the National Research Foundation (NRF) towards this research is hereby acknowledged. Opinions expressed and conclusions arrived at, are those of the author and are not necessarily to be attributed to the NRF."

Declaration

I, Stephanie Shao-Hsuan Lee, hereby declare that the work on which this dissertation/thesis is based is my original work (except where acknowledgements indicate otherwise) and that neither the whole work nor any part of it has been, is being, or is to be submitted for another degree in this or any other university.

I empower the university to reproduce for the purpose of research either the whole or any portion of the contents in any manner whatsoever.

Signature: Signed by candidate

Date: 14 February 2022

Acknowledgements

I wish to express my sincere gratitude to my supervisor, Dr Marcin Jankiewicz, for his invaluable supervision, advice, and constant guidance throughout the duration of my project. I have gained and learned so much from him.

I am extremely thankful to my co-supervisors, Dr Frances Robertson, and Dr Björn Christ. I would like to thank Dr Frances Robertson for all the insightful comments and suggestions that she has provided, as well as for always being available to help in moments of need. I would also like to thank Dr Björn Christ for his patience and for taking the time to teach me the clinical aspects required for this study, your expertise on intra-individual variability has been essential.

I would like to extend my heartfelt thanks to the National Research Foundation (NRF) and the University of Cape Town (UCT) for the financial support which made this project possible.

Special thanks to Joanah Madzime for the countless hours she sacrificed to kindly help and always teach me without hesitation, as well as to Ndivhuwo Magondo for always being there to work through difficulties and challenges together.

Finally, I would like to express my appreciation to my parents, Kevin, and Cathy Lee, for their continuous love and support in everything that I do throughout my life. Thank you to my brother, Spencer Lee, for his ability to always make me laugh and for his constant encouragement. I am grateful for my partner, Cameron Francis, for always believing in me even when I did not believe in myself. Without them, none of this would've been possible.

Table of Contents

Abstract

Research on Alzheimer's disease (AD) has shown white matter (WM) degeneration and structural connectome disruptions measured by diffusion tensor imaging (DTI) as well as increased reaction time intra-individual variability (RT IIV) on neurocognitive testing. However, the relationship between these changes measured on these different modalities remains unexplored. To explore possible relationships between these alterations, this study used tractography to identify WM changes, as indexed by fractional anisotropy (FA) and mean diffusivity (MD), followed by a graph theory-based analysis of the brain structural connectome, and investigated the relationship between these graph theory metrics and RT IIV in 16 AD patients and 20 healthy elderly controls. Within AD patients, we identified WM tracts with lower FA and higher MD mostly located in the cortical and subcortical temporal lobes, such as the hippocampus subregions, compared to healthy elderly controls. We also observed higher FA in the WM tracts within the thalamus as well as between the thalamus and brainstem in AD patients. In the structural brain connectome of these patients, there were regions with altered nodal strength, transitivity, and local efficiency relative to the controls' connectome. Conversely to many studies, we found increases in nodal efficiency across multiple regions and higher global efficiency in AD patients compared to healthy elderly controls. Finally, higher global efficiency was correlated with increased RT IIV on the CRT task in AD patients. In AD, a positive relationship between transitivity in the left cingulate cortex and RT IIV as well as between nodal efficiency in the left cortical temporal lobe and mean RT on the CRT task were observed. On the other hand, lower transitivity in the right thalamus and increased RT IIV, as well as lower transitivity and longer mean RT were found on both the SRT and CRT tasks in AD patients. Our results may show evidence of disruptions and compensatory mechanisms in WM tracts and network metrics in AD. Together, these results revealed WM changes, topological alterations of the brain structural connectome in AD and that these findings can be used in combination with IIV to predict cognitive decline or progression of AD.

List of figures

List of tables

List of abbreviations

AAL	Automated Anatomical Labelling
ACSENT	Applied Cognitive Science and Experimental Neuropsychology Team
AD	Alzheimer's Disease
AFNI	Analysis of Functional Neuroimages
aMCI	Amnestic Mild Cognitive Impairment
AP	Anterior-Posterior
AxD	Axial Diffusivity
BL	Average length in mm of the fibre tracts in each bundle
BML	Bayesian Multilevel
BOLD	Blood Oxygen Level Dependent
CAMCOG-R	Cambridge Examination for Mental Disorders of the Elderly- Revised edition
CANTAB	Cambridge Neuropsychological Test Automated Battery
CDR	Clinical Dementia Rating
CMP	Connectome Mapper
CMTK	Connectome Mapping Toolkit
CNS	Central Nervous System
CRT	Choice Reaction Time
CSF	Cerebrospinal Fluid
CUBIC	Cape University Body Imaging Centre
DMN	Default-Mode Network
DSM-IV	Diagnostic and Statistical Manual – Fourth Edition
DT	Diffusion Tensor
DTI	Diffusion Tensor Imaging
DW	Diffusion-Weighted
DWI	Diffusion-Weighted Imaging
EEG	Electroencephalograph
EPI	Echo Planar Imaging
FA	Fractional Anisotropy
FACTID	Fibre Assessment by Continuous Tracking Including Diagonals
FATCAT	Functional And Tractographic Connectivity Analysis Toolbox
FC	Functional Connectivity
fMRI	Functional Magnetic Resonance Imaging
fNT	Fractional number of tracks in that white matter region of interest
fNV	Fractional volume of tracks compared to masked total volume
FOV	Field of View
GDS	Geriatric Depression Scale

GM	Grey Matter
GSH	Groote Schuur Hospital
HIV/AIDS	Human Immunodeficiency Virus/Acquired Immunodeficiency Deficiency Syndrome
IIV	Intraindividual Variability
IQR	Interquartile Range
iSD	Intra-individual Standard Deviation
LAMICs	Low- And Middle-Income Countries
MCI	Mild Cognitive Impairment
MD	Mean Diffusivity
MEG	Magnetoencephalography
MEMPRAGE	Multi-Echo Magnetisation Prepared Rapid Gradient Echo
MHz	Megahertz
MMSE	Mini-Mental State Examination
MRI	Magnetic Resonance Imaging
ms	milliseconds
NHST	Null Hypothesis Significance Testing
NT	Number of tracks in that white matter region of interest
NV	Number of voxels in that white matter region of interest
PA	Posterior-Anterior
PET	Positron Emission Tomography
PV	Physical volume of tracts
RBA	Region-Based Analysis
RD	Radial Diffusivity
RF	Radiofrequency
R-ILF	Right Inferior Longitudinal Fasciculus
ROI	Region Of Interest
rs-fMRI	Resting-State Functional Magnetic Resonance Imaging
RT	Reaction Time
SD	Standard Deviation
sMRI	Structural Magnetic Resonance Imaging
SPECT	Single-Photon Emission Computed Tomography
SRT	Simple Reaction Time
T	Tesla
T1w	T1-weighted
T2w	T2-weighted
TBSS	Tract-Based Spatial Statistics
TE	Echo Time

TORTOISE	Tolerably Obsessive Registration and Tensor Optimization Indolent Software Ensemble
TR	Repetition Time
UCT	University of Cape Town
VBM	Voxel-Based Morphometry
WM	White Matter
WM-ROI	White Matter Region of Interest

1. Introduction

Over the last century, the world's population showed a greater proportion of older people and, concurrently, an increased rate of age-related brain diseases such as dementia. In 2020, over 55 million people lived with dementia worldwide (Alzheimer's Disease International, 2020). This number is expected to triple to more than 152 million by 2050 (Alzheimer's Association, 2021b). The highest increase in prevalence is predicted to be in developing countries, such as North Africa, eastern sub-Saharan Africa and the Middle East (Prince *et al.*, 2015; World Health Organisation, 2015; Alzheimer's Association, 2021b). The bulk of the research on individuals with age-associated diseases that lead to dementia is performed in high-income countries, even though more than 60% of these individuals currently live in low- and middle-income countries (LAMICs) (Prince *et al.*, 2015; World Health Organisation, 2015) and this percentage is expected to rise to 71% by 2050 (Alzheimer's Disease International, 2020). This increase is caused by both population growth and ageing.

Research has found that only 20-50% of dementia cases in high-income countries have received a formal diagnosis (*Dementia statistics*, 2021). Unfortunately, these numbers are much greater in LAMICs. There is an indication that 90% of the dementia cases are undiagnosed in one of these LAMICs, India (Dias and Patel, 2009; *Dementia India Report 2010*, 2010; Nulkar, Paralikar and Juvekar, 2019). If these figures are similar in other LAMICs, this would mean that approximately three-quarters of people with dementia have not received a formal diagnosis and thus have no access to care and treatment (Alzheimer's Disease International, 2020). One of the biggest problems is the costs that are associated with this disease which puts a huge financial and social strain on the healthcare system, patients as well as the caregivers, especially in LAMICs. In South Africa, which is one of the LAMICs, very little research has been done on the prevalence or progression of dementia.

1.1 AD symptoms

Alzheimer's disease (AD) is characterised as a progressive neurodegenerative disease that primarily affects memory and, to varying degrees, other cognitive domains, with the incidence increasing in the older population. AD is the most common type of dementia and is also known as a "disconnection syndrome" (de LaCoste and White, 1993; Delbeuck, Van

Der Linden and Collette, 2003). AD has been observed to develop over 15 to 20 years before clinical symptoms can be detected (Prince and Morris, 1999; Elias, Beiser and Wolf, 2000). Symptoms occur as parts of the brain responsible for learning, thinking, and memory have been damaged. Eventually, as the disease progresses, other parts of the brain that allow a person to perform basic bodily functions, e.g., walking and swallowing, become affected as well (Alzheimer's Association, 2021b). Some of these clinical symptoms include cognitive deficits such as memory impairment, executive dysfunction, impaired visuospatial and language function deficits as well as behavioural disturbances (McKhann, 2012).

AD affects both the grey matter (GM), which is the functional part of the brain that processes signals/information, and white matter (WM), i.e., the structural part of the brain that transports the signals/information between the GM regions. Information in the form of electric signals being fired within neuronal circuitry, which creates the cellular basis of thoughts, sensations, movements, emotions, skills and memories, flows through these WM connections and travel rapidly through the brain (Alzheimer's Association, 2021a). One of the brain changes of AD is believed to involve the abnormal accumulation of the microscopic brain protein fragment, known as beta-amyloid (Alzheimer's Association, 2017), which is formed from the breakdown of a larger naturally occurring protein (O'Brien and Wong, 2011). Beta-amyloid is a sticky compound that builds up and forms amyloid plaques outside the neurons which disrupts neuron-to-neuron communication and ultimately kills these brain cells (Alzheimer's Association, 2017). Another brain change of AD occurs inside the neurons and are known as tau tangles, which is the build-up of an abnormal form of the tau protein (Alzheimer's Association, 2021a). The function of the tau protein is to stabilise the neuron's internal skeleton (Alzheimer's Association, 2021c). In healthy neurons, the tube-like shape part of the internal skeleton, known as the microtubules, aids the transportation of nutrients and other vital substances to different parts of the neuron that is essential for the normal functioning, as well as the survival of the neuron (Alzheimer's Association, 2021c). In AD, abnormal chemical changes cause the tau proteins to separate from the microtubules, causing the internal skeleton to disintegrate, and bond together to other tau proteins and eventually forming tau tangles (Alzheimer's Association, 2021c). The accumulation of these tau tangles with the disintegrated internal skeleton of neurons leads to the loss of neuronal function and ultimately apoptosis (Kinney *et al.*, 2018). Microglia,

which are immune system cells in the brain that clean out toxic proteins and debris from dead cells, are activated by amyloid plaques and tau tangles (Alzheimer's Association, 2021a). When the microglia can't keep up with all the toxic proteins and debris that need to be cleared, chronic inflammation occurs (Alzheimer's Association, 2021a). Accelerated atrophy, which is caused by cell death and cell loss, is another brain change seen in AD (Braak and Braak, 1991, 1995; Nir *et al.*, 2013; Alzheimer's Association, 2021a). However, the temporal relationship between these changes remains unclear (Jack *et al.*, 2013). Due to the loss of neurons, WM volume is decreased as a result of both axonal loss and myelin degeneration in neural fibre tracts (Hua *et al.*, 2008; Braskie *et al.*, 2011; Nir *et al.*, 2013).

1.2 AD biomarkers

There is currently no effective treatment to stop or reverse the progression of AD. Thus, it is important to establish a set of sensitive biomarkers that can detect structural, functional and cognitive changes at the early stages of the disease before clinical symptoms are present, as well as monitor the progression of the disease (Bachmann *et al.*, 2018).

One method of measurement that may be able to help accomplish this goal and is being utilised more and more in AD research, is intraindividual variability (IIV) in cognitive performance. Compared to traditional cognitive test scores, which are based on measures on central tendency and only assesses the performance of an individual on a single measure administered on a single occasion, IIV measures within-person trial-to-trial variation and assesses fluctuations in the performance of an individual on a single task taken over multiple occasions (Fiske and Rice, 1955; Hultsch, MacDonald and Dixon, 2002; MacDonald, Nyberg and Bäckman, 2006). Specifically, IIV measures within-person inconsistency in performance and across time and can be looked across either longer periods, e.g., week-to-week, or shorter periods, e.g., trial-to-trial (Halliday *et al.*, 2018). IIV is most commonly measured in terms of reaction time (RT) variability where an increase in RT variability is associated with ageing (Bielak *et al.*, 2014), declines in WM volume (Walhovd and Fjell, 2007; Lövdén *et al.*, 2013), lower WM integrity (Fjell *et al.*, 2011; Moy *et al.*, 2011; Mella *et al.*, 2013; Halliday *et al.*, 2019), greater severity of WM hyperintensities (Bunce *et al.*, 2007; Haynes *et al.*, 2017), decrease in hippocampal volume (Bangen *et al.*, 2019), and more rapid cognitive decline in older adults (Hultsch and MacDonald, 2004; Lövdén *et al.*, 2007; Bielak *et al.*, 2010; Grand, Stawski and MacDonald, 2016). Increases in RT variability have also been

found in AD individuals (Duchek *et al.*, 2009; Jackson *et al.*, 2012; Phillips *et al.*, 2013; Halliday *et al.*, 2018). Currently, only one published study explored the association between increased RT variability and WM changes in AD (Jackson *et al.*, 2012).

Another method of measurement that offers insight into structural and functional biomarkers is magnetic resonance imaging (MRI), specifically two MRI modalities: resting-state functional MRI (rs-fMRI); diffusion-tensor-imaging (DTI). Rs-fMRI evaluates functional connectivity (FC) by measuring the low-frequency Blood Oxygen Level Dependent (BOLD) signal variations within and between brain networks when participants are at rest, i.e., not performing a specific task. Regions are considered to be "functionally connected" if there is a notable association between the BOLD signals in these regions, such as positive FC. DTI can be used to map out and quantify the properties of WM connections, i.e., WM tracts, between GM regions. This is known as DTI tractography. Tractography can be used to observe whether there is damage to structural integrity, characterised as low fractional anisotropy (FA) and high mean diffusivity (MD) (Tromp, 2016), that is associated with AD. The consensus among numerous studies is that there are WM disruptions in AD individuals (Bozzali *et al.*, 2002; Naggara *et al.*, 2006; Huang, Friedland and Auchus, 2007; Stahl *et al.*, 2007; Salat *et al.*, 2009; Johnson *et al.*, 2010; Jackson *et al.*, 2012). Bartzokis et al. (2009) suggest that AD could begin with compromised myelin. In AD, increased MD has been found in WM regions (Bozzali *et al.*, 2002; Naggara *et al.*, 2006; Brueggen *et al.*, 2019), indicating tissue damage in those regions (Soares *et al.*, 2013). MD increases in the basal forebrain have also been associated with a higher risk for mild cognitive impairment (MCI) to convert to AD (Brueggen *et al.*, 2015). These studies have also reported a decrease in FA in these AD individuals (Bozzali *et al.*, 2002; Naggara *et al.*, 2006; Brueggen *et al.*, 2019), which reflects a disrupted organisation of WM caused by axonal degeneration (Soares *et al.*, 2013; Brueggen *et al.*, 2019). This impairment of WM networks can already be seen before significant neurodegeneration is detectable (Bartzokis, 2011; Fischer *et al.*, 2015).

Graph theory is a powerful mathematical technique that represents the brain as a complex network of interrelated components, known as the connectome (Bullmore and Sporns, 2009). Graph theory provides a new set of outcomes to characterise a network in terms of the topology of the connectome. Both structural and functional networks can be mapped out and analysed by applying graph theoretical analyses to MRI data (Prescott *et al.*, 2014).

The mathematical construct of a graph is used to represent a brain in terms of nodes and edges, where nodes can be thought of as structural GM areas and the edges are the metrics characterising WM connectivity to other regions as measured by DTI (Sporns, 2018). In previous studies, network properties that have been observed to be affected in AD individuals compared to healthy controls include lower global efficiency (Lo *et al.*, 2010; Kocagoncu *et al.*, 2020), local efficiency (Reijmer *et al.*, 2013), nodal efficiency (Lo *et al.*, 2010; Zajac *et al.*, 2017), nodal strength (Veronese *et al.*, 2019; Wu *et al.*, 2019; Kuang *et al.*, 2020), nodal degree (Dai *et al.*, 2019; Franciotti *et al.*, 2019), transitivity (Pereira *et al.*, 2016; Mijalkov *et al.*, 2017; Si *et al.*, 2019) and both lower (Brier *et al.*, 2014) as well as higher modularity (Pereira *et al.*, 2016; Mijalkov *et al.*, 2017; Si *et al.*, 2019). Thus, this technique may also have the potential to identify early signs of AD.

1.3 Our project

This study is part of a larger research project on the longitudinal trajectory of cognitive decline in AD taking place in Cape Town, South Africa (Christ, Combrinck and Thomas, 2018) and is conducted by the Applied Cognitive Science and Experimental Neuropsychology Team (ACSENT) Laboratory of the University of Cape Town's (UCT) Department of Psychology. A previous study on the same sample found decreased WM integrity in the right inferior longitudinal fasciculus (R-ILF) and the body and the genu of the corpus callosum using voxel-wise analysis of diffusion measures (Engelbrecht, in preparation). The study also observed that increased IIV on RT tasks correlated with lower FA and axial diffusivity (AxD) in a cluster in the R-ILF. Previous studies from the larger research project did not use full-probabilistic DTI tractography nor investigate the structural connectome using graph theoretical measures. The correlation between network measures and RT IIV scores has also never been explored in Alzheimer's disease. In addition, no study has investigated group differences in DTI measures and graph theoretical measures using a region-based analysis (RBA) statistical approach. Based on this rationale, we investigated structural abnormalities associated with AD using full-probabilistic DTI tractography as well as possible relationships between graph theory measures and IIV scores in AD patients and healthy elderly controls.

By using a RBA statistical approach, this study aimed to investigate group differences between AD patients and healthy elderly controls in DTI measures, such as FA, MD, AxD, radial diffusivity (RD), etc. Secondly, we aimed to create structural connectome graphs from

full-probabilistic tractography DT images and analyse the group differences of the connectome topology in each region by using graph theoretical metrics between patients with AD and healthy elderly controls using RBA. Lastly, we aimed to analyse whether connectivity and efficiency across the structural connectome are related to IIV in the two groups, bridging the gap between pathological processes and emerging clinical manifestations.

We hypothesised that:

(1) AD patients will demonstrate decreased structural connectivity (lower FA, higher MD, lower AxD, higher RD) in WM tracts in all parts of the brain, especially in the temporal lobe such as the hippocampus, and in other limbic system structures including the cingulate cortex.
(2) A topographical structure of the network of AD patients will be disrupted, with lower brain network efficiency at both local and global levels compared to healthy elderly controls. Graph theory metrics such as transitivity, efficiency (nodal, local, and global), nodal strength and nodal degree will be lower while modularity will be higher, especially in the temporal lobe and cingulate cortex, in AD patients compared to healthy elderly controls.
(3) Lower transitivity, efficiency (nodal, local, and global), nodal strength and nodal degree in the cingulate cortex and temporal lobe, as well as higher modularity will be associated with greater RT IIV and greater mean RT in AD patients.

2. Background/Literature review

2.1 Intra-individual variability

In neurocognitive testing, IIV is considered to be a marker for neurocognitive impairment (Christ, Combrinck and Thomas, 2018). IIV is believed to be extremely sensitive to even slight changes in cognitive function and is thus suitable for detecting the beginning stages of neurodegenerative diseases, such as AD (Kälin *et al.*, 2014; Costa *et al.*, 2019).

One method of capturing IIV involves using latency-based measures, which evaluates inconsistency in performance on reaction time (RT) tasks. One of the advantages of RT IIV measures is that they are able to detect more subtle individual performance differences compared to traditional cognitive tests as they have larger ranges (Allaire and Marsiske, 2005). Other advantages would be that RT tasks contain multiple trials for one measure,

they are not as sensitive to the re-test effect (Allaire and Marsiske, 2005) and can measure variation in performance over seconds, days, or weeks (micro-timescales). Micro-timescales are less likely to be related to developmental changes and thus would reveal dynamic within-person features, whereas performance variations over months and years (macro-timescales) would be highly affected by development change and ageing (Ram *et al.*, 2012).

RT variability can be measured on tasks such as the simple reaction time (SRT) task and the choice reaction time (CRT) task. SRT requires the detection of a stimulus with a response execution, whereas CRT requires more complex identification of the stimulus with an added factor of selecting the appropriate response (Dykiert *et al.*, 2012). Increased variability during these tasks is suggested to be due to impairment of high-order cognitive processes, e.g., executive and attentional control, and not considered as random noise or a product of error variance (West *et al.*, 2002; Bunce, Macdonald and Hultsch, 2004; Duchek *et al.*, 2009; Vasquez, Binns and Anderson, 2018). Hultsch, MacDonald and Dixon (2002) reported that IIV had a negative relationship with cognitive performance on measures that involved working memory, episodic memory, perceptual speed, and crystallized abilities.

RT IIV has been observed to be a marker of the central nervous system (CNS) function (MacDonald, Hultsch and Dixon, 2003; Burton *et al.*, 2006; Dykiert *et al.*, 2012), where increased RT IIV exhibits deterioration of the CNS. Interestingly, greater RT IIV has also been seen in conditions that only transiently affected the function of the CNS, e.g., alcohol consumption (Maruff *et al.*, 2005). Thus, it would make sense that neurodegenerative diseases affecting the CNS, such as AD, will show greater RT IIV. Literature has found that the link between greater IIV and neurodegenerative diseases include executive dysfunction (West *et al.*, 2002) and disease-associated disruptions in neural networks and functional connectivity (FC) seen in functional neuroimaging studies (Kelly *et al.*, 2008).

An increase in RT variability have been observed to be associated with healthy ageing (Bielak *et al.*, 2014), with more rapid cognitive decline in older adults (Hultsch and MacDonald, 2004; Lövdén *et al.*, 2007; Bielak *et al.*, 2010; Grand, Stawski and MacDonald, 2016). RT IIV has also been found to have the ability to predict cognitive decline (MacDonald, Hultsch and Dixon, 2003; Bielak *et al.*, 2010) and the development from healthy ageing to mild cognitive impairment (MCI) (Cherbuin, Sachdev and Anstey, 2010). Even though RT IIV has been found to increase with age in normal healthy ageing (Dykiert *et*

al., 2012), RT IIV is able to differentiate between healthy ageing and pathological decline with higher RT IIV in individuals with AD compared to healthy control groups (Hultsch *et al.*, 2000; Gorus *et al.*, 2008). In another study that is part of the longitudinal study of our sample, Christ, Thomas and Combrinck (2018) reported that in South Africa, individuals with AD have higher IIV on both time- and accuracy-based tasks compared to healthy elderly controls. Previous studies have found that IIV increased as task complexity increased (Burton *et al.*, 2006; Gorus, Raedt and Mets, 2006). This increase was greater in the AD group compared to both the MCI group and healthy controls group (Hultsch *et al.*, 2000; Gorus *et al.*, 2008).

2.2 Magnetic resonance imaging

Magnetic Resonance Imaging (MRI) has been an extremely powerful tool since its development in the 1970s where it is able to provide information on the structure, function, and physiological processes of the brain in vivo. The main principle of MRI measures the net electromagnetic energy released by protons from hydrogen nuclei in water molecules in the human body (Arora, 2018).

2.2.1 Basics of MRI

The MRI scanner contains radiofrequency (RF) coils, gradient coils, and a large, powerful magnet. This magnet generates an external/static magnetic field, i.e., B_0, of high strength (1.5T, 3T or higher), where 1T (Tesla) is a unit of magnetic flux. In the presence of B_0 in the z-direction, i.e., the inferior-superior orientation of the participant, the protons' spins will align themselves in the direction parallel and anti-parallel to B_0, the number of protons in parallel and anti-parallel direction is different and this creates a nonzero net magnetisation vector. Moreover, in the presence of B_0, the protons will start to precess about the axis of the B_0. The rate at which the spins of the protons precess around B_0 is known as the Larmour frequency (resonance frequency) and can be calculated using the Larmour equation:

$$\omega_0 = \gamma B_0$$

Where ω_0 is the precession frequency in MHz (megahertz), γ is a constant that is specific to each nucleus in MHz/T known as the gyromagnetic ratio, B_0 is the strength of the external

magnetic field in T. For hydrogen's nuclei (a proton), the gyromagnetic ratio is 42.58 MHz/T. And so, at B_0 = 1.5T, protons precess at 64 MHz and at B_0 = 3T they precess at 128 MHz.

The component of the magnetisation vector along the direction of B_0 is called longitudinal magnetisation (Hashemi, Bradley and Lisanti, 2004; Arora, 2018). In order to generate an MR signal, an RF pulse (B_1 ; also known as the excitation pulse) is generated by a transmit RF coil. The pulse is usually applied perpendicular to B_0 and makes spins precess about the B_1 direction in the rotating frame for as long as the pulse is on. As a result of B_1, a transverse component of the magnetisation vector is being produced (van Geuns *et al.*, 1999; Sands and Levitin, 2004). Once the RF pulse is turned off, the protons lose energy as they return to equilibrium (i.e., predominantly aligned with B_0). As spins precess, they release RF energy which is measurable using a receive RF coil (van Geuns *et al.*, 1999). Two independent time constants of the decaying RF signal are measured: (1) T1 is the time it takes for the original net magnetisation to regain at least 63% of the longitudinal magnetisation, (2) T2 is the time it takes for at least 63% of the transverse magnetisation to be lost, i.e., time of the signal to decay to 37% of the original signal *(Figure 1)*.

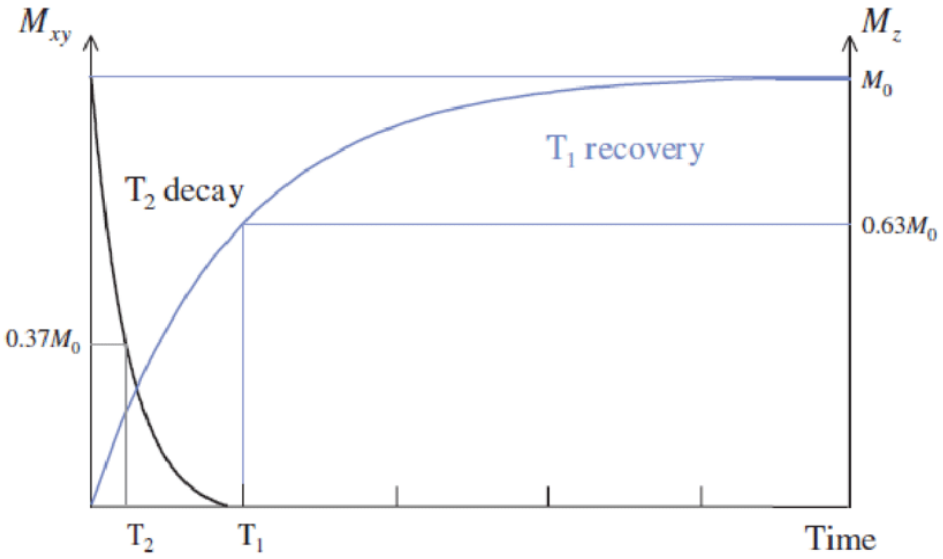

Figure 1: T1 recovery time and T2 decay time constants (adapted from (McRobbie et al., 2006)).

Image contrast is created due to different signal intensities of different tissues, i.e., differences in T1 and T2 values and the proton density of the different tissues, which is the concentration of hydrogen protons in the tissue (Wehrli and Kanal, 1987).

However, this signal mentioned above only contains information of the entire imaged part of the body, with no spatial information (Arora, 2018). To resolve this, gradients are used to produce a linear magnetic field non-uniformity along all three axes (Hashemi, Bradley and Lisanti, 2004). To image a specific slice, an RF pulse of a specific frequency is selected to only excite that specific slice while applying the slice-selection gradient in the direction of the B_0 field, i.e., the z-axis (Sands and Levitin, 2004). After selecting a slice, a frequency-encoding gradient is applied perpendicular to the slice-selection gradient, i.e., the x-axis (Sands and Levitin, 2004). The frequency-encoding gradient affects the precession frequency of the protons (Sands and Levitin, 2004). A phase-encoding gradient is applied perpendicular to both the slice-selection and frequency-encoding gradient, i.e., the y-axis. It is used to induce phase differences between protons that have different y coordinates (Sands and Levitin, 2004).

For completeness, we should note that most of MR sequences used in neuroimaging are based on two types of sequences: a single-echo sequence, where the excitation RF pulse is 90˚ and an echo is generated by 180° RF pulse; a gradient-echo sequence, where the flip-angle of the excitation RF pulse can be set to an arbitrary value, and the echo is generated by a gradient.

Extrinsic parameters, i.e., repetition time (TR) and echo time (TE), can also be changed to define an image contrast. TR is the time interval between two consecutive RF excitation pulses. TE is the time interval between the transmitted RF pulse and the echo (a maximum of the received signal) (Hashemi, Bradley and Lisanti, 2004). Images such as T1-weighted, T2-weighted and proton density-weighted images can be formed by adjusting TR and TE.

2.2.2 Structural imaging and Alzheimer's disease

In literature, there are two main pathopsychological hypotheses regarding WM damage in AD that have been discussed. The first model is known as the Wallerian degeneration model, where microstructural damage to WM has been found to occur secondary to neuronal loss, i.e., GM atrophy, (Duan *et al.*, 2006; Huang, Friedland and Auchus, 2007). The

other model is known as the retrogenesis model of AD which states that axons with a smaller axonal circumference that are last to myelinate are the first to degenerate as they are more susceptible to damage as AD progresses (Reisberg *et al.*, 1999, 2002; Stricker *et al.*, 2009; Bartzokis, 2011).

Structural MRI studies of AD showed the extensive loss of neurons and atrophy in GM (Frisoni *et al.*, 2002; Atiya *et al.*, 2003; Chetelat and Baron, 2003; Thompson *et al.*, 2003) as well as WM volume reductions (Salat *et al.*, 2009; Guo *et al.*, 2010) in the brain. According to the Braak staging system of AD, neurofibrillary degeneration is first observed in temporal lobe structures; including the transentorhinal cortex, then spreads medially to the entorhinal cortex and subsequently affects the amygdala and hippocampus (Atiya *et al.*, 2003; Du *et al.*, 2004; Pennanen *et al.*, 2004; Li *et al.*, 2011; Chandra *et al.*, 2019; Kulason *et al.*, 2020), before it extends to the rest of the neocortex as the disease progresses (Braak and Braak, 1991; Atiya *et al.*, 2003; Thompson *et al.*, 2003; Pini *et al.*, 2016). Atrophy also occurs in other regions, including the parahippocampal, fusiform and medial temporal gyri and temporal pole (Salat *et al.*, 2009; Guo *et al.*, 2010; Li *et al.*, 2011). Similarly, AD has been found to affect additional limbic structures, such as the cingulate gyrus and thalamus (Thompson *et al.*, 2003; De Jong *et al.*, 2008; Guo *et al.*, 2010). Damage was also then extended to frontal and parietal brain areas, as well as the basal forebrain cholinergic system, putamen, and brainstem later on in the disease (Sowell *et al.*, 2003; De Jong *et al.*, 2008; Guo *et al.*, 2010; Kilimann *et al.*, 2014; J. H. Lee *et al.*, 2015).

Whole-brain voxel-based morphometry (VBM) investigations (Frisoni *et al.*, 2002; Hirata *et al.*, 2005) have also shown that atrophy in the medial and lateral temporal regions was more pronounced compared to other regions (Serra *et al.*, 2010).

2.2.3 Diffusion tensor imaging

2.2.2.1 Principles of DTI

Diffusion is a phenomenon resulting from the random motion of molecules from one spatial location to other locations (Alexander *et al.*, 2007). Diffusion-weighted imaging (DWI) uses the differences in the magnitude of diffusion of water molecules within the brain to create image contrast (Huisman, 2010). DWI adds a pulse sequence to the conventional spin-echo sequence that includes a pair of large-gradient pulses, i.e., diffusion gradients, on both sides

of the 180° refocusing RF pulse (Alexander *et al.*, 2007; Huisman, 2010). The first gradient pulse dephases the magnetisation across the voxels, i.e., gives molecules phase shifts, whereas the second pulse rephases the magnetisation, i.e., cancels the acquired phase shift by rephrasing stationary spins (Alexander *et al.*, 2007; Huisman, 2010). If the molecules are stationary, i.e., non-diffusing, the phases generated by the pair of gradient pulses will completely cancel, the magnetisation will be uniform and thus, there will be no signal loss (Alexander *et al.*, 2007; Huisman, 2010). On the other hand, if there is a coherent flow in the direction of the applied gradient, these moving spins will produce a net phase difference causing signal attenuation, depending on the degree of diffusion (Mori and Zhang, 2006; Alexander *et al.*, 2007; Huisman, 2010). The higher the degree of diffusion, i.e., random motion, the greater the MR signal loss, e.g., in cerebrospinal fluid.

The magnitude of diffusion is different in different types of matter and brain structures (Huisman, 2010). In WM, water molecules diffuse more rapidly in the parallel direction to the fibre orientation and are somewhat unrestricted (Alexander *et al.*, 2007; Gold *et al.*, 2011; Behrman-Lay *et al.*, 2015). On the other hand, water diffusion is greatly impeded and hindered in the directions perpendicular to the fibres due to barriers inflicted by myelin sheaths and axonal membranes (Alexander *et al.*, 2007; Acosta-Cabronero *et al.*, 2010; Gold *et al.*, 2011; Behrman-Lay *et al.*, 2015). The diffusion in WM regions is generally more anisotropic (graphically represented as an ellipsoid), whereas GM regions are less anisotropic and cerebrospinal fluid is more isotropic (Alexander *et al.*, 2007; Huisman, 2010; Soares *et al.*, 2013; Behrman-Lay *et al.*, 2015). Since WM is highly anisotropic, water diffusion in healthy WM is highly directional along the direction of the tissue fibre, thus if diffusion is isotropic, this may be an indication of structural integrity loss.

In the context of WM, DTI measures the extracellular diffusion of water molecules to further quantify the density of WM-insulated axonal bundles that connect different regions of the brain. DTI through quantification of the WM microstructures, by extension, can be used to study the structural network created by the brain's WM.

The movement of molecules in each direction and the relationship between these directions are represented as a 3 × 3 diffusion tensor (D) and its different components can be calculated for each voxel by introducing diffusion gradients, as described above, for many gradient directions repeatedly (Mori and Zhang, 2006).

$$D = \begin{bmatrix} D_{xx} & D_{xy} & D_{xz} \\ D_{yx} & D_{yy} & D_{yz} \\ D_{zx} & D_{zy} & D_{zz} \end{bmatrix}$$

Because we assume that this diffusion tensor is symmetric, therefore it can be diagonalised, and as a result three eigenvalues (λ_1, λ_2, λ_3) and three corresponding eigenvectors (ε_1, ε_2, ε_3) are calculated. These define the directions and apparent diffusivities along the axes of principal diffusion (Alexander *et al.*, 2007). Once diagonalised, the diffusion tensor can be seen as a three-dimensional ellipsoid (Basser, Mattiello and LeBihan, 1994), where the eigenvalues represent the ellipsoidal radii, i.e., the relative amount of diffusion in each direction, and the eigenvectors signifying the directions of the principal axes *(Figure 2)* (Basser, Mattiello and LeBihan, 1994; Alexander *et al.*, 2007).

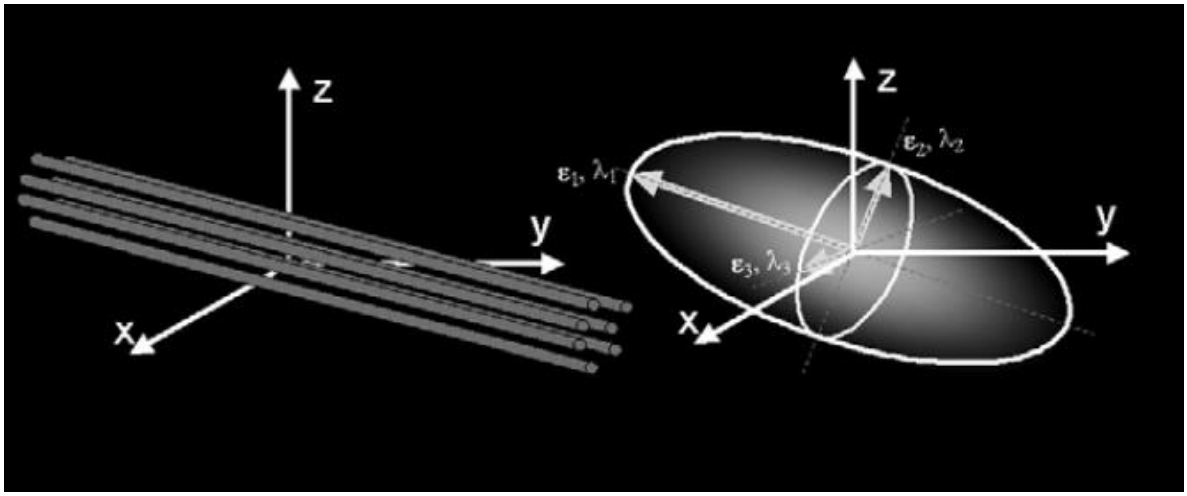

Figure 2: The diffusion tensor can be represented as an ellipsoid (adapted from (Alexander et al.*, 2007)).*

If the eigenvalues are approximately equal (e.g., $\lambda_1 \approx \lambda_2 \approx \lambda_3$), diffusion is classified as being isotropic. If the eigenvalues are significantly different in size (e.g., $\lambda_1 > \lambda_2 > \lambda_3$), diffusion is anisotropic. The first eigenvalue, λ_1, which is also known as axial diffusivity (AxD), reflects the diffusion coefficient along the direction of maximal 'apparent' diffusion (Gold *et al.*, 2011; Daianu *et al.*, 2016), i.e., overall displacement parallel to the axon. The second and third eigenvalues (λ_2, λ_3) are the diffusion coefficients along the two perpendicular directions and are in the plane orthogonal to the main diffusion *(Figure 2)* (Basser, Mattiello and LeBihan, 1994; Gold *et al.*, 2011).

Microstructural changes in WM, such as healthy physiological changes, disease and tissue injury may alter the magnitude of the eigenvalues. Therefore, the diffusion tensor is a

sensitive marker to illustrate both healthy and unhealthy tissue microstructure (Alexander *et al.*, 2007).

Diffusion within each voxel can be described by four scalar parameters that are derived from the eigenvalues of the diffusion tensor. These scalar parameters are known as fractional anisotropy (FA), mean diffusivity (MD), axial diffusivity (AxD) and radial diffusivity (RD) (O'Donnell and Westin, 2011).

Fractional anisotropy (FA) is a normalised standard deviation of the eigenvalues and reflects the total degree of water diffusion along the tissue fibre, i.e., to what extent diffusion is anisotropic (Hagmann *et al.*, 2006; Dietrich *et al.*, 2010; O'Donnell and Westin, 2011). FA is represented as a scalar value between 0 and 1, where 0 describes the diffusion as being isotropic and 1 represents diffusion as anisotropic, i.e., diffusion is only along one axis and is fully hindered along the perpendicular directions (Soares *et al.*, 2013). This DTI measure is commonly used as an index of overall WM microstructural integrity (Pierpaoli and Basser, 1996).

FA is calculated as:

$$FA = \sqrt{\frac{3}{2}} \frac{\sqrt{(\lambda_1 - MD)^2 + (\lambda_2 - MD)^2 + (\lambda_3 - MD)^2}}{\sqrt{\lambda_1^2 + \lambda_2^2 + \lambda_3^2}}$$

Where MD = $\lambda_1 + \lambda_2 + \lambda_3$ / 3. Higher FA values suggest more intact and dense packing of axons, which would mean higher restriction on diffusion and lower intercellular space (Hoeft *et al.*, 2007) as well as increased myelination (Alexander *et al.*, 2011), while lower FA values indicate the change or loss of WM integrity due to demyelination of axonal structures (Rose, Janke and Chalk, 2008; Nir *et al.*, 2013; Soares *et al.*, 2013).

Mean diffusivity (MD) is another DTI metric that quantifies the total diffusion rate, within a voxel independent of diffusion direction (Gao *et al.*, 2011; Nir *et al.*, 2013; Barrio-Arranz *et al.*, 2015; Behrman-Lay *et al.*, 2015; Daianu *et al.*, 2016).

MD is defined as an average of the three eigenvalues:

$$MD = \frac{\lambda_1 + \lambda_2 + \lambda_3}{3}$$

Increased MD is possibly due to WM injury such as the loss/damage of neurons, e.g., damage to myelin sheaths on axons and dendrites (Phillips *et al.*, 2016), which are normal barriers to diffusion.

Both FA and MD are sensitive to age-related changes in WM (Behrman-Lay *et al.*, 2015). Healthy WM is related to relatively high FA (usually > 0.2) and lower MD values (Mori and Zhang, 2006) *(Figure 3)*.

Radial diffusivity (RD) captures the average diffusivity transverse to axonal fibres, i.e., overall displacement perpendicular to the axon. It is derived by calculating the average of the two eigenvalues, λ_2 and λ_3:

$$RD = \frac{\lambda_2 + \lambda_3}{2}$$

While RD indicates transverse diffusion, axial diffusivity (AxD), i.e., the largest eigenvalue *(λ_1)*, represents diffusion parallel to axonal fibres (Nir *et al.*, 2013). When RD is disrupted, it appears to be an indication of demyelination (Alexander *et al.*, 2007; Klawiter *et al.*, 2011; Nir *et al.*, 2013), whereas AxD may be a more specific marker for axonal damage/loss (Alexander *et al.*, 2007; Phillips *et al.*, 2016). However, some studies have found an absence of myelin and axonal damage with an increase in RD and no change in AxD (Song *et al.*, 2002), while others have reported both increases in RD and decreases in AxD which may suggest fibre reorganisation (Dubois *et al.*, 2008).

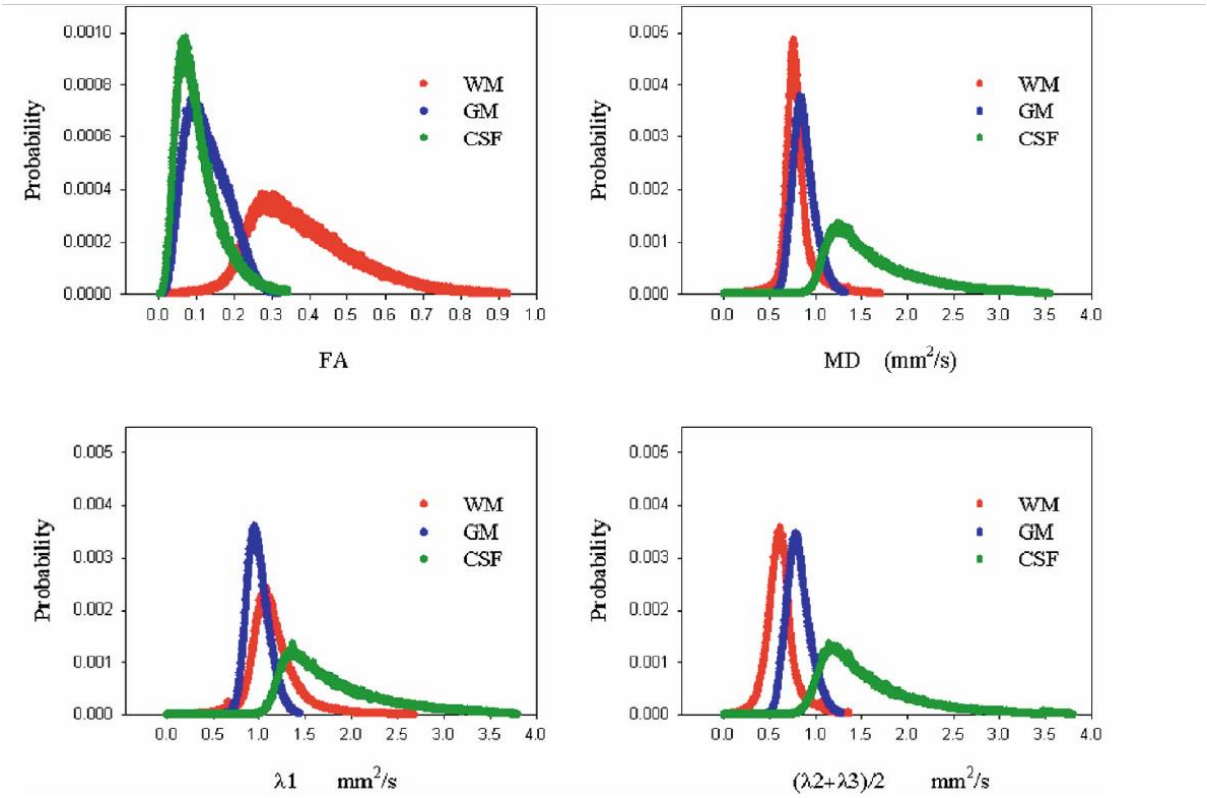

Figure 3: Histograms of FA, MD, AxD and RD in healthy white matter (WM), grey matter (GM) and cerebrospinal fluid (CSF) (adapted from (Alexander et al., 2007)).

2.2.2.2 DTI and AD

DTI measures are good detectors of WM integrity alterations at a microscopic level in both healthy and diseased older individuals (Behrman-Lay *et al.*, 2015).

A vast number of previous DTI studies have observed lower FA in AD patients compared to control participants in all four lobes in the brain, i.e., frontal lobe (Choi *et al.*, 2005; Gao *et al.*, 2011; Liu *et al.*, 2011; Chandra *et al.*, 2019), temporal lobe (Chandra *et al.*, 2019), such as the medial (Gao *et al.*, 2011) and left temporal lobe (Damoiseaux *et al.*, 2009; Serra *et al.*, 2010), parietal lobe (Sugihara *et al.*, 2004; Rose, Janke and Chalk, 2008) as well as occipital lobe (Chandra *et al.*, 2019). Specifically, lower FA has been seen in the corpus callosum (Stricker *et al.*, 2009; Serra *et al.*, 2010; Gao *et al.*, 2011; Liu *et al.*, 2011), thalamus (Rose, Janke and Chalk, 2008; Damoiseaux *et al.*, 2009; Serra *et al.*, 2010), cingulum (Damoiseaux *et al.*, 2009; Stricker *et al.*, 2009; Liu *et al.*, 2011; Chandra *et al.*, 2019), parahippocampus (Stricker *et al.*, 2009; Liu *et al.*, 2011), fornix (Serra *et al.*, 2010; Liu *et al.*, 2011), brainstem (Liu *et al.*, 2011) as well as the superior lateral/longitudinal fasciculus and uncinate fasciculus (Damoiseaux *et al.*, 2009; Liu *et al.*, 2011; Chandra *et al.*, 2019). In addition, numerous studies have reported that there is a relationship between greater cognitive

impairment and lower anisotropy in some of these regions (Stricker *et al.*, 2009; Guo *et al.*, 2010; Liu *et al.*, 2011; Nir *et al.*, 2013). Xie et al. (2006) used DTI and VBM to examine FA and volumetric abnormalities in AD compared to controls. They found that the reduction in FA was evident in WM regions, and was observed to be close in location to GM regions that showed cortical volume reductions, such as the bilateral medial temporal structures, in the AD group compared to controls. This is consistent with other MRI studies investigating WM and GM volumes (Guo *et al.*, 2010). Higher FA was also observed in motor associated brain areas, including the corticospinal tract (Teipel *et al.*, 2007, 2014; Douaud *et al.*, 2011) and cerebellum (Teipel *et al.*, 2014). Conversely, some studies did not find any regions with a change in FA in the AD group compared to healthy controls (Stahl *et al.*, 2007).

Studies have reported significantly elevated MD within several regions when comparing AD participants to healthy controls. AD patients had higher MD measures within parietal, medial temporal, frontal lobe regions, specifically the hippocampus, amygdala, temporal gyrus, the entorhinal cortex, anterior and posterior regions of the cingulate gyrus (bilaterally), medial frontal gyrus, parahippocampal gyrus and anterior thalamic radiations (bilaterally) (Rose, Janke and Chalk, 2008; Serra *et al.*, 2010). A meta-analysis of 41 case-control DTI studies found increases in MD globally, i.e., in the frontal, parietal, occipital and temporal lobes including the hippocampus, in the AD group with increases absent in the frontal and occipital regions in the MCI group (Sexton *et al.*, 2011). Conversely, Serra et al. (2010) only found higher MD, specifically in the bilateral anterior thalamic radiations, in the anterior part of the inferior longitudinal fasciculus and the hippocampal part of the left cingulum, in the AD group compared to the healthy controls, but not in the MCI group.

An increase in AxD in both normal ageing and AD (Acosta-Cabronero *et al.*, 2010; Sullivan, Rohlfing and Pfefferbaum, 2010; Agosta *et al.*, 2011; Nir *et al.*, 2013) has been reported. Additionally, an elevated AxD associated with clinical impairment (Nir *et al.*, 2013) was found. Gao et al. (2011) compared a group of healthy older individuals as well as a group of participants with AD to a group of healthy young adults in six fibre bundles. These fibre bundles included commissural, posterior and anterior fibre bundles in the genu and splenium of the corpus callosum, bilateral corticospinal tract in the posterior internal capsule, and an area close to the anterior limb of the internal capsule and external capsule. They found that the healthy older individuals showed higher RD values in the anterior

bundles and the right posterior internal capsule, while the AD group showed higher RD and AxD in all six fibre bundles that they investigated compared to the healthy young adult group.

By observing all four measures, AD patients presented significantly lower FA and higher MD across all lobes in the brain when compared to healthy controls (Mito *et al.*, 2018), specifically in the medial temporal lobe (Xie *et al.*, 2006; Zhang *et al.*, 2007; Stebbins and Murphy, 2009). Regions that showed both increases in MD and decreases in FA could suggest changes in microstructural integrity associated with tissue atrophy and increased diffusion in the brain (Sen and Basser, 2005; Gold *et al.*, 2011). In addition, FA and MD abnormalities have been found to be associated with memory and executive dysfunction in AD (Sjöbeck *et al.*, 2010; Hirni *et al.*, 2013). Studies have found lower FA and higher MD in AD in regions such as the fornix and the cingulum bundle (Zhang *et al.*, 2007; Mielke *et al.*, 2009; Qiu *et al.*, 2010).

WM neuropathology regularly causes FA to decrease, which may be due to the increase in RD and reduced AxD, or both (Alexander *et al.*, 2007). Nir et al. (2013) revealed higher mean MD, AxD and RD values in AD patients compared to healthy controls. Other longitudinal studies replicated these findings (Nowrangi *et al.*, 2013; Firbank *et al.*, 2016). Conversely, Kitamura et al. (2013) investigated individuals with mild AD over a period of 18 months and reported decreases in FA and increases in RD, but no changes in MD or AxD. Another study that was part of this study's longitudinal project (Engelbrecht, in preparation) detected group differences in the right inferior longitudinal fasciculus (R-ILF) with AD patients having lower FA and RD values compared to controls.

2.3 Graph Theory

In graph theory, a network comprises nodes and edges between them *(Figure 4A)*. In the context of neuroimaging, nodes represent regions of interest (ROIs) obtained from anatomical or functional atlases, while edges represent the structural or functional associations between the nodes (Dai and He, 2014). Both structural and functional networks can be mapped out and analysed by applying graph theoretical analyses to MRI data (Prescott *et al.*, 2014). Structural associations can be either cortical thickness or volume between the ROIs in structural imaging or properties of WM tracts in diffusion MRI (Dai and He, 2014). The functional associations are the temporal correlations measured in

electroencephalograph (EEG), magnetoencephalography (MEG) or resting-state functional MRI (rs-fMRI) (Dai and He, 2014).

2.3.1 Graph theoretical measures of interest

The topology of brain networks can be investigated by using graph theory metrics that assess integration and segregation (Rubinov and Sporns, 2010). Segregation is defined by partitioning a network into groups of regions, i.e. modules, which form the structural part of a brain to perform a function, and is quantified using measures such as transitivity, local efficiency and modularity (Watts and Strogatz, 1998; Newman and Girvan, 2004; Prescott *et al.*, 2014; Pereira *et al.*, 2018). **Transitivity** measures the overall probability that neighbours of a node are also connected to each other (Mears and Pollard, 2016). It can be calculated by dividing the observed number of closed triplets by the maximum possible number of closed triplets (Mijalkov *et al.*, 2017) *(Figure 4H)*. Higher transitivity indicates stronger segregation of the network (Luo, Greene and Constable, 2021), i.e., which may affect the brain's ability to undergo specialised computations. A decrease in transitivity may represent transitory myelin damage (Kocevar, Gabriel Stamile *et al.*, 2016). **Modularity** is the presence of closely interconnected groups of regions known as modules. High modularity represents strong connectivity of nodes within a module and sparsely connected between modules (Newman and Girvan, 2004; Brier *et al.*, 2014; Pereira *et al.*, 2018) *(Figure 4G)*. **Local efficiency** describes how efficiently information is transferred between a node and its immediate neighbours (Lee *et al.*, 2019) *(Figure 4E)* and measures the fault tolerance of the network, which represents the exchange of information when the node of interest is removed (Ma *et al.*, 2018). Decreased local efficiency is a consequence of the loss of short-range connections between the neighbourhood regions (Sun *et al.*, 2019). High segregation is an indication of high complexity in a network thus, a decrease in segregation can be a sign that the network has a more random topologic organisation (Prescott *et al.*, 2014).

Integration is defined as the capacity of the network to be interconnected and the ability of brain networks to combine information from different brain regions at a rapid speed, this includes measures such as global efficiency (Watts and Strogatz, 1998; Latora and Marchiori, 2001; Pereira *et al.*, 2018). **Global efficiency** is calculated by averaging the efficiency for all node pairs (Tuladhar *et al.*, 2016) and shows how well information is transmitted across the

entire network (Bullmore and Sporns, 2009; Rubinov and Sporns, 2010; Contrerass *et al.*, 2020) *(Figure 4D)*.

Other graph theory measures include nodal efficiency, nodal degree, and nodal strength. **Nodal efficiency** measures how efficiently information is exchanged between a node and all other nodes in a network *(Figure 4F)*. A node that has low nodal efficiency indicates lower information flow and may be inefficiently connected to other nodes in the network and vice versa (Kim *et al.*, 2014). The **degree of a node** is the total number of edges, i.e., connections, that is connected to the node (Mears and Pollard, 2016) *(Figure 4C)*. Even with regional

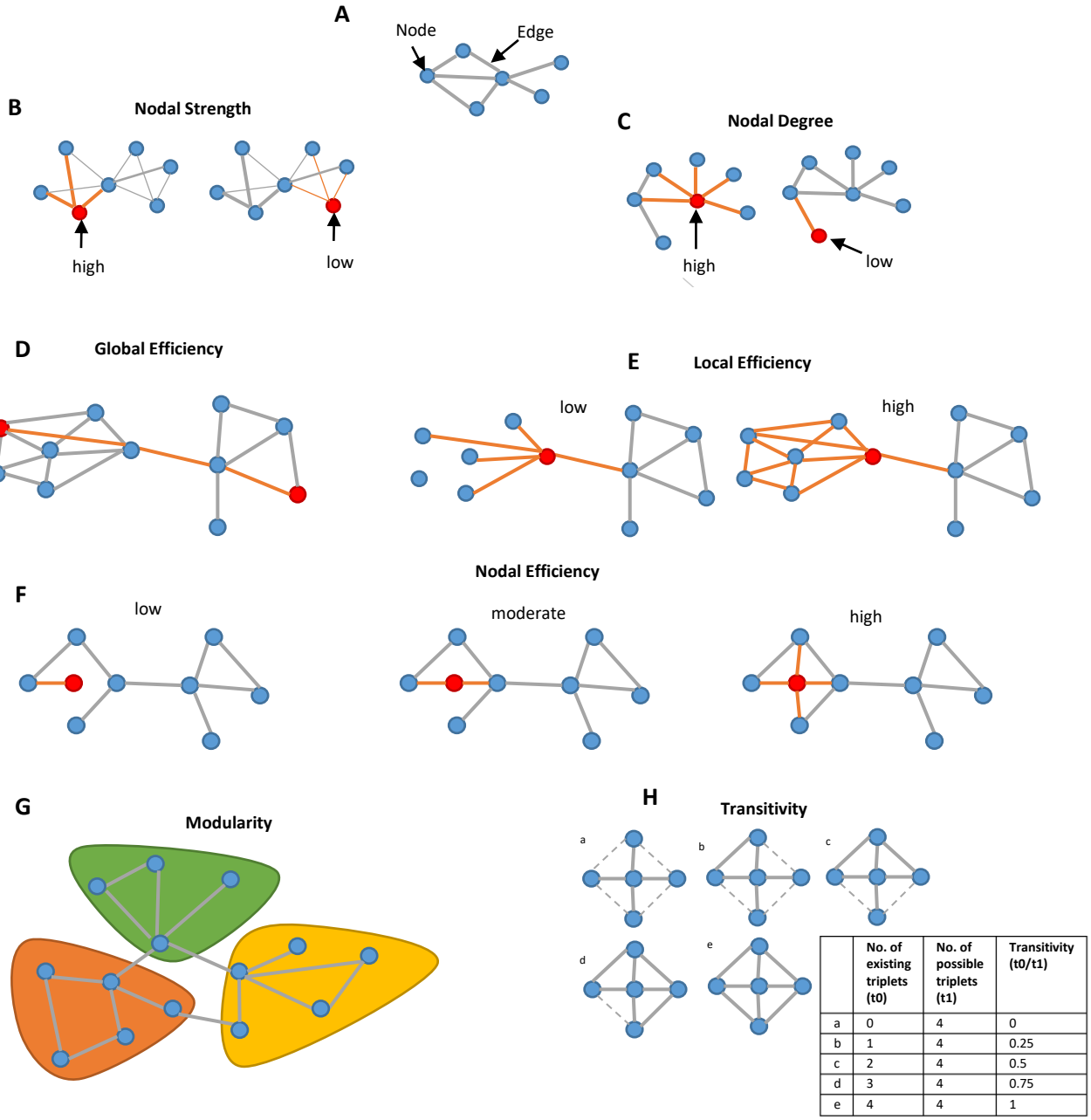

	No. of existing triplets (t0)	No. of possible triplets (t1)	Transitivity (t0/t1)
a	0	4	0
b	1	4	0.25
c	2	4	0.5
d	3	4	0.75
e	4	4	1

Figure 4: Graph theoretical measures. Red circle shows the node of interest and orange lines show the edges of interest.

brain atrophy, an increase in the nodal degree suggests more robust connectivity. **Nodal strength** is given by the sum of the edge weights linked to a node, i.e., higher nodal strength means stronger connectivity (Mijalkov *et al.*, 2017; Kim and Min, 2020) *(Figure 4B).*

2.3.2 Structural and functional connectome and Alzheimer's disease

The brain's structural and functional connectome shows disrupted topological organisation in patients with mild cognitive impairment (MCI) (Wang *et al.*, 2013; Filippi *et al.*, 2018; Sun *et al.*, 2019) and in cognitively healthy patients with amyloid deposition and neurodegeneration (Pereira *et al.*, 2018). This disruption is more severe in patients who progress to AD, particularly in the regions that form part of the default-mode network (DMN) (Wang *et al.*, 2013; Sun *et al.*, 2019), which is a set of brain regions characterised by increased neural activity during rest and deactivation during goal-orientated tasks in healthy subjects (Raichle *et al.*, 2002; Buckner, Andrews-Hanna and Schacter, 2008). Progressive degeneration is associated with the breakdown of anatomical connections, most affecting connections to the left hippocampus (Filippi *et al.*, 2018), a region that is found to decline early in AD.

Previous studies have reported that patients with amnestic mild cognitive impairment (aMCI) who were at high risk of converting to AD showed lower global and local efficiency (Shu *et al.*, 2012; Fischer *et al.*, 2015; X. N. Wang *et al.*, 2016; Zhao *et al.*, 2017; Sun *et al.*, 2019) compared to controls. This decrease in global efficiency indicates a disruption in long-distance connections or a loss of ability to effectively transmit information to distant regions in the brain (X. N. Wang *et al.*, 2016; Pereira *et al.*, 2018), and may be linked to the degeneration of WM fibre bundles used to transfer information (Lo *et al.*, 2010; Dai *et al.*, 2019). In a study using resting-state magnetoencephalography, López-Sanz et al. (2017) observed a decrease in transitivity and an increase in modularity in the MCI group. These changes in graph-theoretical measures suggest that structural and functional impairment of brain regions may be already measurable at the preclinical stage of AD.

Similar results have been found in patients with AD compared to controls using a number of different imaging modalities. Franciotti et al. (2019) showed that AD patients had a reduction in the number of edges, i.e., decrease in nodal degree, as well as a loss of local and global efficiency in a resting-state EEG study. They also found a reduction in the strength of information transfer among occipital and parieto-temporal areas (Franciotti *et*

al., 2019). Similarly, Kocagoncu et al. (2020) also found decreases in both global and local efficiency with increase in Tau burden using both electro-magnetoencephalography and positron emission tomography (PET) scanning. In another PET study, the hippocampus and inferior parietal cortex presented with the highest increase in nodal strength in the AD group compared to controls (Veronese *et al.*, 2019).

There were mixed results when studying the functional brain networks using resting-state fMRI. Zhao et al. (2012) reported lower global efficiency and higher local efficiency, conversely, Supekar et al. (2008) found no differences in global efficiency and lower local efficiency in AD compared to controls. These disrupted brain regions were mainly found in the DMN, in the temporal lobe and the subcortical structures in AD (Zhao *et al.*, 2012). In a sMRI study that studied both MCI and AD patients observed that AD individuals had significant nodal degree increases in the right insula, left medial orbitofrontal, bilateral posterior cingulate gyri, and rostral anterior cingulate as well as decreases in right inferior parietal gyri, the left middle temporal and right precentral compared to controls (Mijalkov *et al.*, 2017). Some of these regions that presented with changes in the number of edges belong to the structural regions that correspond to regions found in the DMN of the functional connectome, including the anterior cingulate and posterior cingulate gyri as well as the medial orbitofrontal (Mijalkov *et al.*, 2017). Local efficiency increases were found in the left entorhinal cortex and bilateral temporal pole as well as decreases in several regions in the frontal, temporal and parietal lobes (Mijalkov *et al.*, 2017). The authors also found decreased transitivity with increased modularity in both the MCI and AD groups (Mijalkov *et al.*, 2017). Similar results on transitivity and modularity have been found in another sMRI study (Pereira *et al.*, 2016). Conversely, in a rs-fMRI study, Brier et al. (2014) reported a decrease in modularity with advancing clinical status.

In DTI AD studies, impairment of network properties has been found in AD which suggests that structural connectivity is altered by WM degeneration in these individuals (Lo *et al.*, 2010). These network properties include lower global efficiency (Lo *et al.*, 2010; Wu *et al.*, 2019; Kuang *et al.*, 2020), local efficiency (Reijmer *et al.*, 2013), nodal degree (Dai *et al.*, 2019), nodal strength (Wu *et al.*, 2019; Kuang *et al.*, 2020), nodal efficiency (Lo *et al.*, 2010; Zajac *et al.*, 2017), transitivity (Pereira *et al.*, 2016; Mijalkov *et al.*, 2017; Si *et al.*, 2019) and both lower (Brier *et al.*, 2014) as well as higher modularity (Pereira *et al.*, 2016; Mijalkov *et*

al., 2017; Si *et al.*, 2019) in AD relative to controls. Daianu et al. (2015) observed significantly lower strength of connections between nodes in AD patients compared to controls in 13 brain regions, including the bilateral precuneus, bilateral parahippocampal regions, left rostral middle frontal lobe, left rostral anterior cingulate gyrus, left middle temporal lobe, bilateral fusiform, left lingual, bilateral isthmus of the cingulate gyri and the right superior parietal lobe. Compared to controls, the AD group revealed lower nodal degree in the right middle frontal gyrus, insula, and middle temporal gyrus (Dai *et al.*, 2019). Nodal efficiency has also been found to be lower in AD individuals compared to controls in the left thalamus (Zajac *et al.*, 2017) as well as the right frontal lobe and right temporal regions (Lo *et al.*, 2010). Lo et al. (2010) also found that WM networks of the AD group had no changes in local efficiency, but showed decreases in global efficiency.

2.4 Relationship between imaging and IIV

Several studies have looked at the relationship between IIV and different imaging measures in healthy individuals over a broad age range. In sMRI studies, Walhovd and Fjell (2007) proposed that there is a negative correlation between RT IIV and WM volume. Using T2-weighted MRI, Bunce et al. (2007) investigated the relationship between WM hyperintensities and cognitive performance in 469 healthy adults aged 60 to 64 years and observed only frontal lobe WM hyperintensities to be associated with RT IIV. This is consistent with another study that observed patients with frontal lobe lesions and found that patients with lesions in the dorsolateral prefrontal cortex and/or in the superior medial frontal cortex, in particular, showed the highest variability (Stuss *et al.*, 2003). In fMRI studies, a study consisting of 42 subjects with age range between 18 to 46 years, found a positive correlation between measures of response variability and activation in the right thalamic, inferior parietal, inferior frontal and bilateral middle frontal regions (Bellgrove, Hester and Garavan, 2004). These regions form part of a distributed neural network known to be involved in sustained attention and inhibitory processing (Bellgrove, Hester and Garavan, 2004). Conversely, MacDonald et al. (2008) observed that decreasing IIV was associated with increased activation in the inferior parietal cortex, as well as better recognition and shorter latencies.

Previous studies that have looked at the relationship between DTI measures and IIV reported that higher IIV, which suggests less effective behavioural and attentional control

that may be due to inefficient neural and network activation (Rabbitt *et al.*, 2001), is associated with a decrease in FA (Moy *et al.*, 2011; Mella *et al.*, 2013), as well as an increase in radial diffusivity (RD) (Moy *et al.*, 2011; Mella *et al.*, 2013) and MD (Moy *et al.*, 2011; Grydeland *et al.*, 2013; Halliday *et al.*, 2019) in WM fibre tracts. Moy et al. (2011) also found that the association between WM changes and age-related RT IIV increases involved most of the interhemispheric and intrahemispheric corticocortical connections. Conversely, another DTI study has found that higher values of FA were associated with higher average RT and greater variability with the opposite outcome for MD, specifically in the frontal regions (Booth *et al.*, 2019).

A limited amount of literature has investigated the relationship between IIV and different imaging measures in MCI and AD individuals. In a study of 451 MCI participants and 285 healthy controls between the age of 55 and 90, Bangen et al. (2019) found that there was a significant negative relationship between IIV and entorhinal cortical thickness, but not with hippocampal volume in the MCI group. In addition, the authors also examined whether IIV would predict longitudinal change in hippocampal volume and entorhinal cortical thickness over a 24-month follow-up period. They observed that there was an association between higher IIV and greater reduction in entorhinal cortex thickness over time in both groups, but only found a significant association between higher IIV and hippocampal volume over time in the MCI group.

As mentioned in previous sections, the only published work that looked at the relationship between IIV and WM integrity in AD individuals found that there was a negative relationship between RT IIV and WM volume (Jackson *et al.*, 2012). These WM regions include the posterior cingulate, precuneus, superior frontal gyrus, as well as the ventral and dorsolateral prefrontal cortex volumes (Jackson *et al.*, 2012), some of which form part of the default-mode network (DMN), which has been found to be implicated in both AD and IIV (Greicius *et al.*, 2004; Kelly *et al.*, 2008). Another study, which is a substudy of a larger research project from which our sample is drawn from, extended these findings and observed an association between IIV on simple and choice RT tasks and micro-structural WM changes, as indexed by DTI (Engelbrecht, in preparation). One of the main findings from this study was a negative relationship between RT IIV and AxD, but not RD, in the right inferior longitudinal fasciculus (R-ILF) (Engelbrecht, in preparation). This may suggest that changes in IIV may be

caused by disruptions in the integrity of the axonal structure and not in myelin (Engelbrecht, in preparation).

The only study to date that looked at the relationship between graph theory measures and IIV was a resting-state functional connectivity MRI (rs-fMRI) study where the authors found that modularity and small-worldness both predicted intra-individual variation in memory capacity (Stevens *et al.*, 2012). To our knowledge, no study has investigated the association between IIV and graph-theoretical properties using DTI full-probabilistic tractography in AD.

3. Methodology

3.1 Design and setting

This study examined (1) white matter (WM) changes and graph theoretical measures in patients diagnosed with possible or probable Alzheimer's disease (AD) compared to healthy elderly controls and (2) the association between these WM structural connectome properties and intra-individual variability (IIV) on neurocognitive tests between the two groups. The sample is from a larger research project on the longitudinal trajectory of cognitive decline in AD that took place in Cape Town, South Africa (Christ, Combrinck and Thomas, 2018) and was conducted by the Applied Cognitive Science and Experimental Neuropsychology Team (ACSENT) Laboratory of the University of Cape Town's (UCT) Department of Psychology. The parent study made use of a measurement-burst design to measure IIV (Fiske and Rice, 1955; Nesselroade, 1991), where the same task is taken multiple times and over multiple time-frames. Over 12 months, each participant goes through three intervals of serial testing (T1, T2, and T3). Within each interval, there are three testing sessions and each of these sessions are further divided into two blocks that consist of 30 trials within each block *(Figure 5)*. The cognitive tests were taken in a private room in the Geriatric Unit at Groote Schuur Hospital (GSH) in Cape Town, or in the participant's home. Furthermore, magnetic resonance imaging (MRI) scans were also acquired of each participant sometime over the 12 months at the Cape University Body Imaging Centre (CUBIC) in GSH.

This study used the reaction time (RT) outcome data of two different RT tasks, simple and choice RT task, from the parent study's neuropsychological test battery and is only from one test interval. For each participant, the six blocks (180 trials) of each RT task were utilised to

compute the net IIV *(Figure 5).* The interval chosen for each participant (either T1, T2 or T3) were selected according to the interval that was derived closest to the MRI scan date of that participant.

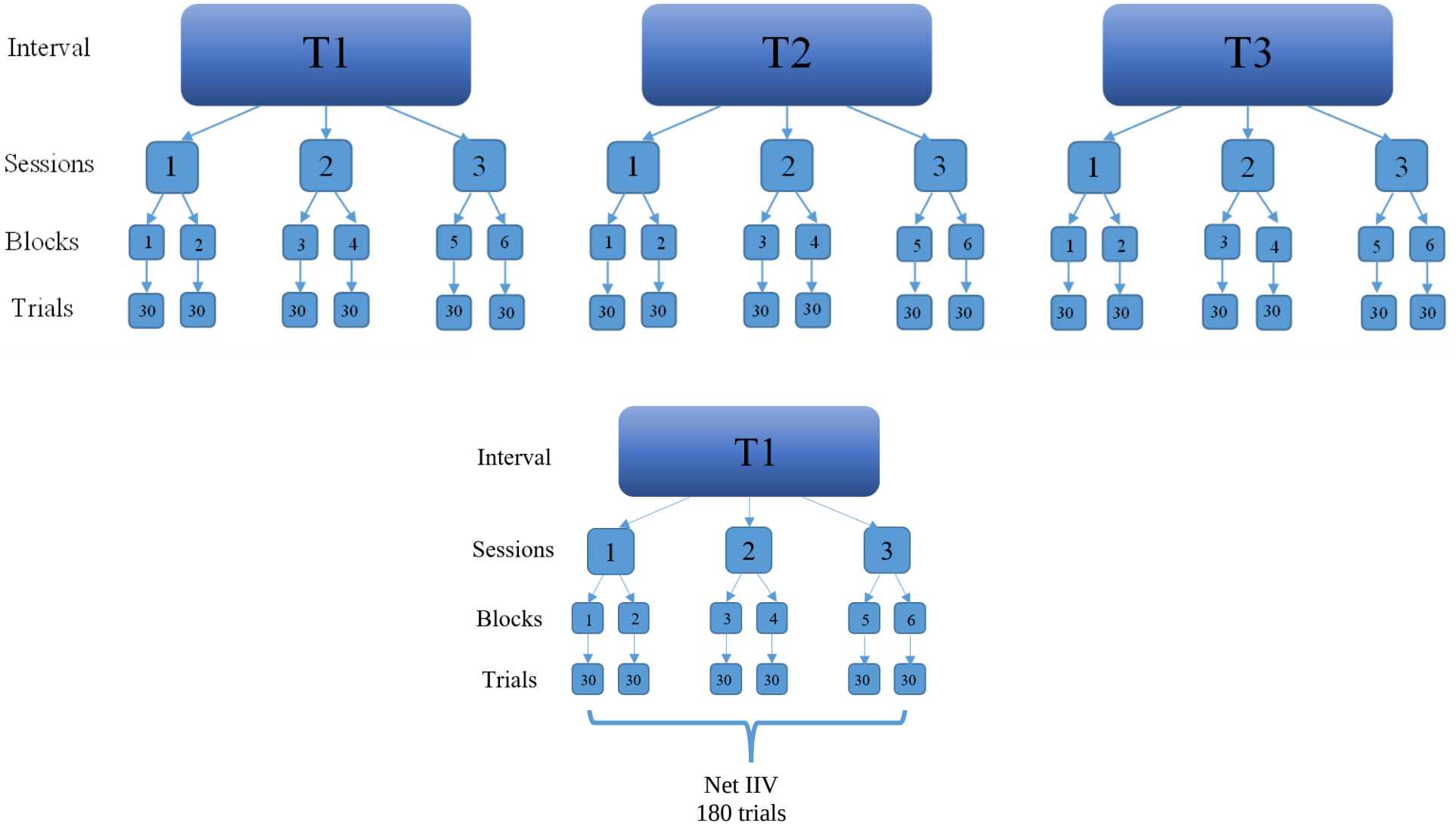

Figure 5: Measurement-burst design of parent study. Flowchart of how reaction time data was collected and how the net intra-individual variability for each participant was calculated.

3.2 Participants

Eligibility criteria: The eligibility criteria in this study were identical to the criteria in the parent study. Only participants who (1) were 55 years of age or older, (2) had an accessible medical health history available, (3) were capable of speaking, reading, and writing in English and (4) had a family member or caretaker who was available to follow up on recent changes in cognitive function were included in the study.

Participants were excluded if they were (1) diagnosed with HIV/AIDS, uncontrolled diabetes mellitus, uncontrolled hypertension or any other medical condition that could affect their cognitive function, (2) any current or past psychiatric illnesses, (3) had any major neurological disorder such as Parkinson's disease, or a history of a significant cerebrovascular accident or traumatic brain injury within the last two years, (4) current alcohol or drug abuse, or were a heavy smoker (more than 20 cigarettes a day), (5) had a Geriatric Depression Scale (GDS) (Yesavage *et al.*, 1982) score greater than 15 out of 30, or (6) scored less than 12 on the Mini-Mental State Examination (MMSE) (Folstein, Folstein and McHugh, 1975). These criteria were applied based on results from previous studies on cognitive performance in both healthy controls and AD (Grant, Contoreggi and London, 2000; Arvanitakis *et al.*, 2004; Swan and Lessov-Schlaggar, 2007; Gorelick *et al.*, 2011; Van Den Kommer *et al.*, 2013; Bernardin, Maheut-Bosser and Paille, 2014; Jokinen *et al.*, 2015).

Healthy elderly controls: Control participants (*n* = 26; 20 women; mean age = 70.31) were volunteers who were notified about the study through informal information sessions at old age homes, seniors' clubs and retirement villages or flyers handed out at these establishments in and around Cape Town, South Africa. Some control individuals were the healthy relatives of the clinical participants.

AD patients: The clinical participants (*n* = 26; 17 women; mean age = 75.42) were recruited into the parent study from the Memory Clinic in GSH (government-funded hospital) if they met the NINCDS-ADRDA criteria (McKhann *et al.*, 1984) for mild-to-moderate stage of possible or probable AD. Health professionals, such as a neurologist and a neuropsychologist, who work at the Memory Clinic, monitored the recruitment of these clinical participants.

The Memory Clinic, which is managed by UCT's Division of Geriatric Medicine and the Albertina and Walter Sisulu Institute of Ageing in Africa, consists of patients that were referred from primary healthcare institutions in and around Cape Town (Kalula *et al.*, 2010) if the patients were presumed to have age-related memory disorders. One of the staff members at the Memory Clinic approached potential clinical participants and presented the study's information to them.

All clinical participants met the (1) Diagnostic and Statistical Manual – Fourth Edition (DSM-IV; American Psychiatric Association, 2013) diagnostic criteria for AD and (2) were all classified to be of mild-to-moderate severity on the Clinical Dementia Rating (CDR) scale.

For the current study, the participants were not categorised by disease severity and were evaluated as one group.

Study protocols and procedures were approved by the Human Research Ethics Committee of UCT's Faculty of Health Sciences. Procedures followed the guidelines published in the Declaration of Helsinki (World Medical Association, 2013).

3.3 Procedure

The data were from five sessions. The first session was for screening, which was followed by three neurocognitive test sessions within a week or less (but no more than 30 days later) and the fifth session as the imaging session. The three test sessions took place over a two-week period and the sessions were identical to one another. Only the test order was varied, to control for order effects. Since the interval for each participant were selected according to the interval that was derived closest to the MRI scan date of that participant for this study, the MR images were either not more than 7 months before the participants' first test session or after the participants' third test session depending on which interval was closest to the MRI scan *(Table 1*). See *Supplementary Table 1* to see chosen interval and test order for each participant.

Table 1: Examples of how an interval for each participant was selected.

								The chosen interval for this specific participant		
Participant	**MRI scan date**	**TI 1, Sess. 1**	**TI 1, Sess. 2**	**TI 1, Sess. 3**	**TI 2, Sess. 1**	**TI 2, Sess. 2**	**TI 2, Sess. 3**	**TI 3, Sess. 1**	**TI 3, Sess. 2**	**TI 3, Sess. 3**
Participant 1	2016/06/07	2015/03/13	2015/03/23	2015/03/27	2015/09/23	2015/10/07	2015/10/14	2016/05/24	2016/05/31	2016/06/07
					The chosen interval for this specific participant					
Participant 2	2017/01/17	2016/09/06	2016/09/14	2016/09/22	2017/03/16	2017/03/24	2017/04/03	2017/10/25	2017/11/02	2017/11/08
Key: TI, Time Interval; Sess., Session										

Screening: Before the screening, all participants signed consent forms, with all clinical participants signing with a guardian, caregiver, or relative present. Screening was carried out depending on the participant's preference, either in a private research room in the Geriatric Unit at GSH or at the participant's home. The scores of each screening measure (listed under *section 3.4.1*) for each participant were then calculated and checked against the eligibility criteria.

Testing: The testing phase began within 30 days of the screening phase *(Figure 6)*. Testing was carried out depending on the participant's preference, either in a private research room in the Geriatric Unit at GSH or at the participant's home. Reaction time data, namely the simple reaction time (SRT) and choice reaction time (CRT) task, was collected during the three testing sessions of each interval, i.e., three sessions each for the SRT and CRT task. Each of the three test sessions took place 7 days apart, over the course of 2 weeks *(Figure 6)*. Two SRT and two CRT blocks were administered in each of the three sessions, i.e., a total of six blocks for the SRT task and six blocks for the CRT task in each interval. Each of these blocks consisted of 30 trials, i.e., 60 trials in each session *(Figure 5)*. Therefore, this study comprised of 180 trials of SRT data and 180 trials of CRT data for each participant *(Figure 5)*.

Neuroimaging: All scans were conducted at CUBIC, GSH. Written informed consent, as well as an MRI compatibility checklist, was obtained from all participants upon arrival at the scanning centre. Imaging study protocols were undertaken with the approval of the Human Research Ethics Committee of UCT.

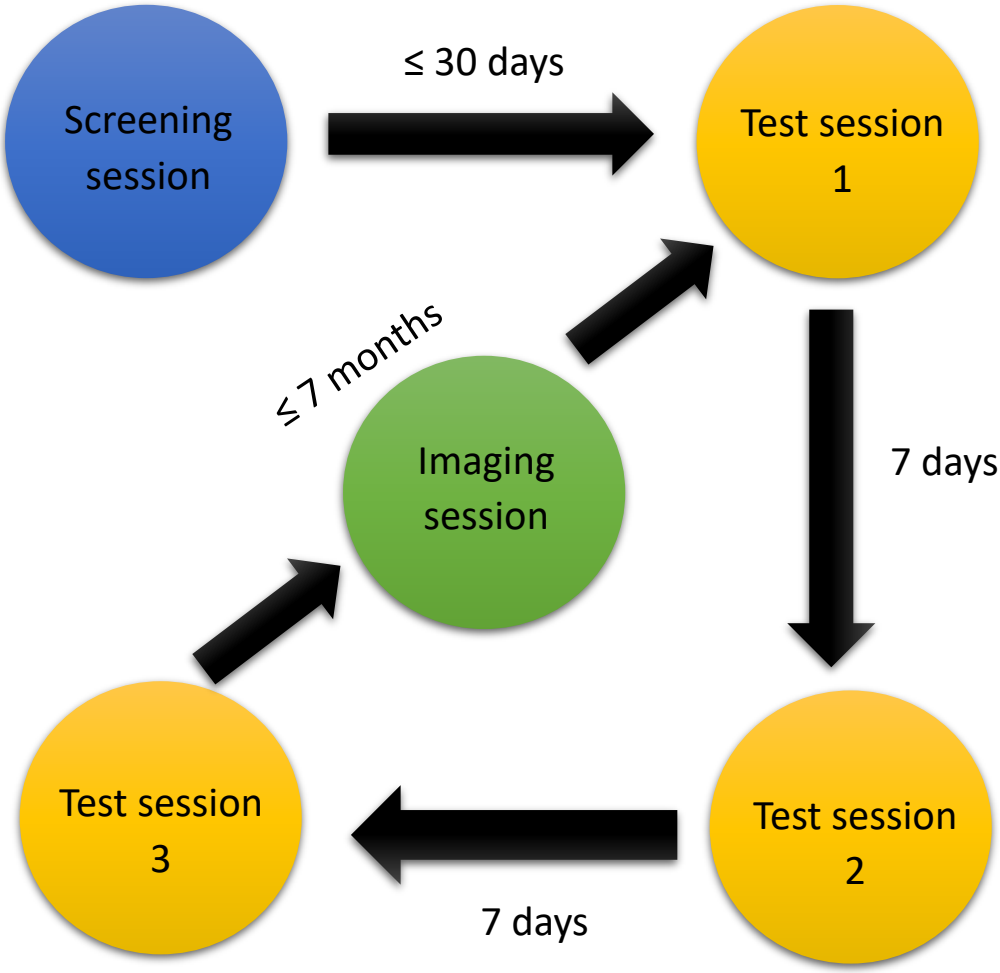

Figure 6: Timeline of the procedure - screening, testing, and imaging sessions.

3.4 Measures

3.4.1 Screening measures

The screening process, which included (1) taking a clinical history, (2) the Geriatric Depression Scale (GDS) (Yesavage *et al.*, 1982), (3) the MMSE (Folstein, Folstein and McHugh, 1975), and (4) the Cambridge Examination for Mental Disorders of the Elderly-Revised edition (CAMCOG-R) (Huppert *et al.*, 1995), ensured that the previously described eligibility criteria were met.

Geriatric Depression Scale (GDS): The Geriatric Depression Scale is used to identify symptoms of depression in older adults (Yesavage *et al.*, 1982). It is a 30-item questionnaire consisting of yes or no questions where participants answer according to how they felt over the past week (Yesavage *et al.*, 1982). A score between (1) 0-9 is considered normal, (2) 10-

19 indicates mild depression and (3) 20-30 is considered as severe depression (Yesavage *et al.*, 1982). The GDS can be used on healthy older adults, older adults with mild-to-moderate cognitive impairments (Yesavage *et al.*, 1982) as well as medically ill older adults and has been used successfully in a South African setting (Dorsey, Rodriquez and Brathwaite, 2002).

Mini-Mental State Examination (MMSE): The Mini-Mental State Exam is a questionnaire consisting of 30 points that is widely used to measure cognitive impairment among the elderly (Folstein, Folstein and McHugh, 1975). This examination has the ability to test for orientation, memory, language, attention, and visual-spatial skills (Folstein, Folstein and McHugh, 1975). If an individual obtains a score between 24-30, they are considered to have no cognitive impairment, a score between 19-23 is classified as mild cognitive impairment, a score between 10-18 is classified as moderate cognitive impairment and less than 9 is considered to be severe cognitive impairment (Folstein, Folstein and McHugh, 1975). The MMSE has been used successfully in the South African setting (Ramlall *et al.*, 2013; James *et al.*, 2015; Adam, Godlwana and Maleka, 2016; Christ, Combrinck and Thomas, 2018).

The Cambridge Examination for Mental Disorders of the Elderly- Revised edition (CAMCOG-R): The CAMCOG-R is a standardised instrument that is part of the Cambridge Examination for Mental Disorders of the Elderly – Revised (Huppert *et al.*, 1995). It is used as a cognitive screening tool for early diagnosis of dementia in the elderly (Leeds *et al.*, 2001) as well as for the assessment of cognitive function. This measure consists of 67 items and evaluates language, attention, orientation, perception, praxis, calculation, memory, and abstract thinking. This study uses a version that has been adapted for the South African population (James *et al.*, 2015).

3.4.2 IIV testing measures

Neurocognitive testing consisted of a 12-test cognitive battery that included a range of reaction time (RT)- and accuracy-based tasks. The current study used two RT tasks from that battery that are part of the Cambridge Neuropsychological Test Automated Battery (CANTAB) (Fray, Robbins and Sahakian, 1996) to measure performance variability. These CANTAB tests were administered on a Windows 8.1 touchscreen device with a press pad.

The CANTAB is a computerised neuropsychological test battery and is widely used and reviewed in the literature (Lowe and Rabbitt, 1998; Égerházi *et al.*, 2007).

Reaction time (RT) is defined as the time between the appearance of a stimulus and the participant's response to that stimulus. The first is a simple reaction time (SRT) task, where the participant is required to hold down a press pad while monitoring for the presence of a yellow dot inside a white circle on a computer screen. Once the yellow dot appears, the participant must, as soon as possible, release the press pad and select the white circle on the screen *(Figure 7a)*. The yellow dot, i.e., the stimulus, would appear on the screen for 250ms and the participant needs to respond to the yellow dot in 5s before the next trial would begin, with an inter-stimulus delay of between 750 and 2250ms. The second is a choice reaction time (CRT) task, which works similarly to the SRT task, except instead of only one white circle, there are five white circles where the yellow dot may appear and the participant is required to select the one out of the five white circles in which the yellow dot appeared *(Figure 7b)*. Both tasks had a 10-trial practice phase before the actual test phase. Participants could move on to the testing phase if they achieve 90% accuracy for the first practice phase, however, if they fail the first phase, they can attempt a second practice phase. Thereafter, the participants would progress to the testing phase irrespective of the result, i.e., whether a pass or fail. The testing phase for both SRT and CRT tasks consisted of 30 trials, which took about 5 minutes to complete. Two SRT blocks and two CRT blocks were administered for each session, i.e., 60 trials in each session. Therefore, this study comprised of 180 trials of SRT data and 180 trials of CRT data for each participant *(Figure 5)*. These RT tasks can assess motor and mental response speeds, as well as measure response accuracy, impulsivity, movement time and reaction time (Cambridge Cognition).

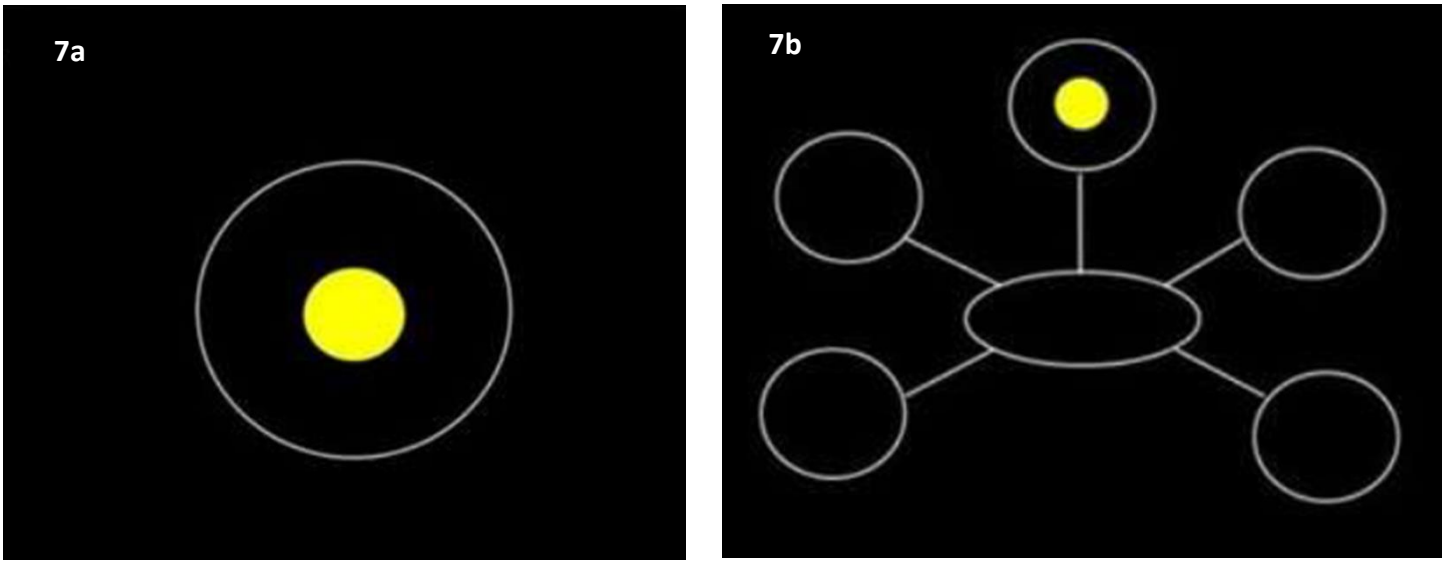

Figure 7a: Cambridge Neuropsychological Test Automated Battery – Simple reaction time task.
Figure 7b: Cambridge Neuropsychological Test Automated Battery – Choice reaction time task.

3.4.3 Structural and DTI imaging

3.4.3.1 Image acquisition

This study's DTI data were acquired from the parent study's MRI data. A 3 Tesla Skyra MRI scanner (Siemens, Erlangen, Germany) was used to image participants at the Cape Universities Body Imaging Centre (CUBIC) at the University of Cape Town. Structural T1-weighted (T1w) images were acquired using a multi-echo magnetisation prepared rapid gradient echo (MEMPRAGE) sequence (van der Kouwe *et al.*, 2008) (voxel size = 1.0 × 1.0 × 1.0 mm^3, FOV = 224 × 224 × 176 mm^3, TR = 2530 ms, TI = 1100 ms, TEs = 1.69/3.54/5.39/7.24 ms, flip angle = 7°) and two diffusion-weighted (DW) sets with opposite phase encodings (here, anterior-posterior and posterior-anterior, AP-PA) using a spin-echo sequence (voxel size = 2.0 × 2.0 × 2.0 mm^3, FOV = 244 × 244 × 148 mm^3, TR/TE = 9800/92 ms, 30 non-collinear gradient directions with DW factor b = 1000 s mm^{-2}, and five non-DW b = 0 s mm^{-2} (b_0) acquisitions).

3.4.3.2 Image processing

Structural and DW images were pre-processed using the Analysis of Functional Neuroimages (AFNI) toolbox (Cox, 1996), and software packages namely Freesurfer (Freesurfer, v6.0.1) and the Tolerably Obsessive Registration and Tensor Optimization Indolent Software

Ensemble (TORTOISE, v3.1.4) (Pierpaoli and Walker, 2010). The processing pipeline included the following steps *(Figure 9)*:

a. Conversion of raw DICOM (structural and DW) images to NIfTI format using the dcm2niix_afni tool;
b. Skullstripping and GM segmentation of structural dataset;
c. T1w images that were acquired during scanning were converted to T2-weighted (T2w)-like anatomical images using AFNI's *fat_proc_imit2w_from_t1w* function;
d. All the diffusion-weighted images went through manual visual inspection and the distorted volumes were discarded;
e. DWI artefacts, e.g., motion, EPI distortion and eddy current distortion correction, were corrected by applying TORTOISE's *DIFFPREP* function using each participant's T2w anatomical image;
f. TORTOISE's *DRBUDDI* function was used for the correction of DWI distortion as well as co-registration and merging of the remaining anterior-posterior (AP) and posterior-anterior (PA) DW volumes, to form a final DW set of volumes;
g. Diffusion parameters and tensors, including all 3 eigenvectors (L1, L2, and L3) and 3 of their eigenvalues (V1, V2, V3), FA, MD, AxD and RD, were estimated using AFNI's *fat_proc_dwi_to_dt* function;
h. Before tractography, the data of each participant was flipped in the z-direction, i.e., gradient flipping.
i. Structural images (T1w) and the corresponding parcellations were warped to DW space and co-registered to the DW images;
j. Full-probabilistic DTI tractography was performed with AFNI's Functional And Tractographic Connectivity Analysis Toolbox (FATCAT) (Taylor and Saad, 2013) using GM seeds identified in step b (More details in *Tractography section*).

Note to step b.: In this step, GM regions were identified through parcellation using the Connectome Mapper (CMP) 3 (v3.0.0-RC4), which is part of the Connectome Mapping Toolkit (CMTK) and is an open-source MRI processing pipeline that utilises raw T1-weighted, T2-weighted, diffusion or blood oxygen level-dependent (BOLD) data to map structural and

functional connectivity matrices (Daducci *et al.*, 2012). This software includes a tool, known as the Multi-Scale Brain Parcellator, that uses a 5-scale brain grey matter parcellation (Cammoun *et al.*, 2012), and is obtained from the Desikan-Killiany atlas (Desikan *et al.*, 2006), with added on new structures to create the final parcellation at each scale. These new structures include 4 sub-structures of the brainstem (Iglesias, Van Leemput, *et al.*, 2015), the thalamus subdivided into 7 nuclei (Najdenovska *et al.*, 2018) and the hippocampus sectioned into 12 segments (Iglesias, Augustinack, *et al.*, 2015). For this study, we chose the Lausanne 2018 scale 1 (Daducci *et al.*, 2012) which consists of 126 regions of interest (ROI) *(Supplementary Table 2)*. Therefore, the brain of each participant was parcellated into 126 ROIs of the Lausanne 2018 scale 1 segmentation and an individual 126 × 126 structural connectivity matrix was built for each of these participants.

For the purpose of graph-theoretical analysis, the GM regions produced at this step were interpreted as graph nodes and at the same time were used as seeds in full-probabilistic DTI tractography to characterise the WM tracts - or graph edges - connecting the nodes.

Note to step c.: DW volumes that were distorted because of motion and signal drop-out caused by EPI field distortion were removed from both AP and PA data sets.

Note to step d.: Participants were eligible for further processing if they had more than 15 diffusion volumes, i.e., not less than 50% of the DWI volumes and had at least one b_0 volume.

Note to step f.: *DIFFPREP* had to be done before *DRBUDDI* as *DRBUDDI* uses *DIFFPREP's* output to perform motion and eddy current distortion as well as EPI distortions.

Note to step g.: The three eigenvectors are not completely orthogonal to each other and thus uncertainty and errors arise. Therefore, a file that contained data about the uncertainty of the DT parameters were also part of the output at this step created by the *3dDWUncert.* The *3dDWUncert* function calculates the bias and standard deviation (SD) using V2 and V3 as the reference as well as the bias and SD of FA.

Note to step h.: Sometimes, there may be a systematic sign change in the recorded gradient components when gradients are stored in DICOMs. This is a problem as a single component of each gradient will appear to have its sign flipped in the output file.

DWIs processed using TORTOISE v3.1.4 seem to require the signs of gradient components to be flipped in the z-directions before tractography. This sign change does not influence scalar parameters due to the symmetry properties of the diffusion tensor. However, this sign change will cause the eigenvectors to rotate, which is greatly evident in tractography (Taylor *et al.*, 2015) *(Figure 8)*.

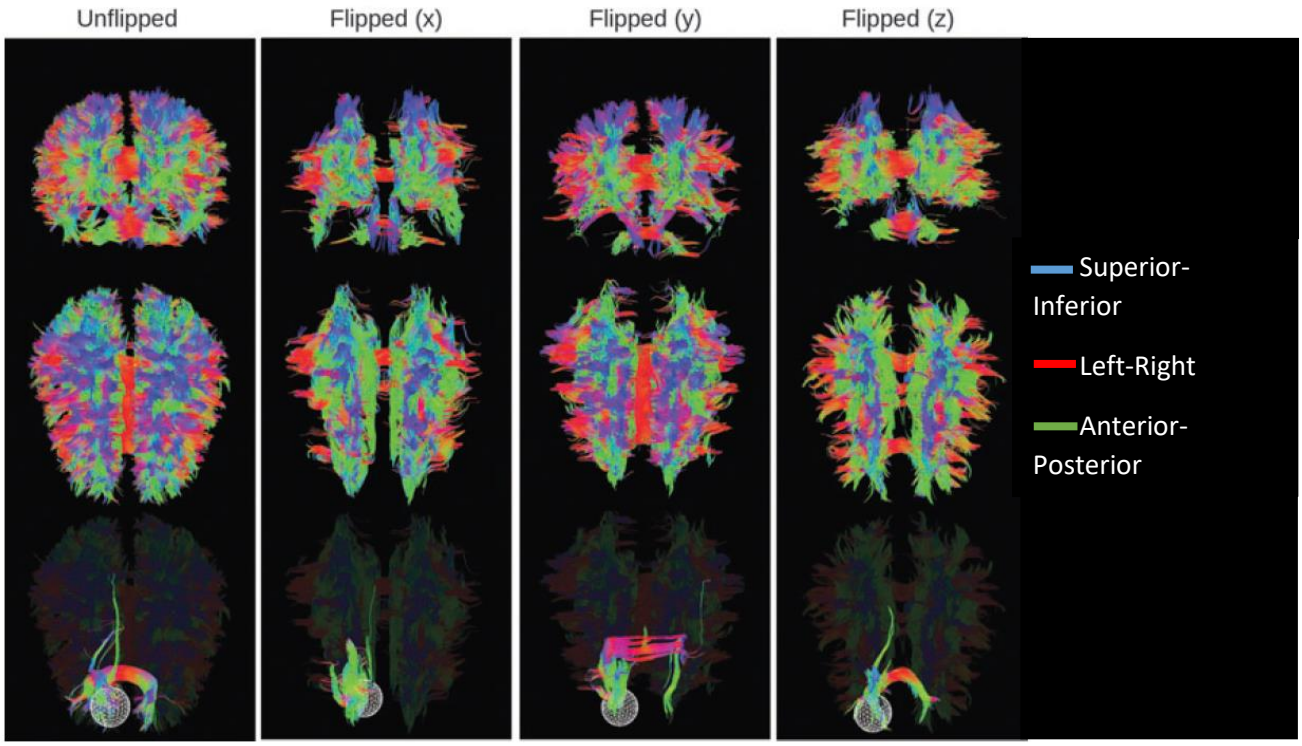

Figure 8: Sets of whole-brain tractographic reconstruction. Set of data, from the left, which has been properly flipped, and the next three sets in need of each potential kind of flip, i.e., x, y, and z (adapted from (Taylor et al., 2015)).

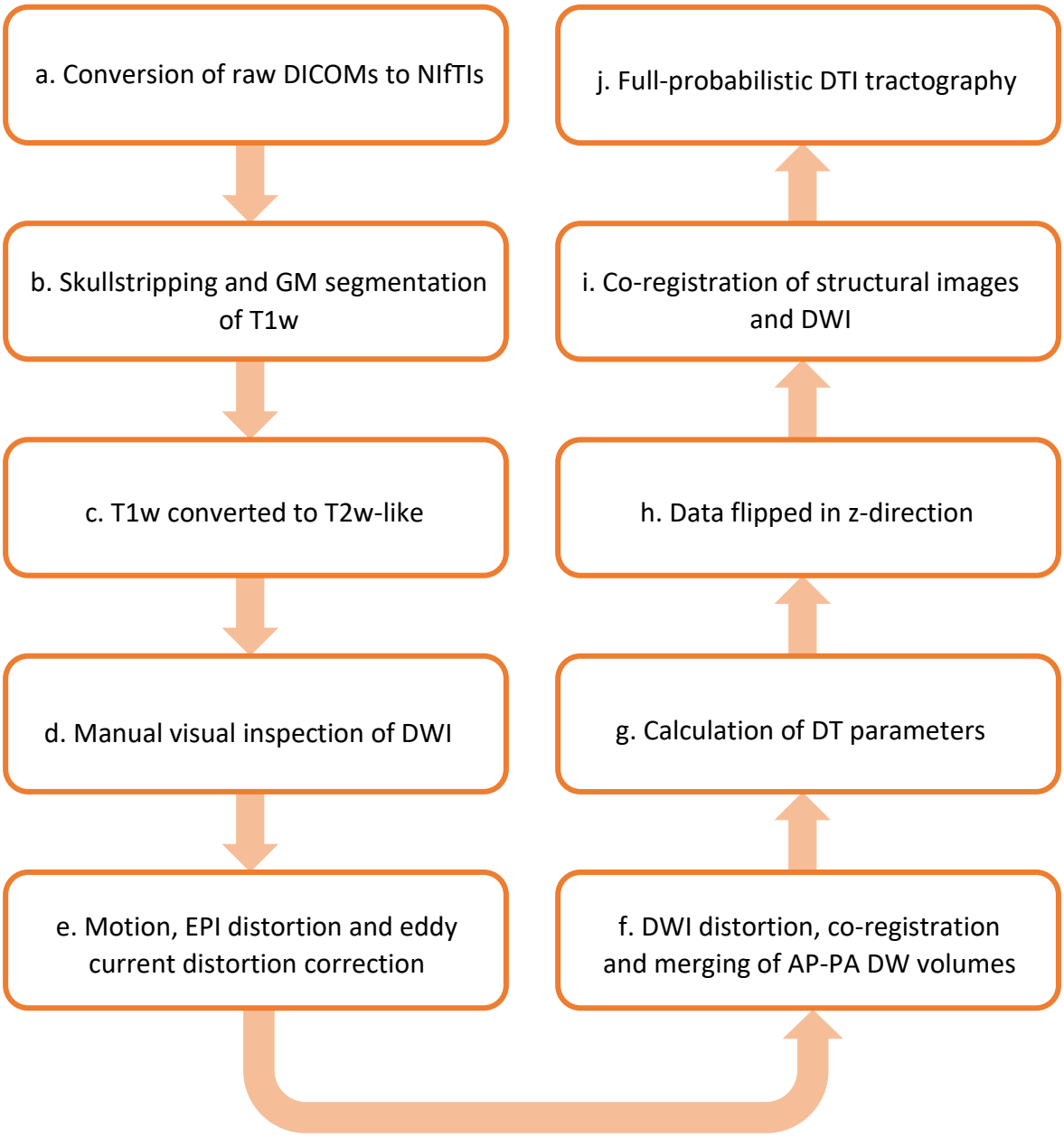

Figure 9: Image processing pipeline.

3.4.3.3 Tractography

Tractography is a technique used to estimate properties of WM tracts connecting pairs of seeds in a set of GM regions in the brain. DTI reveals WM tracts through 3-dimensional fibre tracking. Firstly, a certain number of seed points in a voxel is selected (Descoteaux, Deriche and Anwander, 2007). Subsequently, from the estimated diffusion tensors, paths taken by nerve fibres that connect functionally associated regions can be modelled using the principal axis of diffusion (axonal diffusivity) in each voxel, forming tracts. This allows for an in-vivo

reconstruction of the fibre bundles (Christidi *et al.*, 2016). From voxel to voxel, tracts will propagate according to the axonal diffusivity direction in each voxel. Propagation persists until one of the tracking threshold parameters is reached, i.e., the tract possibly does not pass through that specific voxel. The tracking threshold parameters in this study included: (1) a turning angle > 60˚ so that the propagation of the tract does not make a U-turn, (2) A minimum of 0.2 for FA as to only include WM in the analysis (Mori and Van Zijl, 2002) and not e.g., grey matter (GM) or cerebrospinal fluid (CSF) (Feldman *et al.*, 2010) and (3) tract length < 20mm to ensure that the propagated WM bundle is a tract.

In this project, full-probabilistic tractography was performed using AFNI's FATCAT (Taylor and Saad, 2013), which uses repeated iterations of whole-brain tracking to estimate the probability of structural WM connections between all pairs of seed regions. FATCAT uses the algorithm called "fibre assessment by continuous tracking including diagonals (FACTID)". The command *3dTrackID* estimates the locations of WM associated with the seeds and is able to run in three different modes, namely deterministic, mini-probabilistic and full-probabilistic. When tracts cross within a voxel and consequently the AxD direction does not signify the initial tract that was tracked, problems may arise (Feldman *et al.*, 2010). Full-probabilistic, which is what was used in this study to perform whole-brain tractography on the parcellated brain, considers all possible directions of a tract to prevent this problem (Descoteaux, Deriche and Anwander, 2007). After the seed point is chosen in the voxel, a random angle and direction are then selected for the tract to propagate while taking into consideration the uncertainty of that direction. The *3dDWUncert* function is used before *3dTrackID* to produce an uncertainty information file and is utilised as the input for *3dTrackID* to estimate the uncertainty in diffusion tensor eigenvectors and the tensor fitted data for each participant. The function *3dTrackID* uses each participant's own diffusion data and uses repeated iterations of whole-brain tracking to estimate where the location of WM pathways, i.e., WM mask, most likely are between ROIs (Taylor *et al.*, 2012; Freedberg *et al.*, 2021). The tract propagates voxel to voxel until the tracking threshold parameters are reached. The tract then stops propagating and a different random angle and direction are selected also starting from the same initial seed point. As a result, a thousand iterations of tracts could possibly propagate from one single seed point. A group-level WM mask was generated by co-registering FA maps of each participant.

3dTrackID generates a '*.grid' file output that contains 126 × 126 matrices of output statistics for each participant. This file output includes the means and SD of parameter quantities (such as FA, MD, AxD, RD and BL) as well as the number (NT) and volume of tracts (PV) of tractographic connections between all pairs of nodes, i.e., GM ROIs (Taylor *et al.*, 2012; Freedberg *et al.*, 2021). Other measures from this output file include fNT, fNV and NV. Please refer to the *Supplementary material (Page 136* and *137* as well as *Supplementary Table 5, 6, 7* and *8)* for more information and results on these other DTI measures. This resulted in a single value for FA, MD, AxD, RD, BL, NT, PV, fNT, fNV and NV for each viable pathway for each participant. For each DTI measure, tracts were considered outliers using the criteria $Q_L - 1.5\ (IQR) < DTI\ parameter\ value < Q_U + 1.5\ (IQR)$ and were removed.

Mini-probabilistic tractography (Taylor *et al.*, 2015) is a combination of deterministic and full-probabilistic tractography as it is comprised of multiple seed points per voxel with fewer iterations. For the analyses in this study, we used the full-probabilistic tractography's output for our statistical analyses and mini-probabilistic tractography for presentation as the output from full-tractography cannot be visualised. *Figure 10* shows an example of whole-brain tractography results in a randomly selected control participant.

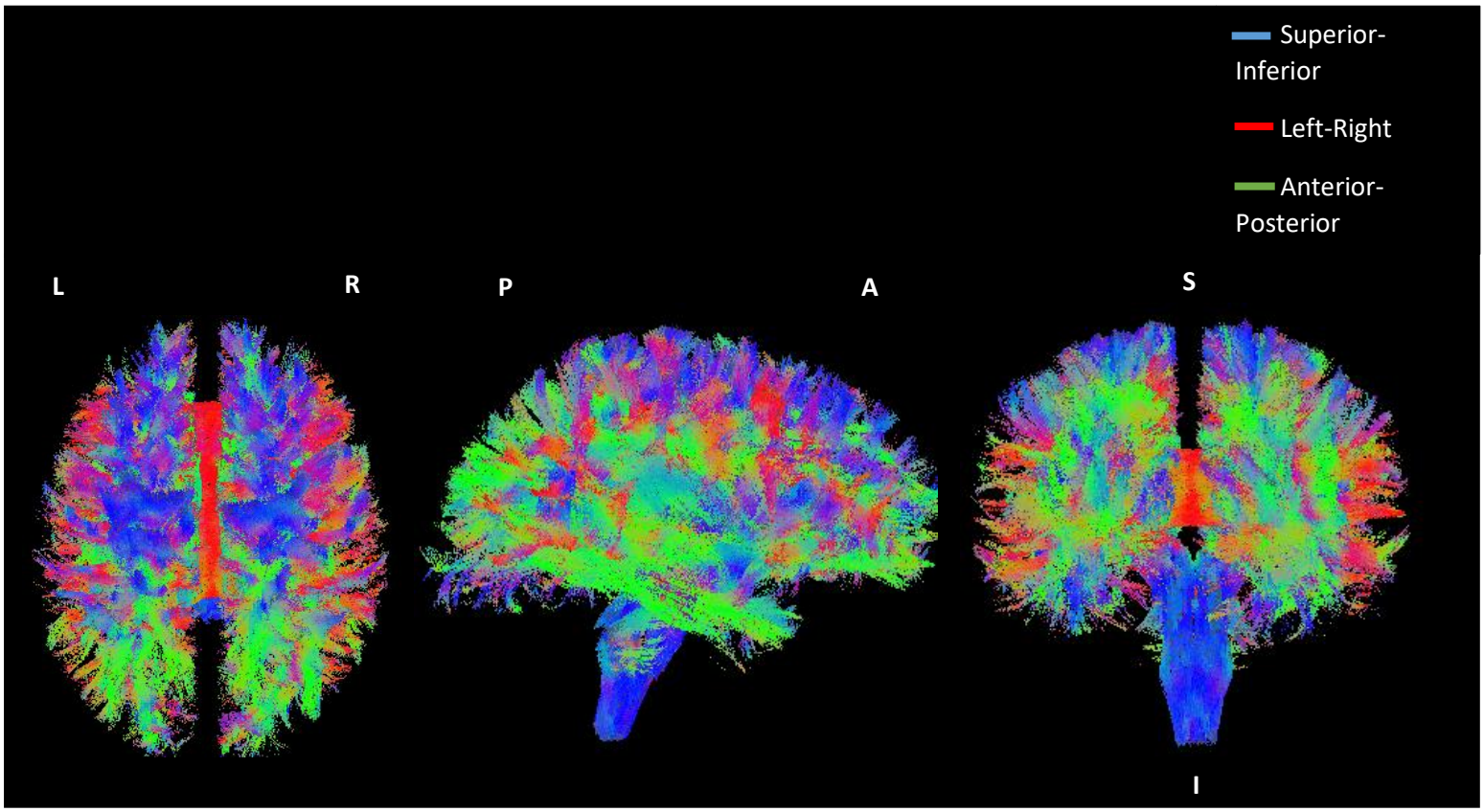

Figure 10: Whole-brain tractography. The different colours represent the direction of the white matter tracts: red = transverse tracts; green = anterioroposterior tracts; blue: craniocaudal fibres.

After tractography, we found that 110 regions had tracts that were common among all the participants, so for the rest of the analyses after tractography, 110 nodes/ROIs were used, i.e., 16 regions were excluded from the original 126 ROIs.

3.4.3.4 Graph theory

ROIs were identified, extracted and imported into R (v3.6.2). A graph-theoretical framework was applied to analyse the local and global topological features, such as global, local and nodal efficiency, nodal strength, transitivity, modularity, and nodal degree, of structural networks in AD patients and healthy elderly controls.

We calculated graph metrics using the *igraph* (v3.6.2) and *brainGraph* brain network analysis packages in R. The nodes of the graph were identified using the CMP parcellation scheme and the graphs' edges were identified through full-probabilistic tractography in FATCAT.

In our analyses, we used the measures from the output of tractography as the anatomical pairwise connectivity between nodes. Pairwise fNT values were used to generate a 110 × 110 adjacency matrix (110 regions identified after tractography), where the dimensions of this matrix were obtained from the 110 ROIs of the 126 ROIs from the Lausanne 2018 scale 1 segmentation, for each participant. fNT is defined as the probabilistic number of tracts between the nodes divided by the total number of probabilistic tracts in the whole brain (Tinaz *et al.*, 2017). The graphs generated are weighted graphs. *Figure 11* shows a flowchart of the imaging data processing.

For each graph theoretical measure, regions were considered outliers using the criteria $Q_L - 1.5\ (IQR) <$ graph theoretical measure $< Q_U + 1.5\ (IQR)$. For global efficiency and modularity, participants were considered outliers using the criteria $Q_L - 1.5\ (IQR) <$ graph theoretical measure $< Q_U + 1.5\ (IQR)$ and were removed. Outliers were removed if they were found to be influential.

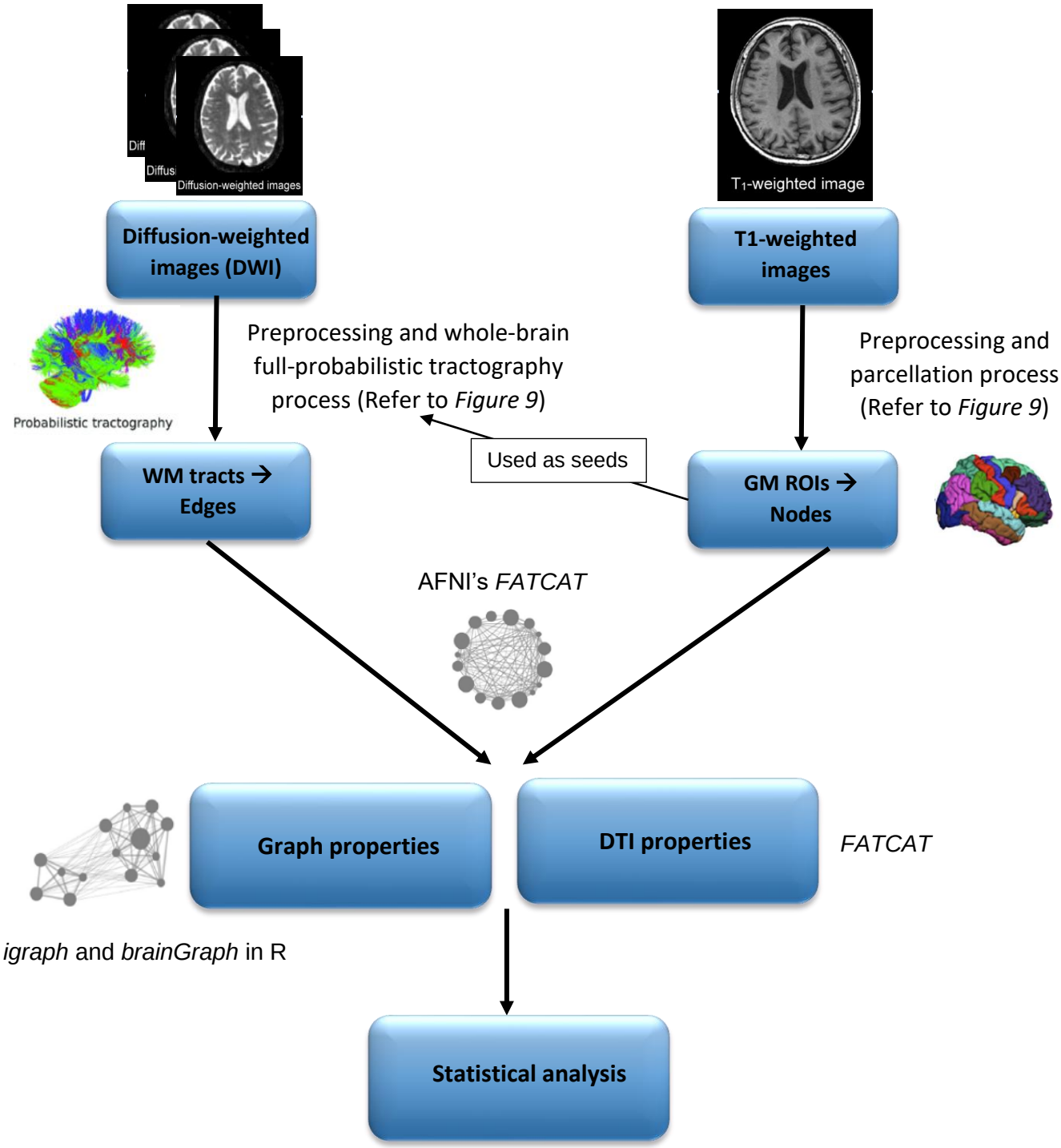

Figure 11: Flowchart of imaging data processing.

3.5 Statistical analyses

All IIV scores statistical analyses were conducted in SPSS (v28.0) and all imaging statistical analyses were performed in R (v3.6.2).

3.5.1 IIV data preparation

3.5.1.1 Filtering of RT data

We followed the filtering approach described by Hultsch and colleagues (2000, 2002, 2008). The RT data were filtered by removing outliers in the data because extremely slow or fast responses caused by, for example, interruption, fast guesses, or temporary distraction, may represent inaccurate performance and incorrect results.

Responses were considered as outliers and were removed if they were either (1) less than the lower limit of 150 milliseconds (ms) or (2) greater than an upper limit of 3 standard deviations (SD) above the mean of each testing block, calculated separately for the AD patients and healthy elderly controls. This limit criterion is consistent with other RT IIV studies (Hultsch *et al.*, 2000; Bielak *et al.*, 2010; Garrett, MacDonald and Craik, 2012). The lower limit is set based on the finding from a study by Thorpe, Fize and Marlot (1996), where they reported that the average adult takes about 150 ms to assess visual stimuli and respond. Thus, any responses below 150 ms were considered to have not gone through any decision-making processes.

Values that were identified as outliers and missing data, due to invalid responses, were filled in using a regression-based multiple imputations method (Lachaud and Renaud, 2011) in SPSS. This method allows for the uncertainty of the missing data by generating multiple different duplicates of the dataset, with the missing values replaced by imputed values, and combines the results obtained from each of these datasets (Huque *et al.*, 2018). Multiple imputations can present conservative estimates of performance variability (Hultsch, MacDonald and Dixon, 2002) whereas, if directly substituting the outliers and missing values with the mean values of the block, unavoidably reduce variability and lead to bias. In this study, we selected the “Mersenne Twister” random generator and set the starting point at 2 000 000. Only the trials from its specific block were used as predictors for each block of both tasks. SPSS then ran five imputations and the average value was calculated across the five imputations for each of the outliers and missing values. The missing values are then substituted by the average values that were calculated.

3.5.1.2 Extracting and calculating IIV

In this study, we drew on the work by Hultsch *et al*. (2000, 2002, 2008). To capture IIV scores, we first needed to remove systematic effects, such as time-on-task effects (e.g., test order, RT trials, etc.) and group effects (e.g., group status, age, education, etc.) from the RT data. Raw SDs is associated with mean RT, thus systematic effects may arise as there is a strong negative relationship between mean RTs and SDs (Hale *et al.*, 1988; Hultsch *et al.*, 2008). Therefore, it is crucial to partial out any factors that may have an impact on the mean RT performance before computing intra-individual standard deviation (*iSD*), i.e., the variance that can be explained by within-person variability alone.

To partial out these effects, a mixed-effect random intercept model was run on each of the SRT and CRT datasets with either SRT or CRT latency as the outcome variable. A random intercept model is able to fit one trendline/intercept for each participant, i.e., repeated measures of each individual, instead of only one trendline for all data like in a general linear model, and thus improves the fit to data. Main effects were added to one model: (1) interval, blocks, trials, and test order to determine the impact of time-on-task effects and (2) monthly household income, group status, age, years of education and sex to determine the influence of group effects. These were added as fixed effects in the models to test whether any of the time-on-task variables (trials, blocks, sessions, test-order) or group variables (monthly household income, group status, age, years of education, sex) had an effect on the dependent variable, i.e., reaction time.

$$Y_{ij} = \mathrm{B}_{0j} + \mathrm{B}_{1j}X_{1ij} + \mathrm{B}_{2j}X_{2ij} + \mathrm{B}_{3j}X_{3ij} + \mathrm{B}_{4j}X_{4ij} + \mathrm{B}_{5j}X_{5ij} + \mathrm{B}_{6j}X_{6ij} + \mathrm{B}_{7j}X_{7ij} + \mathrm{B}_{8j}X_{8ij} + \mathrm{B}_{9j}X_{9ij} + u_{0j} + e_{ij}$$

Where Y_{ij} = Reaction time (Simple or Choice) for the *j*-th individual in the *i*-th group, B_{0j} = Intercept, B_{nj} = Coefficients, X_{1ij} = Trials, X_{2ij} = Blocks, X_{3ij} = Sessions, X_{4ij} = Test Order, X_{5ij} = Monthly Household Income, X_{6ij} = Group, X_{7ij} = Age in years, X_{8ij} = Education in years, X_{9ij} = Sex, u_{0j} = Random effect term for intercept B_{0j}, e_{ij} = Error term

In this study, we identified group, interval, sessions, and blocks as fixed effects that contributed significantly to SRT latency in the first mixed-effects random intercept model. The second mixed-effects random intercept model identified sex, group, test order, interval, trials, sessions and blocks as fixed effects that significantly contributed to CRT latency.

We then added all these significant fixed effects identified by the two models as predictors together in one random slope model for each of the SRT and CRT datasets. This model was a maximum effects model where we exhausted all the variables and their high order interactions with one another. A random slope model has one intercept for each individual and varies according to the slope of each individual. The slope is the degree by which the data correlates, i.e., degree by which the predictor correlates with the outcome. In this way, it not only predicts but also allows to vary according to the strength of the prediction, thus adding a greater level of sensitivity.

In this study, the random slopes model included a random term for trials to allow each subject's intercept to vary its slope across trials as we were interested in explaining all the systematic variance, i.e., the effect of the mean, that could account for RT performance over time, i.e., the performance across trials. This represents the change over time for each individual. In order to add a random term to a variable, that variable must be added as a fixed effect in order to add a random term to it.

SRT:

$$Y_{ij} = \mathrm{B}_{0j} + \mathrm{B}_{1j}X_{1ij} + \mathrm{B}_{2j}X_{2ij} + \mathrm{B}_{3j}X_{3ij} + \mathrm{B}_{4j}X_{4ij} + \mathrm{B}_{5j}X_{5ij} + u_{0j} + u_{1j}X_{1ij} + e_{ij}$$

Where Y_{ij} = Simple reaction time for the *j*-th individual in the *i*-th group, B_{0j} = Intercept, B_{nj} = Coefficients, X_{1ij} = Trials, X_{2ij} = Interval, X_{3ij} = Sessions, X_{4ij} = Blocks, X_{5ij} = Group, u_{0j} = Random effect term for intercept B_{0j}, u_{1j} = Random term to the coefficient of X_{1ij}, e_{ij} = Error term

CRT:

$$Y_{ij} = \mathrm{B}_{0j} + \mathrm{B}_{1j}X_{1ij} + \mathrm{B}_{2j}X_{2ij} + \mathrm{B}_{3j}X_{3ij} + \mathrm{B}_{4j}X_{4ij} + \mathrm{B}_{5j}X_{5ij} + \mathrm{B}_{6j}X_{6ij} + \mathrm{B}_{7j}X_{7ij} + u_{0j} + u_{1j}X_{1ij} + e_{ij}$$

Where Y_{ij} = Choice reaction time for the *j*-th individual in the *i*-th group, B_{0j} = Intercept, B_{nj} = Coefficients, X_{1ij} = Trials, X_{2ij} = Sex, X_{3ij} = Group, X_{4ij} = Test Order, X_{5ij} = Interval, X_{6ij} = Sessions, X_{7ij} = Blocks, u_{0j} = Random effect term for intercept B_{0j}, u_{1j} = Random term to the coefficient of X_{1ij}, e_{ij} = Error term

The residuals, which are the unexplained variance in the dataset, from these analyses were then captured and transformed into standardised scores, i.e., z-scores. Subsequently, these z-scores were transformed into t-scores with the equation: T-scores = (Z-scores × 10) + 50. It is convention in IIV research to convert the residuals to t-scores in order to standardise the

data, which allows for cross-study comparisons of IIV scores. This method is consistent with other IIV studies (Hultsch *et al.*, 2000; Hultsch, MacDonald and Dixon, 2002). As a final step, the SD was calculated across the t-scores (n = 180) of each participant for the two tasks. This was determined as the overall *iSD* for each participant for each task.

3.5.2 Inferential statistical analysis

All inferential statistical analyses were done in R (v3.6.2).

3.5.2.1 Between-group differences

Differences between groups in demographic variables (e.g., years of education, age) and cognitive performance (neuropsychological scores: CAMCOG-R and MMSE scores, IIV scores: *iSD* SRT and CRT values as well as mean SRT and CRT values) were analysed using a two-sample t-test if the continuous numerical data were normally distributed or the Mann-Whitney U test if the continuous numerical were not normally distributed. Sex and monthly household income data were observed with the Chi-squared test. These analyses were done in R (v3.6.2).

To evaluate differences between groups for DTI measures and in graph metrics, comparisons were performed using the Bayesian multilevel (BML) modelling applied to a Region-Based Analysis (RBA) (Chen *et al.*, 2019) in AFNI. With this integrative approach, data from all 110 ROIs (110 regions identified after tractography) were included simultaneously in a single multilevel model and the effects of interest were evaluated (Lima Portugal *et al.*, 2020). The null hypothesis significance testing (NHST) framework has gained increased scepticism over the years, specifically, the threshold of 0.05 has become a debatable topic with some researchers believing that the threshold is not strict enough (Benjamin *et al.*, 2018) or for the use of p-values to be discarded completely (McShane *et al.*, 2019). The BML framework looks at the probability of the effect being positive or negative. In other words, it does not consider a binary threshold, i.e., either “significant” or “not significant”, but rather in a graded fashion, to assess statistical evidence (Chen *et al.*, 2020). This method estimates the probability of the research hypothesis (H) with the given data, $P(H|\text{data})$. BML summarises effect inference through its entire probability density distribution, called the posterior density distribution (Chen *et al.*, 2020). This distribution is associated with

P(θ|data), where θ is the parameter being estimated. Such a probability can be calculated by using Bayes' rule (Kruschke, 2010).

The output of RBA gives the posterior distribution which quantifies a value known as posterior probability (P+), which is essentially the area under the curve, and also the probability of the effect being positive. For example, for P(θ > 0 | data), P+ is the area under the curve above 0 (Limbachia *et al.*, 2021). We could also look at the posterior distribution with "tail probabilities" *(Figure 12)*, which represents two-sided 90% and 95% uncertainty intervals. If the P+ values are closer to 1, the effect of interest, such as the means and the difference in means, is > 0 and conversely, P+ values closer to 0 shows the negative effect (Limbachia *et al.*, 2021). Thus, if the P+ values equal 0.01, the probability of the effect being positive is only 0.01 with the probability of the effect being negative is 0.99 (Limbachia *et al.*, 2021).

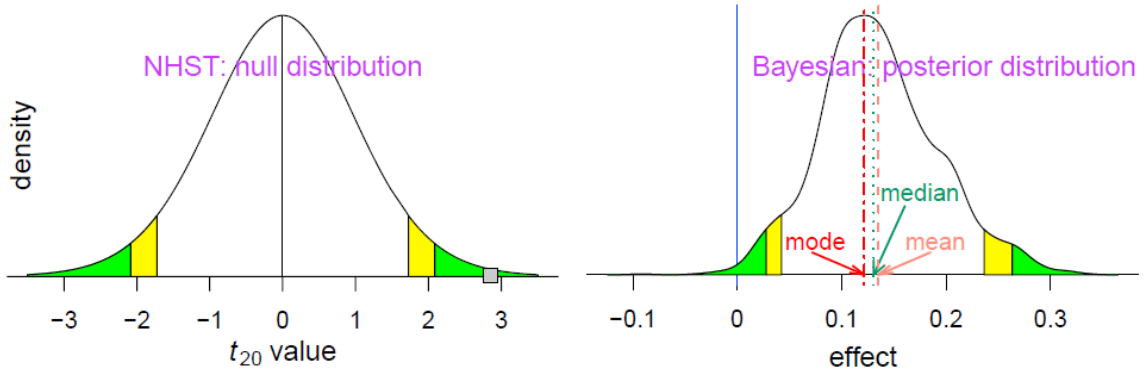

Figure 12: Different probability definitions and focus between the conventional and Bayesian frameworks (adapted from (Chen et al., 2020)).

Figure 12 above (Chen *et al.*, 2020) shows the difference between the NHST and the Bayesian framework. For the NHST (left curve), the green or yellow tails symbolises a two-sided significance level of 0.05 or 0.1. If a t_{20} value falls in one of these tails, one may say that there is strong evidence for the effect. For the Bayesian framework (right curve), the blue line represents the "zero effect" so to the right of this blue line is anything above 0, i.e., the effect is positive. Anything to the left of this blue line is less than 0, i.e., the effect is negative. As we can see in this diagram *(Figure 12)*, the area under the curve to the right of the blue line is much bigger (about 99%), meaning that the P+ value is probably about 0.99. On the other hand, if the P+ value is equal to 0.01, the probability of the effect being positive is only 0.01 with the probability of the effect being negative is 0.99 (the blue line

would then be on the other side). There are some differences between the two densities in *Figure 12* above: (1) The x-axes are not the same, (2) due to the assumption of a standard curve, the shape of the null distribution under NHST is smooth and regular, whereas the shape of the posterior distribution under the Bayesian framework is irregular from the random samples through Markov chain Monte Carlo simulations and (3) the posterior density of the Bayesian framework provides more information such as the shape, spread and skewness compared to the confidence interval presented by NHST.

One of the advantages of this approach is that correction for multiple comparisons is not required as only one model is employed and data regarding the effect in one region is shared across all the regions (technically via "partial pooling") through the assumption that there is a normal distribution of ROI contributions (Lima Portugal *et al.*, 2020; Limbachia *et al.*, 2021). Posteriors of the effects for every region can be plotted individually (Lima Portugal *et al.*, 2020; Limbachia *et al.*, 2021). The Bayesian multilevel model produces an output that consists of only one overall posterior that is generated as a joint distribution in high-dimensional parameter space, where the dimensionality is the number of parameters in the model (Chen *et al.*, 2020). Conversely, for the standard testing approach, correction for multiple comparisons is required as the effect in each region is assessed independently from other regions, i.e., no data is shared between the regions (Lima Portugal *et al.*, 2020; Limbachia *et al.*, 2021).

The effects of sex, age, years of education and monthly household income were adjusted for all these analyses. Age and years of education were entered as covariates due to significant group differences in our sample, and sex and household income were included because of results reported by previous studies (Kidron *et al.*, 1997; Karp *et al.*, 2004; Carter *et al.*, 2012; Sattler *et al.*, 2012; Andrew and Tierney, 2018; Cavedo *et al.*, 2018; Deckers *et al.*, 2019). Age and years of education were standardised. For the RBA analyses, P+ values that were between 0.025 and 0.05 or between 0.95 and 0.975 were considered to have strong evidence supporting group differences. Very strong evidence supporting group differences were represented by P+ values that were smaller than 0.025 or larger than 0.975.

We also had an additional general linear model that included all the above covariates as well as the interactions between these variables and group, i.e., group: sex, group: age, group:

education, group: household income, to see whether there were any significant interactions to include in the final model.

$$Y = \beta_0 + \beta_1 X_1 + \beta_2 X_2 + \beta_3 X_3 + \beta_4 X_4 + \beta_5 X_5 + \beta_6 X_1 X_2 + \beta_7 X_1 X_3 + \beta_8 X_1 X_4 + \beta_9 X_1 X_5 + \varepsilon$$

Where Y = DTI measure, β_0 = Intercept, β_n = Coefficients, X_1 = Group, X_2 = Age in years (standardised), X_3 = Sex, X_4 = Education in years (standardised), X_5 = Monthly Household Income, ε = Error term

Refer to *Supplementary material Section A* for RBA scripts of final models for DTI measures and graph theory measures.

A multiple regression model was used to investigate whether group predicted global efficiency and modularity while controlling for sex, age, years of education and monthly household income. Results were considered statistically significant if $p \leq 0.05$.

$$Y = \beta_0 + \beta_1 X_1 + \beta_2 X_2 + \beta_3 X_3 + \beta_4 X_4 + \beta_5 X_5 + \varepsilon$$

Where Y = Global Efficiency/Modularity, β_0 = Intercept, β_n = Coefficients, X_1 = Group, X_2 = Age in years (standardised), X_3 = Sex, X_4 = Education in years (standardised), X_5 = Monthly Household Income, ε = Error term

3.5.2.2 Relationship between network metrics and IIV scores

We then investigated the relationship between network metrics and RT IIV, i.e., *iSD*, in both groups separately. Lastly, we investigated the relationship between network metrics and mean RT of the two tasks in both groups separately. Multiple regression models controlling for the effects of sex, age, years of education and monthly household income were conducted. Results were considered statistically significant if $p \leq 0.05$.

$$Y = \beta_0 + \beta_1 X_1 + \beta_2 X_2 + \beta_3 X_3 + \beta_4 X_4 + \beta_5 X_5 + \varepsilon$$

Where Y = Graph theory measure, X_1 = iSD or mean reaction time (For both SRT and CRT), X_2 = Age in years (standardised), X_3 = Sex, X_4 = Education in years (standardised), X_5 = Monthly Household Income

4. Results

Sample characteristics

The final statistical analyses consisted of data from 20 (14 women) healthy elderly controls and 16 (12 women) AD patients *(Table 2)*. Six healthy elderly controls were excluded as:

(a) Segmentation failed for 5 individuals' structural images;

(b) 1 individual withdrew from the study before the imaging session.

Ten AD patients were excluded as:

(a) Segmentation failed for 5 individuals' structural images;

(b) 2 individuals had less than 15 diffusion volumes, i.e., less than 50% of the diffusion-weighted imaging (DWI) volumes, or did not have b_0 volumes due to motion artefacts;

(c) 1 individual had incomplete diffusion tensor imaging (DTI) acquisitions;

(d) 1 individual did not meet the eligibility criteria described above in *section 5.2*;

(e) 1 individual's tractography was of poor quality.

Analyses revealed no significant between-group differences in monthly household income, sex distribution and current depressive symptomatology (GDS). However, there were significant differences between the two groups in terms of age, where the patients were on average 2 years older than controls, and years of education, with the controls having completed more years of formal schooling. The controls also scored significantly higher in both CAMCOG-R outcome measures as well as the MMSE *(Table 2)*.

Table 2: Comparison of demographic and general cognitive functioning data between the two groups of the study sample.

Variable	**Group**			
	All	**Healthy elderly controls**	**Mild-to-moderate stage of possible or probable clinical AD[a]**	**p-value**
Sample size (N)	36	20	16	
Sex (F:M)	26:10	14:6	12:4	1
Age (years)[b] Median (IQR)	72.44 (69.02; 78.42)	70.13 (66.98; 76.31)	76.06 (72.59; 79.84)	**0.02***
Education (years)[c] Median (IQR)	10 (8; 14)	12 (10; 14)	8.5 (8; 10.25)	**0.01****

Household Income (%)[d]				
Level 1	0 (0)	0 (0)	0 (0)	
Level 2	1 (2.78)	1 (5)	0 (0)	
Level 3	4 (11.11)	3 (15)	1 (6.25)	0.19
Level 4	11 (30.56)	3 (15)	8 (50)	
Level 5	7 (19.44)	4 (20)	3 (18.75)	
Level 6	13 (36.11)	9 (45)	4 (25)	
GDS[e]				
Median (IQR)	5 (2.5; 7)	5.5 (1.75; 8)	5 (3; 6)	0.61
CAMCOG-R Total Score[e]				
Median (IQR)	86 (69; 93.5)	93 (90; 96.25)	68 (56.5; 72)	**< 0.001*** **
CAMCOG-R Memory Composite[e]				**< 0.001*** **
Median (IQR)	21 (10; 22)	22 (21; 24.25)	8 (6; 10.5)	
MMSE[e]				
Median (IQR)	27 (22; 29)	29 (27.75; 29.25)	21 (19.5; 24.5)	**< 0.001*** **

Key: AD, Alzheimer's Disease; IQR, Interquartile Range; GDS, Geriatric Depression Scale; CAMCOG-R, Cambridge Cognitive Examination for Mental Disorders of the Elderly-Revised; MMSE, Mini-Mental State Examination

Note: Numbers in parentheses represent the interquartile range when the median is presented and represent the percentage when quantity is presented.

[a]Diagnosed according to the NINCDS-ADRDA criteria (McKhann *et al.*, 1984).

[b]All participants were over the age of 55 years.

[c]Highest level of education attained.

[d]Monthly household income, categorised on a 1-6 scale, where 1 = ZAR 0 – 499, 2 = ZAR 500 – 999, 3 = ZAR 1000 – 2499, 4 = ZAR 2500 – 5499, 5 = ZAR 5500 – 9999 and 6 = ZAR 10000+.

[e]Missing data for 1 AD participant.

P-values represent group difference between healthy controls and AD patients, where p ≤ 0.05, **p < 0.01, ***p < 0.001.

4.1 Between-group differences in RT IIV and mean RT

Table 3: Comparison of RT IIV and mean RT data between the two groups of the study sample.

	Group				95% Confidence interval	
Variable	**Healthy elderly controls (N = 20)**	**Mild-to-moderate stage of possible or probable clinical AD[a] (N = 16)**	**t**	**p**	**Lower**	**Upper**
iSD[b]						
SRT	8.78 (1.61)	11.03 (2.34)	-3.42	**0.002****	-3.60	-0.92
CRT	9.08 (1.28)	10.82 (2.06)	-3.11	**0.004****	-2.88	-0.60
Mean RT[c]						
SRT	318.08 (33.37)	346.78 (53.93)	-1.96	0.06	-58.45	1.05
CRT	349.12 (32.71)	384.32 (53.85)	-2.60	**0.01****	-66.31	-8.10

Key: AD, Alzheimer's Disease; SRT, Simple Reaction Time task; CRT, Choice Reaction Time task; *iSD*, Intra-individual Standard Deviation; RT, Reaction Time.

Note: Means with standard deviations in parentheses are presented.

[a]Diagnosed according to the NINCDS-ADRDA criteria (McKhann *et al.*, 1984).

[b]*iSD* represents RT IIV.

[c]The mean reaction time is measured by averaging reaction time scores across 180 trials of task performance.

[bc]Measured in milliseconds.

*p ≤ 0.05, **p < 0.01, ***p < 0.001

There were significant between-group differences on both SRT and CRT tasks when it came to RT IIV, i.e., *iSD*. In both tasks, the AD patients presented with significantly higher RT IIV *(Table 3)*.

For mean RT, there was only a significant between-group difference on the CRT task, and not on the SRT task. However, in both tasks, the average response time of the AD patients was slower than that of the controls *(Table 3)*.

4.2 Between-group differences in DTI measures

After tractography, we found that 110 regions had tracts that were common among all the participants, so for the rest of the analyses, 110 nodes/ROIs were used, i.e., 16 regions were excluded from the original 126 ROIs *(Figure 13)*.

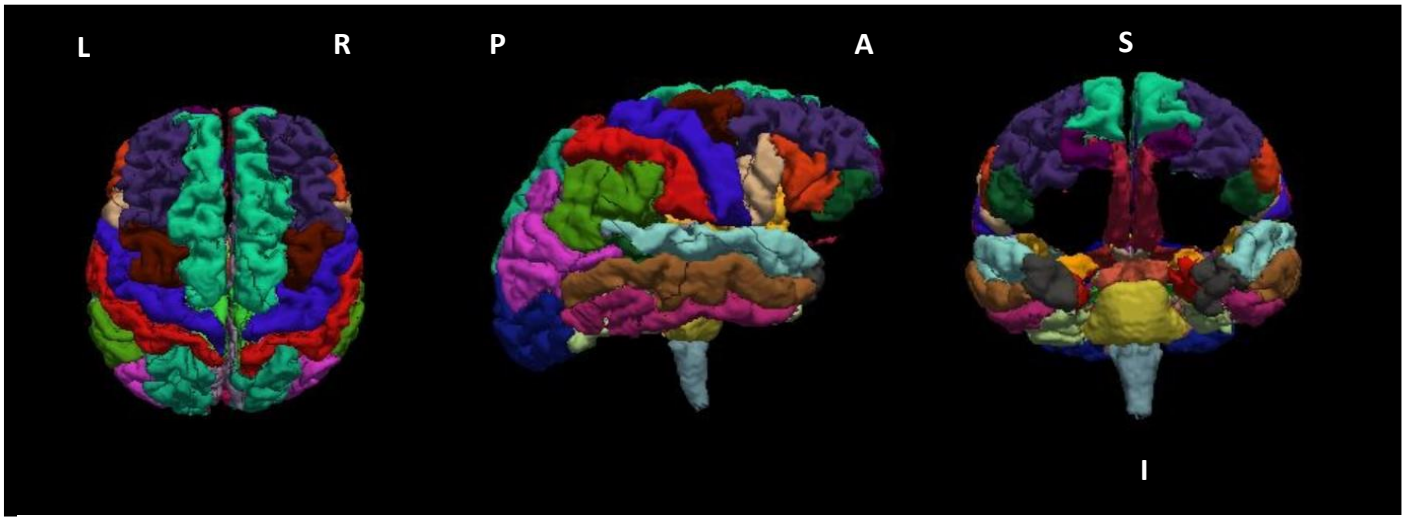

Figure 13: 110 ROIs included as seeds for DTI tractography and graph analysis. Different colours represent different seeds.

Refer to *Supplementary Figure 1* to find common connections across all participants in the sample with a total of 110 regions and 301 connections.

In the general linear model that included sex, age, years of education and monthly household income as covariates as well as the interactions between these variables and group, i.e., group:

sex, group: age, group: education, group: household income, we found that there were no statistically significant interactions after correcting for multiple comparisons. Thus, in the final model, we only included sex, age, years of education and monthly household income as covariates and did not include any interactions.

Table 4: Abbreviations with full names of the regions of interest and location of these regions.

Abbreviation	Full name	Location
lat-OF	Lateral Orbitofrontal Cortex	Cortical Frontal Lobe
ParsOrbitalis	Pars Orbitalis	Cortical Frontal Lobe
med-OF	Medial Orbitofrontal Cortex	Cortical Frontal Lobe
ParsTriangularis	Pars Triangularis	Cortical Frontal Lobe
ParsOpercularis	Pars Opercularis	Cortical Frontal Lobe
ros-mid-F	Rostral Middle Frontal Gyrus	Cortical Frontal Lobe
sup-F	Superior Frontal Gyrus	Cortical Frontal Lobe
caud-mid-F	Caudal Middle Frontal Gyrus	Cortical Frontal Lobe
Precentral	Precentral Gyrus	Cortical Frontal Lobe
Paracentral	Paracentral Lobule	Cortical Frontal Lobe
ros-ant-Cing	Rostral Anterior Cingulate Cortex	Cortical Cingulate Cortex
caud-ant-Cing	Caudal Anterior Cingulate Cortex	Cortical Cingulate Cortex
pos-Cing	Posterior Cingulate Cortex	Cortical Cingulate Cortex
isthmus-Cing	Isthmus of the Cingulate Gyrus	Cortical Cingulate Cortex
Postcentral	Postcentral Gyrus	Cortical Parietal Lobe
Supramarginal	Supramarginal Gyrus	Cortical Parietal Lobe
sup-P	Superior Parietal Lobule	Cortical Parietal Lobe
inf-P	Inferior Parietal Lobule	Cortical Parietal Lobe
Precuneus	Precuneus Cortex	Cortical Parietal Lobe
Cuneus	Cuneus Cortex	Cortical Occipital Lobe
Pericalcarine	Pericalcarine Cortex	Cortical Occipital Lobe
lat-Occ	Lateral Occipital Gyrus	Cortical Occipital Lobe
Lingual	Lingual Gyrus	Cortical Occipital Lobe
Fusiform	Fusiform Gyrus	Cortical Temporal Lobe
Parahippo	Parahippocampal Gyrus	Cortical Temporal Lobe
Entorhinal	Entorhinal Cortex	Cortical Temporal Lobe
Tpole	Temporal Pole	Cortical Temporal Lobe
inf-T	Inferior Temporal Gyrus	Cortical Temporal Lobe
mid-T	Middle Temporal Gyrus	Cortical Temporal Lobe
banks-sup-Tsulcus	Banks of the Superior Temporal Sulcus	Cortical Temporal Lobe
sup-T	Superior Temporal Gyrus	Cortical Temporal Lobe
trans-T	Transverse Temporal Gyrus	Cortical Temporal Lobe
Insula	Insula	Insula
Pulvinar	Pulvinar	Subcortical Thalamus
ant	Anterior Thalamus	Subcortical Thalamus
med-dors	Mediodorsal Thalamus	Subcortical Thalamus
vent-lat-dors	Ventral Latero-Dorsal Nucleus Thalamus	Subcortical Thalamus
cent-lat-lat-pos-med-Pulvinar	Central Lateral-Lateral Posterior-Medial Pulvinar	Subcortical Thalamus
vent-ant	Ventral Anterior Thalamus	Subcortical Thalamus

vent-lat-vent	Ventral Latero-Ventral Thalamus	Subcortical Thalamus
Caudate	Caudate Nucleus	Subcortical Basal Ganglia
Pu	Putamen	Subcortical Basal Ganglia
Pal	Pallidum	Subcortical Basal Ganglia
Acc-area	Nucleus Accumbens Area	Subcortical Basal Ganglia
Amygdala	Amygdala	Subcortical Temporal Lobe
Hippo	Hippocampus	Subcortical Temporal Lobe
Hippo-Presubiculum	Hippocampus Presubiculum	Subcortical Hippocampus Subregions (Subcortical Temporal Lobe)
Hippo-Subiculum	Hippocampus Subiculum	Subcortical Hippocampus Subregions (Subcortical Temporal Lobe)
Hippo-CA1	Hippocampus CA1	Subcortical Hippocampus Subregions (Subcortical Temporal Lobe)
Hippo-MolecularLayerHP	Hippocampus Molecular Layer HP Dentate Gyrus	Subcortical Hippocampus Subregions (Subcortical Temporal Lobe)
Hippo-Tail	Hippocampus Tail	Subcortical Hippocampus Subregions (Subcortical Temporal Lobe)
vent-DC	Ventral Diencephalon	Ventral Diencephalon
Hypothalamus	Hypothalamus	Hypothalamus (Diencephalon)
Brain-Stem-Midbrain	Brainstem Midbrain	Brainstem
Brain-Stem-Pons	Brainstem Pons	Brainstem
Brain-Stem-Medulla	Brainstem Medulla	Brainstem
Brain-Stem-SCP	Brainstem SCP	Brainstem

4.2.1 FA

Figure 14 shows connections with either very low or very high P+ values, i.e., strong to very strong evidence of group differences in FA, where low P+ means Controls > AD and high P+ means Controls < AD. *Figures 15, 16, 17* and *18* show the corresponding AxD and RD group differences for these connections. Refer to *Supplementary Table 3* for these results in table form.

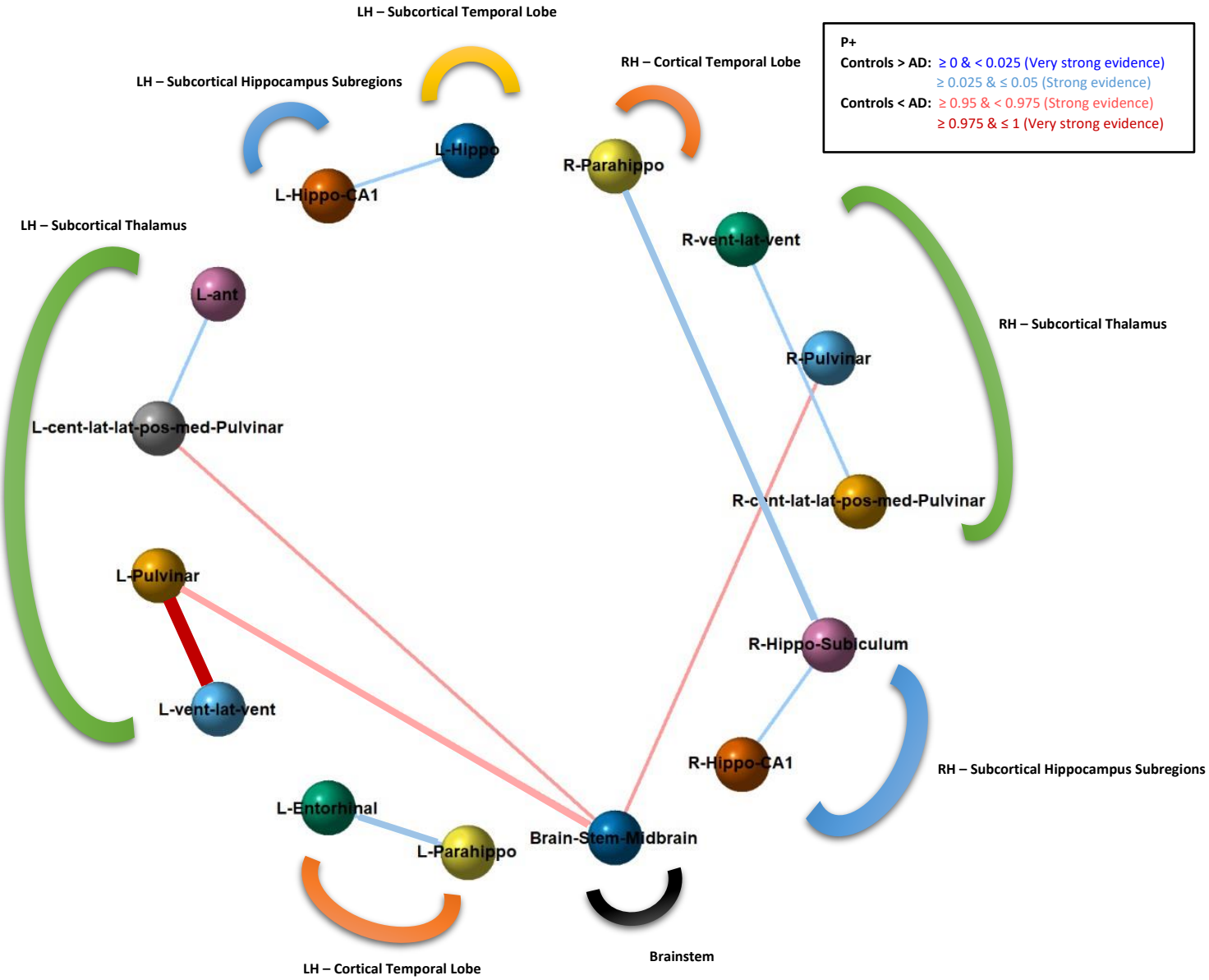

Figure 14: Connections that have either very low or very high P+ values for FA. Blue lines represent low P+ (Controls > AD), red lines represent high P+ (Controls < AD) in FA. Line thickness indicates strength of inter-regional relationships.

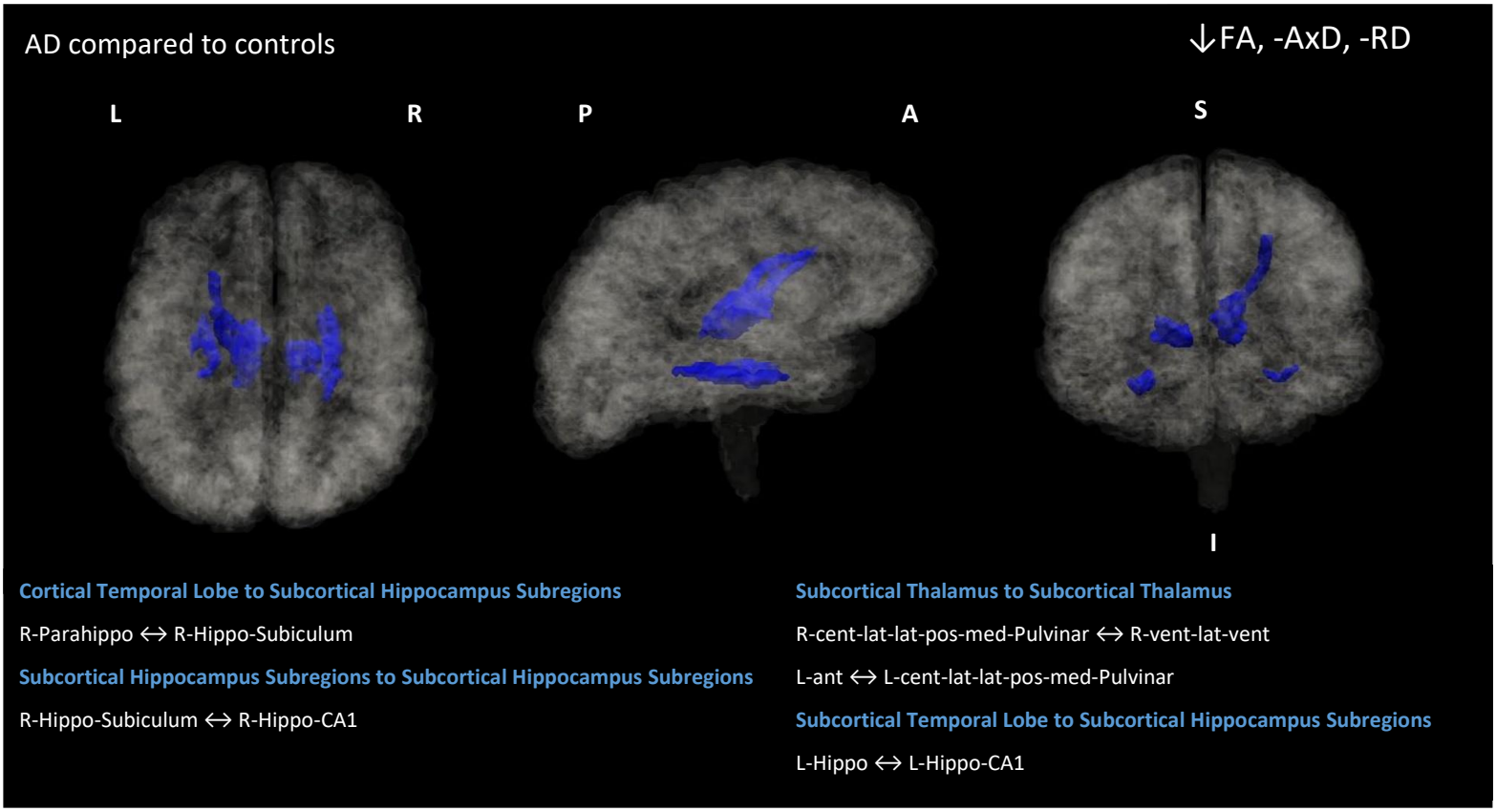

Figure 15: Connections that show lower FA with similar AxD and RD in AD patients compared to healthy elderly controls.

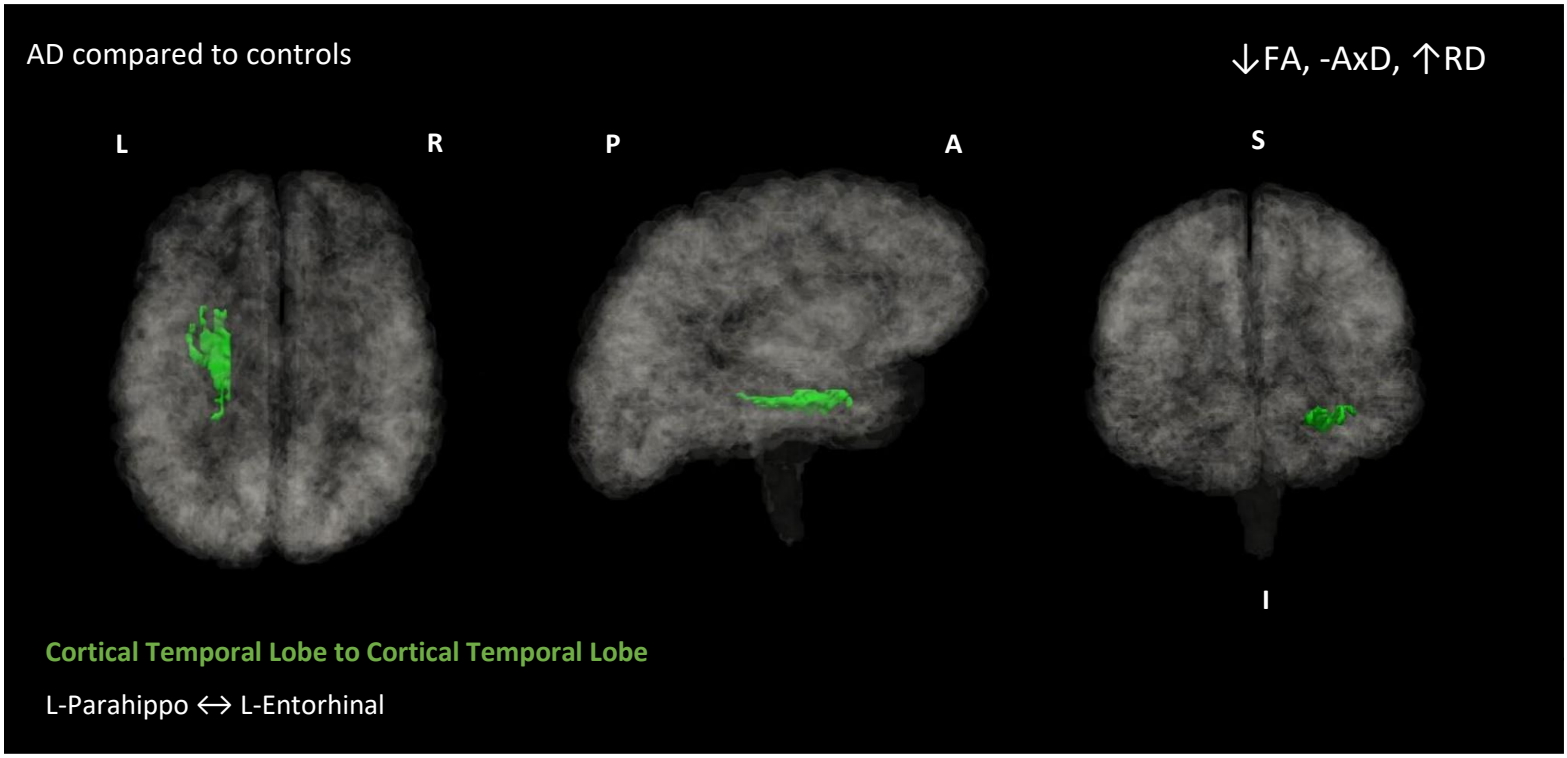

Figure 16: Connections that show lower FA with similar AxD and higher RD in AD patients compared to healthy elderly controls.

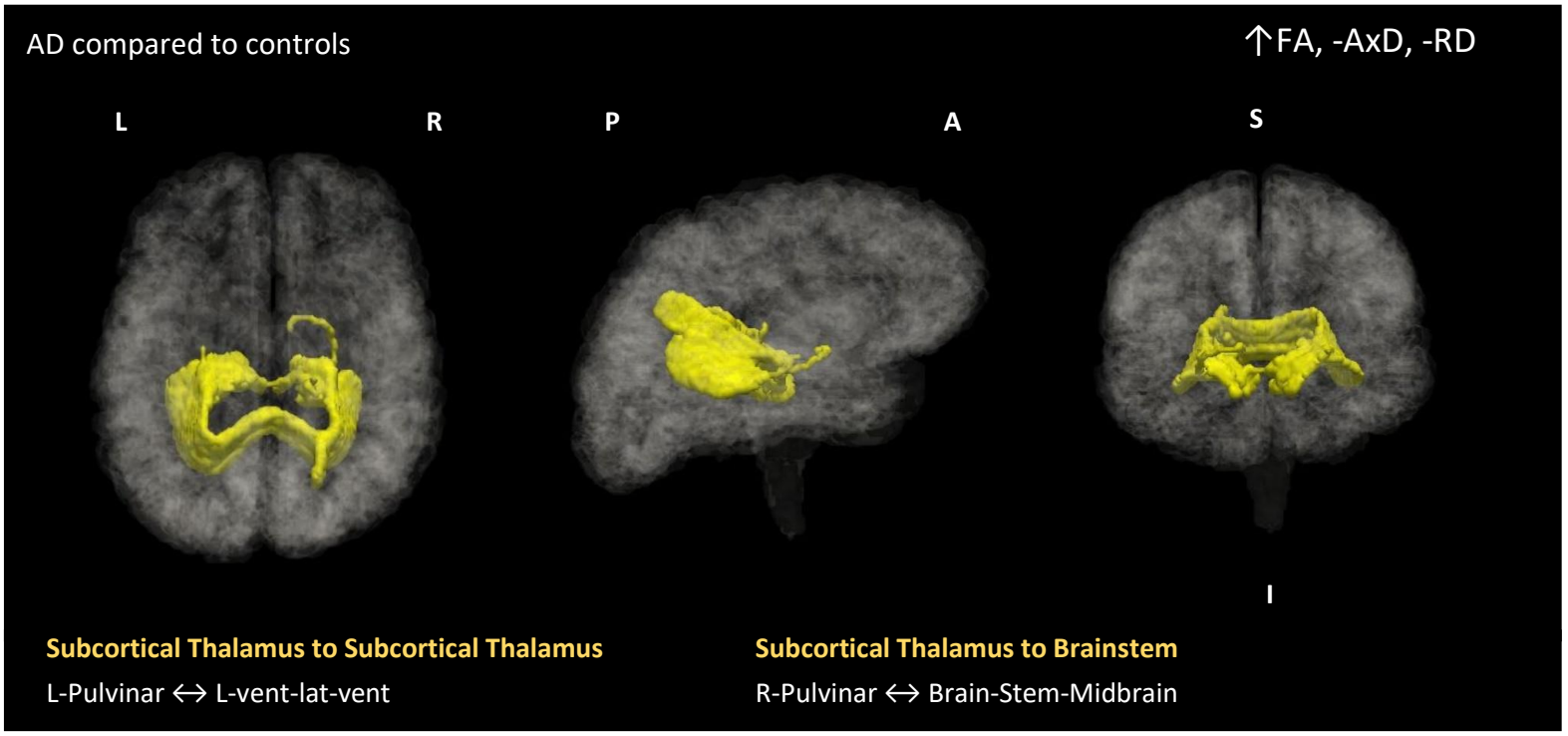

Figure 17: Connections that show higher FA with similar AxD and RD in AD patients compared to healthy elderly controls.

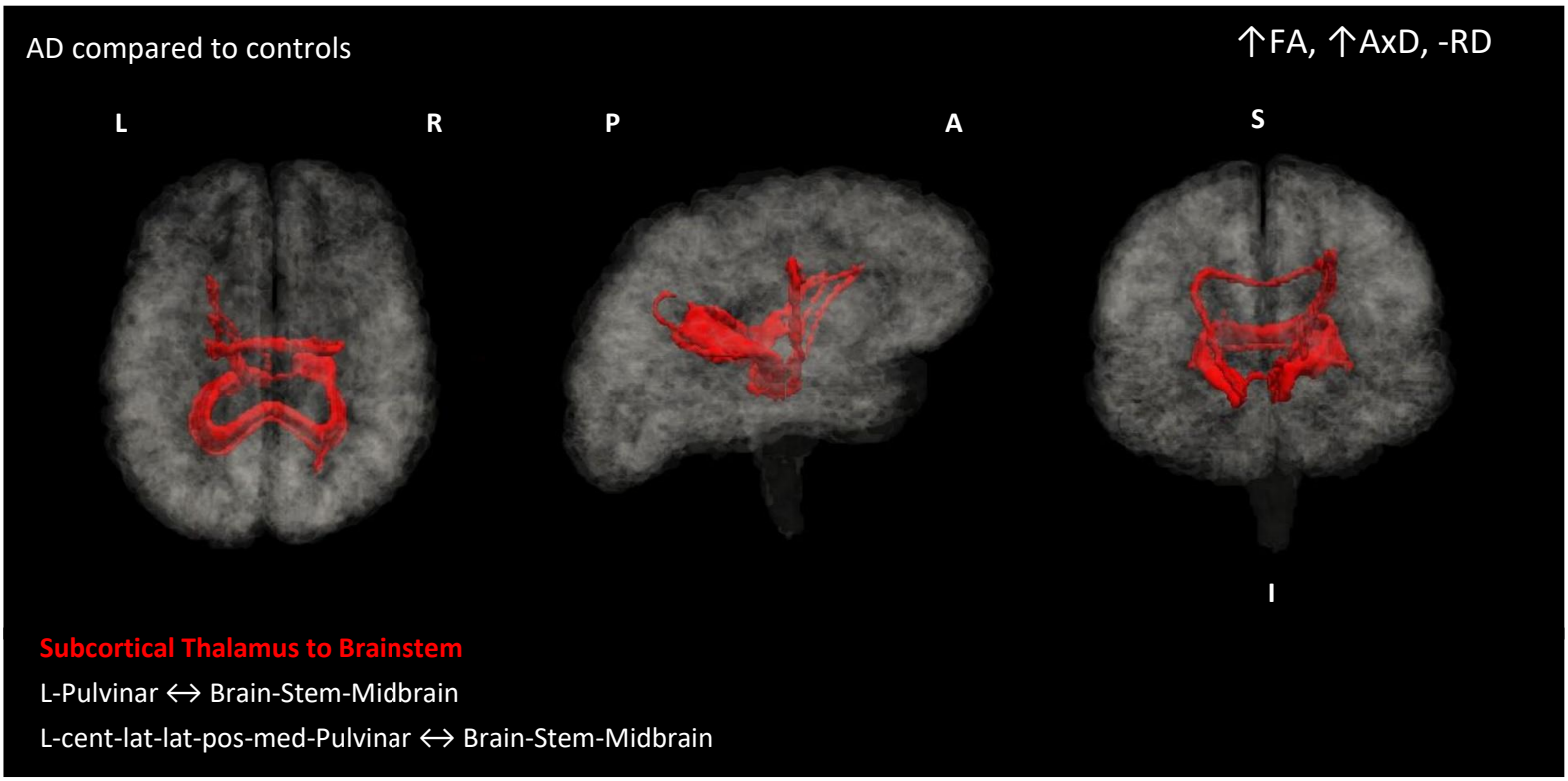

Figure 18: Connections that show higher FA as well as higher AxD and similar RD in AD patients compared to healthy elderly controls.

4.2.2 MD

Figure 19 shows either very low or very high P+ values, i.e., strong to very strong evidence of group differences in MD, where low P+ means Controls > AD and high P+ means Controls < AD. *Figures 20, 21* and *22* show the corresponding AxD and RD group differences for these connections. Refer to *Supplementary Table 4* for these results in table form.

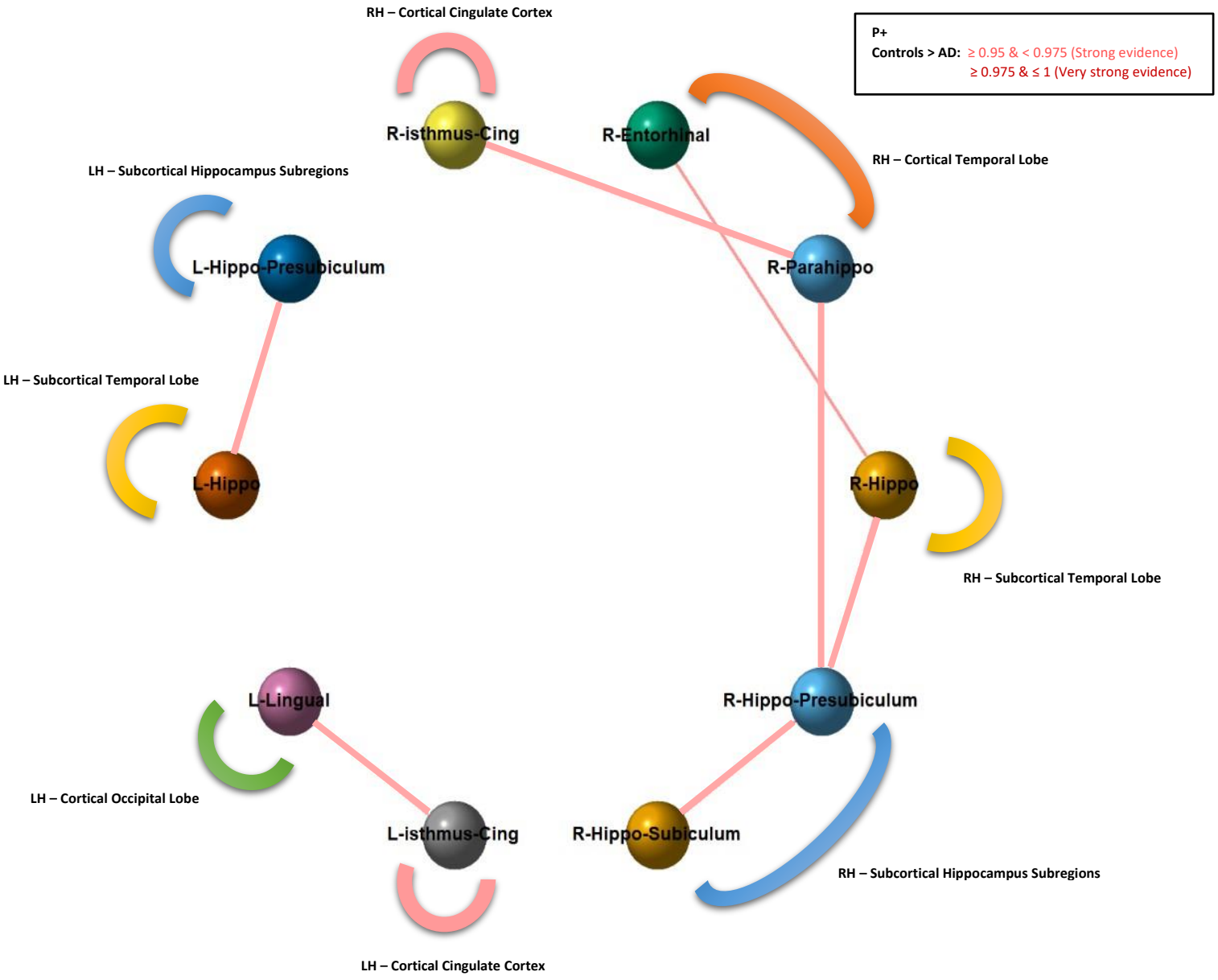

Figure 19: Connections that showed very high P+ values for MD. Red lines represents high P+ (Controls < AD) in MD. Line thickness indicates strength of inter-regional relationships.

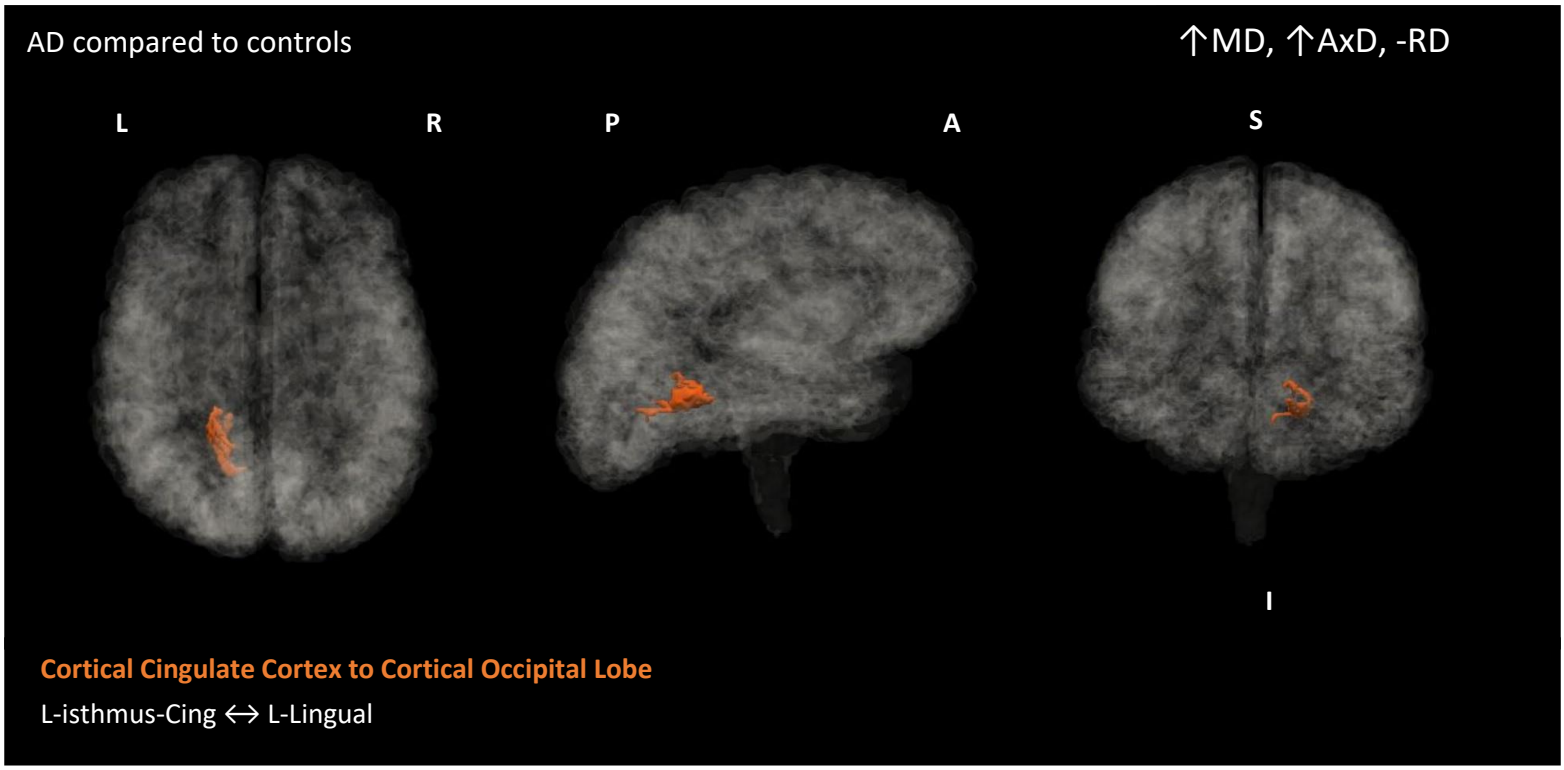

Figure 20: Connections that show higher MD as well as higher AxD with similar RD in AD patients compared to healthy elderly controls.

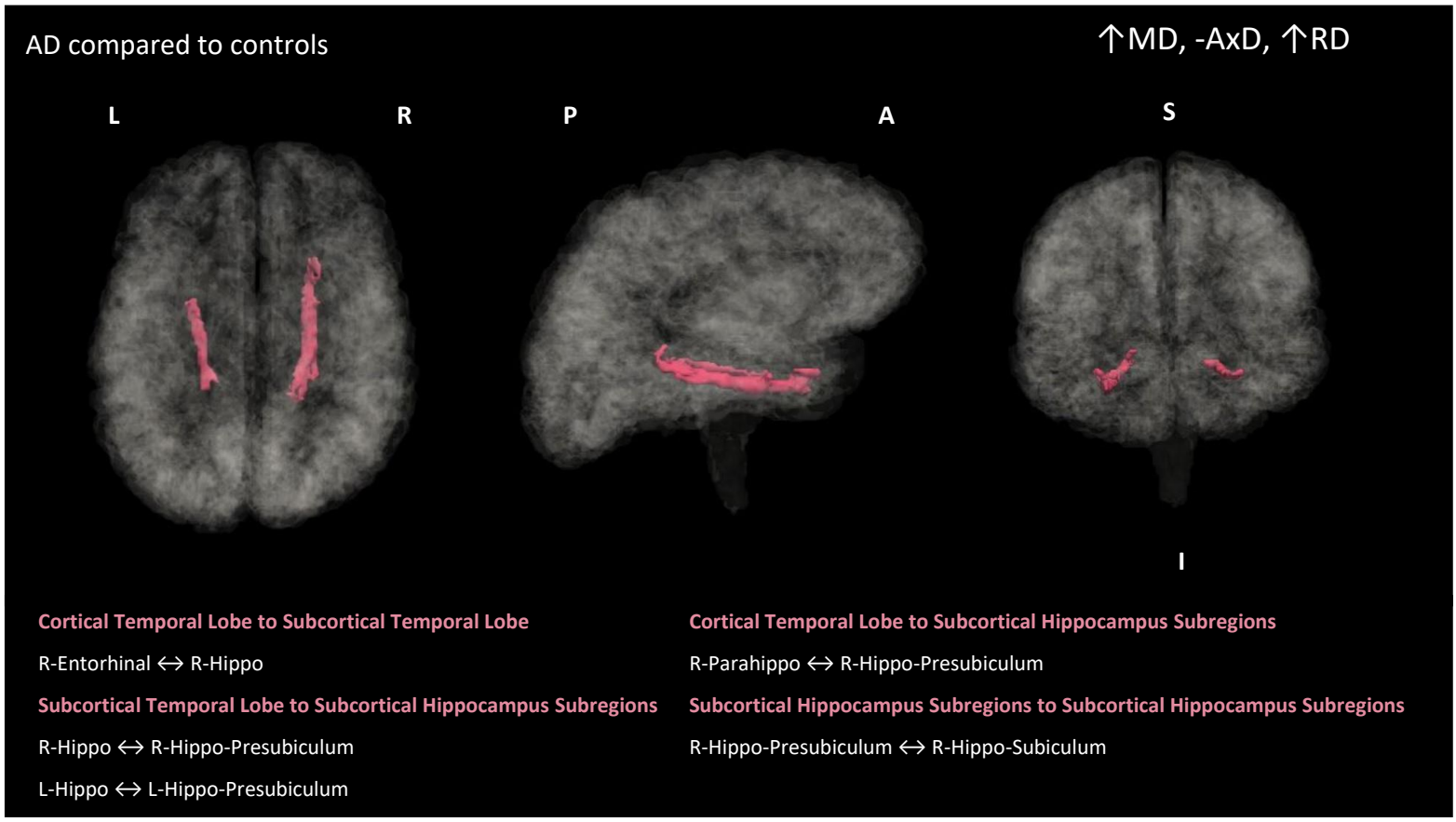

Figure 21: Connections that show higher MD with similar AxD and higher RD in AD patients compared to healthy elderly controls.

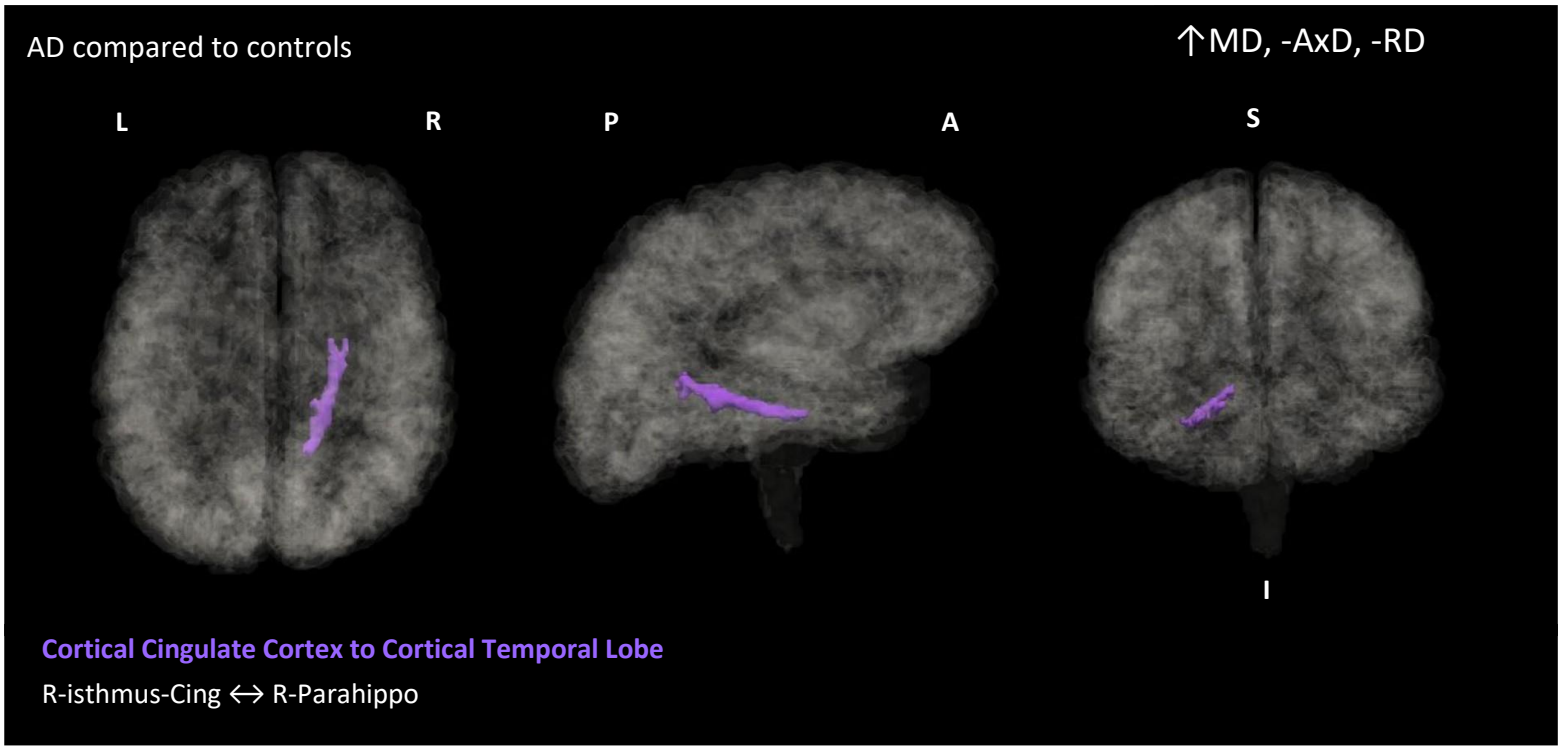

Figure 22: Connections that show higher MD with similar AxD and RD in AD patients compared to healthy elderly controls.

4.3 Between-group differences in graph theory measures

Nodal degree and modularity showed no statistically significant between-group differences. Refer to *Supplementary Figure 2, Supplementary Figure 3* and *Supplementary Table 9* for these network measure graphs and data. *Table 5* show regions that had either very low or very high P+ values, i.e., strong to very strong evidence showing group differences where low P+ means Controls > AD and high P+ means Controls < AD for nodal strength, transitivity, nodal efficiency, and local efficiency. *Figures 23, 24, 25, 26, 27, 28* and *29* show results in the brain of the AD patients compared to the healthy elderly controls. Multiple regression showed higher global efficiency in AD patients than in healthy elderly controls *(Table 6 and Figure 30).*

Table 5: Regions with either very low or very high P+ values, where low P+ means Controls > AD and high P+ means Controls < AD, for each graph theory measure.

Region	Mean (SD)	P+	Quantile intervals				
			2.5%	5%	50%	95%	97.5%
Local Efficiency							
Cortical Parietal Lobe							
R-Precuneus	-2737.66 (858.09)	<0.01**	-4349.53	-4085.97	-2775.81	-1232.80	-926.01
L-Postcentral	7836.87 (3059.98)	0.98**	575.32	1892.96	8343.83	11650.24	12163.26
Cortical Temporal Lobe							
R-Entorhinal	-5588.76 (1533.79)	<0.01**	-8413.25	-7934.37	-5727.52	-2891.95	-2458.78
R-sup-T	1613.8 (533.26)	>0.99**	502.99	708.76	1633.75	2452.98	2618.98

L-Fusiform	2485.16 (910.07)	>0.99**	633.67	976.87	2505.18	3917.75	4210.98
L-Entorhinal	-2985.84 (1262.91)	<0.01**	-5313.64	-5010.34	-3007.02	-850.97	-459.03
Subcortical Temporal Lobe							
R-Hippo	10836.94 (5892.08)	>0.99**	4619.41	5391.69	9162.50	26017.22	28849.52
Subcortical Hippocampus Subregions							
R-Hippo-Presubiculum	-11045.26 (3198.65)	<0.01**	-16267.79	-15277.52	-11862.25	-5219.31	-4723.26
R-Hippo-Subiculum	46053.6 (5057.21)	>0.99**	24180.51	39131.84	46966.32	50395.09	51902.22
R-Hippo-CA1	-11092.51 (3294.13)	<0.01**	-16919.34	-15626.45	-11870.46	-5231.73	-4771.22
Ventral Diencephalon							
L-vent-DC	3302.14 (1082.69)	>0.99**	1003.01	1480.19	3352.90	4871.70	5312.03
Nodal Efficiency							
Cortical Occipital Lobe							
R-lat-Occ	717.76 (392.92)	0.97*	-11.36	108.11	700.99	1397.07	1552.27
Cortical Temporal Lobe							
R-Fusiform	1026.82 (653.41)	0.96*	-165.67	32.00	997.99	2102.89	2436.59
L-Fusiform	4953.51 (1237.33)	>0.99**	2149.36	2620.42	5115.14	6718.56	6979.16
R-Parahippo	10697.51 (1762.24)	>0.99**	7498.33	8543.63	10842.67	12781.80	13294.58
L-Tpole	1769.95 (752.91)	>0.99**	254.29	458.89	1804.14	2957.78	3187.74
L-mid-T	2341.62 (862.23)	>0.99**	678.71	904.60	2354.19	3734.66	4018.32
Subcortical Temporal Lobe							
R-Hippo	2124.58 (1035.06)	>0.99**	414.31	645.85	1990.55	4001.49	4419.86
L-Hippo	3528.08 (1451.21)	0.98**	195.36	732.90	3716.57	5582.70	5919.48
Subcortical Hippocampus Subregions							
R-Hippo-Subiculum	2370.68 (1161.47)	>0.99**	438.97	732.46	2255.62	4372.94	4906.57
R-Hippo-MolecularLayer HP	1869.97 (1341.68)	0.97*	-64.58	158.07	1595.66	4481.10	5140.21
L-Hippo-CA1	508.64 (398.28)	0.95*	-73.80	-0.73	441.07	1282.03	1549.75
Subcortical Thalamus							
L-vent-lat-vent	892.36 (551.76)	0.96*	-104.89	54.82	859.66	1821.23	2051.49
Subcortical Basal Ganglia							
L-Acc-area	552.97 (349.75)	0.97*	-33.78	45.19	515.65	1179.33	1318.03
Nodal Strength							
Cortical Cingulate Cortex							
R-pos-Cing	9.85×10^{-4} (6.02×10^{-4})	0.97*	-1.28×10^{-5}	1.36×10^{-4}	9.10×10^{-4}	2.10×10^{-3}	2.42×10^{-3}
L-pos-Cing	1.32×10^{-3} (7.05×10^{-4})	0.96*	-1.42×10^{-4}	1.34×10^{-4}	1.34×10^{-3}	2.43×10^{-3}	2.65×10^{-3}
Subcortical Thalamus							

R-med-dors	-1.93× 10^{-3} (9.10 × 10^{-4})	0.03*	-3.49 × 10^{-3}	-3.27 × 10^{-3}	-2.01 × 10^{-3}	-3.22 × 10^{-4}	9.22 × 10^{-5}
R-cent-lat-lat-pos-med-Pulvinar	-1.68 × 10^{-3} (7.48 × 10^{-4})	0.02**	-3.04 × 10^{-3}	-2.81× 10^{-3}	-1.72 × 10^{-3}	-3.57 × 10^{-4}	-6.61 × 10^{-5}
R-vent-lat-vent	-1.43 × 10^{-4}(8.27 × 10^{-4})	0.04*	-3.24 × 10^{-3}	-2.79 × 10^{-3}	-1.39 × 10^{-3}	-1.34 × 10^{-4}	1.18 × 10^{-4}
L-Pulvinar	-1.94 × 10^{-3} (7.94 × 10^{-4})	<0.01**	-3.58 × 10^{-3}	-3.30 × 10^{-3}	-1.88 × 10^{-3}	-7.18 × 10^{-4}	-5.09 × 10^{-4}
L-vent-lat-dors	-1.66 × 10^{-3} (7.16 × 10^{-4})	0.02**	-3.01 × 10^{-3}	-2.77 × 10^{-3}	-1.69 × 10^{-3}	-3.83 × 10^{-4}	-1.27 × 10^{-4}
L-vent-lat-vent	-4.44 × 10^{-4}(1.02 × 10^{-3})	<0.01**	-6.74 × 10^{-3}	-6.28 × 10^{-3}	-4.35 × 10^{-3}	-2.96 × 10^{-3}	-2.68 × 10^{-3}
Subcortical Basal Ganglia							
R-Pal	-2.73 × 10^{-3} (9.52 × 10^{-4})	<0.01**	-4.60 × 10^{-3}	-4.31 × 10^{-3}	-2.71 × 10^{-3}	-1.18 × 10^{-3}	-8.53 × 10^{-4}
Hypothalamus (Diencephalon)							
R-Hypothalamus	1.88 × 10^{-3} (1.05 × 10^{-3})	0.97*	-1.10 × 10^{-4}	2.36 × 10^{-4}	1.87 × 10^{-3}	3.57 × 10^{-3}	4.12 × 10^{-3}
Cortical Frontal Lobe							
L-Precentral	1.58 × 10^{-3} (5.08 × 10^{-4})	>0.99**	6.28 × 10^{-4}	7.94 × 10^{-4}	1.57 × 10^{-3}	2.42 × 10^{-3}	2.64 × 10^{-3}
Cortical Parietal Lobe							
L-Postcentral	1.53 × 10^{-3} (4.36 × 10^{-4})	>0.99**	6.37 × 10^{-4}	7.96 × 10^{-4}	1.54 × 10^{-3}	2.23 × 10^{-3}	2.35 × 10^{-3}
L-inf-P	8.80 × 10^{-4} (3.89 × 10^{-4})	0.99**	1.02 × 10^{-4}	2.44 × 10^{-4}	8.85 × 10^{-4}	1.52 × 10^{-3}	1.65 × 10^{-3}
Cortical Temporal Lobe							
L-mid-T	9.91 × 10^{-4} (5.00 × 10^{-4})	0.98**	2.88 × 10^{-5}	1.64 × 10^{-4}	9.91 × 10^{-4}	1.81 × 10^{-3}	1.96 × 10^{-3}
L-sup-T	1.2 × 10^{-3}(4.96 × 10^{-4})	>0.99**	3.15 × 10^{-4}	4.48 × 10^{-4}	1.16 × 10^{-3}	2.06 × 10^{-3}	2.31 × 10^{-3}
Insula							
L-Insula	1.16 × 10^{-3} (6.32 × 10^{-4})	0.97*	-5.75 × 10^{-5}	1.24 × 10^{-4}	1.17 × 10^{-3}	2.19 × 10^{-3}	2.37 × 10^{-3}
Subcortical Temporal Lobe							
L-Hippo	-1.03 × 10^{-3} (4.10 × 10^{-4})	0.01**	-1.82 × 10^{-3}	-1.69 × 10^{-3}	-1.04 × 10^{-3}	-3.39 × 10^{-4}	-1.98 × 10^{-4}
Ventral Diencephalon							
L-vent-DC	-4.32 × 10^{-3} (1.56 × 10^{-3})	<0.01**	-7.26 × 10^{-3}	-6.65 × 10^{-3}	-4.40 × 10^{-3}	-1.45 × 10^{-3}	-9.14 × 10^{-4}
Brain Stem							
Brain-Stem-Pons	5.72 × 10^{-3} (1.78 × 10^{-3})	>0.99**	3.04 × 10^{-3}	3.49 × 10^{-3}	5.44 × 10^{-3}	9.98 × 10^{-3}	1.08 × 10^{-2}
Brain-Stem-Medulla	-2.64 × 10^{-3} (8.23 × 10^{-4})	<0.01**	-4.36 × 10^{-3}	-3.99 × 10^{-3}	-2.63 × 10^{-3}	-1.37 × 10^{-3}	-1.09 × 10^{-3}
Brain-Stem-SCP	-1.56 × 10^{-3} (9.61× 10^{-4})	0.03*	-3.53 × 10^{-3}	-3.27 × 10^{-3}	-1.46 × 10^{-3}	-1.50 × 10^{-4}	5.00 × 10^{-5}
Transitivity							
Cortical Temporal Lobe							
R-Fusiform	1.46 × 10^{-2} (9.29 × 10^{-3})	0.96*	-2.23 × 10^{-3}	7.12 × 10^{-4}	1.39 × 10^{-2}	3.07 × 10^{-2}	3.34 × 10^{-2}
R-Entorhinal	1.25 × 10^{-2} (5.76 × 10^{-3})	0.98**	1.07 × 10^{-3}	3.08 × 10^{-3}	1.28 × 10^{-2}	2.13 × 10^{-2}	2.29 × 10^{-2}
R-inf-T	2.47 × 10^{-2} (5.54 × 10^{-3})	>0.99**	1.30 × 10^{-2}	1.62 × 10^{-2}	2.49 × 10^{-2}	3.29 × 10^{-2}	3.49 × 10^{-2}
L-Tpole	4.78 × 10^{-2} (6.78 × 10^{-3})	>0.99**	2.89 × 10^{-2}	3.40 × 10^{-2}	4.87 × 10^{-2}	5.66 × 10^{-2}	5.80 × 10^{-2}
L-inf-T	8.99 × 10^{-3} (3.91 × 10^{-3})	0.98**	8.91 × 10^{-5}	2.00 × 10^{-3}	9.35 × 10^{-3}	1.47 × 10^{-2}	1.58 × 10^{-2}

L-sup-T	-1.22×10^{-2} (6.16×10^{-3})	0.03*	-2.38×10^{-2}	-2.20×10^{-2}	-1.24×10^{-2}	-1.87×10^{-3}	4.48×10^{-5}
Subcortical Thalamus							
R-vent-lat-dors	1.59×10^{-2} (6.50×10^{-3})	0.99**	2.91×10^{-3}	4.80×10^{-3}	1.66×10^{-2}	2.55×10^{-2}	2.69×10^{-2}
R-vent-ant	2.29×10^{-2} (1.07×10^{-2})	0.99**	3.56×10^{-3}	6.88×10^{-3}	2.28×10^{-2}	3.90×10^{-2}	4.15×10^{-2}
L-ant	-1.09×10^{-2} (5.70×10^{-3})	0.04*	-2.07×10^{-2}	-1.94×10^{-2}	-1.14×10^{-2}	-8.65×10^{-4}	1.23×10^{-3}
L-vent-ant	-6.09×10^{-3} (3.60×10^{-3})	0.05*	1.29×10^{-2}	-1.19×10^{-2}	-6.21×10^{-3}	-4.45×10^{-5}	1.25×10^{-3}
Subcortical Basal Ganglia							
R-Caudate	-3.22×10^{-2} (6.94×10^{-3})	<0.01**	-4.26×10^{-2}	-4.13×10^{-2}	-3.33×10^{-2}	-1.92×10^{-2}	-1.65×10^{-2}
R-Pu	-2.12×10^{-2} (6.83×10^{-3})	0.01**	-3.05×10^{-2}	-2.94×10^{-2}	-2.29×10^{-2}	-6.88×10^{-3}	-3.22×10^{-3}
L-Pu	-1.41×10^{-2} (7.73×10^{-3})	0.01**	-3.03×10^{-2}	-2.86×10^{-2}	-1.27×10^{-2}	-3.25×10^{-3}	-1.26×10^{-3}
Cortical Frontal Lobe							
L-sup-F	1.76×10^{-2} (6.76×10^{-3})	0.98**	3.37×10^{-4}	5.47×10^{-3}	1.82×10^{-2}	2.72×10^{-2}	2.93×10^{-2}
L-Paracentral	1.58×10^{-2} (7.82×10^{-3})	0.96*	-1.88×10^{-3}	1.60×10^{-3}	1.67×10^{-2}	2.65×10^{-2}	2.90×10^{-2}
Cortical Cingulate Cortex							
L-caud-ant-Cing	-6.19×10^{-3} (3.29×10^{-3})	0.04*	-1.24×10^{-2}	-1.13×10^{-2}	-6.32×10^{-3}	-5.79×10^{-4}	5.38×10^{-4}
L-pos-Cing	-9.42×10^{-3} (5.80×10^{-3})	0.05*	-2.11×10^{-2}	-1.91×10^{-2}	-9.39×10^{-3}	1.32×10^{-4}	1.79×10^{-3}
Cortical Parietal Lobe							
L-Supramarginal	1.03×10^{-2} (4.56×10^{-3})	0.99**	2.04×10^{-3}	3.43×10^{-3}	9.86×10^{-3}	1.84×10^{-2}	2.08×10^{-2}
L-inf-P	-2.19×10^{-2} (9.35×10^{-3})	0.01**	-3.65×10^{-2}	-3.49×10^{-2}	-2.29×10^{-2}	-4.60×10^{-3}	-2.22×10^{-3}
Hypothalamus (Diencephalon)							
L-Hypothalamus	-1.10×10^{-2} (5.72×10^{-3})	0.02**	-2.23×10^{-2}	-2.05×10^{-2}	-1.09×10^{-2}	-1.94×10^{-3}	-3.65×10^{-4}

Key: SD, Standard Deviation; R, Right; L, Left

Note: Data presented are group difference means with standard deviations in parentheses.

*Strong evidence, **Very strong evidence

P+ ≤ 0.05: Controls > AD, P+ ≥ 0.95: Controls < AD

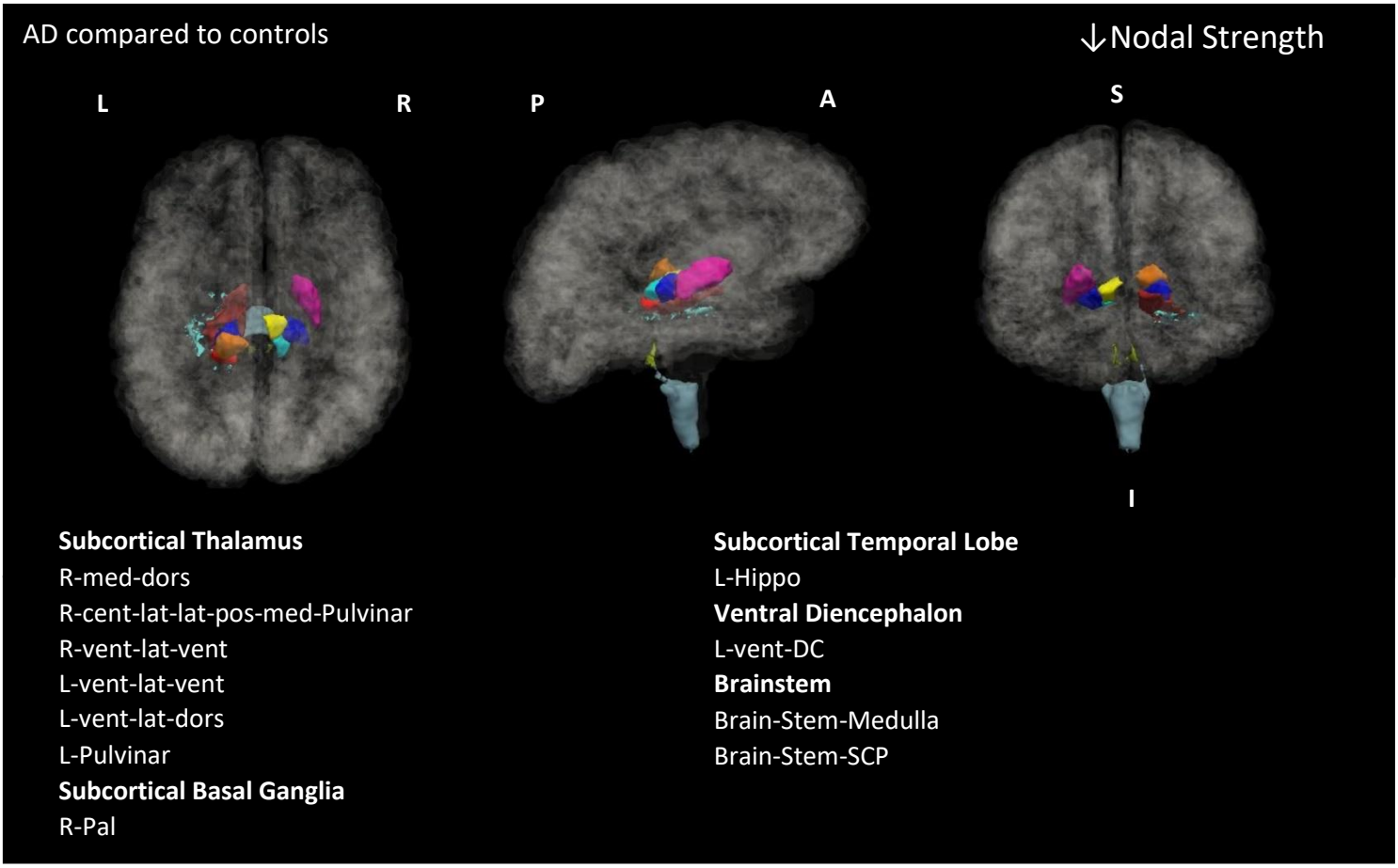

Figure 23: Regions that show lower nodal strength in AD patients compared to healthy elderly controls.

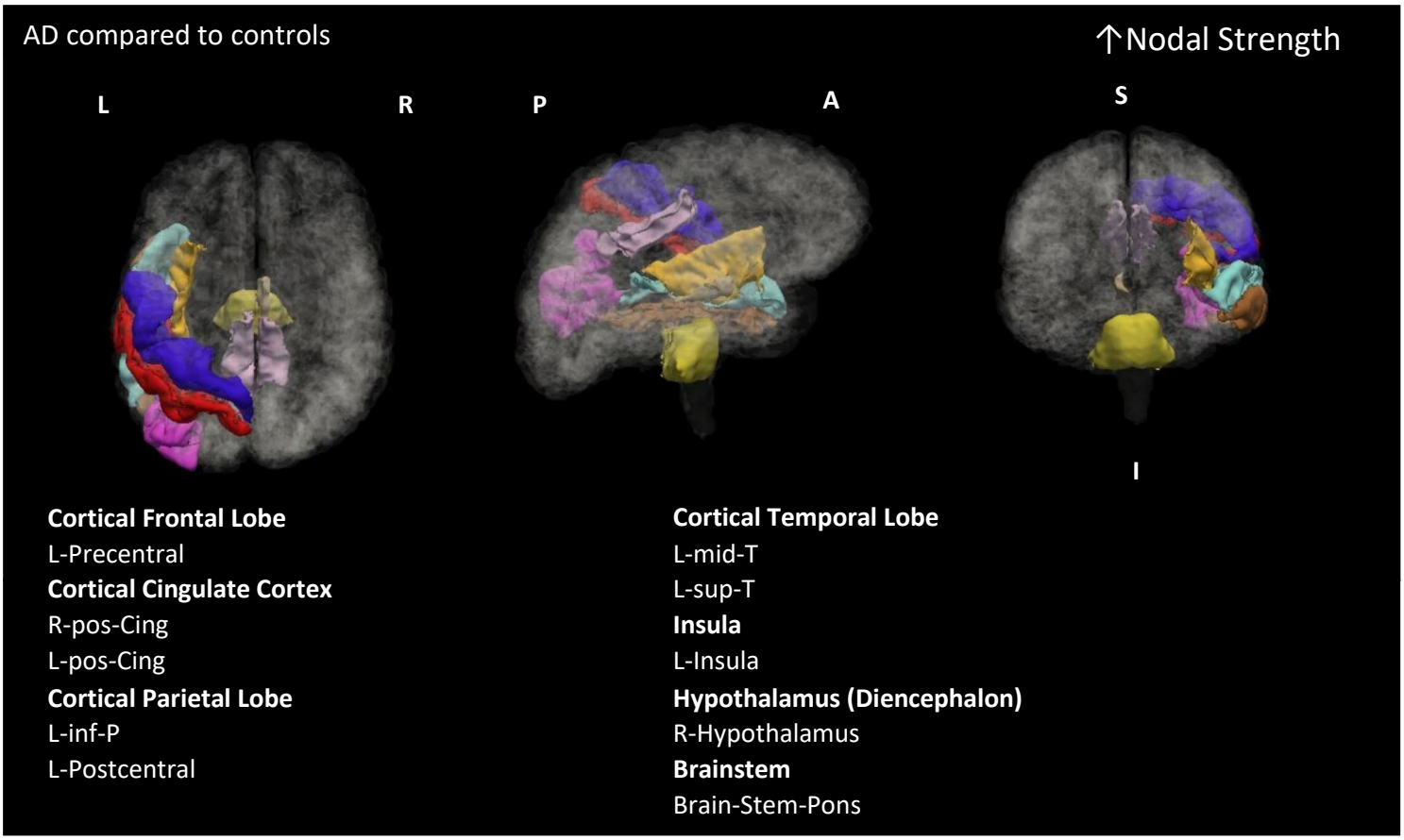

Figure 24: Regions that show higher nodal strength in AD patients compared to healthy elderly controls.

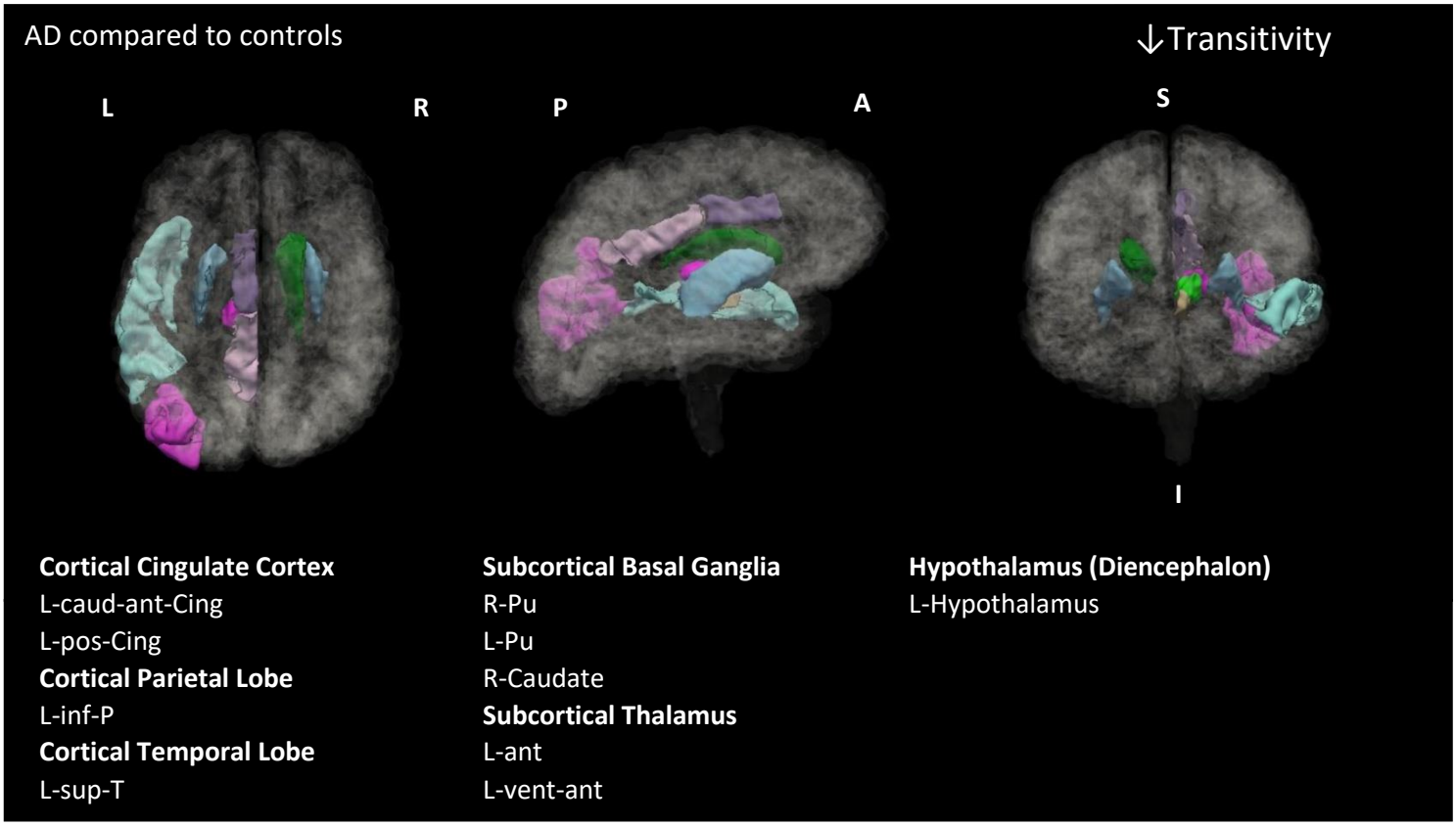

Figure 25: Regions that show lower transitivity in AD patients compared to healthy elderly controls.

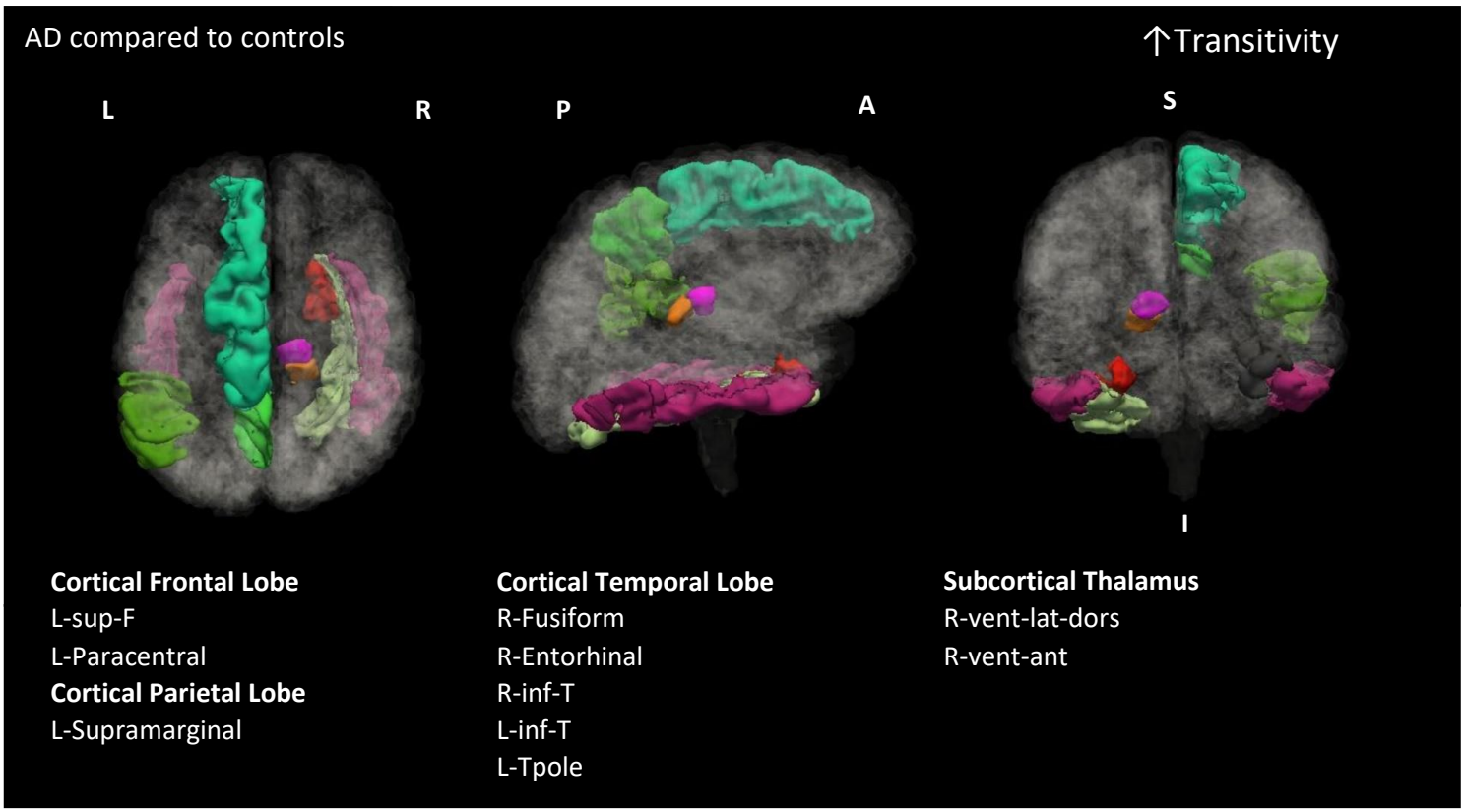

Figure 26: Regions that show higher transitivity in AD patients compared to healthy elderly controls.

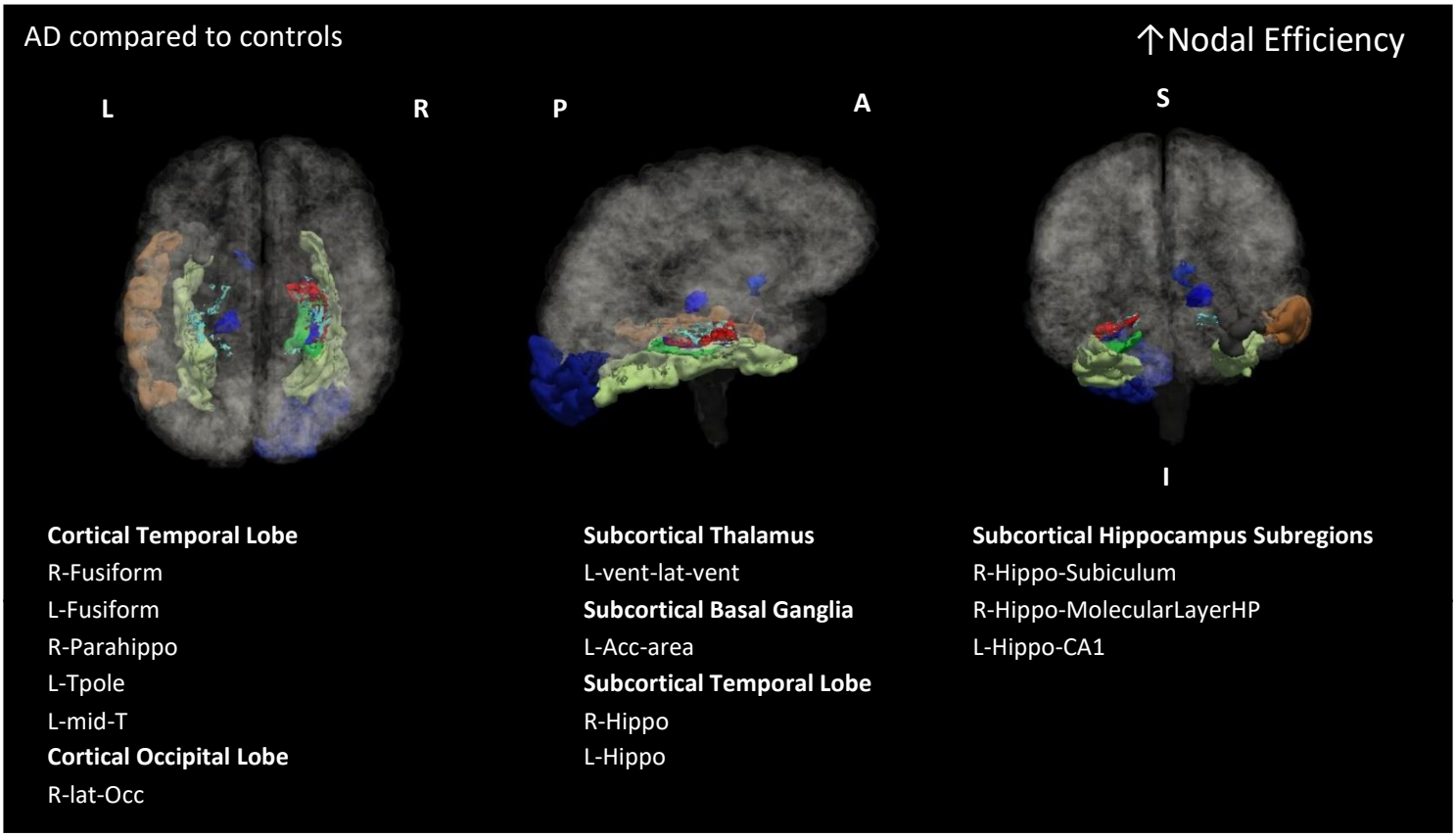

Figure 27: Regions that show higher nodal efficiency in AD patients compared to healthy elderly controls.

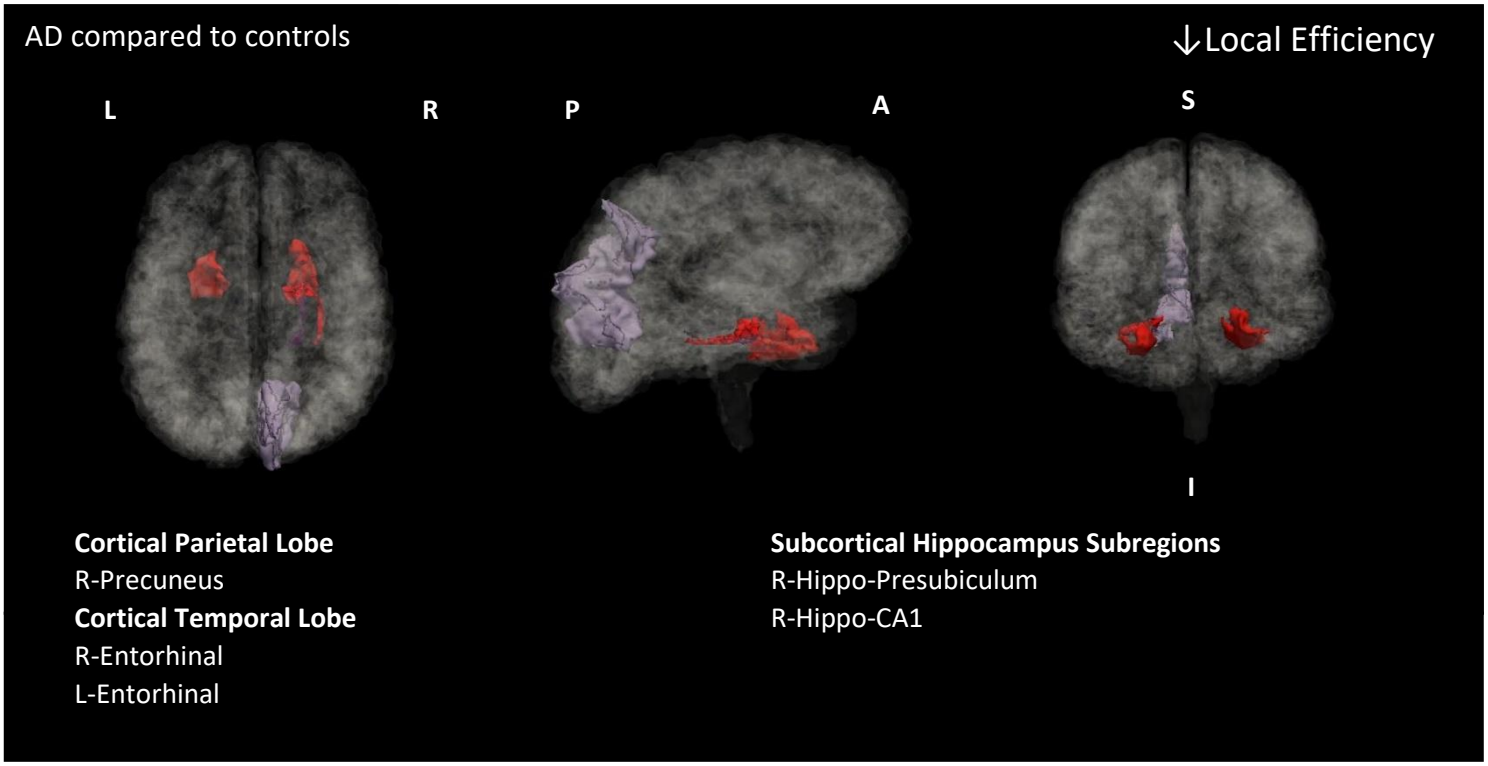

Figure 28: Regions that show lower local efficiency in AD patients compared to healthy elderly controls.

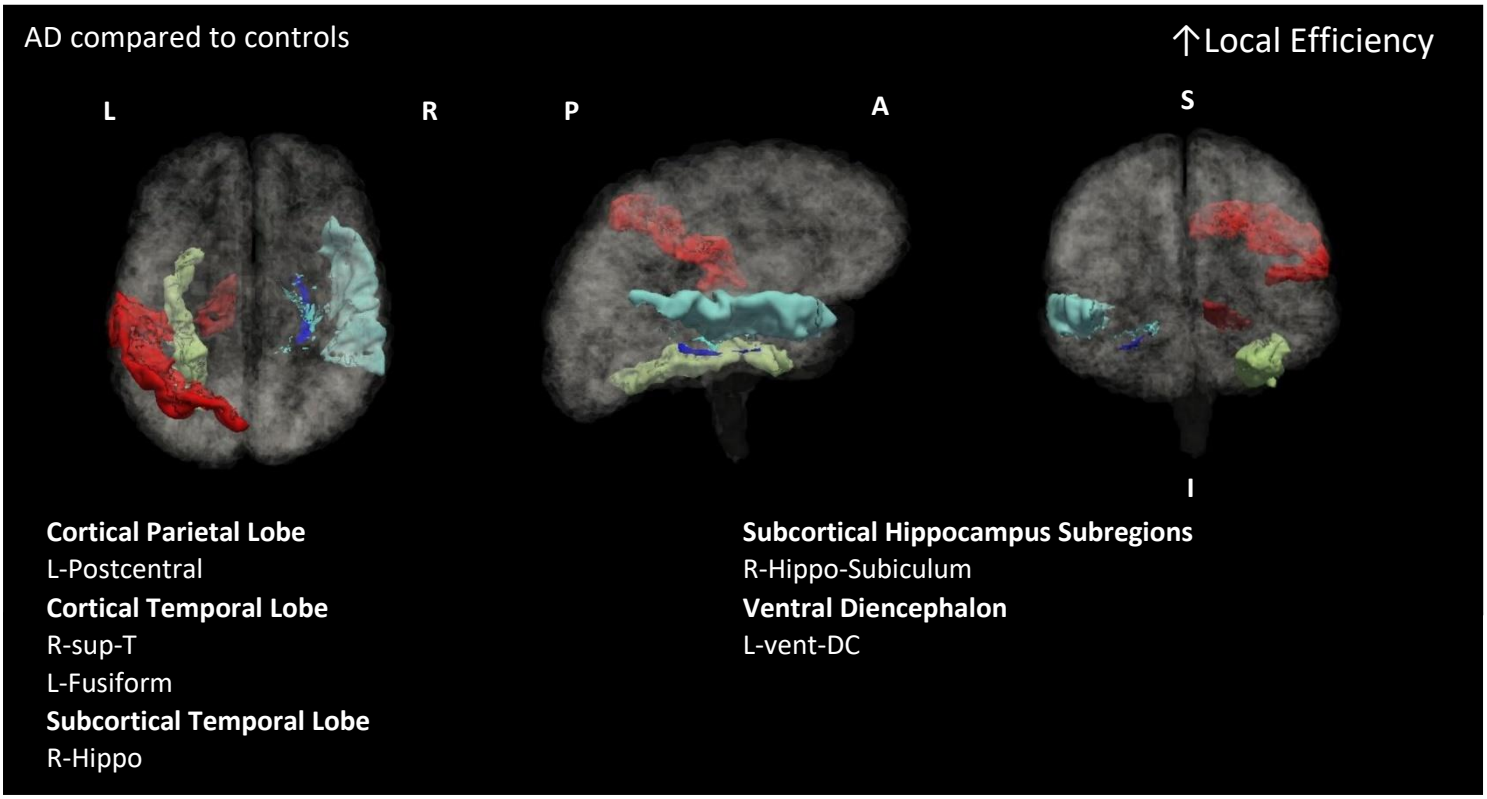

Figure 29: Regions that show higher local efficiency in AD patients compared to healthy elderly controls.

Table 6: Multiple linear regression analysis results with global efficiency as the dependent variable.

Effect	Coefficient Estimate (Standard Error)	*t*	95% Confidence Interval	*p*
Intercept	10228.70 (2807.30)	2.64	4434.79; 16022.65	**< 0.001*** **
Group[a]				
Controls	(reference)		(reference)	(reference)
AD	7296.60 (2472.90)	2.95	2192.83; 12400.40	**0.007** **
Sex[b]				
Female	(reference)		(reference)	(reference)
Male	-5755.70 (2939.00)	-1.96	-11821.47; 310.16	0.06
Age in years[c]	189.10 (1234.00)	0.15	-2357.65; 2735.92	0.88
Education in years[c]	265.70 (1425.30)	0.19	-2675.92; 3207.34	0.85
Monthly Household Income[d]				
Level 2	-8332.20 (7032.50)	-1.19	-22846.58; 6182.18	0.25
Level 3	-5869.00 (4227.20)	-1.39	-14593.43; 2855.48	0.18
Level 4	(reference)		(reference)	(reference)
Level 5	-212.90 (3449.50)	-0.06	-7332.32; 6906.55	0.95
Level 6	-1063.00 (3100.70)	-0.34	-7462.54; 5336.51	0.73

Key: AD, Alzheimer's Disease

[a]Group is represented as 1 dummy variable with "Controls" serving as the reference group.

[b]Sex is represented as 1 dummy variable with "Female" serving as the reference group.

[c]Variable was standardised.

[d]Monthly Household Income is represented as 4 dummy variables with "Level 4" serving as the reference group.

*p ≤ 0.05, **p < 0.01, ***p < 0.001

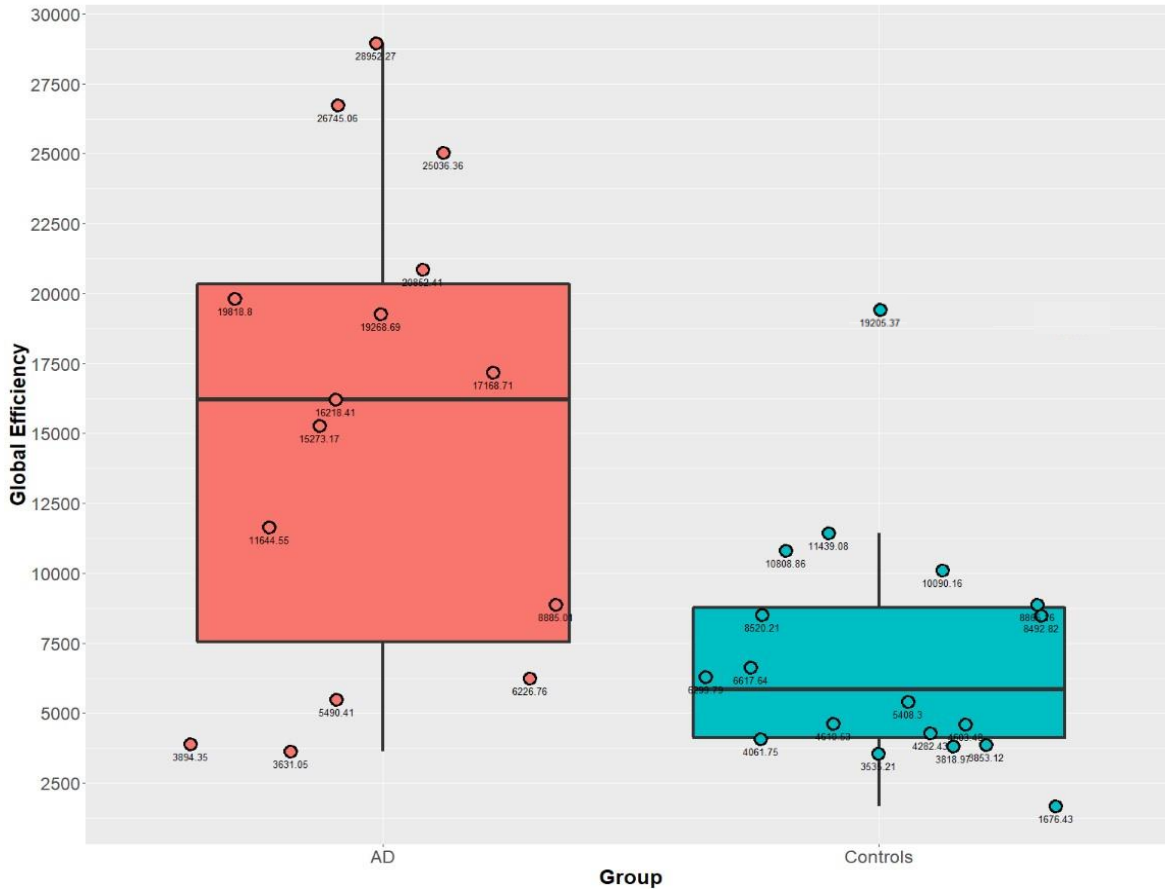

Figure 30: Box-and-whiskers plots showing global efficiency in each group. Points represent the global efficiency of each individual in each group.

4.4 Relationship between graph theory metrics and IIV

We investigated the relationship between network metrics and RT IIV for nodes that had significant group differences in network metrics identified in *section 4.3* above. Multiple regression models were performed separately for the controls and the AD patients, controlling for sex, age, years of education and monthly household income.

SRT *iSD* was negatively associated with transitivity of the left anterior cingulate cortex (L-ant) (β = -0.01, SE < 0.01, *p* = 0.02) *(Figure 31A)* in the controls, but not in the AD patients. SRT *iSD* was negatively associated with transitivity of the right ventral latero-dorsal nucleus thalamus (R-vent-lat-dors) (β = -0.01, SE < 0.01, *p* = 0.02) *(Figure 31B)* in the AD patients, but not in the controls.

CRT *iSD* was positively associated with nodal efficiency of the left ventral latero-ventral thalamus (L-vent-lat-vent) (β = 18580.94, SE = 7621.00, *p* = 0.03) *(Figure 31C)* as well as negatively associated with nodal efficiency of the left nucleus accumbens area (L-Acc-area) (β = -774.01, SE = 342.90, *p* = 0.05) *(Figure 31D)* and nodal strength of the right mediodorsal thalamus (R-med-dors) (β < -0.01, SE < 0.01, *p* = 0.02) *(Figure 31E)* in the controls, but not in the AD patients.

CRT *iSD* was positively associated with transitivity of the left posterior cingulate cortex (L-pos-Cing) (β < 0.01, SE < 0.01, *p* = 0.05) *(Figure 31F)* and global efficiency (β = 2558.10, SE = 984.70, *p* = 0.04) *(Figure 31G)* in the AD patients, but not in the controls.

Neither SRT *iSD* nor CRT *iSD* showed an association with local efficiency in any region.

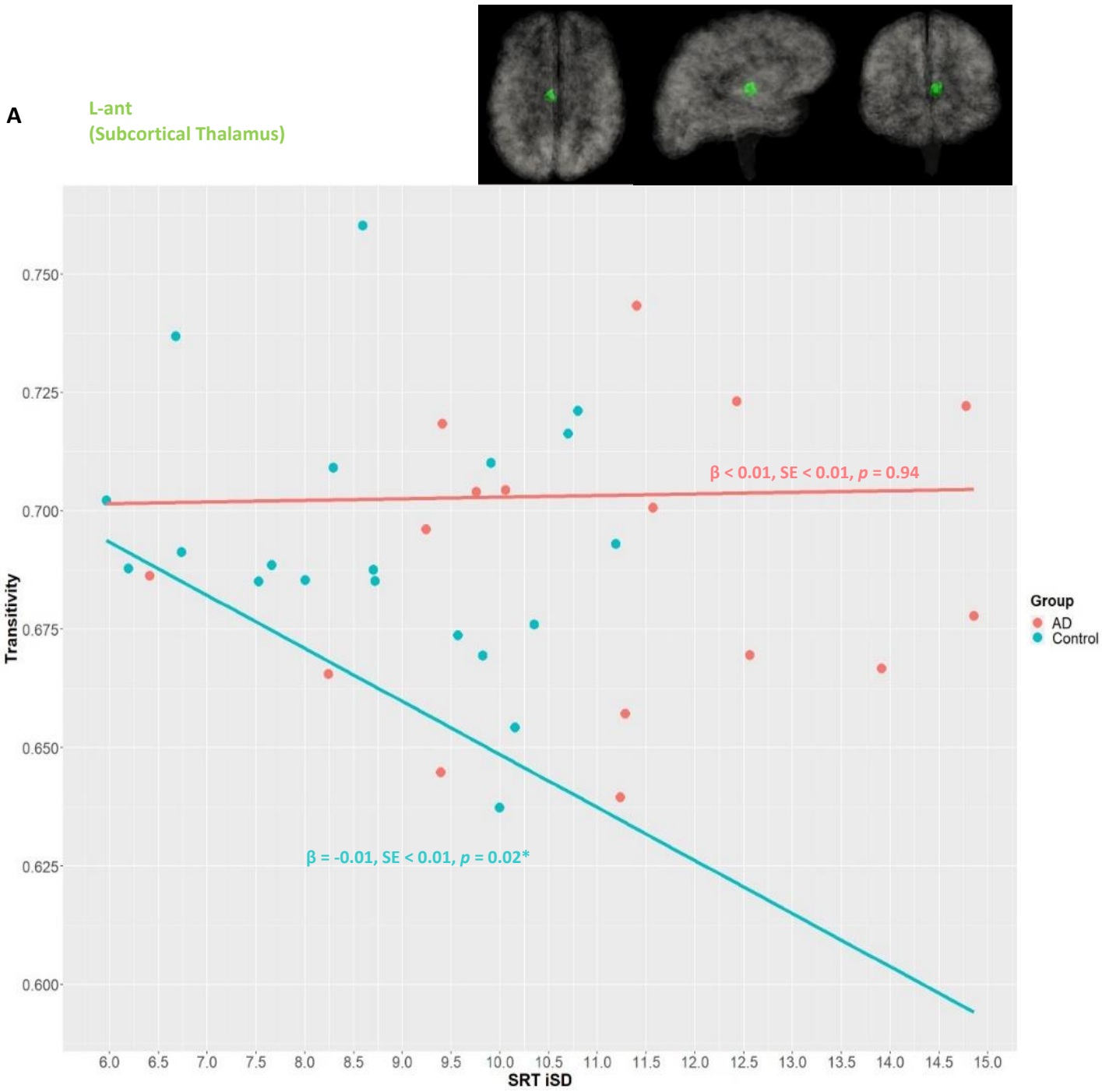

B

R-vent-lat-dors
(Subcortical Thalamus)

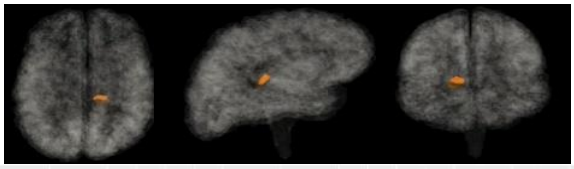

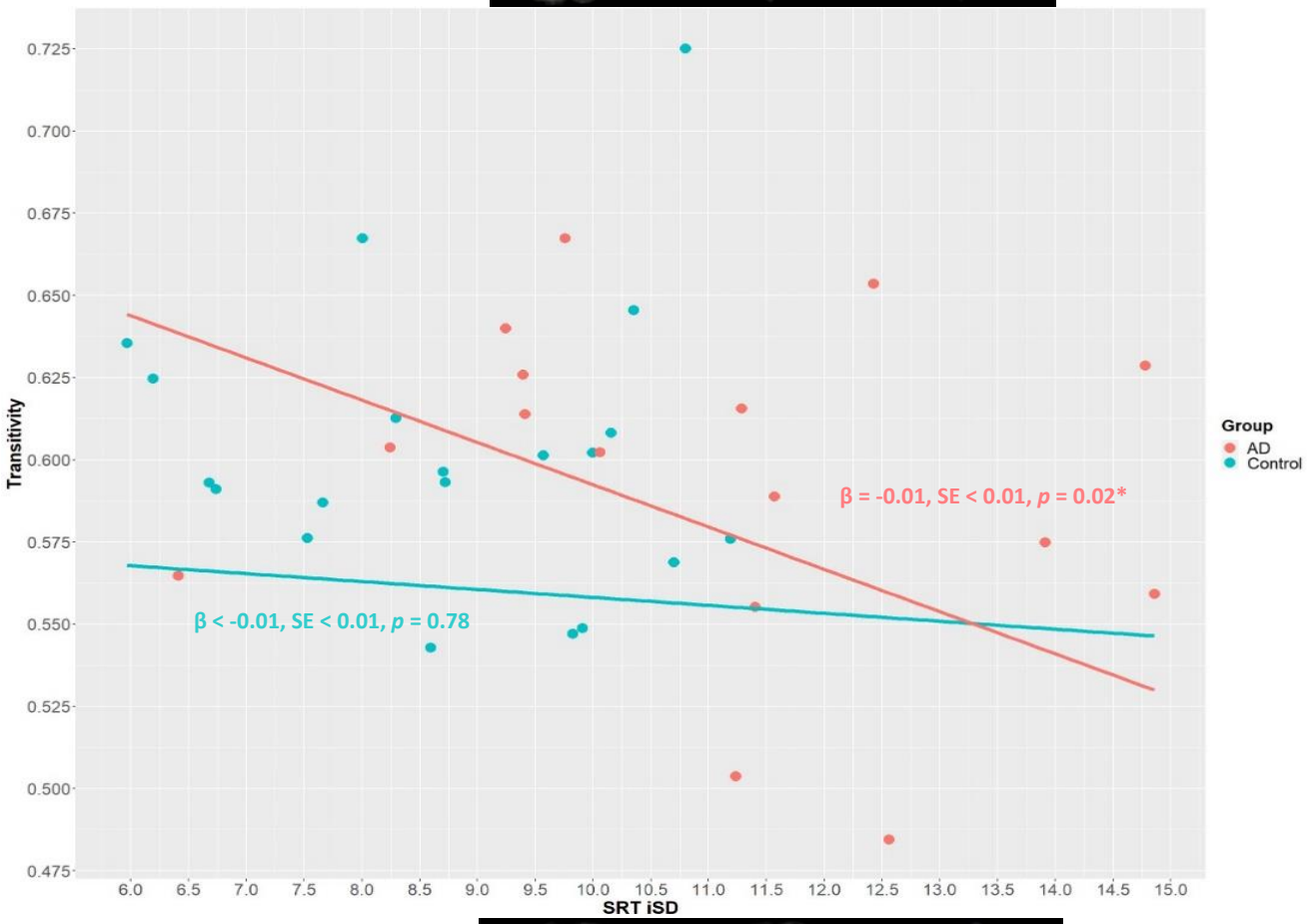

C

L-vent-lat-vent
(Subcortical Thalamus)

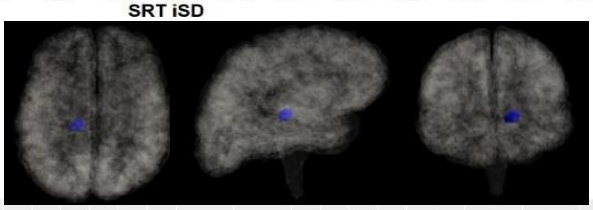

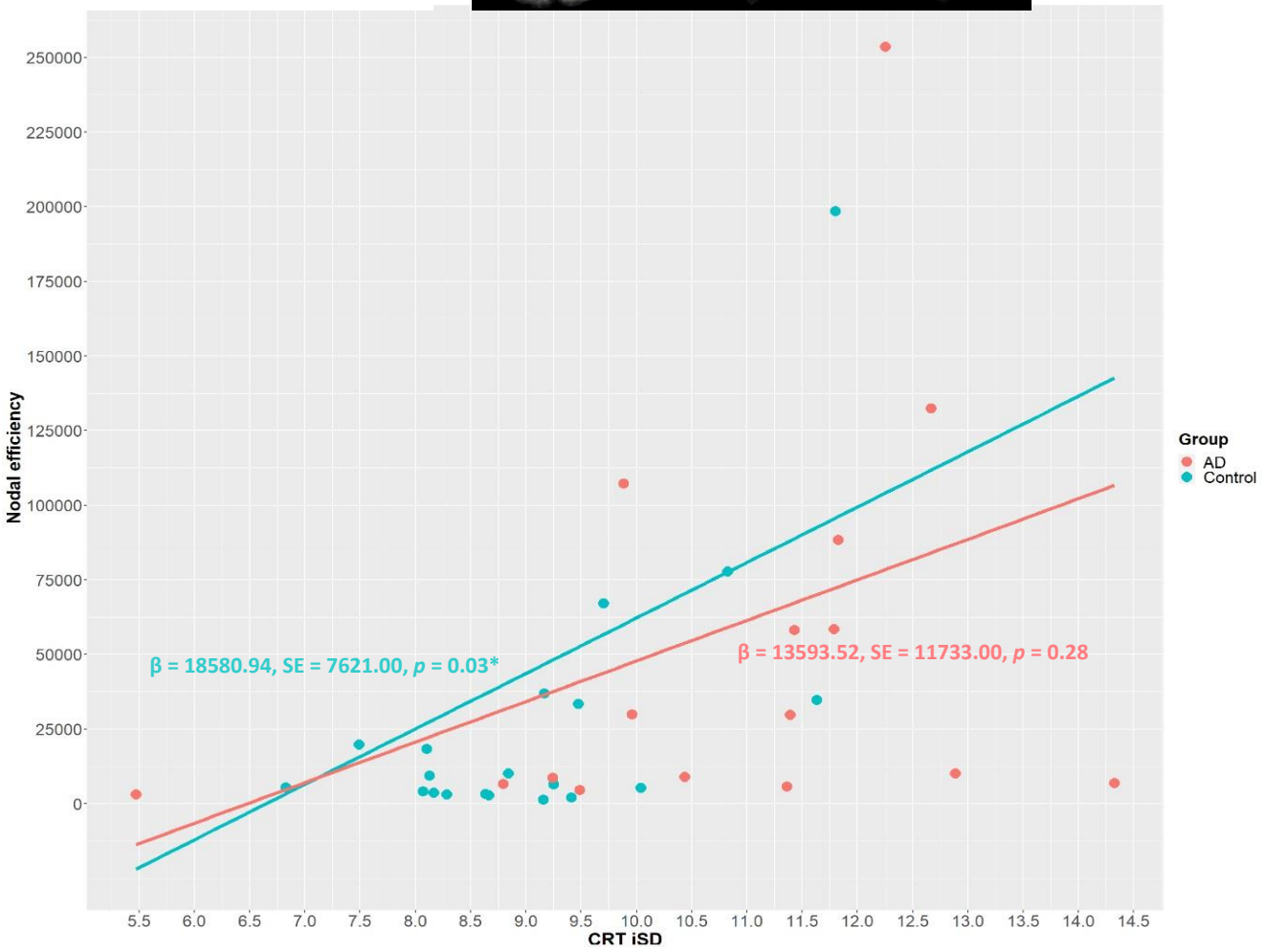

D

L-Acc-area
(Subcortical Basal Ganglia)

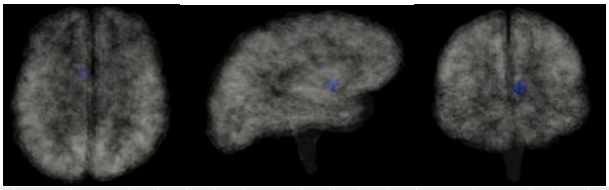

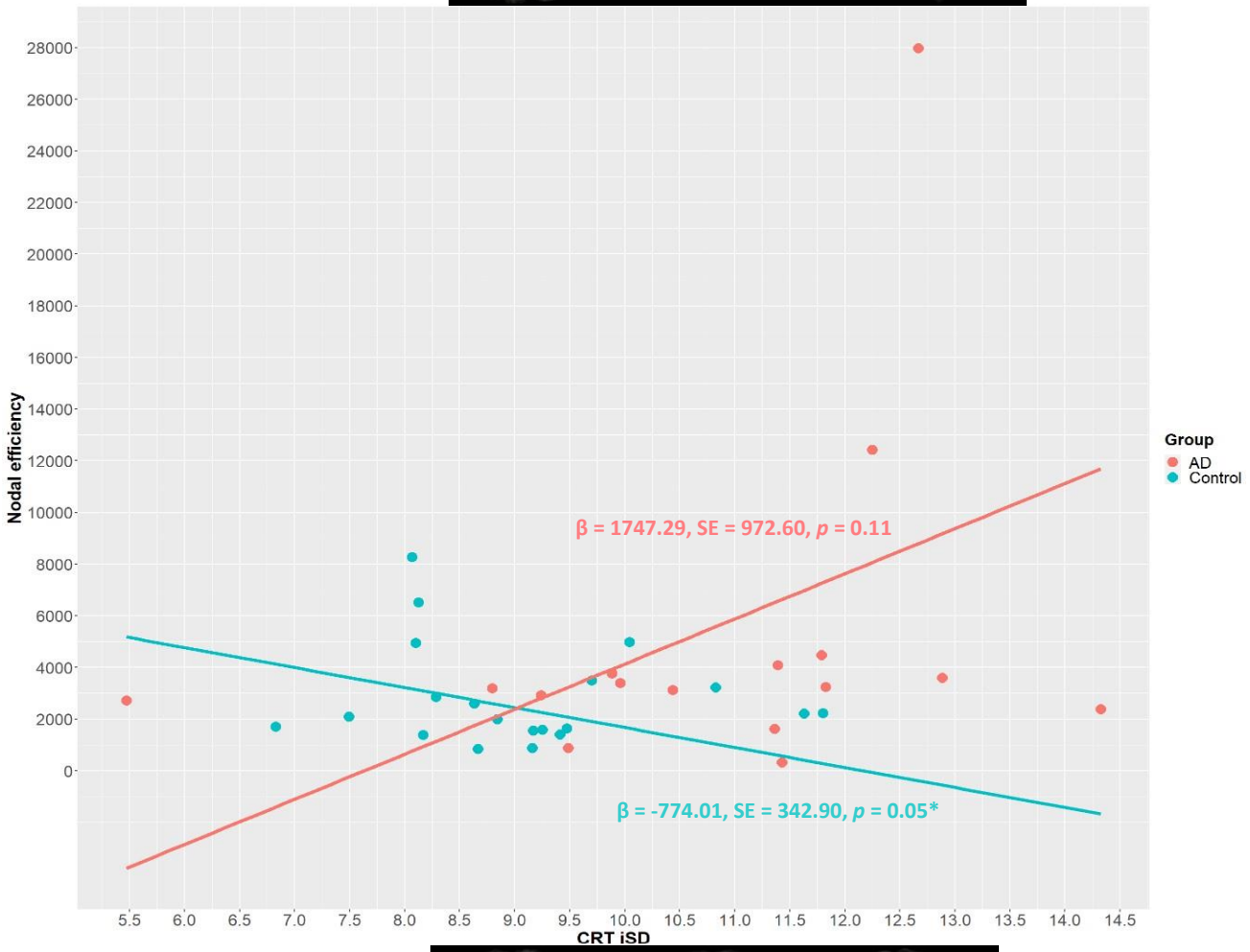

E

R-med-dors
(Subcortical Thalamus)

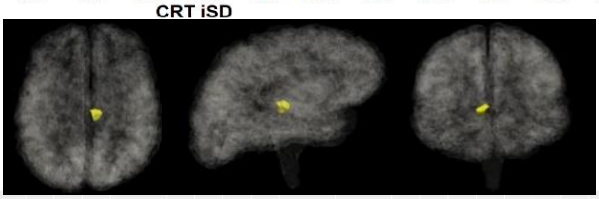

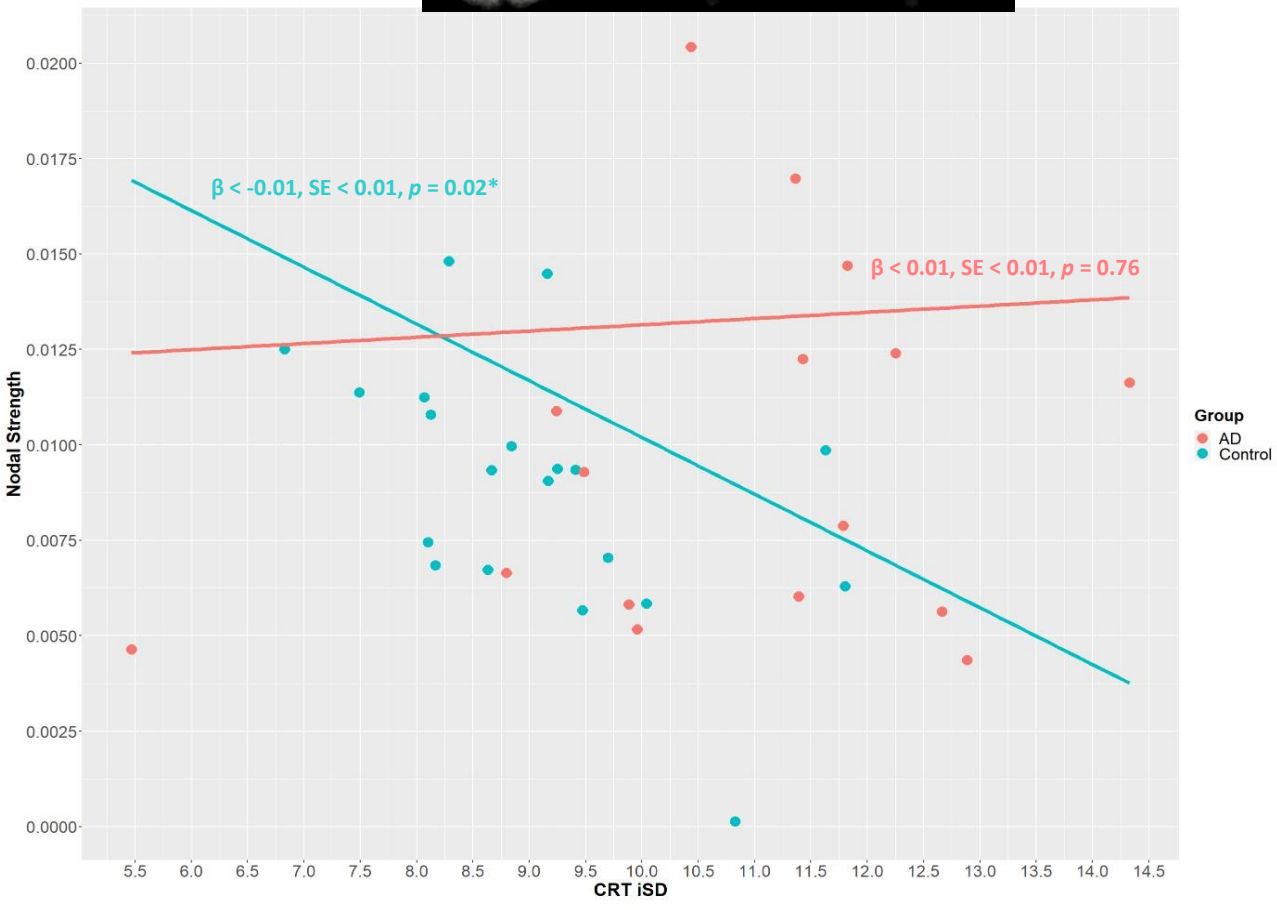

F

L-pos-Cing
(Cortical Cingulate Cortex)

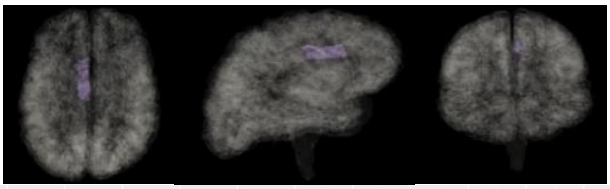

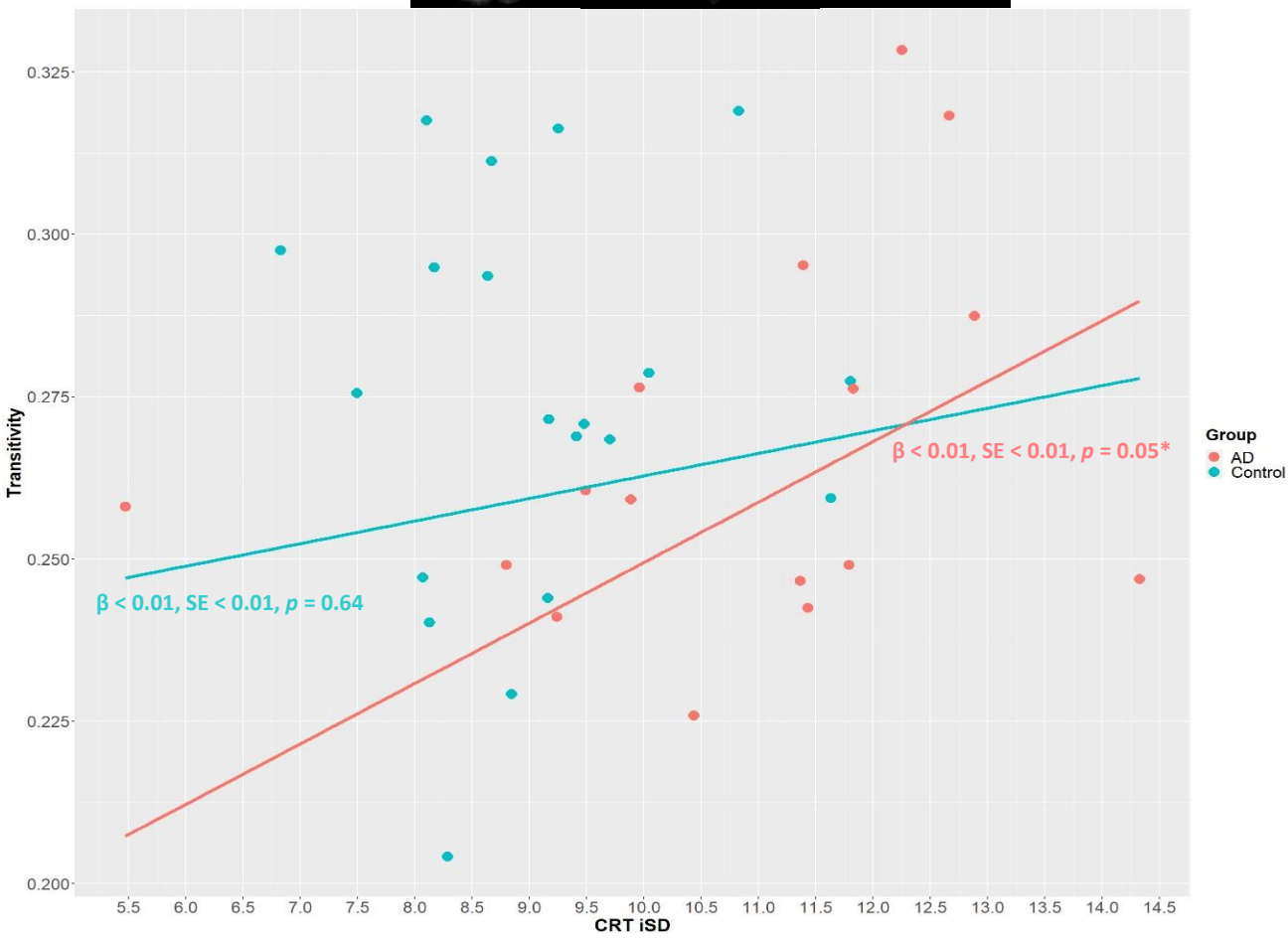

G

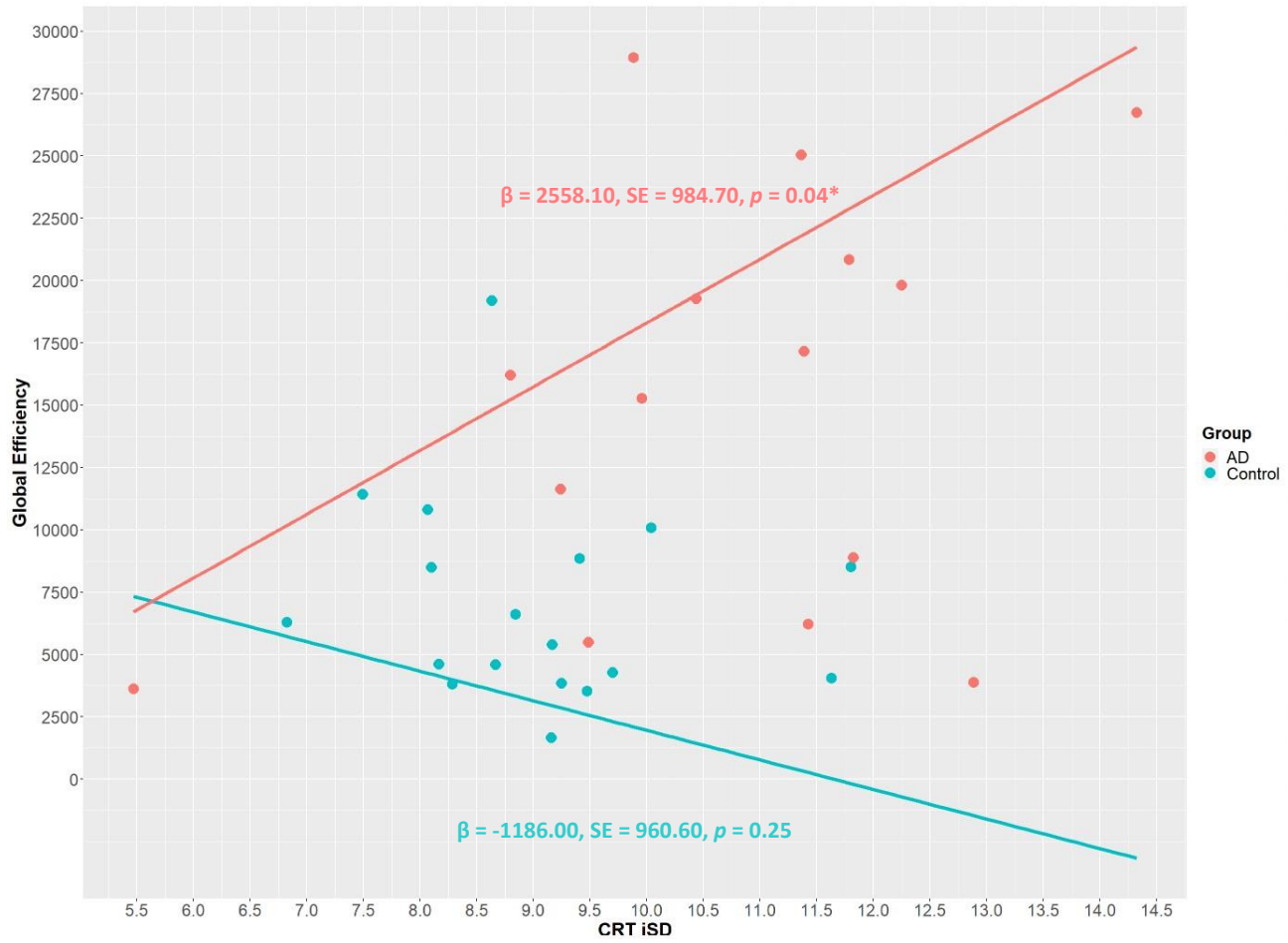

Figure 31: Scatterplots showing the relationship between graph theory measures (nodal strength, nodal efficiency, transitivity, and global efficiency) and RT IIV (SRT iSD and CRT iSD). Regression line was calculated after controlling for all covariates (sex, age, years of education, and monthly household income).

Finally, we investigated the relationship between mean RT of the two tasks and graph theory measures.

Mean SRT latency was negatively associated with transitivity of the left temporal pole (L-Tpole) (β < -0.01, SE < 0.01, p = 0.05) *(Figure 32A)* in the controls, but not in the AD patients. In the AD patients, but not in the controls, mean SRT latency was negatively associated with transitivity of the right ventral latero-dorsal nucleus thalamus (R-vent-lat-dors) (β < -0.01, SE < 0.01, p = 0.02) *(Figure 32B)*.

Mean CRT latency was negatively associated with transitivity of the left temporal pole (L-Tpole) (β < -0.01, SE < 0.01, p = 0.04) *(Figure 32C)* and positively associated with transitivity of the left caudal anterior cingulate cortex (L-caud-ant-Cing) (β < 0.01, SE < 0.01, p = 0.04) *(Figure 32D)* in the controls, but not in the AD patients. Mean CRT latency was negatively associated with transitivity of the right ventral latero-dorsal nucleus thalamus (R-vent-lat-dors) (β < -0.01, SE < 0.01, p = 0.01) *(Figure 32E)* and positively associated with nodal efficiency of the left fusiform gyrus (L-Fusiform) (β = 651.63, SE = 264.50, p = 0.04) *(Figure 32F)* in the AD patients, but not in the controls.

Neither mean SRT latency nor mean CRT latency showed an association with nodal strength and local efficiency in any region. There was also no relationship between global efficiency and mean RT on either task.

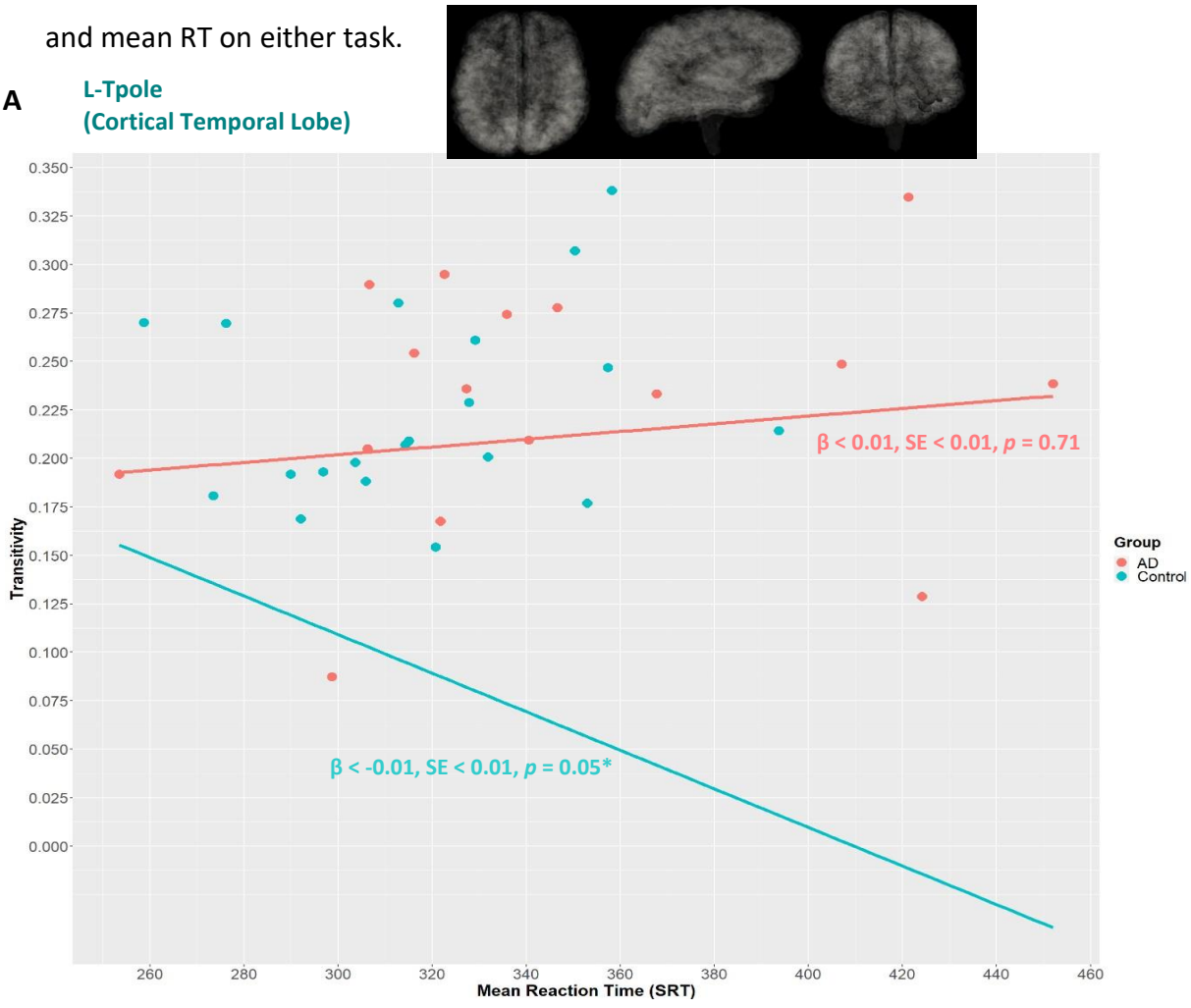

B

R-vent-lat-dors
(Subcortical Thalamus)

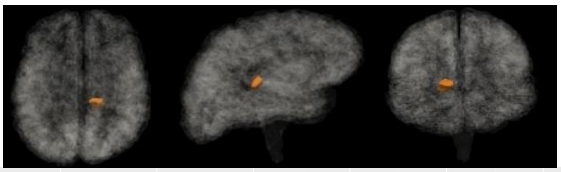

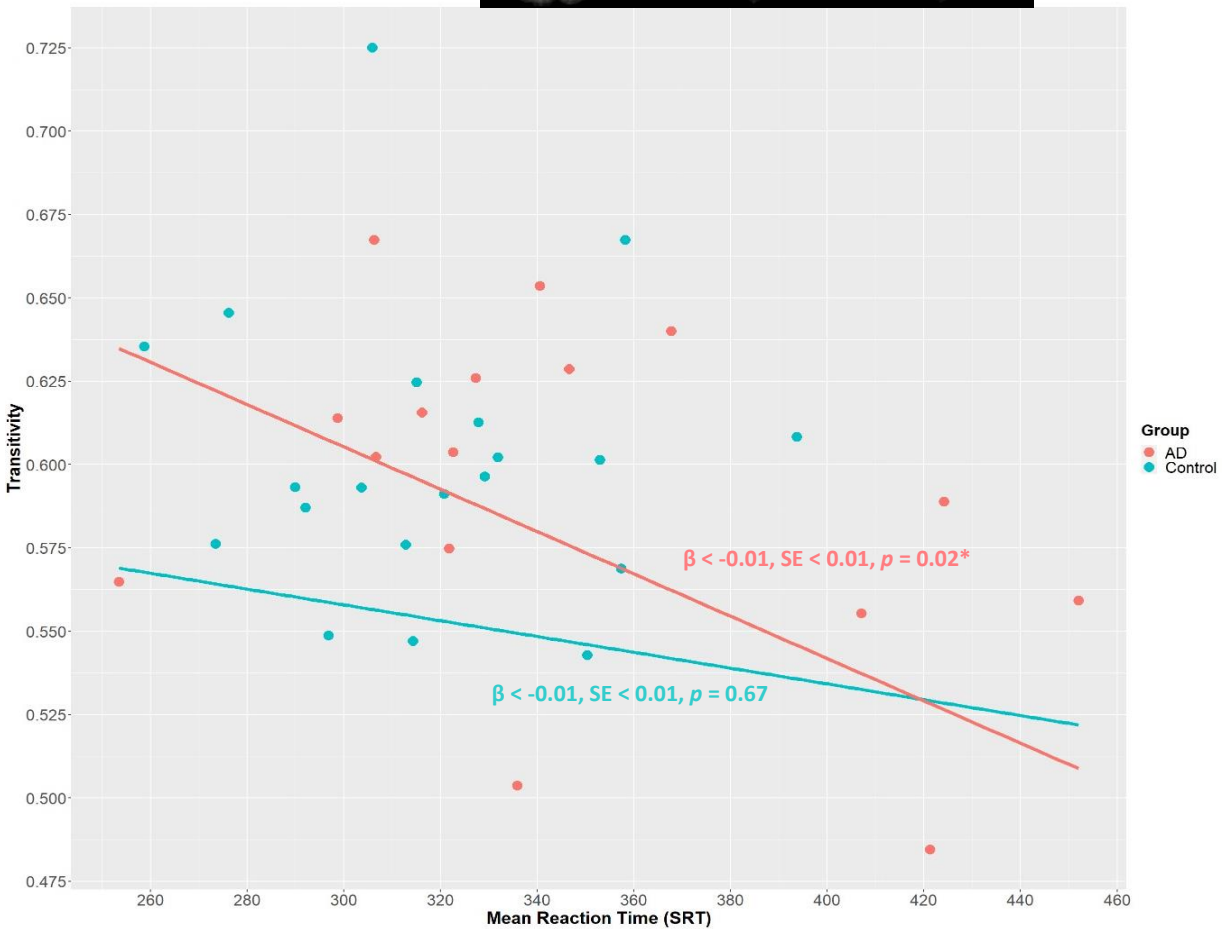

C

L-Tpole
(Cortical Temporal Lobe)

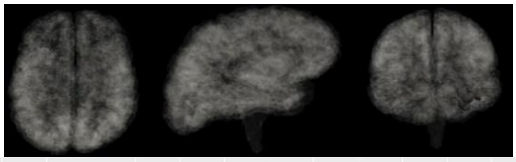

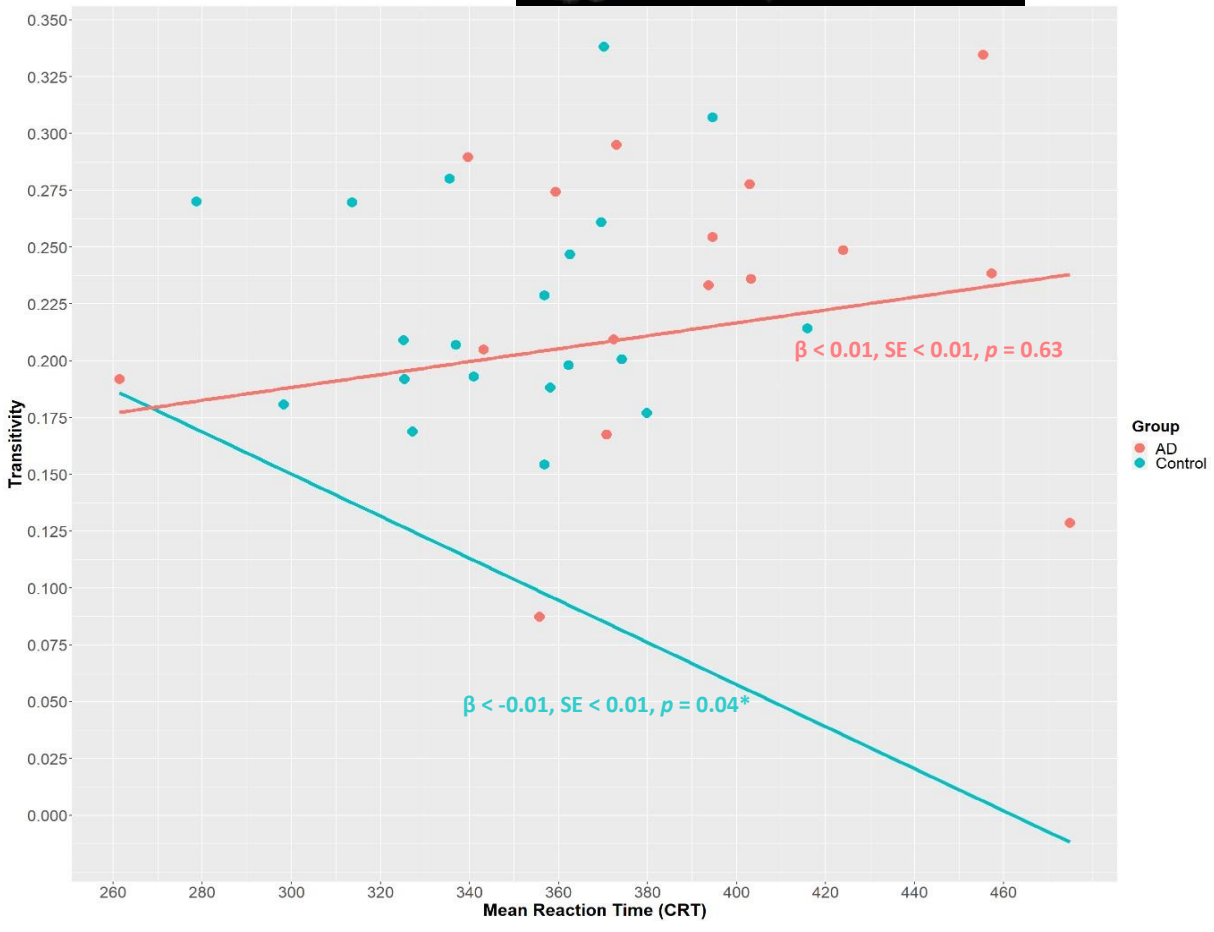

D

L-caud-ant-Cing
(Cortical Cingulate Cortex)

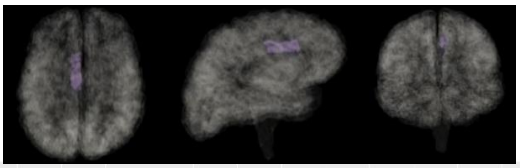

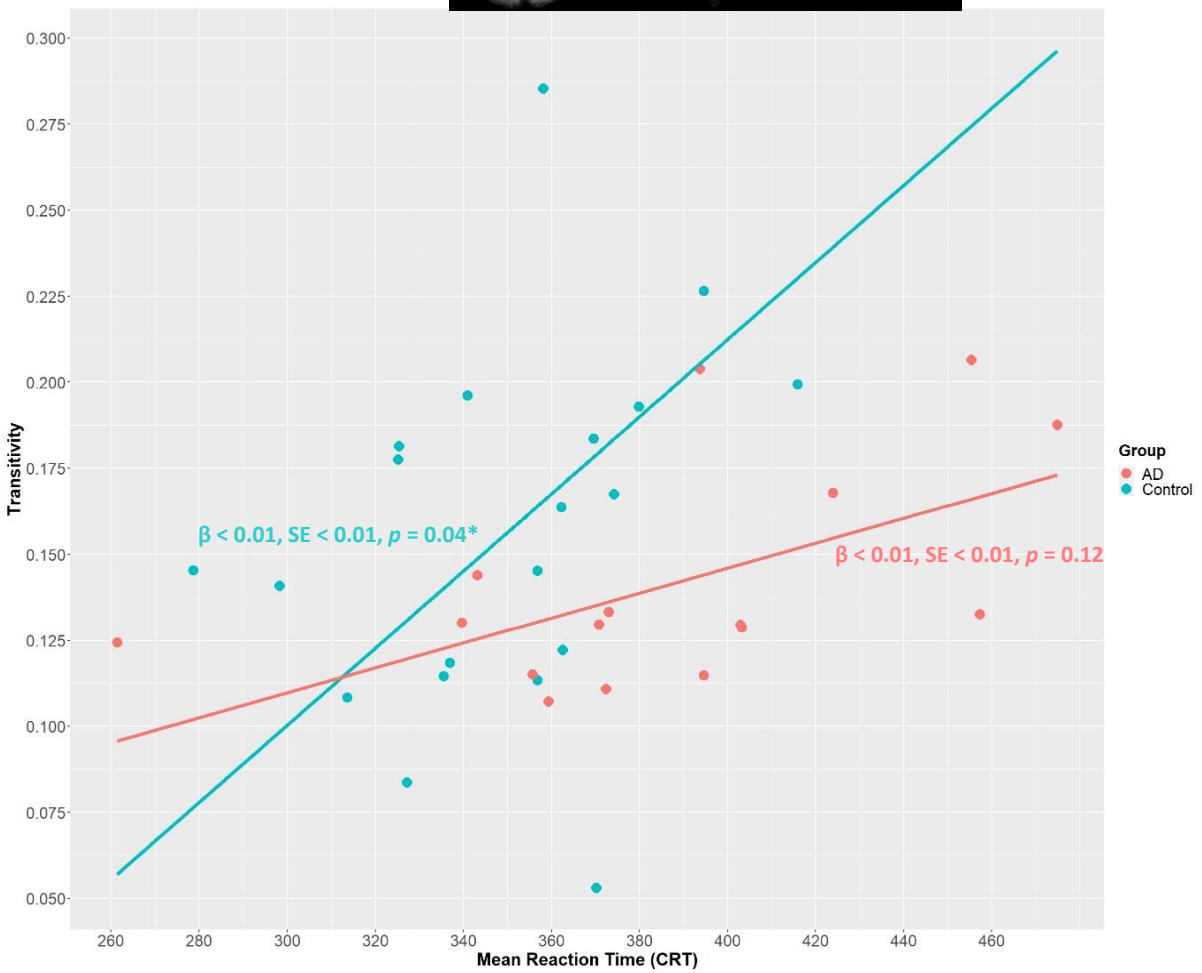

E

R-vent-lat-dors
(Subcortical Thalamus)

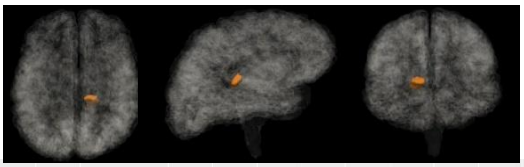

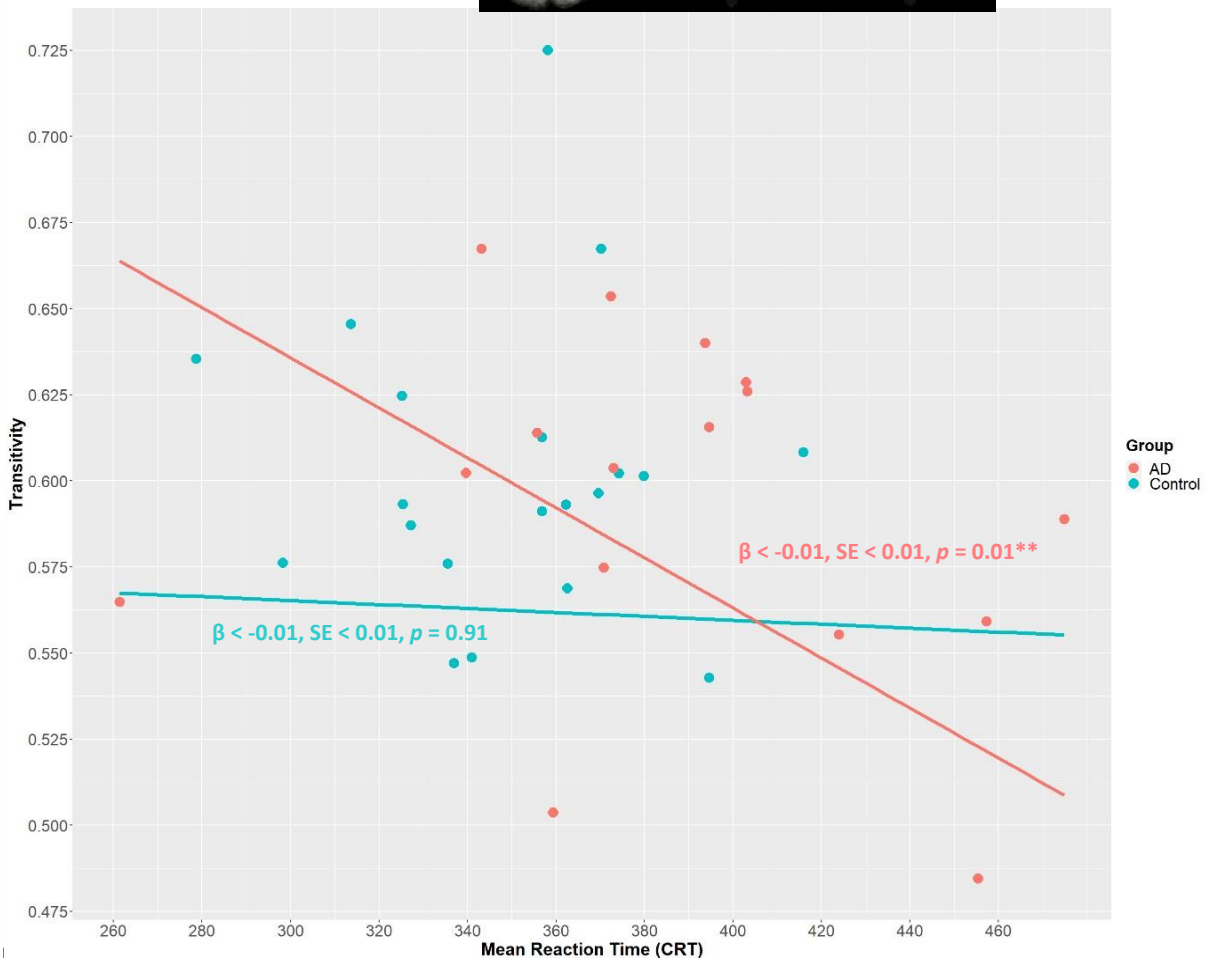

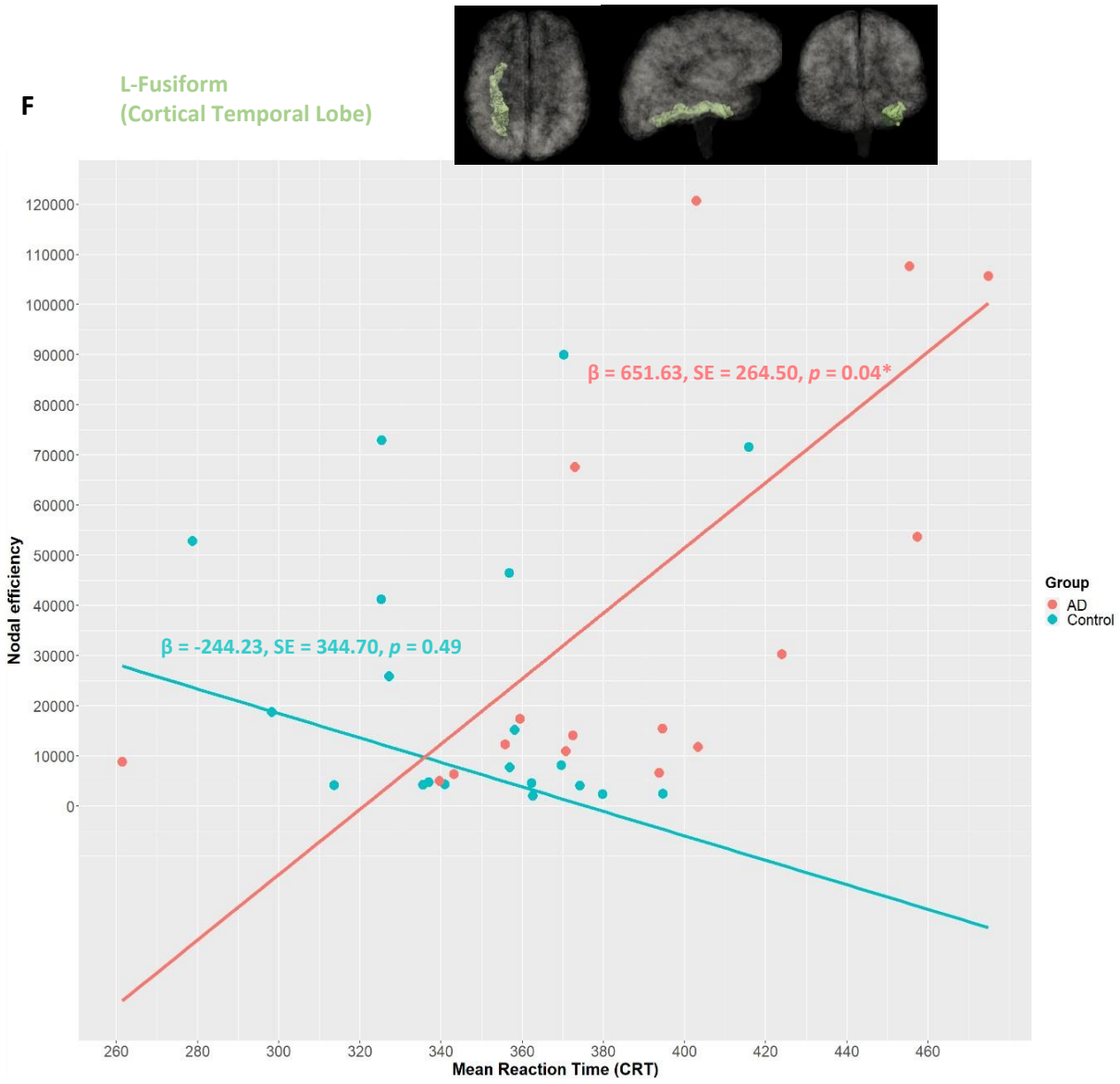

Figure 32: Scatterplots showing the relationship between graph theory measures (nodal efficiency and transitivity) and mean RT (SRT and CRT). Regression line was calculated after controlling for all covariates (sex, age, years of education, and monthly household income).

5. Discussion

Using diffusion MRI tractography, the present study sought to determine whether there are alterations in WM structural connectivity and the connectome in AD patients relative to healthy elderly controls and whether these changes contribute to intra-individual variability (IIV) on reaction time (RT) tasks.

The following were the main findings of this study:

IIV: IIV on both simple and choice RT tasks was significantly higher in the AD patients compared to healthy elderly controls *(Table 3)*. The AD patients also had significantly longer mean RT latencies than healthy elderly controls in the CRT task, but not in the SRT task *(Table 3)*.

DTI measures: In AD patients, white matter (WM) tracts with lower FA compared to healthy elderly controls were predominately located in the bilateral cortical temporal lobes, left subcortical temporal lobe and bilateral subcortical hippocampus subregions *(Figure 14, 15 and 16)*. AD patients had higher FA than controls in WM tracts from the thalamus bilaterally to the brainstem *(Figure 14, 17 and 18)*. Certain WM tracts within the thalamus had higher FA in controls than in AD patients *(Figure 15)*, whereas others had lower FA in controls *(Figure 17)*.

AD patients had higher MD in WM tracts in the bilateral cingulate cortex, left cortical occipital lobe, bilateral subcortical temporal lobes, bilateral subcortical hippocampus subregions, and right cortical temporal lobe *(Figure 19, 20, 21 and 22)*. WM tracts with lower FA and higher MD in AD patients were part of the right cortical temporal lobe, left subcortical temporal lobe, and bilateral hippocampus subregions *(Figure 15 and 21).*

Graph theory metrics: Interestingly, compared to healthy elderly controls, the AD patients had higher nodal efficiency across multiple regions *(Table 5 and Figure 27)*, as well as higher global efficiency *(Figure 30 and Table 6)*. There were group differences in graph theory measures in the cortical frontal, cortical parietal, cortical occipital, cortical and subcortical temporal lobes, as well as cortical cingulate cortex, subcortical thalamus, insula, subcortical basal ganglia, subcortical hippocampus subregions and brainstem *(Table 5)*. Some nodes had lower, and some had higher nodal strength, transitivity and local efficiency in the AD patients compared to healthy elderly controls *(Table 5, 23, 24, 25, 26, 28 and 29)*. There were no group differences in nodal degree and modularity *(Supplementary Figure 2, 3 and Supplementary Table 9)*.

Relationship between graph theory metrics and IIV: In AD patients, global efficiency was positively correlated with RT IIV on the CRT task *(Figure 31G)*. Transitivity in the left cingulate cortex and nodal efficiency in the left cortical temporal lobe were also positively correlated with RT IIV and mean RT on the CRT task in AD patients *(Figure 31F and 32F)*. On the other hand, negative relationships between transitivity in the right thalamus and RT IIV as well as between transitivity and mean RT were found on both the SRT and CRT tasks in AD *(Figure 31B, 32B and 32E)*.

5.1 RT IIV and mean RT latencies in AD

Although we found no significant group differences in mean RT latency on the SRT task, previous studies have found that mean RT on SRT tasks was significantly longer in the patient group compared to controls (Sano *et al.*, 1995; Hultsch *et al.*, 2000; Anstey *et al.*, 2007). One possible reason for these conflicting findings could be that the patient group in the Hultsch et al. (2000) and Anstey et al. (2007) studies did not only contain individuals with AD but instead consisted of individuals diagnosed with a broader range of cognitive deficits, whereas this current study only contained patients with mild-to-moderate AD. The presence of a warning signal before the target stimulus may have benefited the healthy elderly controls (Sano *et al.*, 1995) and may explain why these studies making use of warning signals found significant group differences in the SRT task (Sano *et al.*, 1995; Hultsch *et al.*, 2000). A warning signal may have caused unconscious preparedness and thus improved performance on SRT tasks.

We did, however, observe significant group differences in mean latency on the CRT task *(Table 3)*. Both SRT and CRT tasks require a component of psychomotor speed, while CRT tasks need an additional choice decision and visuospatial attention component (Levinoff, Saumier and Chertkow, 2005; Tuch *et al.*, 2005). The results from this current study may suggest that our AD patients did not have impairment in psychomotor speed and thus performed similarly to the controls on the SRT task, unlike patient groups from the previous studies (Sano *et al.*, 1995; Hultsch *et al.*, 2000; Anstey *et al.*, 2007). However, this performance was not maintained with the increased demands of the CRT task as brain mechanisms needed to perform CRT tasks may be impaired in AD patients. These would include brain regions responsible for decision-making and visuospatial attention, such as the prefrontal and frontoparietal cortex (Guo *et al.*, 2013; Somers and Sheremata, 2014). Longer latency responses may be due to an inability to sustain attention, which has been found to be affected in AD (Gorus *et al.*, 2008). Similarly, Pate et al. (1992) found that RT was slowed in the AD group compared to controls only on the CRT task, whereas Hultsch et al. (2000) and Anstey et al. (2007) found significant group differences in both tasks.

Although there were no significant group differences in mean RT latency on the SRT task, when observing RT IIV, AD patients had significantly higher *iSD* than controls on the same

task *(Table 3)*. These results may suggest that RT IIV has the ability to detect slight changes in cognitive function when mean RT was unable to. When it comes to RT IIV, our results are consistent with other studies where higher variability has been observed in AD compared to controls on both SRT and CRT tasks (Hultsch *et al.*, 2000; Gorus *et al.*, 2008; Duchek *et al.*, 2010; Kälin *et al.*, 2014; Halliday *et al.*, 2018).

These studies also reported that IIV increased with task complexity, with this increase being greatest in the AD group (Hultsch *et al.*, 2000; Gorus *et al.*, 2008). By contrast, our findings showed that only the healthy elderly controls, but not the AD patients, had higher IIV on the CRT task compared to the SRT task *(Table 3)*, i.e., IIV is only higher in more complex tasks in cognitively healthy individuals. A possibility for this could be that brain mechanisms involved in upholding constant performance are intensely impaired, thus causing AD patients to perform similarly on both tasks in spite of the increase in complexity. Similar results were previously reported in a substudy (DTI voxel-wise analysis) of the parent study done on the same cohort (Engelbrecht, in preparation).

5.2 Higher integration and altered segregation in AD

Overall, this study found regions with altered nodal strength, transitivity, and local efficiency with higher global efficiency and nodal efficiency in AD relative to healthy elderly controls. This suggests that there are both integration and segregation alterations in AD. The higher nodal strength, transitivity, nodal, local, and global efficiency in AD patients are likely compensatory mechanisms to maintain neuronal activity despite structural abnormalities. The higher global efficiency is an indication of greater network-wide interconnectivity (Rubinov and Sporns, 2010) and may indicate that atrophy in various brain regions of our AD patients resulted in the relatively unaffected regions requiring greater connectivity to work efficiently. Higher global efficiency may reflect an intrinsic alteration in brain wiring patterns. Since optimal brain function requires a balance between local segregation and global integration (Lord *et al.*, 2017), the observed combination of higher global efficiency (integration) and lower local efficiency across multiple nodes (segregation) in AD patients suggests an interruption in this balance and thus a more random network topology.

Most studies have found lower global efficiency in the WM networks of AD patients relative to controls (Lo *et al.*, 2010; T. Wang *et al.*, 2016; Zajac *et al.*, 2017). However, there are a

few studies in line with our results. In a recent rs-fMRI study, Contreras et al. (2020) observed higher global efficiency in functional networks of the AD individuals. The authors commented that even though the functional network of the AD patients had a higher mean global efficiency value relative to the controls across all ROIs (whole-brain network level), the number of ROIs with greater nodal efficiency[1] was less than that of the controls. By contrast, we observed higher nodal efficiency in AD across many regions, although local efficiency also tended to be lower, especially in the cortical temporal lobe and hippocampus subregions. In another rs-fMRI study, Supekar et al. (2008) found higher global connectivity in AD depending on the frequency band investigated. Interestingly, Wright et al. (2021) observed that their AD patients also presented with higher global efficiency than the control group, however, these were calculated through cognitive networks, in which cognitive tests were the nodes, and statistical inter-nodal significance represented the edges of the network.

We found the same number of modules in AD patients and healthy elderly controls, i.e., no group differences in modularity *(Supplementary Figure 2, 3 and Supplementary Table 9).* However, regions in the modules and connections between these regions differed between the AD patients and healthy elderly controls *(Supplementary Figure 2).* This indicates that AD patients may undergo reorganisation of structural networks, which is interpreted as effects of brain plasticity (delEtoile and Adeli, 2017). Previous studies have reported modular organisation with lower modularity in the functional network of AD patients compared to healthy controls (Brier *et al.*, 2014; Dai *et al.*, 2019), whereas other studies observed higher functional and structural networks modularity in the AD patients (Pereira *et al.*, 2016; Mijalkov *et al.*, 2017; Si *et al.*, 2019). We also did not find group differences in nodal degree, whereas Dai et al. (2019) observed lower nodal degree in both structural and functional connectomes in AD patients compared to controls.

[1] Contreras et al. (2020) described global efficiency for each node (ROI level), i.e., nodal global efficiency, as well as global efficiency across all the ROIs (whole-brain level), which corresponds to nodal efficiency and global efficiency in our study.

5.3 Alterations in WM tracts and the corresponding nodes in AD

Nodes in the cortical occipital, cortical temporal, and subcortical temporal lobes, subcortical hippocampus subregions, cortical cingulate cortex, subcortical thalamus, and brainstem, showed alterations in graph theory measures as well as alterations in DTI measures in the corresponding tracts. We present a discussion of the DTI and graph theory findings focused on the implicated WM connections and the corresponding nodes.

5.3.1 Cortical temporal, subcortical temporal lobes, and subcortical hippocampus subregions (temporal lobe)

5.3.1.1 Lower FA as well as higher MD and RD in AD patients

Temporal lobe regions, such as the entorhinal cortex, may be the very first and most severely affected by AD (Braak and Braak, 1991). In this study, four of the nine WM tracts that were identified to have group differences in FA, namely WM between the **left parahippocampal gyrus (L-Parahippo)** and the **left entorhinal cortex (L-Entorhinal),** WM between the **right parahippocampal gyrus (R-Parahippo)** and the **right hippocampus subiculum (R-Hippo-Subiculum),** WM between the **left hippocampus (L-Hippo)** and the **left hippocampus CA1 (L-Hippo-CA1),** as well as WM between the **right hippocampus subiculum (R-Hippo-Subiculum)** and the **right hippocampus CA1 (R-Hippo-CA1),** presented lower *FA* with no change in *MD* in the AD patients *(Figure 14, 15 and 16)*. Kitamura et al. (2013) investigated individuals with mild AD over a period of 18 months and similarly reported lower FA and higher RD, but no changes in MD or AxD. Lower FA values found in these regions may indicate the change or loss of WM integrity due to demyelination of axonal structures (Rose, Janke and Chalk, 2008; Nir *et al.*, 2013; Soares *et al.*, 2013). A vast number of previous DTI studies have observed lower FA in AD patients compared to control participants in the temporal lobe (Damoiseaux *et al.*, 2009; Serra *et al.*, 2010; Gao *et al.*, 2011; Chandra *et al.*, 2019), including the parahippocampal gyrus (Stricker *et al.*, 2009; Salat *et al.*, 2010; Liu *et al.*, 2011) and hippocampus (Hong *et al.*, 2013).

Furthermore, WM regions that had reduced FA in the AD group have been observed to be close in location to GM regions showing cortical volume reductions, such as the bilateral medial temporal structures (Xie *et al.*, 2006). Prior studies have noted changes including the accumulation of neurofibrillary tangles and amyloid-beta plaques as well as neuronal loss in

the medial temporal lobe, including the hippocampus CA1 and subiculum subregions and entorhinal cortex, as well as overall hippocampal atrophy in the early stages of AD (Monte, 1989; Braak and Braak, 1991; Arriagada *et al.*, 1992; Price *et al.*, 2001; Machulda *et al.*, 2009). Given the critical role of the temporal lobe in information storage and memory retrieval (Squire, Stark and Clark, 2004), these observations may be related to impaired memory function of AD and MCI patients. This is further supported by fMRI studies, where decreased medial temporal lobe activation has been found in mild-to-moderate dementia patients when they attempted to learn new information (Rombouts *et al.*, 2000; Machulda *et al.*, 2009).

The five other WM tracts, specifically WM between the **left hippocampus (L-Hippo)** and the **left hippocampus presubiculum (L-Hippo-Presubiculum),** WM between the **right hippocampus (R-Hippo)** and the **right hippocampus presubiculum (R-Hippo-Presubiculum),** WM between the **right parahippocampal gyrus (R-Parahippo)** and the **right hippocampus presubiculum (R-Hippo-Presubiculum),** WM between the **right entorhinal cortex (R-Entorhinal)** and the **right hippocampus (R-Hippo),** as well as WM between the **right hippocampus presubiculum (R-Hippo-Presubiculum)** and the **right hippocampus subiculum (R-Hippo-Subiculum),** displayed with higher *MD* with no change in *FA* in the AD patients *(Figure 19 and 21)*. Interestingly, most tracts with higher MD in this study are in the right hemisphere. MD is associated with structural organisation, with lower values indicating well-organised structure, for example, denser axonal packing. We also found higher RD in these tracts, and since MD is the linear summation of AxD and RD, significant increases of either AxD or RD causes higher MD. Higher MD is possibly due to WM injury, such as the loss or damage to myelin sheaths on axons and dendrites (Phillips *et al.*, 2016) which are normal barriers to diffusion. Similar to these findings, previous studies have also observed higher MD within the medial temporal lobe, specifically the hippocampus, amygdala, temporal gyrus, the entorhinal cortex and parahippocampal gyrus in AD patients (Rose, Janke and Chalk, 2008; Serra *et al.*, 2010; Hong *et al.*, 2013).

WM tracts in the cortical temporal lobe, subcortical temporal lobe and subcortical hippocampus subregions showed no group differences in *AxD*, which may mean an absence of axonal damage (Alexander *et al.*, 2007; Phillips *et al.*, 2016), however, most tracts presented higher *RD* in AD patients pointing to regional myelin damage, reduced

myelination or myelin loss (Alexander *et al.*, 2007). It is, therefore, reasonable to speculate that the lower FA and higher MD found was driven mainly by RD, similarly to the observation made by Stricker et al. (2009). Supporting this, previous animal studies in triple-transgenic AD mice showed indications of myelin disruptions in the entorhinal cortex and hippocampus even prior to beta-amyloid plaques and neurofibrillary tangles formation (Desai *et al.*, 2009). When controlling for T2 intensity, Salat et al. (2010) also observed that regionally overlapping changes in FA and MD (lower FA, higher MD and RD) was greatest in the medial temporal lobe.

Areas in the brain that are the last to myelinate, such as the hippocampus and entorhinal cortex, are also the first to degenerate in AD (Braak and Braak, 1991; Reisberg *et al.*, 1999, 2002; Stricker *et al.*, 2009; Bartzokis, 2011). These regions are mainly in the temporal lobe, both cortical and subcortical, and are most vulnerable to the pathological changes seen in AD (Atiya *et al.*, 2003; Du *et al.*, 2004; Pennanen *et al.*, 2004; Salat *et al.*, 2009; Guo *et al.*, 2010; Li *et al.*, 2011; Chandra *et al.*, 2019; Kulason *et al.*, 2020). This concurs with whole-brain voxel-based morphometry (VBM) investigations (Frisoni *et al.*, 2002; Hirata *et al.*, 2005), where atrophy in the medial and lateral temporal regions has been found to be more pronounced compared to other regions (Serra *et al.*, 2010), and PET imaging studies, where hypometabolism in the temporal lobes has been observed (Herholz *et al.*, 2002; Langbaum *et al.*, 2009).

5.3.1.2 Higher transitivity and nodal efficiency, altered local efficiency and lower nodal strength in AD patients

The following regions had group differences in both DTI measures and graph theoretical measures in the temporal lobe: the **entorhinal cortex bilaterally (R-Entorhinal, L-Entorhinal),** the **right parahippocampal gyrus (R-Parahippo),** the **hippocampus bilaterally (R-Hippo, L-Hippo),** the **right hippocampus subiculum (R-Hippo-Subiculum),** the **right hippocampus presubiculum (R-Hippo-Presubiculum)** and the **hippocampus CA1 bilaterally (R-Hippo-CA1, L-Hippo-CA1)**. Results found in the parahippocampal gyrus will be discussed in *section 5.3.2.2* below.

Compared to controls, AD patients showed:

1) Higher *transitivity* in the **right entorhinal cortex** *(Table 5 and Figure 26).*

2) Lower *local efficiency* in the **entorhinal cortex bilaterally,** the **right hippocampus CA1** and the **right hippocampus presubiculum**, as well as higher *local efficiency* in the **right hippocampus subiculum** and the **right hippocampus** *(Table 5, Figure 28 and 29).*
3) Higher *nodal efficiency* in the **right parahippocampal gyrus,** the **hippocampus bilaterally,** the **right hippocampus subiculum** and the **left hippocampus CA1** *(Table 5, Figure 27).*
4) Lower *nodal strength* in the **left hippocampus** *(Table 5 and Figure 23).*

We observed lower local efficiency and nodal strength, mainly in the hippocampus. Conversely, in a PET imaging study, Veronese et al. (2019) reported that the highest increase in terms of strength was found in the hippocampus. Lower nodal strength may suggest weaker connectivity and reduced WM integrity, specifically in the hippocampus. Since DTI results in the hippocampus WM tracts included both lower FA and higher MD in the AD patients, degeneration of fibre bundles used for information transmission in the hippocampus is likely present. This may indicate abnormal connections between the temporal lobes.

The lower local efficiency observed may suggest structural disruptions of short-range connections within regions involved in memory function, mostly in and around the hippocampus, and may be related to impairment in functional segregation in episodic memory. Previous sMRI studies similarly found lower local efficiency in the hippocampus, but simultaneously found higher local efficiency in the left entorhinal cortex (Mijalkov *et al.*, 2017), where we observed lower local efficiency.

In line with these observations, reduced local efficiency in aMCI patients that converted to AD compared to controls has been reported in the temporal cortices, namely the left superior temporal gyrus, right temporal pole, and bilateral hippocampus (Sun *et al.*, 2019). Furthermore, Filippi et al. (2018) investigated alterations in structural and functional connectivity as well as changes in the structural and functional connectome along the AD continuum. They identified structural connectivity disruptions, i.e., lower FA and higher MD (which we also observed in this study), with decreased FC as well as lower nodal strength and local efficiency in the hippocampal, medial and lateral temporal nodes bilaterally in AD.

However, we also found higher local efficiency and higher nodal efficiency in some parts of the hippocampus, e.g., the right hippocampus subiculum, in AD patients. This could be due to the brain network losing some of its long-distance connections to these parts of the hippocampus resulting in a relative increase in the number of connections to a node's immediate neighbours, thus leading to the formation of new paths for communication. Increase in local connections could lead to a more segregated pattern of connectivity and is an indication of abnormal network function. Sheng et al. (2021) proposed that regional brain compensation may start from the medial temporal lobe, as they reported more elevated nodal properties with increased AD progression. Rs-fMRI studies reported reduced connectivity within the medial temporal lobe in AD patients (Filippi *et al.*, 2018), whereas MCI patients showed increased connectivity (Das *et al.*, 2013; Berron *et al.*, 2020). It is, therefore, possible that the current analyses detected higher local efficiency and higher nodal efficiency because our observations may be more influenced by the AD patients at the earlier stage of the disease, i.e., mild AD. Contrary to our results, Zajac et al. (2017) observed lower nodal efficiency in the left hippocampus and the left entorhinal cortex in AD patients relative to controls.

We observed varying local efficiency and higher nodal efficiency in the CA1 and subiculum hippocampal subregions: areas that show accumulation of neurofibrillary tangles and amyloid-beta plaques and neuronal loss in the early stages of AD (Monte, 1989; Arriagada *et al.*, 1992; Price *et al.*, 2001). Due to these pathological changes and atrophy in the hippocampus, these regions may increase connectivity with their neighbouring nodes to maintain certain functions.

We also observed higher transitivity in the right entorhinal cortex in AD patients compared to healthy elderly controls. This finding may suggest that the entorhinal cortex is so severely damaged in AD, as reported in previous studies (Braak and Braak, 1991; Reisberg *et al.*, 1999, 2002; Stricker *et al.*, 2009; Bartzokis, 2011), that the neighbouring nodes connect to each other to maintain function.

5.3.1.3 Higher local efficiency, nodal efficiency and nodal strength and altered transitivity without DTI alterations in AD patients

Some regions in the temporal lobe showed group differences in graph theory measures but no differences in DTI measures. These regions showed:

1) Higher *nodal efficiency* in the **right hippocampus molecular layer HP (R-Hippo-MolecularLayerHP),** the **left middle temporal gyrus (L-mid-T)**, the **bilateral fusiform gyrus (R-Fusiform, L-Fusiform)** and the **left temporal pole (L-Tpole)** *(Table 5 and Figure 27).*
2) Higher *nodal strength* in the **left middle temporal gyrus (L-mid-T)** and the **left superior temporal gyrus (L-sup-T)** *(Table 5 and Figure 24).*
3) Lower *transitivity* in the **left superior temporal gyrus (L-sup-T),** as well as higher *transitivity* in the **right fusiform gyrus (R-Fusiform),** the **bilateral inferior temporal gyrus (R-inf-T, L-inf-T)** and the **left temporal pole (L-Tpole)** *(Table 5, Figure 25 and 26)***.**
4) Higher *local efficiency* in the **right superior temporal gyrus (R-sup-T)** and the **left fusiform gyrus (L-Fusiform)** *(Table 5 and Figure 29).*

Although we found elevated nodal efficiency in AD in widespread regions of the temporal lobe and hippocampus, Lo et al. (2010), investigating the topological organisation of structural cortical networks in AD using DTI tractography, reported lower nodal efficiency, mainly in the frontal regions, with only one region in the temporal lobe: the temporal pole. Another study by Wang et al. (2016) also found lower nodal efficiency in the right middle temporal pole and right fusiform gyrus in the temporal lobe. The discrepancies in findings could be due to methodological differences, as we used full-probabilistic tractography to construct the WM networks whereas Lo et al. (2010) used streamline tractography and thus did not study subcortical regions, such as the hippocampus.

Interestingly, the higher nodal strength, nodal efficiency, local efficiency, and transitivity in AD patients are mostly seen in the cortical temporal lobe regions. These increases could reflect a compensatory mechanism where the number of local connections to the cortical temporal lobe increases in order to compensate for the loss of connections between distant areas. In a structural imaging study, Mijalkov et al. (2017) observed higher local efficiency in the temporal lobe, specifically in the bilateral temporal pole and left entorhinal cortex.

However, although we found lower local efficiency in the left as well as the right entorhinal cortex in AD, we found higher transitivity and nodal efficiency but no difference in local efficiency in the temporal pole. Mijalkov et al. (2017) also found lower local efficiency in the bilateral inferior temporal lobe, whereas we found higher transitivity in this region.

5.3.2 Cortical cingulate cortex, cortical occipital, and cortical temporal lobes

5.3.2.1 Higher MD and AxD in AD patients

The current results observed higher *MD* with no change in *FA* and *RD* in WM tracts between the cortical cingulate cortex, cortical occipital and cortical temporal lobes, specifically WM between the **right isthmus of the cingulate gyrus (R-isthmus-Cing)** and the **right parahippocampal gyrus (R-Parahippo),** as well as WM between the **left isthmus of the cingulate gyrus (L-isthmus-Cing)** and the **left lingual gyrus (L-Lingual),** in the AD patients compared to healthy elderly controls *(Figure 19, 20 and 22).* This may indicate increased fibre degeneration, possibly from axonal membrane disruption or myelin loss in these tracts. These results are consistent with another DTI tractography study that consisted of 25 AD patients, 19 aMCI patients and 15 healthy controls, where Pievani et al. (2010) found significant WM damage in aMCI and AD in the limbic pathways, such as the cingulum and fornix, as well as the major cortico-cortical WM tracts. They reported significantly higher MD in the cingulum, without FA, AxD and RD changes. These MD changes in the WM of the cingulum have also been found to be located next to areas of macroscopic GM atrophy, including the hippocampus (Serra *et al.*, 2010), which are regions that have been found to be implicated in AD individuals (Atiya *et al.*, 2003; Du *et al.*, 2004; Pennanen *et al.*, 2004; Li *et al.*, 2011; Chandra *et al.*, 2019; Kulason *et al.*, 2020). Another study found more widespread changes in MD than FA, with higher MD in the ventromedial frontal, occipital, temporal, precuneus and cingulum regions (Salat *et al.*, 2010). Similarly, lower MD has also been observed in the parahippocampal gyrus (Zhang *et al.*, 2007; Rose, Janke and Chalk, 2008; Salat *et al.*, 2010; Serra *et al.*, 2010). In contrast to the current findings, Ryan et al. (2013) found reduced MD and AxD in the right cingulum in pre-symptomatic patients affected by a familial AD gene variant.

While we did not detect FA changes in the WM tracts mentioned above, other studies have reported lower FA in the cingulum of AD (Xie *et al.*, 2005; Zhang *et al.*, 2007, 2013; Damoiseaux *et al.*, 2009; Stricker *et al.*, 2009; Liu *et al.*, 2011; S.-H. Lee *et al.*, 2015; Chandra *et al.*, 2019), such as the isthmus of the cingulum, with higher RD (Zhang *et al.*, 2013; S.-H. Lee *et al.*, 2015) and AxD (S.-H. Lee *et al.*, 2015). Lower FA has also been observed in the parahippocampus (Zhang *et al.*, 2007; Stricker *et al.*, 2009; Salat *et al.*, 2010; Liu *et al.*, 2011) and lingual gyrus in the occipital lobe (Ibrahim *et al.*, 2009).

We also found higher *AxD* in the WM from the left isthmus of the cingulate cortex to the left lingual gyrus *(Figure 20)*, with no change in *AxD* between the right isthmus of the cingulate cortex and parahippocampal gyrus *(Figure 22*). However, a shorter average length (BL) of the latter was also detected *(Supplementary Table 7)*. The higher *MD* and the lower *BL* may suggest that these tracts, due to WM injury or atrophy, such as the loss or damage of neurons, have caused the average length of that bundle to be shorter in AD patients. This is a reasonable speculation as atrophy is known to occur in the parahippocampus (Salat *et al.*, 2009; Guo *et al.*, 2010; Wang *et al.*, 2012) and limbic structures, such as the cingulate gyrus (Thompson *et al.*, 2003; De Jong *et al.*, 2008; Mcevoy *et al.*, 2009; Guo *et al.*, 2010), in AD. Structurally, the WM tracts mentioned above are connected to each other. The isthmus of the cingulate cortex connects inferiorly with the parahippocampal gyrus, and the front of the lingual gyrus continues on the surface of the temporal lobe and joins the parahippocampal gyrus (Murphy, 2017; Jumah and Dossani., 2021). In a structural imaging study, Yang et al. (2019) observed significant reductions in cortical thickness in the left isthmus of the cingulate cortex, left lingual gyrus as well as the right parahippocampal gyrus in the AD patients compared to controls, with these three regions also significantly reduced when comparing patients with AD to patients with aMCI. In rs-fMRI studies, the posterior/isthmus cingulate cortex presented reduced FC during the preclinical and clinical AD stages (Buckner *et al.*, 2005, 2009).

Salat et al. (2010) also found higher AxD in the lateral occipital/lingual gyrus, periventricular, and callosal regions. Some studies have also reported higher AxD in both normal ageing and AD (Acosta-Cabronero *et al.*, 2010; Sullivan, Rohlfing and Pfefferbaum, 2010; Agosta *et al.*, 2011; Bosch *et al.*, 2012; Nir *et al.*, 2013) while others have noted very little to no change in AxD with age (Lebel *et al.*, 2008). Additionally, an elevated AxD associated with clinical

impairment (Nir *et al.*, 2013) was found. Acosta-Cabronero et al. (2012) studied 21 very mild, 22 mild AD patients with 26 controls and proposed that early MD increases are paired with an increase in AxD. RD and FA, on the other hand, showed more pronounced changes as disease severity increased, while AxD remained relatively stable. They proposed that MD alternations seen in more severe disease stages may be affected by the higher RD. Therefore, our MD findings may indicate that WM tracts between the cingulate cortex and occipital lobe are one of the firsts to be affected in AD, while WM tracts between the cingulate cortex to temporal lobe are only implicated later on as disease progresses. This contradicts the findings of previous studies where the temporal lobe has been found to be first affected in AD (Atiya *et al.*, 2003; Du *et al.*, 2004; Pennanen *et al.*, 2004; Li *et al.*, 2011; Chandra *et al.*, 2019; Kulason *et al.*, 2020). Consistent with our findings, Huang et al. (2013) also reported increased MD with increased AxD in projection tracts, however, they found that these features were most pronounced in regions less affected in AD. Another speculation is that this change in AxD is due to inflammation and microglial activation in AD and may represent something more than just axonal loss.

Notably, studies have found higher AxD and RD in combination with MD in AD patients compared to healthy controls (Nir *et al.*, 2013; Nowrangi *et al.*, 2013; Firbank *et al.*, 2016) bilaterally in the WM of the caudal cingulum bundle, caudal corpus callosum, parahippocampal gyrus, caudal temporal and parietal regions, where temporal pole, rostral corpus callosum, prefrontal WM and caudal occipital lobe were spared (Acosta-Cabronero *et al.*, 2010).

5.3.2.2 Higher nodal efficiency in AD patients

With respect to graph theoretical measures in the cortical cingulate cortex, cortical occipital, and cortical temporal lobes, we only found one region that also had higher MD in AD patients in these locations: the **right parahippocampus gyrus (R-Parahippo)**. Our results showed higher *nodal efficiency* in the **right parahippocampus gyrus** in AD patients compared to healthy elderly controls. Interestingly, this region had the biggest difference in mean nodal efficiency between the two groups of all the regions. This is consistent with observations in a recent study, where the authors investigated differences in network properties as well as the relationship between these network properties, impaired cognition, and pathological biomarkers between 34 healthy controls, 70 MCI and 40 AD

patients. They reported higher nodal properties in the medial temporal lobe, specifically the right parahippocampal gyrus and right amygdala, with increased AD progression (Sheng *et al.*, 2021). The authors proposed that this could be due to the reorganisation/compensatory mechanisms of structural networks and thus show high resilience to network integrity damages in AD patients, which has also been seen in MCI individuals in other studies (Liu *et al.*, 2020). Conversely, Wang et al. (2016) found lower nodal efficiency in the right parahippocampal gyrus. In addition, Zhao et al. (2017) reported significant correlations between lower nodal efficiency and impaired memory performance in the bilateral parahippocampal gyrus of aMCI patients, but not controls.

5.3.2.3 Higher nodal efficiency and nodal strength as well as lower transitivity without DTI alterations in AD patients

Some regions in the cingulate cortex, cortical occipital and cortical temporal lobes showed group differences in graph theory measures but no differences in DTI measures. When comparing AD patients to healthy elderly controls, we found that AD patients had:

1) Higher *nodal efficiency* in the **right lateral occipital gyrus (R-lat-Occ)** *(Table 5 and Figure 27).*
2) Higher *nodal strength* in the **bilateral posterior cingulate cortex (R-pos-Cing, L-pos-Cing)** *(Table 5 and Figure 24).*
3) Lower *transitivity* in the **left posterior cingulate cortex (L-pos-Cing)** and the **left caudal anterior cingulate cortex (L-caud-ant-Cing)** *(Table 5 and Figure 25).*

These results are surprising as a node with high nodal efficiency and strength indicates higher information flow and may be efficiently connected to other nodes in the network (Kim *et al.*, 2014), i.e., more robust connectivity (Mijalkov *et al.*, 2017; Kim and Min, 2020). One of the major areas responsible for visual object processing includes the lateral occipital gyrus (Nagy, Greenlee and Kovács, 2012). As mentioned above, these results of this enhanced variation may indicate a compensatory mechanism to maintain a high level of visual object processing despite the pathological process. Our findings involving the occipital lobe corresponds to the same region, i.e., the lateral occipital cortex, that has been reported to show a faster rate of atrophy with increased impairment in AD patients compared to controls (McDonald *et al.*, 2009). In contrast to our findings, Wang et al. (2016) observed

reduced nodal efficiency in the bilateral superior occipital gyri, the right middle occipital gyrus, right inferior occipital gyrus and bilateral cuneus.

We also observed lower transitivity, specifically in the left anterior and posterior cingulate cortex. Lower transitivity may represent transitory myelin damage (Kocevar, Gabriel Stamile *et al.*, 2016), suggesting that these regions are poorly connected to their neighbouring areas and that their neighbouring areas are also poorly connected to each other. Although we did not find any MD changes in these particular tracts, they are all situated very close to regions where we found higher MD. However, Zhang et al. (2007) observed both lower FA and higher MD in the posterior cingulate cortex with FA reductions extending to the splenium of the corpus callosum in AD. This could indicate that the WM and GM are affected around the posterior cingulate cortex, i.e., neighbouring nodes. Current findings include both higher nodal strength and lower transitivity in the posterior cingulate cortex. However, the lower transitivity is only seen in the left hemisphere.

Thompson et al. (2003) observed that GM loss tends to occur faster in the left hemisphere than the right as time progresses, with most significant impairments in the temporal, parietal and occipital lobes as well as the cingulate cortices with the frontal lobe being relatively spared earlier in AD. Our observations of higher nodal strength in the left hemisphere suggest that the connections between the posterior cingulate cortex to the neighbouring nodes are stronger in AD patients. However, there is a lower probability that these neighbour nodes are also connected to each other, i.e., lower transitivity. Hence, there may be a lot of information being transmitted to and from the posterior cingulate cortex, but because there is no change in nodal efficiency or local efficiency, this information is not transferred efficiently. In addition, the lower transitivity in the posterior cingulate cortex may indicate that although a lot of information is transferred from this region to its neighbouring regions because these regions aren't connected, the information transfer stops around the posterior cingulate cortex.

The posterior cingulate cortex is believed to be involved in self-referential thought and episodic memory (Raichle, 2015), and thus we propose that the right hemisphere posterior cingulate cortex may show a compensatory mechanism to at least partially keep up with episodic memory and self-referential thought. This hyperconnectivity may result in early disease states (Hillary *et al.*, 2015). We speculate that the cingulate cortex is severely

affected in our AD patients as both the anterior and posterior cingulate cortex has reduced transitivity, which indicates weak segregation in the cingulate cortex and that its regions are not well connected to each other. Catheline et al. (2008) examined the cingulum tract and observed both the anterior and posterior regions to have disruptions in AD.

We did not find any group differences in nodal degree. On the other hand, other studies have observed that AD patients showed changes in the number of connections in regions that are part of the DMN, such as the anterior cingulate and posterior cingulate gyri, compared to controls or patients with MCI (Mijalkov *et al.*, 2017). A possible reason why we did not find differences in nodal degree in these regions could be that these regions had the same amount of connections to the surrounding regions, but that neighbouring regions are not connected to each other. Neighbouring regions around the anterior and posterior cingulate cortex include the retrosplenial cortex and corpus callosum, which we did not investigate, but have been found to be implicated in AD in previous studies (Acosta-Cabronero *et al.*, 2010; Tan *et al.*, 2013). There is consistent evidence that the cingulate cortex is one of the earliest sites affected by AD where atrophy rates are among the greatest (Thompson *et al.*, 2003; Buckner *et al.*, 2005; De Jong *et al.*, 2008; Mcevoy *et al.*, 2009; Guo *et al.*, 2010; Zhao *et al.*, 2019).

5.3.3 Subcortical thalamus and brainstem

5.3.3.1 Lower within-thalamus FA and higher FA in tracts between thalamus and brainstem

Prior structural imaging studies observed AD to affect limbic structures, such as the thalamus (De Jong *et al.*, 2008; Guo *et al.*, 2010; Zarei *et al.*, 2010). Most previous studies have found thalamic abnormalities to occur secondary to entorhinal cortex alterations, although this idea has been challenged in recent years (Aggleton *et al.*, 2016). A recent study that assessed GM volume using VBM analysis in a large cohort of individuals showed that at the start of cognitive decline, GM loss was observed in the bilateral ventrolateral regions of the thalamus (Van De Mortel, Thomas and Van Wingen, 2021). However, with disease progression, the GM loss seemed more prominent in areas such as the hippocampus and parahippocampal gyrus, while the magnitude of GM loss of the thalamus does not further progress (Van De Mortel, Thomas and Van Wingen, 2021). There is some evidence that the thalamus, specifically the anterodorsal thalamic nucleus, undergoes neurofibrillary

changes at the same time as the hippocampus, which have been found to be affected in the early stage of the disease (Braak and Braak, 1991).

The thalamus is involved in attention and episodic memory functioning, which have been seen to be implicated in AD (Gorus *et al.*, 2008). It possesses an abundant number of connections to medial temporal structures, which are well recognised to be responsible for memory. In the current study, all WM tracts found to have AD-related alterations in the thalamus and brainstem showed either higher or lower *FA* with no change in *MD.* Lower *FA* was observed in WM tracts between regions within the thalamus, particularly WM between the **right central lateral-lateral posterior-medial pulvinar (R-cent-lat-lat-pos-med-Pulvinar)** and the **right ventral latero-ventral thalamus (R-vent-lat-vent),** as well as WM between the **left anterior thalamus (L-ant)** and the **left central lateral-lateral posterior-medial pulvinar** (**L-cent-lat-lat-pos-med-Pulvinar)** in AD patients *(Figure 14 and 15)*. These results concur with previous DTI studies in AD (Rose, Janke and Chalk, 2008; Damoiseaux *et al.*, 2009; Serra *et al.*, 2010).

The WM tract between the right central lateral-lateral posterior-medial pulvinar and right ventral latero-ventral thalamus also presented with a lower number of tracts *(NT) (Supplementary Table 6)*. A lower number of tracts could be the reason for lower FA, as lower FA values indicate the loss of WM integrity. Similarly, Van De Mortel, Thomas and Van Wingen (2021) reported the largest volume reductions occurred around the pulvinar in the posterior thalamus, a structure involved in visual information processing.

Interestingly, current findings presented higher *FA* in the WM between the **left central lateral-lateral posterior-medial pulvinar (L-cent-lat-lat-pos-med-Pulvinar)** and the **brainstem midbrain (Brain-Stem-Midbrain),** WM between the **left pulvinar (L-Pulvinar)** and the **brainstem midbrain (Brain-Stem-Midbrain),** WM between the **right pulvinar (R-Pulvinar)** and the **brainstem midbrain (Brain-Stem-Midbrain),** as well as WM between the **left pulvinar (L-Pulvinar)** and the **left ventral latero-ventral thalamus (L-vent-lat-vent)** in AD patients compared to healthy elderly controls *(Figure 14, 17 and 18).* A previous study investigated subjects with pre-symptomatic and symptomatic carriers of an autosomal dominant gene variant predisposing them to AD and found that at the pre-symptomatic stage, individuals displayed reduced volumes of the left thalamus and bilateral caudate as well as higher FA of bilateral thalamus and left caudate compared to controls (Ryan *et al.*,

2013). FA did not differ from controls at the symptomatic stage, but MD was higher (Ryan *et al.*, 2013). The high FA in the WM tracts between the thalamus and brainstem observed in the current study may therefore be driven by the mild AD patients in our study. We propose that FA first appears to increase with GM loss in the thalamus during the very early stages of the disease. The marked anisotropy of the thalamus and brainstem may be due to their compartmentalised cytoarchitectural organisation as well as large numbers of WM fibres passing through these locations. This is further supported by our finding of higher AxD, number of voxels *(NV)* and physical volume of the tracts *(PV) (Supplementary Table 6).* As these tracts did not display RD group differences, demyelination would not explain the FA differences observed between AD patients and healthy elderly controls. Mole et al. (2016) proposed that higher FA observed in motor tracts in Parkinson's disease may reflect compensatory reorganisation of neural circuits, indicating adaptive or extended neuroplasticity. This may also explain our findings of high FA in WM tracts between the thalamus and brainstem in AD. In contrast to our findings, Liu et al. (2011) observed lower FA in both MCI and AD patients compared to controls in WM tracts of the brainstem using voxel-based analysis and ROI-based analysis.

It has been postulated that since the brainstem is connected with several cortical structures and is responsible for numerous autonomic, behavioural and cognitive functions, it may be involved in the progression of AD (J. H. Lee *et al.*, 2015). Neuropathological studies suggest that tau pathology occurs earliest in the brainstem before cortical changes (Grinberg *et al.*, 2009; Simic *et al.*, 2009; Braak *et al.*, 2011), with the largest amount of amyloid deposited in the midbrain compared to other parts of the brainstem (Brilliant *et al.*, 1992). Structural imaging studies reported that the AD group exhibited smaller volumes of the midbrain, whole brainstem (J. H. Lee *et al.*, 2015; Dutt *et al.*, 2020), locus coeruleus and pons (Dutt *et al.*, 2020) relative to healthy controls. In addition, Dutt et al. (2020) observed smaller midbrain volumes in the elderly controls who later developed AD relative to those who did not progress to AD, suggesting that these volumes are predictive of AD progression. These observed pathological changes and structural alterations in earlier stage AD attracted interest towards the brainstem, bringing about new studies on the region and rethinking/testing old hypotheses.

5.3.3.2 Lower nodal strength and transitivity and higher nodal efficiency in AD

The following regions showed group differences in both DTI measures and graph theory measures: the **right central lateral-lateral posterior-medial pulvinar (R-cent-lat-lat-pos-med-Pulvinar),** the **ventral latero-ventral thalamus bilaterally (R-vent-lat-vent, L-vent-lat-vent),** the **left pulvinar (L-Pulvinar) and** the **left anterior thalamus (L-ant).**

In these regions, compared to controls, AD patients presented with:

1) Lower *nodal strength* in the **right central lateral-lateral posterior-medial pulvinar,** the **ventral latero-ventral thalamus bilaterally and** the **left pulvinar** *(Table 5 and Figure 23).*
2) Higher *nodal efficiency* in the **left ventral latero-ventral thalamus** *(Table 5 and Figure 27).*
3) Lower *transitivity* in the **left anterior thalamus** *(Table 5 and Figure 25).*

The lower nodal strength, i.e., weaker connectivity, in the thalamus suggests damage to WM integrity, which may result in longer pathways to connect different regions in the brain. Our current findings identified higher nodal efficiency in AD in the left subsection of the thalamus, i.e., the left ventral latero-ventral thalamus. Similarly, a recent rs-fMRI study found higher nodal efficiency in the thalamus in AD patients compared to healthy controls (Ng *et al.*, 2021). Another study investigating network efficiency of functional brain networks in primary insomnia patients reported higher nodal efficiency in regions mainly belonging to the DMN and emotional circuits, such as the thalamus (Ma *et al.*, 2018). This may somewhat explain our results as sleep changes and insomnia are common in AD (Dauvilliers, 2007). Conversely, nodal efficiency in the left thalamus has been found to be lower in AD individuals compared to controls (Zajac *et al.*, 2017). Anatomically, the hippocampus connects directly to the anterior thalamus through the fornix and to the pulvinar through the temporopulvinar tract. Since the current study found altered local efficiency, higher nodal efficiency, and lower nodal strength in the hippocampus, we propose that these WM and GM between the hippocampus and thalamus may also be affected. Thus, the lower nodal strength in these subregions of the thalamus may indicate lower connectivity within the thalamus as well as between the hippocampus and the thalamus and its neighbouring regions, such as the fornix (we did not investigate the fornix). The lower transitivity may indicate that regions neighbouring the thalamus are so impaired

that they are not connected to each other. This is supported by a rs-fMRI study, where the authors found decreased FC between the thalamus and multiple other brain regions in the early stages of AD (Wang *et al.*, 2011).

5.3.3.3 Altered nodal strength and higher transitivity without DTI alterations in AD

Other regions that only showed graph theory group differences in the thalamus and brainstem included:

1) Lower *nodal strength* in the **right mediodorsal thalamus (R-med-dors),** the **left ventral latero-dorsal nucleus thalamus (L-vent-lat-dors),** the **brainstem medulla (Brain-Stem-Medulla),** the **brainstem SCP (Brain-Stem-SCP)** as well as higher *nodal strength* in the **brainstem pons (Brain-Stem-Pons)** *(Table 5, Figure 23 and 24).*
2) Higher *transitivity* in the **right ventral latero-dorsal nucleus thalamus (R-vent-lat-dors),** the **right ventral anterior thalamus (R-vent-ant),** as well as lower *transitivity* in the **left ventral anterior thalamus (L-vent-ant)** *(Table 5, Figure 25 and 26).*

There are minimal studies using graph theory to investigate the brainstem in AD. Our study found altered nodal strength in the brainstem subregions of AD patients, suggesting topological disruptions, which needs to be further investigated in future studies.

5.3.4 Cortical frontal lobe

5.3.4.1 Higher nodal strength and transitivity without DTI alterations in AD

Frontal lobe regions are responsible for attention, memory, language, and executive function (Chayer and Freedman, 2001). Although we did not find DTI alterations in the frontal lobe, we observed higher *nodal strength* in the **left precentral gyrus (L-Precentral)** as well as higher *transitivity* in the **left superior frontal gyrus (L-sup-F)** and the **left paracentral lobule (L-Paracentral)** *(Table 5, Figure 24 and 26)* in the AD patients compared to healthy elderly controls. Similarly, Weiler et al. (2018) observed that it was mostly frontal regions that showed increased functional network local efficiency in aMCI patients.

The ability of AD patients to perform memory tasks was related to how well their brains could recruit additional prefrontal areas during the task, suggesting that this may be an adaptive response to functional loss and the degenerative disease process (Grady *et al.*, 2003). Moreover, Sheng et al. (2021) observed that compensation at a whole-brain network level gradually spreads from the frontal lobe to the rest of the cortex as AD progresses. In

line with these observations, Behfar et al. (2020) classified both the right and left precentral gyri, as well as the right middle frontal gyrus as compensatory ROIs as they identified a more robust nodal connectivity, despite atrophy in these regions, in MCI patients. The authors proposed that these compensatory ROIs play an essential part in recruiting additional cognitive resources to achieve a normal level of cognition in MCI patients. As frontal regions are only affected in later stages of the disease (Braak and Braak, 1991), the increase in nodal strength and transitivity we observed reflects that frontal regions are working extra hard and act as compensatory ROIs for the rest of the nodes in the network.

5.3.5 Cortical parietal lobe

5.3.5.1 Higher nodal strength as well as altered transitivity and local efficiency without DTI alterations in AD

Although we did not find DTI alterations, we found the following changes in graph network measures in the parietal lobe in the AD patients compared to healthy elderly controls:

1) Higher *nodal strength* in the **left inferior parietal cortex (L-inf-P)** and the **left postcentral gyrus (L-Postcentral)** *(Table 5 and Figure 24).*

2) Lower *transitivity* in the **left inferior parietal cortex (L-inf-P)** as well as higher *transitivity* in the **left supramarginal gyrus (L-Supramarginal)** *(Table 5, Figure 25 and 26).*

3) Higher *local efficiency* in the **left postcentral gyrus (L-Postcentral)** as well as lower *local efficiency* in the **right precuneus cortex (R-Precuneus)** *(Table 5, Figure 28 and 29).*

The lower transitivity and local efficiency found in the parietal regions may be attributed to the WM degeneration, indicating disrupted connections between these cortical regions. These regions, namely the precuneus and inferior parietal cortex, are part of the DMN (Raichle *et al.*, 2002), which is a network that contains regions implicated in AD in both structural and functional studies (Baron *et al.*, 2001; Buckner *et al.*, 2005; Karas *et al.*, 2007; Sorg, Riedl and Muhlau, 2007; Zhao *et al.*, 2012; Wang *et al.*, 2013; Sun *et al.*, 2019). Previous studies reported abnormal FC of the precuneus in AD (Buckner *et al.*, 2005, 2009), and this altered connectivity has been associated with worse episodic memory in preclinical and clinical AD stages (Bai *et al.*, 2012).

Our study found higher nodal strength in some parietal lobe regions, namely the left inferior parietal cortex and left postcentral gyrus. Similarly, in a PET study, Veronese et al. (2019)

found that AD patients showed higher nodal strength compared to controls in the inferior parietal cortex, which showed the greatest group difference in strength. Furthermore, Behfar et al. (2020) observed that regions that they considered to be compensatory ROIs, e.g., regions in the precentral gyrus and superior parietal lobe, demonstrated an increase in connectivity with other ROIs, such as the postcentral gyrus. This suggests that nodes in the parietal lobe may work together with frontal lobe nodes to compensate for the loss of connections elsewhere in the brain.

5.3.6 Cortical insula

5.3.6.1 Higher nodal strength without DTI alterations in AD

Although we did not find DTI alterations in the insula, the AD patients in our sample showed higher *nodal strength* in the **left insula (L-Insula)** compared to healthy elderly controls *(Table 5 and Figure 24).* Lin et al. (2017) proposed that in the very early stage of AD, the left insula and inferior frontal gyrus may be essential for the maintenance of memory performance with AD-related pathology. Thus, higher nodal strength in the left insula may be necessary to maintain memory performance in the early stages in our AD patients.

5.3.7 Subcortical basal ganglia

5.3.7.1 Lower nodal strength and transitivity and higher nodal efficiency without DTI alterations in AD

Our findings included lower *nodal strength* in the **right pallidum (R-Pal)**, lower *transitivity* in the **putamen bilaterally (R-Pu, L-Pu)** and the **right caudate nucleus (R-Caudate),** as well as higher *nodal efficiency* in the **left nucleus accumbens area (L-Acc-area)** in the AD patients compared to the controls *(Table 5, Figure 23, 25 and 27).* We found lower transitivity in regions of the basal ganglia where previous studies have observed regional atrophy in AD patients at baseline, namely the bilateral putamen and the right caudate nucleus (Cho *et al.*, 2014) as well as the left nucleus accumbens area (Nie *et al.*, 2017). These regions have also been found to have a reduction in local efficiency in aMCI patients (Sun *et al.*, 2019), however, we found only lower transitivity. Although we did not find any DTI alterations in the basal ganglia, studies have reported MD increases in the basal forebrain to be associated with a higher risk for mild cognitive impairment (MCI) to convert to AD (Brueggen *et al.*, 2015).

5.4 Relationship between graph theory metrics and IIV

We found a positive relationship between global efficiency and RT IIV on the CRT task in AD patients. With every unit increase in RT IIV on the CRT task, there is an average expected 2558.10 unit increase in global efficiency in AD. This means that the greater the variability in RT, the greater the global efficiency in the AD patients *(Figure 31F).* This suggests that even with greater global efficiency, connected regions are not connected in the right way to function properly, i.e., disconnection between brain regions with coordinated activity and connection between brain regions that are more isolated or do not form part of a network. In other words, there may be an unsuccessful attempt to compensate or interference from other networks that contributes to poor performance on these tasks. Conversely, previous studies found that higher global efficiency correlated with better scores on different neuropsychological tests in AD patients and aMCI converters (Lo *et al.*, 2010; Sun *et al.*, 2019).

It was recently postulated that episodic memory impairment in AD is not only affected by damages in the medial temporal lobe but also impacted by a dysfunctional integrated network (Nestor, Fryer and Hodges, 2006; Rose, Janke and Chalk, 2008). The implicated network regions included the thalamus, posterior cingulate and the medial temporal lobe, in all of which we found significant relationships between graph theory measures and RT IIV in AD.

5.4.1 Cortical temporal lobe

The temporal pole has been found to be activated during ambiguous decision-making (Guo *et al.*, 2013) and visual processing (Herlin, Navarro and Dupont, 2021), which are components needed for the performance of the CRT task. In the controls, this study found **negative** relationships between *transitivity* in the **left temporal pole (L-Tpole)** and *mean RT on both the SRT and CRT tasks (Figure 32A and 32C)*. This may indicate that the temporal pole and its adjacent areas in the temporal lobe may be needed to perform well on the SRT and CRT tasks. Similarly, previous studies have reported that IIV correlated negatively with WM volumes in the prefrontal, temporal and parietal fibre tracts in healthy males between ages 19 and 49 (Ullén *et al.*, 2008).

In the AD patients, our results included a **positive** relationship between *nodal efficiency* in the **left fusiform gyrus (L-Fusiform)** and *mean RT on the CRT task (Figure 32F),* indicating that increased nodal efficiency leads to decreased performance. In a recent study, Sheng et al. (2021) reported higher nodal efficiency in the right parahippocampal gyrus and the right amygdala, with worse neuropsychological performance, including visuospatial tasks, in AD patients. Visuospatial processing is required for the performance of CRT tasks, so their results, together with ours, suggest that structural connectome alterations do not necessarily reflect brain function. Other fMRI studies have shown increased activity in the fusiform gyrus during both resting-state and cognitive tasks in MCI patients (Bokde *et al.*, 2006; He *et al.*, 2007).

5.4.2 Cortical cingulate cortex

The positive cingulate cortex is highly connected, both structurally and functionally, and is extremely metabolically active. It is part of the DMN, a set of brain regions characterised by increased neural activity during rest and deactivation during goal-orientated tasks in healthy subjects (Raichle *et al.*, 2002; Buckner, Andrews-Hanna and Schacter, 2008). However, other evidence suggests that the posterior cingulate cortex plays a pivotal role in regulating the focus of attention and executive control (Leech and Sharp, 2014) with increased DMN activity when attention is internally directed, such as episodic memory retrieval (Spreng, 2012) or self-referential processing (Buckner, Andrews-Hanna and Schacter, 2008). The cingulate cortex is also responsible for psychomotor speed processing (Hwang *et al.*, 2016), which in addition to attention control, is also needed for the performance on the RT tasks.

Our study found a **positive** association between *transitivity* in the **left posterior cingulate cortex (L-pos-Cing)** and *RT IIV on the CRT task* in AD patients (*Figure 31F*). Weissman et al. (2006) proposed that a failure to suppress DMN activity was associated with attentional lapses, which have been seen to be associated with an increase in IIV and longer response times during a selective attention task (Kelly *et al.*, 2008). Similarly, other studies have found that failure to deactivate the posterior cingulate cortex in both healthy and diseased groups as cognitive load increases is associated with inefficient cognitive function (Sonuga-Barke and Castellanosa, 2007; Greicius, 2008; Bonnelle *et al.*, 2011).

A possible explanation for the positive association between transitivity and RT IIV observed in the posterior cingulate cortex is that denser local connectivity results in AD patients failing to deactivate this region, with interference from mind-wandering or other task-unrelated thoughts across the trials leading to an increase in RT IIV.

In healthy adults, a positive relationship between working memory accuracy and the strength of FC between the anterior medial prefrontal cortex and posterior cingulate cortex has been shown (Hampson *et al.*, 2006). This connection is considered a longer-range connection and thus, could explain that in our AD patients, in order for them to maintain working memory, they needed to increase transitivity, i.e., the number of local connections between neighbouring nodes.

The anterior cingulate cortex is known to be responsible for error detection and monitoring of emotional responses (Carter *et al.*, 1998; Bush, Luu and Posner, 2000). In this current study, we found a **positive** relationship between *transitivity* in the **left caudal anterior cingulate cortex (L-caud-ant-Cing)** and *mean RT on the CRT task* in the controls *(Figure 32D)*. Increased activation of the anterior cingulate cortex is linked to error detection, emotional distress associated with the error and anticipatory anxiety (Bush, Luu and Posner, 2000; Botvinick, Cohen and Carter, 2004; Straube *et al.*, 2009). This suggests that higher transitivity found in this region in controls with longer mean RT could be due to the controls being conscious of how quickly they should respond, together with the anxiety to react quickly but because of this, perform worse, i.e., denser anterior cingulate cortex connectivity leads to heightened performance anxiety and slower response times in the controls.

5.4.3 Subcortical thalamus

In this study, we found that there was a **negative** association between *transitivity* in the **left anterior thalamus (L-ant)** and *RT IIV on the SRT task*, a **negative** association between *nodal strength* in the **right mediodorsal thalamus (R-med-dors)** and *RT IIV on the CRT task,* as well as a **positive** relationship between the *nodal efficiency* in the **left ventral latero-ventral thalamus (L-vent-lat-vent)** and *RT IIV on the CRT task* in the controls *(Figure 31A, 31C and 31E*).

There is strong evidence that deficits in executive control cause higher IIV on cognitive tasks (Bellgrove, Hester and Garavan, 2004). Executive control is known to recruit regions of the prefrontal cortex. Regions within the medial thalamus, such as the mediodorsal nucleus, the nucleus reuniens, and the anterior thalamic nuclei, have been found to support prefrontal cortex function (Aggleton *et al.*, 2016). This could be why we see thalamus connectivity affecting IIV and executive control. Other functions of the thalamus include generating attention and declarative memory functioning (Werf *et al.*, 2003; Bourbon-Teles *et al.*, 2014).

In healthy individuals, higher IIV on an executive control task was associated with increased functional activation in the bilateral middle frontal areas, as well as the right inferior parietal and thalamic regions, which form part of a network associated with inhibitory and attentional control (Bellgrove, Hester and Garavan, 2004). The thalamus is involved in psychomotor processing speed (Hwang *et al.*, 2016). Decreased volume of the thalamus with age has been demonstrated between 21 to 82 years, which correlated with worse performance on cognitive speed tests (Van Der Werf *et al.*, 2001). Since both SRT and CRT tasks require psychomotor speed, this may explain why we see a negative association between the left anterior thalamus transitivity and RT IIV on the SRT task.

Schmitt et al. (2017) showed in mice that the mediodorsal thalamus amplifies local cortical connectivity, i.e., signalling strength, to sustain attentional control, revealing the flexibility of the mammalian brain to make complex decisions. Thus, it makes sense that we observed a negative relationship between nodal strength in the right mediodorsal thalamus and RT IIV on the CRT task in the controls, as the CRT task needs an additional decision-making component.

Interestingly, we also found lower FA and lower nodal efficiency in the left ventral latero-ventral thalamus in the controls compared to AD patients. This region of the thalamus is known to be responsible for motor control. Taken together with the positive relationship of nodal efficiency with RT IIV, these results could suggest that lower nodal efficiency and lower FA in this region of the thalamus may instead cause problems in executive function in our sample.

In the AD patients, there were **negative** relationships between *transitivity* in the **right ventral latero-dorsal nucleus thalamus (R-vent-lat-dors)** and *RT IIV and mean RT on the SRT*

task, as well as *mean RT on the CRT task (Figure 31B, 32B and 32E).* This subsection of the thalamus has been found to be responsible for spatial learning and memory (Bezdudnaya and Keller, 2009). Previous studies have explored the pattern of thalamic degeneration in AD using both DTI and sMRI and identified regional thalamic atrophy, observing that affected regions were mainly connected to the hippocampus, temporal cortex and prefrontal cortex (Zarei *et al.*, 2010). Degeneration of middle frontal gyrus connectivity with the thalamus bilaterally contributes to dysfunction of attention, working memory and executive function in early MCI patients (Cai *et al.*, 2015). These are functions that play a role in both SRT and CRT tasks. Thus, the loss of connections between this subregion of the thalamus and regions such as the temporal cortex and frontal lobe, i.e., decreased transitivity, may cause worse performance.

Interestingly, we found higher transitivity in AD patients compared to healthy controls, but a negative relationship between transitivity and RT IIV and mean RT in these patients. This suggests that this is a compensatory adaptation to preserve performance and that individuals with less well-developed compensatory thalamus connections, i.e., lower transitivity, show greater RT IIV as well as longer mean RT on the SRT and CRT tasks.

5.4.4 Subcortical basal ganglia

We observed a **negative** relationship between *nodal efficiency* in the **left nucleus accumbens area (L-Acc-area)** and *RT IIV on the CRT task* in the controls *(Figure 31D)*. The primary role of the nucleus accumbens is to receive information from limbic regions and cortical brain regions, such as the prefrontal cortex, and send the information to motor-related structures. It is thus responsible for goal-directed behaviours, such as learning and decision-making (West, Moschak and Carelli, 2018). Therefore, higher nodal efficiency in the nucleus accumbens appears to facilitate the decision-making component needed for the CRT task.

6. Limitations and future work

This study had a few limitations. Firstly, our AD patients varied from mild-to-moderate stages of the disease, making it challenging to elucidate and distinguish the changes we observed. Secondly, the AD patients in this study were older than the controls; thus, it is unclear whether our results were completely affected by AD or also by age-related changes.

Thirdly, graph theory-based approaches are still under development and evolving. Some of the graph metrics may artificially introduce some extent of uncertainty and arbitrariness as they involved a dichotomisation step. Therefore, their reliability and informativeness require further investigation. Lastly, our results are limited by the small sample size (Number of controls = 20, number of AD = 16), thus more evidence is needed to show that these findings can be inferred to a population. Due to the small sample size, the study is underpowered and could possibly be the reason why we also could not detect interaction effects in the models.

Future work could group the AD patients according to disease severity and investigate structural connectivity using DTI in conjunction with global and local volume alterations due to atrophy, or FC using rs-fMRI in our study sample, to see whether the alterations/disruptions in structural connectivity coincide with changes in FC and volume. The integration of different modalities (e.g., DTI and rs-fMRI) could allow us to explore how the alterations of anatomical networks are associated with changes in functional networks.

7. Summary and conclusions

To our knowledge, our study is the only study that has investigated DTI measures and graph measures using RBA methods in application to Alzheimer's disease. Our findings showed mixed results with evidence of compensatory mechanisms in WM tracts and network metrics in AD patients. Our results demonstrated alterations in both DTI measures and graph theory measures in both hemispheres, mainly in the bilateral temporal, occipital lobes, thalamus, cingulate cortex, and brainstem. This may be due to our sample consisting of mild-to-moderate stage of possible or probable AD patients; our results thus show effects in the brain during the earlier stages of AD. This is consistent with other studies that suggest AD pathology spreads from the limbic/paralimbic areas to other brain regions (Mesulam, 2000; Thompson *et al.*, 2003). The current findings present some evidence that the thalamus and brainstem may be affected early in the disease, however, we will need histopathology to support this. One of the strengths of this study was the ability to provide insight into multiple nuclei/subregions of the thalamus, which not many studies have done before in AD. Therefore, there was a higher likelihood of detecting AD-related alterations nuclei if they were present in this smaller subset of the thalamic nuclei, as post-mortem studies have indicated (Braak and Braak, 1991).

In conclusion, as hypothesised in our first hypothesis, we found structural connectivity disruptions (lower FA, higher MD) in WM tracts mostly located in the cortical and subcortical temporal lobes, including the bilateral hippocampus subregions, in AD patients compared to healthy controls. However, we also observed altered FA within the WM tracts of the thalamus as well as higher FA between the thalamus and brainstem in AD patients. In addition, we found either no changes or higher AxD and RD in these WM tracts. Higher MD in WM tracts between the cingulate cortex and occipital lobe were also observed in AD patients.

Interestingly, contrary to our second hypothesis, this study detected higher nodal efficiency across multiple regions as well as higher global efficiency in AD patients. There were some nodes with lower and some with higher nodal strength, transitivity and local efficiency in the AD patients compared to healthy elderly controls except for modularity and nodal degree, where we found no group differences.

Finally, although we hypothesised that lower global efficiency would be associated with greater RT IIV and greater mean RT in AD patients in our third hypothesis, we observed that higher global efficiency was associated with increased RT IIV on the CRT task. We also hypothesised that lower transitivity and nodal efficiency in the cingulate cortex and temporal lobe would be associated with greater RT IIV and greater mean RT in AD patients. However, we found a positive relationship between transitivity in the left cingulate cortex and RT IIV as well as between nodal efficiency in the left cortical temporal lobe and mean RT on the CRT task in AD. In the right thalamus, we observed a correlation between lower transitivity and increased RT IIV as well as lower transitivity and longer mean RT, in both tasks in AD.

Our results may show evidence of disruptions and compensatory mechanisms in the WM tracts as well as the structural connectome of AD patients.

Possible reasons for inconsistent findings between previous studies and ours may be due to the differences in disease stages of the AD patients, different methodological and statistical approaches, as well as different imaging modalities. Furthermore, node definition by different parcellation schemes may also produce different brain network properties. For example, using 78 regions of the automated anatomical labelling (AAL) template (Lo *et al.*, 2010) versus 126 regions of the Lausanne 2018 scale 1 segmentation used in this study

(Daducci *et al.*, 2012). Another possible reason for the discrepancies in findings may be due to the difference in covariates that were included in the models, e.g., linear regression with sex and age as covariates (Lo *et al.*, 2010) compared to RBA with sex, age, years of education and monthly household income as confounders used in this study.

This study sheds some light on structural connectivity and connectome alterations in AD and that these results may be used in combination with IIV to predict cognitive decline or progression of AD.

References

Acosta-Cabronero, J., Williams, G. B., Pengas, G. and Nestor, P. J. (2010) 'Absolute diffusivities define the landscape of white matter degeneration in Alzheimer's disease', *Brain*, 133(2), pp. 529–539.

Acosta-Cabronero, Julio, Alley, Stephanie, Williams, Guy B., Pengas, George and Nestor, Peter J. (2012) 'Diffusion Tensor Metrics as Biomarkers in Alzheimer ' s Disease', 7(11). doi: 10.1371/journal.pone.0049072.

Adam, S., Godlwana, L. and Maleka, D. (2016) 'Changes in short-term cognitive function following a hip fracture in the elderly and the effect of cognitive function on early post-operative function', *The South African Orthopaedic Journal (SAOJ)*, 15(1), pp. 77–82. doi: 10.17159/2309-8309/2016/v15n1a9.

Aggleton, John P., Pralus, Agathe, Nelson, Andrew J. D. and Hornberger, Michael (2016) 'Thalamic pathology and memory loss in early Alzheimer's disease: Moving the focus from the medial temporal lobe to Papez circuit', *Brain*, 139(7), pp. 1877–1890. doi: 10.1093/brain/aww083.

Agosta, F., Pievani, M., Sala, S., Geroldi, C., Galluzzi, S., Frisoni, G. B. and Filippi, M. (2011) 'White matter damage in Alzheimer disease and its relationship to gray matter atrophy.', *Radiology*, 258(3), pp. 853–863.

Alexander, A. L., Hurley, S. A., Samsonov, A. A., Adluru, N., Hosseinbor, A. P., Mossahebi, P. and Field, A. S. (2011) 'Characterization of Cerebral White Matter Properties Using Quantitative Magnetic Resonance Imaging Stains.', *AJNR Am J Neuroradiology*, 37(12), pp. 2363–2369.

Alexander, Andrew L., Lee, Jee Eun, Lazar, Mariana and Field, Aaron S. (2007) 'Diffusion Tensor Imaging of the Brain', *Neurotherapeutics*, 4(3), pp. 316–329. doi: 10.1016/j.nurt.2007.05.011.

Allaire, JC and Marsiske, M. (2005) 'Intraindividual variability may not always indicate vulnerability in elders' cognitive performance', *Psychology and Aging*, 20(3), pp. 390–401.

Alzheimer's Association (2017) *Beta-amyloid and the amyloid hypothesis*. Available at: https://www.alz.org/national/documents/topicsheet_betaamyloid.pdf.

Alzheimer's Association (2021a) *2021 ALZHEIMER ' S DISEASE FACTS AND FIGURES - Race , Ethnicity and Alzheimer's in America*. Available at: https://www.alz.org/media/documents/alzheimers-facts-and-figures.pdf.

Alzheimer's Association (2021b) *Global Dementia Cases Forecasted to Triple by 2050*. Available at: https://www.alz.org/aaic/releases_2021/global-prevalence.asp.

Alzheimer's Association (2021c) *Tau*. Available at: https://www.alz.org/media/Documents/alzheimers-dementia-tau-ts.pdf.

Alzheimer's Disease International (2020) *Dementia Statistics*. Available at: https://www.alzint.org/about/dementia-facts-figures/dementia-statistics/.

American Psychiatric Association (2013) *Diagnostic and statistical manual of mental disorders (dsm-5)*. Fifth Edit.

Andrew, Melissa K. and Tierney, Mary C. (2018) 'The puzzle of sex, gender and Alzheimer's disease: Why are women more often affected than men?', *Women's Health*, 14. doi: 10.1177/1745506518817995.

Anstey, Kaarin J., Mack, Holly A., Christensen, Helen, Li, Shu Chen, Reglade-Meslin, Chantal, Maller, Jerome, Kumar, Rajeev, Dear, Keith, Easteal, Simon and Sachdev, Perminder (2007) 'Corpus callosum size, reaction time speed and variability in mild cognitive disorders and in a normative sample', *Neuropsychologia*, 45(8), pp. 1911–1920. doi: 10.1016/j.neuropsychologia.2006.11.020.

Arora, Harneet (2018) 'Review of Basic Concepts Involved in Magnetic Resonance Imaging', *Biomedical*, 5(4), pp. 6804–6807. doi: 10.26717/BJSTR.2018.08.001726.

Arriagada, P. V, Growdon, J. H., Hedley-Whyte, E. T. and Hyman, B. T. (1992) 'Neurofibrillary tangles but not senile plaques parallel duration and severity of Alzheimer's disease', *Neurology*, 42(3).

Arvanitakis, Zoe, Wilson, Robert S., Bienias, Julia L., Evans, Denis A. and Bennett, David A. (2004) 'Diabetes Mellitus and Risk of Alzheimer Disease and Decline in Cognitive Function', *Archives of Neurology*, 61(5), pp. 661–666. doi: 10.1001/archneur.61.5.661.

Atiya, Monika, Hyman, Bradley T., Albert, Marilyn S. and Killiany, Ronald (2003) 'Structural Magnetic Resonance Imaging in Established and Prodromal Alzheimer Disease : A Review', 17(3), pp. 177–195.

Bachmann, Claudia, Jacobs, Heidi I. L., Porta Mana, PierGianLuca, Dillen, Kim, Richter, Nils, von Reutern, Boris, Dronse, Julian, Onur, Oezguer A., Langen, Karl-Josef, Fink, Gereon R., Kukolja, Juraj and Morrison, Abigail (2018) 'On the Extraction and Analysis of Graphs From Resting-State fMRI to Support a Correct and Robust Diagnostic Tool for Alzheimer's Disease', *Frontiers in Neuroscience*, 12(September), pp. 1–24. doi: 10.3389/fnins.2018.00528.

Bai, F., Shu, N., Yuan, Y., Shi, Y., Yu, H., Wu, D., Wang, J., Xia, M., He, Y. and Zhang, Z. (2012) 'Topologically convergent and divergent structural connectivity patterns between patients with remitted geriatric depression and amnestic mild cognitive impairment.', *Journal of Neuroscience*, 32, pp. 4307–4318.

Baker, LM, Laidlaw, DH, Conturo, TE, Hogan, J., Zhao, Y., Luo, X., Correia, S., Cabeen, R., Lane, EM, Heaps, JM, Bolzenius, J.,

Salminen, LE, Akbudak, E., McMichael, AR, Usher, C., Behrman, A. and Paul, RH (2014) 'White matter changes with age utilizing quantitative diffusion MRI.', *Neurology*, 83(3), pp. 247–252.

Bangen, Katherine J., Weigand, Alexandra J., Thomas, Kelsey R., Delano-Wood, Lisa, Clark, Lindsay R., Eppig, Joel, Werhane, Madeleine L., Edmonds, Emily C. and Bondi, Mark W. (2019) 'Cognitive dispersion is a sensitive marker for early neurodegenerative changes and functional decline in nondemented older adults', *Neuropsychology*, 33(5), pp. 599–608. doi: 10.1037/neu0000532.

Baron, J. C., Chételat, G., Desgranges, B., Perchey, G., Landeau, B., De La Sayette, V. and Eustache, F. (2001) 'In vivo mapping of gray matter loss with voxel-based morphometry in mild Alzheimer's disease', *NeuroImage*, 14(2), pp. 298–309. doi: 10.1006/nimg.2001.0848.

Barrio-Arranz, Gonzalo, De Luis-García, Rodrigo, Tristán-Vega, Antonio, Martín-Fernández, Marcos and Aja-Fernández, Santiago (2015) 'Impact of MR acquisition parameters on DTI scalar indexes: A tractography based approach', *PLoS ONE*, 10(10), pp. 1–19. doi: 10.1371/journal.pone.0137905.

Bartzokis, George (2011) 'Alzheimer's disease as homeostatic responses to age-related myelin breakdown', *Neurobiology of Aging*, pp. 1341–1371. doi: 10.1016/j.neurobiolaging.2009.08.007.

Basser, P., Mattiello, J. and LeBihan, D. (1994) 'MR Diffusion Tensor Spectroscopy and Imaging.', *Biophysical Journal*, 66, pp. 259–267.

Behfar, Qumars, Behfar, Stefan Kambiz, Reutern, Boris Von, Richter, Nils, Dronse, Julian, Fassbender, Ronja, Fink, Gereon R., Onur, Oezguer A. and Marco, Matteo De (2020) 'Graph Theory Analysis Reveals Resting-State Compensatory Mechanisms in Healthy Aging and Prodromal Alzheimer ' s Disease', 12(October), pp. 1–13. doi: 10.3389/fnagi.2020.576627.

Behrman-Lay, Ashely M., Usher, Christina, Conturo, Thomas E., Correia, Stephen, Laidlaw, David H., Lane, Elizabeth M., Bolzenius, Jacob, Heaps, Jodi M., Salminen, Lauren E., Baker, Laurie M., Cabeen, Ryan, Akbudak, Erbil, Luo, Xi, Yan, Peisi and Paul, Robert H. (2015) 'Fiber bundle length and cognition: A length-based tractography MRI study', *Brain Imaging and Behavior*, 9(4), pp. 765–775. doi: 10.1007/s11682-014-9334-8.Fiber.

Bellgrove, Mark A., Hester, Robert and Garavan, Hugh (2004) 'The functional neuroanatomical correlates of response variability: Evidence from a response inhibition task', *Neuropsychologia*, 42(14), pp. 1910–1916. doi: 10.1016/j.neuropsychologia.2004.05.007.

Benjamin, Daniel J., Berger, James O., Johnson, Valen E., *et al.* (2018) 'Redefine statistical significance', *Nature Human Behaviour*. Springer US, 2(1), pp. 6–10. doi: 10.1038/s41562-017-0189-z.

Bernardin, Florent, Maheut-Bosser, Anne and Paille, François (2014) 'Cognitive impairments in alcohol-dependent subjects', *Frontiers in Psychiatry*, 5(JUL). doi: 10.3389/fpsyt.2014.00078.

Berron, David, van Westen, Danielle, Ossenkoppele, Rik, Strandberg, Olof and Hansson, Oskar (2020) 'Medial temporal lobe connectivity and its associations with cognition in early Alzheimer's disease', *Brain*, 143(3), pp. 1233–1248. doi: 10.1093/brain/awaa068.

Bezdudnaya, Tatiana and Keller, Asaf (2009) 'Laterodorsal Nucleus of the Thalamus: A Processor of Somatosensory Inputs', *Journal of Comparative Neurology*, 507(6), pp. 1979–1989.

Bielak, A. M., Cherbuin, N., Bunce, D. and Anstey, K. J. (2014) 'Intraindividual variability is a fundamental phenomenon of aging: Evidence from an 8-year longitudinal study across young, middle, and older adulthood.', *Developmental Psychology*, 50, pp. 143–151.

Bielak, Allison A. M., Hultsch, David F., Strauss, Esther, MacDonald, Stuart W. S. and Hunter, Michael A. (2010) 'Intraindividual Variability in Reaction Time Predicts Cognitive Outcomes 5 Years Later', *Neuropsychology*, 24(6), pp. 731–741. doi: 10.1037/a0019802.

Bokde, A., Lopez-Bayo, P., Meindl, T., Pechler, S. and Born, C. (2006) 'Functional connectivity of the fusiform gyrus during a face-matching task in subjects with mild cognitive impairment.', *Brain*, 129, pp. 1113–1124.

Bonnelle, V., Ham, TE, Leech, R., Kinnunen, KM, Mehta, MA and Greenwood, RJ (2011) 'Default mode network connectivity predicts sustained attention deficits after traumatic brain injury.', *Journal of Neuroscience*, 31, pp. 13442–13451.

Booth, Tom, Dykiert, Dominika, Corley, Janie, Gow, Alan J., Morris, Zoe, Munoz Maniega, Susana, Royle, Natalie A., Del Valdes Hernandez, Maria C., Starr, John M. and Penke, Lars (2019) 'Reaction time variability and brain white matter integrity', *Neuropsychology*, 33(5), pp. 642–657. doi: 10.1037/neu0000483.

Bosch, Beatriz, Arenaza-Urquijo, Eider M., Rami, Lorena, Sala-Llonch, Roser, Junqué, Carme, Solé-Padullés, Cristina, Peña-Gómez, Cleofé, Bargalló, Núria, Molinuevo, José Luis and Bartrés-Faz, David (2012) 'Multiple DTI index analysis in normal aging, amnestic MCI and AD. Relationship with neuropsychological performance', *Neurobiology of Aging*. Elsevier Inc., 33(1), pp. 61–74. doi: 10.1016/j.neurobiolaging.2010.02.004.

Botvinick, Matthew M., Cohen, Jonathan D. and Carter, Cameron S. (2004) 'Conflict monitoring and anterior cingulate cortex: An update', *Trends in Cognitive Sciences*, 8(12), pp. 539–546. doi: 10.1016/j.tics.2004.10.003.

Bourbon-Teles, José de, Bentley, Paul, Koshino, Saori, Shah, Kushal, Dutta, Agneish, Malhotra, Paresh, Egner, Tobias,

Husain, Masud and Soto, David (2014) 'Thalamic Control of Human Attention Driven by Memory and Learning', *Curr Biol.*, 24(9), pp. 993–999.

Bozzali, M., Falini, A., Franceschi, M., Cercignani, M., Zuffi, M., Scotti, G., Comi, G. and Filippi, M. (2002) 'White matter damage in Alzheimer's disease assessed in vivo using diffusion tensor magnetic resonance imaging', *Journal of Neurology Neurosurgery and Psychiatry*, 72(6), pp. 742–746. doi: 10.1136/jnnp.72.6.742.

Braak, H. and Braak, E. (1991) 'Neuropathological stageing of Alzheimer-related changes', *Acta Neurologica Scandinavica*, pp. 239–259.

Braak, H. and Braak, E. (1995) 'Staging of Alzheimer's Disease-Related Neurofibrillary Changes', *Neurobiology of Aging*, 16, pp. 271–284.

Braak, Heiko, Thal, Dietmar R., Ghebremedhin, Estifanos and Tredici, Kelly Del (2011) 'Stages of the pathologic process in Alzheimer disease: age categories from 1 to 100 years', *Journal of Neuropathology & Experimental Neurology*, 70(11), pp. 960–969.

Braskie, Meredith N., Jahanshad, Neda, Stein, Jason L., Barysheva, Marina, McMahon, Katie L., de Zubicaray, Greig I., Martin, Nicholas G., Wright, Margaret J., Ringman, John M., Toga, Arthur W. and Thompson, Paul M. (2011) 'Common Alzheimer's Disease Risk Variant Within the CLU Gene Affects white Matter Microstructure in young Adults', *Journal of Neuroscience*, 31(18), pp. 6764–6770. doi: 10.1523/JNEUROSCI.5794-10.2011.

Brier, Matthew R., Thomas, Jewell B., Fagan, Anne M., Hassenstab, Jason, Holtzman, David M., Benzinger, Tammie L., Morris, John C. and Ances, Beau M. (2014) 'Functional connectivity and graph theory in preclinical Alzheimer's disease', *Neurobiology of Aging*. Elsevier Ltd, 35(4), pp. 757–768. doi: 10.1016/j.neurobiolaging.2013.10.081.

Brilliant, Mikhail, Rodger, J. Elbl., Ghobrial, Mona and G.Struble, Robert (1992) 'Distribution of amyloid in the brainstem of patients with Alzheimer disease', *Neuroscience Letters*, 148(1–2), pp. 23–26.

Brueggen, Katharina, Dyrba, Martin, Barkhof, Frederik, Hausner, Lucrezia, Filippi, Massimo, Nestor, Peter J., Hauenstein, Karlheinz, Klöppel, Stefan, Grothe, Michel J., Kasper, Elisabeth and Teipel, Stefan J. (2015) 'Basal forebrain and hippocampus as predictors of conversion to Alzheimer's disease in patients with mild cognitive impairment-a multicenter DTI and volumetry study', *Journal of Alzheimer's Disease*, 48(1), pp. 197–204. doi: 10.3233/JAD-150063.

Brueggen, Katharina, Dyrba, Martin, Cardenas-Blanco, Arturo, Schneider, Anja, Fliessbach, Klaus, Buerger, Katharina, Janowitz, Daniel, Peters, Oliver, Menne, Felix, Priller, Josef, Spruth, Eike, Wiltfang, Jens, Vukovich, Ruth, Laske, Christoph, Buchmann, Martina, Wagner, Michael, Röske, Sandra, Spottke, Annika, Rudolph, Janna, Metzger, Coraline D., Kilimann, Ingo, Dobisch, Laura, Düzel, Emrah, Jessen, Frank and Teipel, Stefan J. (2019) 'Structural integrity in subjective cognitive decline, mild cognitive impairment and Alzheimer's disease based on multicenter diffusion tensor imaging', *Journal of Neurology*, 266(10), pp. 2465–2474. doi: 10.1007/s00415-019-09429-3.

Buckner, RL, Andrews-Hanna, JR and Schacter, DL (2008) 'The brain's default network: anatomy, function, and relevance to disease', *Annals of the New York Academy of Sciences*, 1124, pp. 1–38.

Buckner, RL, Sepulcre, J., Talukdar, T., Krienen, FM, Liu, H., Hedden, T., Andrews-Hanna, JR, Sperling, RA and Johnson, KA (2009) 'Cortical hubs revealed by intrinsic functional connectivity: mapping, assessment of stability, and relation to Alzheimer's disease.', *Journal of Neuroscience*, 29(6), pp. 1860–1873.

Buckner, RL, Snyder, AZ, Shannon, BJ, LaRossa, G., Sachs, R., Fotenos, AF, Sheline, YI, Klunk, WE, Mathis, CA and Morris, JC (2005) 'Molecular, structural, and functional characterization of Alzheimer's disease: evidence for a relationship between default activity, amyloid, and memory.', *Journal of Neuroscience*, 25(34), pp. 7709–7717.

Bullmore, Ed and Sporns, Olaf (2009) 'Complex brain networks: Graph theoretical analysis of structural and functional systems', *Nature Reviews Neuroscience*, pp. 186–198. doi: 10.1038/nrn2575.

Bunce, David, Anstey, Kaarin J., Christensen, Helen, Dear, Keith, Wen, Wei and Sachdev, Perminder (2007) 'White matter hyperintensities and within-person variability in community-dwelling adults aged 60-64 years', *Neuropsychologia*, 45(9), pp. 2009–2015. doi: 10.1016/j.neuropsychologia.2007.02.006.

Bunce, David, Macdonald, Stuart W. S. and Hultsch, David F. (2004) 'Inconsistency in serial choice decision and motor reaction times dissociate in younger and older adults', pp. 1–25.

Burton, Catherine L., Strauss, Esther, Hultsch, David F., Moll, Alex and Hunter, Michael A. (2006) 'Intraindividual variability as a marker of neurological dysfunction: A comparison of Alzheimer's disease and Parkinson's disease', *Journal of Clinical and Experimental Neuropsychology*, 28(1), pp. 67–83. doi: 10.1080/13803390490918318.

Bush, George, Luu, Phan and Posner, Michael I. (2000) 'Cognitive and emotional influences in anterior cingulate cortex', *Trends in Cognitive Sciences*, 4(6).

Cai, Suping, Huang, Liyu, Zou, Jia, Jing, Longlong, Zhai, Buzhong, Ji, Gongjun, Von Deneen, Karen M., Ren, Junchan, Ren, Aifeng and Alzheimer's Disease Neuroimaging Initiative (2015) 'Changes in thalamic connectivity in the early and late stages of amnestic mild cognitive impairment: A resting-state functional magnetic resonance study from ADNI', *PLoS ONE*, 10(2), pp. 1–22. doi: 10.1371/journal.pone.0115573.

Cambridge Cognition (no date) *CANTAB - Reaction Time (RTI)*, *Cambridge Cognition*. Available at:

https://www.cambridgecognition.com/cantab/cognitive-tests/attention/reaction-time-rti/.

Cammoun, Leila, Gigandet, Xavier, Meskaldji, Djalel, Thiran, Jean Philippe, Sporns, Olaf, Do, Kim Q., Maeder, Philippe, Meuli, Reto and Hagmann, Patric (2012) 'Mapping the human connectome at multiple scales with diffusion spectrum MRI', *Journal of Neuroscience Methods*. Elsevier B.V., 203(2), pp. 386–397. doi: 10.1016/j.jneumeth.2011.09.031.

Carter, Cameron S., Braver, Todd S., Barch, Deanna M., Botvinick, Matthew M., Noll, Douglas and Cohen, Jonathan D. (1998) 'Anterior Cingulate Cortex, Error Detection, and the Online Monitoring of Performance', *Science*, 280.

Carter, Christine L., Resnick, Eileen M., Mallampalli, Monica and Kalbarczyk, Anna (2012) 'Sex and gender differences in Alzheimer's disease: Recommendations for future research', *Journal of Women's Health*, 21(10), pp. 1018–1023. doi: 10.1089/jwh.2012.3789.

Catheline, Gwénaëlle, Periot, Olivier, Amirault, Marion and Braun, Marc (2008) 'Distinctive alterations of the cingulum bundle during aging and Alzheimer ' s disease', 31(2010), pp. 1582–1592. doi: 10.1016/j.neurobiolaging.2008.08.012.

Cavedo, Enrica, Chiesa, Patrizia A., Younesi, Erfan, *et al.* (2018) 'Sex differences in functional and molecular neuroimaging biomarkers of Alzheimer's disease in cognitively normal older adults with subjective memory complaints', *Alzheimer's and Dementia*, 14(9), pp. 1204–1215. doi: 10.1016/j.jalz.2018.05.014.

Chandra, Avinash, Dervenoulas, George, Politis, Marios and Neuroimaging, Disease (2019) 'Magnetic resonance imaging in Alzheimer ' s disease and mild cognitive impairment', *Journal of Neurology*. Springer Berlin Heidelberg, 266(6), pp. 1293–1302. doi: 10.1007/s00415-018-9016-3.

Chayer, Celine and Freedman, Morris (2001) 'Frontal Lobe Functions', *Current Neurology and Neuroscience Reports*, 1, pp. 547–552.

Chen, Gang, Taylor, Paul A., Cox, Robert W. and Pessoa, Luiz (2020) 'Fighting or embracing multiplicity in neuroimaging? neighborhood leverage versus global calibration', *NeuroImage*. Elsevier Ltd, 206(October 2019), p. 116320. doi: 10.1016/j.neuroimage.2019.116320.

Chen, Gang, Xiao, Yaqiong, Taylor, Paul A., Rajendra, Justin K., Riggins, Tracy, Geng, Fengji, Redcay, Elizabeth and Cox, Robert W. (2019) 'Handling Multiplicity in Neuroimaging Through Bayesian Lenses with Multilevel Modeling', *Neuroinformatics*, 17(4), pp. 515–545. doi: 10.1007/s12021-018-9409-6.

Cherbuin, N., Sachdev, P. and Anstey, KJ. (2010) 'Neuropyshchological Predicotrs of Transition From Healthy Cognitive Aging to Mild Cognitive Impairment.pdf', *American Journal of Geriatric Psychiatry*, 18(8), pp. 723–733.

Chetelat, G. and Baron, J. C. (2003) 'Early diagnosis of Alzheimer ' s disease: contribution of structural neuroimaging', *NeuroImage*, 18(2), pp. 525–541.

Cho, Hanna, Kim, Jeong-Hun, Kim, Changsoo, Ye, Byoung Seok, Kim, Hee Jin, Yoon, Cindy W., Noh, Young, Kim, Geon Ha, Kim, Yeo Jin, Kim, Jung-Hyun, Kim, Chang-Hun, Kang, Sue J., Chin, Juhee, Kim, Sung Tae, Lee, Kyung-Han, Na, Duk L., Seong, Joon-Kyung and Seo, Sang Won (2014) 'Shape changes of the basal ganglia and thalamus in AD', *Journal of Alzheimer's Disease*, 40(2), pp. 285–295.

Choi, S. J., Lim, K. O., Monteiro, I. and Reisberg, B. (2005) 'Diffusion tensor imaging of frontal white matter microstructure in early Alzheimer's disease: a preliminary study.', *Journal of Geriatric Psychiatry and Neurology*, 18(1), pp. 12–19.

Christ, Björn U., Combrinck, Marc I. and Thomas, Kevin G. F. (2018) 'Both reaction time and accuracy measures of intraindividual variability predict cognitive performance in Alzheimer's disease', *Frontiers in Human Neuroscience*, 12(April). doi: 10.3389/fnhum.2018.00124.

Christidi, Foteini, Karavasilis, Efstratios, Samiotis, Kostantinos, Bisdas, Sotirios and Papanikolaou, Nikolaos (2016) 'Fiber tracking: A qualitative and quantitative comparison between four different software tools on the reconstruction of major white matter tracts', *European Journal of Radiology Open*, pp. 153–161. doi: 10.1016/j.ejro.2016.06.002.

Contreras, Joey Annette, Aslanyan, Vahan, Sweeney, Melanie D., Sanders, Lianne M. J., Sagare, Abhay P., Zlokovic, Berislav V., Toga, Arthur W., Han, S. Duke, Morris, John C., Fagan, Anne, Massoumzadeh, Parinaz, Benzinger, Tammie L. and Pa, Judy (2020) 'Functional connectivity among brain regions affected in Alzheimer's disease is associated with CSF TNF-α in APOE4 carriers', *Neurobiology of Aging*. Elsevier Inc, 86, pp. 112–122. doi: 10.1016/j.neurobiolaging.2019.10.013.

Costa, Ana Sofia, Dogan, Imis, Schulz, Jörg B. and Reetz, Kathrin (2019) 'Going beyond the mean: Intraindividual variability of cognitive performance in prodromal and early neurodegenerative disorders', *Clinical Neuropsychologist*. Routledge, 33(2), pp. 369–389. doi: 10.1080/13854046.2018.1533587.

Cox, Robert W. (1996) 'AFNI: Software for analysis and visualization of functional magnetic resonance neuroimages', *Computers and Biomedical Research*, 29(3), pp. 162–173. doi: 10.1006/cbmr.1996.0014.

Daducci, Alessandro, Gerhard, Stephan, Griffa, Alessandra, Lemkaddem, Alia, Cammoun, Leila, Gigandet, Xavier, Meuli, Reto, Hagmann, Patric and Thiran, Jean Philippe (2012) 'The Connectome Mapper: An Open-Source Processing Pipeline to Map Connectomes with MRI', *PLoS ONE*, 7(12). doi: 10.1371/journal.pone.0048121.

Dai, Zhengjia and He, Yong (2014) 'Disrupted structural and functional brain connectomes in mild cognitive impairment and Alzheimer's disease', *Neuroscience Bulletin*, 30(2), pp. 217–232. doi: 10.1007/s12264-013-1421-0.

Dai, Zhengjia, Lin, Qixiang, Li, Tao, Wang, Xiao, Yuan, Huishu, Yu, Xin, He, Yong and Wang, Huali (2019) 'Disrupted structural and functional brain networks in Alzheimer's disease', *Neurobiology of Aging*. Elsevier Inc, 75, pp. 71–82. doi: 10.1016/j.neurobiolaging.2018.11.005.

Daianu, Madelaine, Mendez, Mario F., Baboyan, Vatche G., Jin, Yan, Melrose, Rebecca J., Jimenez, Elvira E. and Thompson, Paul M. (2016) 'An advanced white matter tract analysis in frontotemporal dementia and early-onset Alzheimer's disease', *Brain Imaging and Behavior*. Brain Imaging and Behavior, 10(4), pp. 1038–1053. doi: 10.1007/s11682-015-9458-5.

Daianu, Madelaine, Mezher, Adam, Jahanshad, Neda, Hibar, Derrek P., Nir, Talia M., Jack, Clifford R., Weiner, Michael W., Bernstein, Matt A. and Thompson, Paul M. (2015) 'Spectral graph theory and graph energy metrics show evidence for the Alzheimer's disease disconnection syndrome in APOE-4 risk gene carriers', *Proceedings - International Symposium on Biomedical Imaging*, 2015-July, pp. 458–461. doi: 10.1109/ISBI.2015.7163910.

Damoiseaux, JS, Smith, SM, Witter, MP, Arigita, EJ, Barkhof, F., Scheltens, P., Stam, CJ, Zarei, M. and Rombouts, SA (2009) 'White matter tract integrity in aging and Alzheimer's disease', *Human Brain Mapping*, 30, pp. 1051–1059.

Das, Sandhitsu R., Pluta, John, Mancuso, Lauren, Kliot, Dasha, Orozco, Sylvia, Dickerson, Bradford C., Yushkevicha, Paul A. and Wolk, David A. (2013) 'Increased Functional Connectivity within Medial Temporal Lobe in Mild Cognitive Impairment', *Hippocampus*, 23(1), pp. 1–6. doi: 10.1002/hipo.22051.Increased.

Dauvilliers, Yves (2007) 'Insomnia in patients with neurodegenerative conditions', *Sleep Medicine*, 8(Supplementary 4), pp. S27–S34. doi: 10.1016/j.sleep.2007.04.011.

Deckers, Kay, Cadar, Dorina, Van Boxtel, Martin P. J., Verhey, Frans R. J., Steptoe, Andrew and Köhler, Sebastian (2019) 'Modifiable Risk Factors Explain Socioeconomic Inequalities in Dementia Risk: Evidence from a Population-Based Prospective Cohort Study', *Journal of Alzheimer's Disease*, 71(2), pp. 549–557. doi: 10.3233/JAD-190541.

Delbeuck, X., Van Der Linden, M. and Collette, F. (2003) 'Alzheimer's Disease as a Disconnection Syndrome?', *Neuropsychology Review*, pp. 79–92. doi: 10.1023/A:1023832305702.

delEtoile, Jon and Adeli, Hojjat (2017) 'Graph Theory and Brain Connectivity in Alzheimer's Disease', *Neuroscientist*, 23(6), pp. 616–626. doi: 10.1177/1073858417702621.

Dementia India Report 2010 (2010).

Dementia statistics (2021) *Alzheimer's Disease International*. Available at: https://www.alzint.org/about/dementia-facts-figures/dementia-statistics/.

Desai, M. K., Sudol, K. L., Janelsins, M. C., Mastrangelo, M. A., Frazer, M. E. and Bowers, J. W. (2009) 'Triple-transgenic Alzheimer's disease mice exhibit region-specific abnormalities in brain myelination patterns prior to appearance of amyloid and tau pathology.', *Glia*, 57(1), pp. 54–65.

Descoteaux, Maxime, Deriche, Rachid and Anwander, Alfred (2007) 'Deterministic and probabilistic q-ball tractography: from diffusion to sharp fiber distributions', (August), p. 36. doi: 10.1016/j.mcn.2008.05.017.

Desikan, Rahul S., Ségonne, Florent, Fischl, Bruce, Quinn, Brian T., Dickerson, Bradford C., Blacker, Deborah, Buckner, Randy L., Dale, Anders M., Maguire, R. Paul, Hyman, Bradley T., Albert, Marilyn S. and Killiany, Ronald J. (2006) 'An automated labeling system for subdividing the human cerebral cortex on MRI scans into gyral based regions of interest', *NeuroImage*, 31(3), pp. 968–980. doi: 10.1016/j.neuroimage.2006.01.021.

Dias, Amit and Patel, Vikram (2009) 'Closing the treatment gap for dementia in India', *India Journal of Psychiatry*, 51.

Dietrich, O., Biffar, A., Baur-Melnyk, A. and Reiser, M. F. (2010) 'Technical aspects of MR diffusion imaging of the body.', *European Journal of Radiology*, 76(3), pp. 314–322.

Dorsey, Sherrita M., Rodriquez, Helen D. and Brathwaite, Dollie (2002) 'Are things Really so Different? A Research Finding of Satisfaction, Illness and Depression in Rural South Africa Elderly.pdf'.

Douaud, G., Jbabdi, S., Behrens, TE, Menke, RA, Gass, A., Monsch, AU, Rao, A., Whitcher, B., Kindlmann, G., Matthews, PM and Smith, S. (2011) 'DTI measures in crossing fibre areas: Increased diffusion anisotropy reveals early white matter alteration in MCI and mild Alzheimer's disease.', *NeuroImage*, 55, pp. 880–890.

Du, A., Schuff, N., Kramer, J., Ganzer, S., Zhu, X., Jagust, W., Miller, B., Reed, B., Mungas, D. and Yaffe, K. (2004) 'Higher atrophy rate of entorhinal cortex than hippocampus in AD', *Neurology*, 62(3), pp. 422–427.

Duan, Jin-Hai, Wang, Hua-Qiao, Xu, Jie, Lin, Xian, Chen, Shao-Qiong, Kang, Zhuang and Yao, Zhi-Bin (2006) 'White matter damage of patients with Alzheimer's disease correlated with the decreased cognitive function', *Surg Radiol Anat*, 28, pp. 150–156.

Dubois, J., Dehaene-Lambertz, G., Perrin, M., Mangin, J. F., Cointepas, Y., Duchesnay, E., Le Bihan, D. and Hertz-Pannier, L. (2008) 'Asynchrony of the early maturation of white matter bundles in healthy infants: quantitative landmarks revealed noninvasively by diffusion tensor imaging', *Human Brain Mapping*, 29(1), pp. 14–27.

Duchek, Janet M., Balota, David A., Tse, Chi-Shing, Holtzman, David M., Fagan, Anne M. and Goate, Alison M. (2010) 'Tasks as an Early Marker for Alzheimer ' s Disease', *Neuropsychology*, 23(6), pp. 746–758. doi: 10.1037/a0016583.The.

Duchek, Janet M., Balota, David A., Tse, Chi Shing, Holtzman, David M., Fagan, Anne M. and Goate, Alison M. (2009) 'The

Utility of Intraindividual Variability in Selective Attention Tasks as an Early Marker for Alzheimer's Disease', *Neuropsychology*, 23(6), pp. 746–758. doi: 10.1037/a0016583.

Dutt, Shubir, Li, Yanrong, Mather, Mara and Nation, Daniel A. (2020) 'Brainstem volumetric integrity in preclinical and prodromal Alzheimer's disease', *Journal of Alzheimer's Disease*, 77(4), pp. 1579–1594. doi: 10.3233/JAD-200187.Brainstem.

Dykiert, Dominika, Der, Geoff, Starr, John M. and Deary, Ian J. (2012) 'Age Differences in Intra-Individual Variability in Simple and Choice Reaction Time: Systematic Review and Meta-Analysis', *PLoS ONE*, 7(10). doi: 10.1371/journal.pone.0045759.

Égerházi, Anikó, Berecz, Roland, Bartók, Eniko and Degrell, István (2007) 'Automated Neuropsychological Test Battery (CANTAB) in mild cognitive impairment and in Alzheimer's disease', *Progress in Neuro-Psychopharmacology and Biological Psychiatry*, 31(3), pp. 746–751. doi: 10.1016/j.pnpbp.2007.01.011.

Elias, MF, Beiser, A. and Wolf, PA (2000) 'The preclinical phase of Alzheimer disease: a 22-year prospective study of the Framingham Cohort.', *Archives of Neurology*, 57, pp. 808–813.

Engelbrecht, Kara (2019) *Intraindividual Variability and Micro-structural White Matter changes in Alzheimer's Disease*. The University of Cape Town.

Feldman, H., Yeatman, J., Lee, E., Barde, L. and Gaman-Bean, S. (2010) 'Diffusion Tensor Imaging: A Review for Pediatric Researchers and Clinicians', *Journal of Developmental and Behavioral Pediatrics*, 31(4), pp. 346–356. doi: 10.1097/DBP.0b013e3181dcaa8b.Diffusion.

Filippi, Massimo, Basaia, Silvia, Canu, Elisa, Imperiale, Francesca, Magnani, Giuseppe, Falautano, Monica, Comi, Giancarlo, Falini, Andrea and Agosta, Federica (2018) 'Changes in functional and structural brain connectome along the Alzheimer's disease continuum', *Molecular Psychiatry*. Springer US, 25(1), pp. 230–239. doi: 10.1038/s41380-018-0067-8.

Firbank, M. J., Watson, R., Mak, E., Aribisala, B., Barber, R., Colloby, S. J. and O'Brien, J. (2016) 'Longitudinal diffusion tensor imaging in dementia with lewy bodies and Alzheimer's disease.', *Parkinsonism and Related Disorders*, 24, pp. 76–80.

Fischer, Florian Udo, Wolf, Dominik, Scheurich, Armin and Fellgiebel, Andreas (2015) 'Altered whole-brain white matter networks in preclinical Alzheimer's disease', *NeuroImage: Clinical*. Elsevier B.V., 8, pp. 660–666. doi: 10.1016/j.nicl.2015.06.007.

Fiske, Donald W. and Rice, Laura (1955) 'Intra-individual response variability', *Psychological Bulletin*, 52(3), pp. 217–250. doi: 10.1037/h0045276.

Fjell, Anders M., Westlye, Lars T., Amlien, Inge K. and Walhovd, Kristine B. (2011) 'Reduced white matter integrity is related to cognitive instability.', *Journal of Neuroscience*, 31(49), pp. 18060–18072. doi: 10.1523/JNEUROSCI.4735-11.2011.

Folstein, Marshal F., Folstein, Susan E. and McHugh, Paul R. (1975) '"Mini-mental state". A practical method for grading the cognitive state of patients for the clinician', *Journal of Psychiatric Research*, 12(3), pp. 189–198. doi: 10.1016/0022-3956(75)90026-6.

Franciotti, Raffaella, Falasca, Nicola Walter, Arnaldi, Dario, Famà, Francesco, Babiloni, Claudio, Onofrj, Marco, Nobili, Flavio Mariano and Bonanni, Laura (2019) 'Cortical Network Topology in Prodromal and Mild Dementia Due to Alzheimer's Disease: Graph Theory Applied to Resting State EEG', *Brain Topography*. Springer US, 32(1), pp. 127–141. doi: 10.1007/s10548-018-0674-3.

Fray, Paul J., Robbins, Trevor W. and Sahakian, Barbara J. (1996) 'Neuorpsychiatyric applications of CANTAB', *International Journal of Geriatric Psychiatry*, 11(4), pp. 329–336. doi: 10.1002/(SICI)1099-1166(199604)11:4<329::AID-GPS453>3.0.CO;2-6.

Freedberg, Michael, Cunningham, Catherine A., Fioriti, Cynthia M., Murillo, Jorge Dorado, Reeves, Jack A., Taylor, Paul A., Sarlls, Joelle E. and Wassermann, Eric M. (2021) 'Multiple parietal pathways are associated with rTMS-induced hippocampal network enhancement and episodic memory changes', *NeuroImage*. Elsevier Inc., 237(May), p. 118199. doi: 10.1016/j.neuroimage.2021.118199.

Frisoni, GB, Testa, C., Zorzan, A., Sabattoli, F., Beltramello, A., Soininen, H. and Laakso, MP (2002) 'Detection of grey matter loss in mild Alzheimer's disease with voxel based morphometry.', *Journal of Neurology, Neurosurgery and Psychiatry*, 73, pp. 657–664.

Gao, Junling, Cheung, Raymond Tak-fai, Lee, Tatia M. C., Chu, Leung-wing, Sar, Hong Kong, Medical, Maclehose, Centre, Rehabilitation, Sar, Hong Kong, Aging, S. R. T. Healthy, Sar, Hong Kong, Faculty, L. K. S., Sar, Hong Kong, Faculty, L. K. S., Sar, Hong Kong and Sar, Hong Kong (2011) 'Possible Retrogenesis Observed with Fiber Tracking : An Anteroposterior Pattern of White Matter Disintegrity in Normal Aging and Alzheimer ' s Disease', 26, pp. 47–58. doi: 10.3233/JAD-2011-101788.

Garrett, Douglas D., MacDonald, Stuart W. S. and Craik, Fergus I. M. (2012) 'Intrain dividual reaction time variability is malleable: Feedback- and education-related reductions in variability with age', *Frontiers in Human Neuroscience*, 6(MAY 2012), pp. 1–10. doi: 10.3389/fnhum.2012.00101.

van Geuns, RJ, Wielopolski, PA, de Bruin, HG, van Ooijen, PM, Hulshoff, M., Oudkerk, M. and de Feyter, PJ (1999) 'Basic principles of magnetic resonance imaging', *Prog Cardiovasc Dis.*, 42(2), pp. 149–156.

Gold, Brian T., Powell, David A., Andersen, Anders H. and Smith, Charles D. (2011) 'Alterations in multiple measures of

white matter integrity in normal women at high risk of Alzheimer's disease', *NeuroImage*, 52(4), pp. 1487–1494. doi: 10.1016/j.neuroimage.2010.05.036.Alterations.

Gorelick, Philip B., Scuteri, Angelo, Black, Sandra E., Decarli, Charles, Greenberg, Steven M., Iadecola, Costantino, Launer, Lenore J., Laurent, Stephane, Lopez, Oscar L., Nyenhuis, David, Petersen, Ronald C., Schneider, Julie A., Tzourio, Christophe, Arnett, Donna K., Bennett, David A., Chui, Helena C., Higashida, Randall T., Lindquist, Ruth, Nilsson, Peter M., Roman, Gustavo C., Sellke, Frank W. and Seshadri, Sudha (2011) 'Vascular contributions to cognitive impairment and dementia: A statement for healthcare professionals from the American Heart Association/American Stroke Association', *Stroke*, 42(9), pp. 2672–2713. doi: 10.1161/STR.0b013e3182299496.

Gorus, Ellen, De Raedt, Rudi, Lambert, Margareta, Lemper, Jean Claude and Mets, Tony (2008) 'Reaction times and performance variability in normal aging, mild cognitive impairment, and Alzheimer's disease', *Journal of Geriatric Psychiatry and Neurology*, 21(3), pp. 204–218. doi: 10.1177/0891988708320973.

Gorus, Ellen, Raedt, Rudi De and Mets, Tony (2006) 'Diversity , dispersion and inconsistency of reaction time measures : effects of age and task complexity', 18(5).

Grady, Cheryl L., Mcintosh, Anthony R., Beig, Sania, Keightley, Michelle L., Burian, Hana and Black, Sandra E. (2003) 'Evidence from Functional Neuroimaging of a Compensatory Prefrontal Network in Alzheimer ' s Disease', 23(3), pp. 986–993.

Grand, Jacob H. G., Stawski, Robert S. and MacDonald, Stuart W. S. (2016) 'Comparing individual differences in inconsistency and plasticity as predictors of cognitive function in older adults', *Journal of Clinical and Experimental Neuropsychology*, 38(5), pp. 534–550. doi: 10.1080/13803395.2015.1136598.

Grant, Steven, Contoreggi, Carlo and London, Edythe D. (2000) 'Drug abusers show impaired performance in a laboratory test of decision making', *Neuropsychologia*, 38(8), pp. 1180–1187. doi: 10.1016/S0028-3932(99)00158-X.

Greicius, M. (2008) 'Resting-state functional connectivity in neuropsychiatric disorders', *Current Opinion in Neurology*, 21, pp. 424–430.

Greicius, Michael D., Srivastava, Gaurav, Reiss, Allan L. and Menon, Vinod (2004) 'Default-mode network activity distinguishes Alzheimer ' s disease from healthy aging : Evidence from functional MRI'.

Grinberg, LT, Rüb, U., Ferretti, REL, Nitrini, R., Farfel, JM, Polichiso, L., Gierga, K., Jacob-Filho, W. and Heinsen, H. (2009) 'The dorsal raphe nucleus shows phospho-tau neurofibrillary changes before the transentorhinal region in Alzheimers disease. A precocious onset?', *Neuropathology and Applied Neurobiology*, 35, pp. 405–416.

Grydeland, Håkon, Walhovd, Kristine B., Tamnes, Christian K., Westlye, Lars T. and Fjell, Anders M. (2013) 'Intracortical Myelin Links with Performance Variability across the Human Lifespan : Results from T1- and T2- Weighted MRI Myelin Mapping and Diffusion Tensor Imaging', 33(47), pp. 18618–18630. doi: 10.1523/JNEUROSCI.2811-13.2013.

Guo, X., Wang, Z., Li, K., Li, Z., Qi, Z., Jin, Z., Yao, L. and Chen, K. (2010) 'Voxel-based assessment of gray and white matter volumes in Alzheimer's disease', *Neuroscience Letters*, 468(2), pp. 146–150. doi: 10.1016/j.neulet.2009.10.086.Voxel-based.

Guo, Zongjun, Chen, Juan, Liu, Shien, Li, Yuhuan, Sun, Bo and Gao, Zhenbo (2013) 'Brain areas activated by uncertain reward-based decision-making in healthy volunteers', 8(35). doi: 10.3969/j.issn.1673-5374.2013.35.009.

Hagmann, P., Jonasson, L., Maeder, P., Thiran, J. P., Wedeen, V. J. and Meuli, R. (2006) 'Understanding diffusion MR imaging techniques: from scalar diffusion-weighted imaging to diffusion tensor imaging and beyond.', *Radiographics*, 26(Suppl 1), pp. S205-23.

Hale, S., Myerson, J., Smith, G. A. and Poon, L. W. (1988) 'Age, variability, and speed: between-subjects diversity', *Psychol. Aging*, 3, pp. 407–410. doi: 10.1037/0882-7974.3.4.407.

Halliday, Drew, Stawski, Robert, Cerino, Eric, DeCarlo, Correne, Grewal, Karl and MacDonald, Stuart (2018) 'Intraindividual Variability across Neuropsychological Tests: Dispersion and Disengaged Lifestyle Increase Risk for Alzheimer's Disease', *Journal of Intelligence*, 6(1), p. 12. doi: 10.3390/jintelligence6010012.

Halliday, Drew W. R., Gawryluk, Jodie R., Garcia-Barrera, Mauricio A. and MacDonald, Stuart W. S. (2019) 'White Matter Integrity Is Associated With Intraindividual Variability in Neuropsychological Test Performance in Healthy Older Adults', *Frontiers in Human Neuroscience*, 13(October), pp. 1–10. doi: 10.3389/fnhum.2019.00352.

Hampson, Michelle, Driesen, Naomi R., Skudlarski, Pawel, Gore, John C. and Constable, R. Todd (2006) 'Brain Connectivity Related to Working Memory Performance', 26(51), pp. 13338–13343. doi: 10.1523/JNEUROSCI.3408-06.2006.

Hashemi, RH, Bradley, WG and Lisanti, CJ (2004) *MRI: The Basics*. 2nd edn.

Haynes, Becky I., Bunce, David, Kochan, Nicole A., Wen, Wei, Brodaty, Henry and Sachdev, Perminder S. (2017) 'Associations between reaction time measures and white matter hyperintensities in very old age', *Neuropsychologia*. Elsevier, 96(December 2016), pp. 249–255. doi: 10.1016/j.neuropsychologia.2017.01.021.

He, Y., Wang, L., Zang, Y., Tian, L. and Zhang, X. (2007) 'Regional coherence changes in the early stages of Alzheimer's disease: a combined structural and resting-state functional MRI study.', *NeuroImage*, 35, pp. 488–500.

Herholz, K., Salmon, E., Perani, D., Baron, J. C., Holthoff, V., Frolich, L., Schonknecht, P., Ito, K., Mielke, R., Kalbe, E., Zundorf, G., Delbeuck, X., Pelati, O., Anchisi, D., Fazio, F., Kerrouche, N., Desgranges, B., Eustache, F., Beuthien-Baumann, B., Menzel, C., Schroder, J., Kato, T., Arahata, Y., Henze, M. and Heiss, W. D. (2002) 'Discrimination between Alzheimer dementia and controls by automated analysis of multicenter FDG PET', *NeuroImage*, 17, pp. 302–316.

Herlin, Bastien, Navarro, Vincent and Dupont, Sophie (2021) 'The temporal pole: From anatomy to function- A literature appraisal', *Journal of Chemical Neuroanatomy*, 113.

Hillary, FG, Roman, CA, Venkatesan, U., Rajtmajer, SM, Bajo, R. and Castellanos, ND (2015) 'Hyperconnectivity is a fundamental response to neurological disruption.', *Neuropsychology*, 29, p. 59.

Hirata, Y., Matsuda, H., Nemoto, K., Ohnishi, T., Hirao, K., Yamashita, F., Asada, T., Iwabuchi, S. and Samejima, H. (2005) 'Voxel-based morphometry to discriminate early Alzheimer's disease from controls', *Neuroscience Letters*, 382, pp. 269–274.

Hirni, DI, Kivisaari, SL, Monsch, AU and Taylor, KI (2013) 'Distinct neuroanatomical bases of episodic and semantic memory performance in Alzheimer's disease', *Neuropsychologia*, 51, pp. 930–937.

Hoeft, F., Barnea-Goraly, N., Haas, B. W., Golarai, G., Ng, D., Mills, D. and Reiss, A. L. (2007) 'More Is Not Always Better: Increased Fractional Anisotropy of Superior Longitudinal Fasciculus Associated with Poor Visuospatial Abilities in Williams Syndrome.', *Journal of Neuroscience*, 27(44), pp. 11960–11965.

Hong, Yun Jeong, Yoon, Bora, Lim, Sung Chul, Shim, Yong S., Kim, Jee Young, Ahn, Kook Jin, Han, Il Woo and Yang, Dong Won (2013) 'Microstructural changes in the hippocampus and posterior cingulate in mild cognitive impairment and Alzheimer's disease: A diffusion tensor imaging study', *Neurological Sciences*, 34(7), pp. 1215–1221. doi: 10.1007/s10072-012-1225-4.

Hua, Xue, Leow, Alex, Lee, Suh, Klunder, Andrea, Toga, Arthur, Lepore, Natasha, Chou, Yi-Yu and Brun, Caroline (2008) '3D characterization of brain atrophy in Alzheimer's diseas and mild cognitive impairment using tensor-based morphometry', *Neuroimage*, 41(1), pp. 19–34.

Huang, Hao, Fan, Xin, Weiner, Myron, Martin-cook, Kristin, Xiao, Guanghua, Davis, Jeannie, Devous, Michael, Rosenberg, Roger and Diaz-arrastia, Ramon (2013) 'Alzheimer ' s disease with full diffusion tensor characterization', 33(9), pp. 2029–2045. doi: 10.1016/j.neurobiolaging.2011.06.027.Distinctive.

Huang, Juebin, Friedland, R. P. and Auchus, A. P. (2007) 'Diffusion tensor imaging of normal-appearing white matter in mild cognitive impairment and early Alzheimer disease: Preliminary evidence of axonal degeneration in the temporal lobe', *American Journal of Neuroradiology*, 28(10), pp. 1943–1948. doi: 10.3174/ajnr.A0700.

Huisman, T. A. G. M. (2010) 'Diffusion-weighted and diffusion tensor imaging of the brain, made easy', *Cancer Imaging*, 10(SPEC. ISS. A), pp. 163–171. doi: 10.1102/1470-7330.2010.9023.

Hultsch, David F. and MacDonald, Stuart W. S. (2004) 'Intraindividual variability in performance as a theoretical window onto cognitive aging', in *New Frontiers in Cognitive Aging*. doi: 10.1093/acprof:oso/9780198525691.003.0004.

Hultsch, David F., MacDonald, Stuart W. S. and Dixon, Roger A. (2002) 'Variability in reaction time performance of younger and older adults', *Journals of Gerontology - Series B Psychological Sciences and Social Sciences*, 57(2), pp. 101–115. doi: 10.1093/geronb/57.2.P101.

Hultsch, David F., MacDonald, Stuart W. S., Hunter, Michael A., Levy-Bencheton, J. and Strauss, Esther (2000) 'Intraindividual variability in cognitive performance in older adults: comparison of adults with mild dementia, adults with arthritis, and healthy adults.', *Neuropsychology*, 14, pp. 588–598. doi: 10.1037/0894-4105.14.4.588.

Hultsch, David F., Strauss, Esther, Hunter, Michael A. and MacDonald, Stuart W. S. (2008) 'Intraindividual variability, cognition and aging', in Craik, Fergus I. M. and Salthouse, Timothy A. (eds) *The Handbook of Aging and Cognition*. 3rd edn. New York, pp. 491–556.

Huppert, Felicia A., Brayne, Carol, Gill, Caroline, Paykel, E. S. and Beardsall, Lynn (1995) 'CAMCOG—A concise neuropsychological test to assist dementia diagnosis: Socio-demographic determinants in an elderly population sample', *British Journal of Clinical Psychology*, 34(4), pp. 529–541. doi: 10.1111/j.2044-8260.1995.tb01487.x.

Huque, Md Hamidul, Carlin, John B., Simpson, Julie A. and Lee, Katherine J. (2018) 'A comparison of multiple imputation methods for missing data in longitudinal studies 01 Mathematical Sciences', *BMC Medical Research Methodology*. BMC Medical Research Methodology, 18(1), pp. 1–16. doi: 10.1186/s12874-018-0615-6.

Hwang, Misun, Tudorascu, Dana L., Nunley, Karen, Karim, Helmet, Aizenstein, Howard J., Orchard, Trevor J. and Rosano, Caterina (2016) 'Brain Activation and Psychomotor Speed in Middle-Aged Patients with Type 1 Diabetes: Relationships with Hyperglycemia and Brain Small Vessel Disease', *Journal of Diabetes Research*.

Ibrahim, Ibrahim, Horacek, Jiri, Bartos, Ales, Hajek, Milan, Ripova, Daniela, Brunovsky, Martin and Tintera, Jaroslav (2009) 'Combination of voxel based morphometry and diffusion tensor imaging in patients with Alzheimer's disease', *Neuroendocrinology Letters*, 30(1), pp. 39–45.

Iglesias, Juan Eugenio, Augustinack, Jean C., Nguyen, Khoa, Player, Christopher M., Player, Allison, Wright, Michelle, Roy, Nicole, Frosch, Matthew P., McKee, Ann C., Wald, Lawrence L., Fischl, Bruce and Van Leemput, Koen (2015) 'A

computational atlas of the hippocampal formation using ex vivo, ultra-high resolution MRI: Application to adaptive segmentation of in vivo MRI', *NeuroImage*. Elsevier B.V., 115, pp. 117–137. doi: 10.1016/j.neuroimage.2015.04.042.

Iglesias, Juan Eugenio, Van Leemput, Koen, Bhatt, Priyanka, Casillas, Christen, Dutt, Shubir, Schuff, Norbert, Truran-Sacrey, Diana, Boxer, Adam and Fischl, Bruce (2015) 'Bayesian segmentation of brainstem structures in MRI', *NeuroImage*. Elsevier B.V., 113, pp. 184–195. doi: 10.1016/j.neuroimage.2015.02.065.

Jack, Clifford R., Knopman, David S., Jagust, William J., Petersen, Ronald C., Weiner, Michael W., Aisen, Paul S., Shaw, Leslie M., Vemuri, Prashanthi, Wiste, Heather J., Weigand, Stephen D., Lesnick, Timothy G., Pankratz, Vernon S., Donohue, Michael C. and Trojanowski, John Q. (2013) 'Tracking pathophysiological processes in Alzheimer's disease: An updated hypothetical model of dynamic biomarkers', *The Lancet Neurology*, 12(2), pp. 207–216. doi: 10.1016/S1474-4422(12)70291-0.

Jackson, Jonathan D., Balota, David A., Duchek, Janet M. and Head, Denise (2012) 'White matter integrity and reaction time intraindividual variability in healthy aging and early-stage Alzheimer disease', *Neuropsychologia*. Elsevier Ltd, 50(3), pp. 357–366. doi: 10.1016/j.neuropsychologia.2011.11.024.

James, Katharine A., Grace, Laurian K., Thomas, Kevin G. F. and Combrinck, Marc I. (2015) 'Associations between CAMCOG-R subscale performance and formal education attainment in South African older adults', *International Psychogeriatrics*, 27(2), pp. 251–260. doi: 10.1017/S1041610214002233.

Johnson, David K., Barrow, Willis, Anderson, Rae Ann, Harsha, Amith, Honea, Robyn, Brooks, William M. and Burns, Jeffrey M. (2010) 'Diagnostic utility of cerebral white matter integrity in early alzheimer's disease', *International Journal of Neuroscience*, 120(8), pp. 544–550. doi: 10.3109/00207454.2010.494788.

Jokinen, H., Melkas, S., Ylikoski, R., Pohjasvaara, T., Kaste, M., Erkinjuntti, T. and Hietanen, M. (2015) 'Post-stroke cognitive impairment is common even after successful clinical recovery', *European Journal of Neurology*, 22(9), pp. 1288–1294. doi: 10.1111/ene.12743.

De Jong, L., Van der Hiele, K., Veer, I., Houwing, J., Westendorp, R., Bollen, E., De Bruin, P., Middelkoop, H., Van Buchem, M. and Der Van Grond, J. (2008) 'Strongly reduced volumes of putamen and thalamus in Alzheimer's disease: an MRI study', *Brain*, 131, pp. 3277–3285.

Jumah, Fareed R. and Dossani., Rimal H. (2021) 'Neuroanatomy, Cingulate Cortex', *StatPearls*. Available at: https://www.ncbi.nlm.nih.gov/books/NBK537077/.

Kälin, Andrea M., Pflüger, Marlon, Gietl, Anton F., Riese, Florian, Jäncke, Lutz, Nitsch, Roger M. and Hock, Christoph (2014) 'Intraindividual variability across cognitive tasks as a potential marker for prodromal Alzheimer's disease', *Frontiers in Aging Neuroscience*, 6(JUL), pp. 1–8. doi: 10.3389/fnagi.2014.00147.

Kalula, Sebastiana Zimba, Ferreira, Monica, Thomas, Kevin G. F., de Villiers, Linda, Joska, John A. and Geffen, Leon N. (2010) 'Profile and management of patients at a memory clinic', *South African Medical Journal*, 100(7), pp. 449–451. doi: 10.7196/samj.3384.

Karas, G., Scheltens, P., Rombouts, S., van Schijndel, R., Klein, M., Jones, B., van der Flier, W., Vrenken, H. and Barkhof, F. (2007) 'Precuneus atrophy in early-onset Alzheimer's disease: A morphometric structural MRI study', *Neuroradiology*, 49, pp. 967–976.

Karp, Anita, Kåreholt, Ingemar, Qiu, Chengxuan, Bellander, Tom, Winblad, Bengt and Fratiglioni, Laura (2004) 'Relation of Education and Occupation-based Socioeconomic Status to Incident Alzheimer's Disease', *American Journal of Epidemiology*, 159(2), pp. 175–183. doi: 10.1093/aje/kwh018.

Kelly, A. M. Clar., Uddin, Lucina Q., Biswal, Bharat B., Castellanos, F. Xavier and Milham, Michael P. (2008) 'Competition between functional brain networks mediates behavioral variability', *NeuroImage*, 39(1), pp. 527–537. doi: 10.1016/j.neuroimage.2007.08.008.

Kidron, D., Black, S. E., Stanchev, P., Buck, B., Szalai, J. P., Parker, J., Szekely, C. and Bronskill, M. J. (1997) 'Quantitative MR volumetry in Alzheimer's disease - Topographic markers and the effects of sex and education', *Neurology*, 49, pp. 1504–1512.

Kilimann, I., Grothe, M., Heinsen, H., Alho, EJL, Grinberg, L., Amaro, E. Jr, Dos Santos, GAB, Da Silva, RE, Mitchell, AJ and Frisoni, GB (2014) 'Subregional basal forebrain atrophy in Alzheimer's disease: a multicenter study.', *J Alzheimers Dis*, 40, pp. 687–700.

Kim, Dae Jin and Min, Byoung Kyong (2020) 'Rich-club in the brain's macrostructure: Insights from graph theoretical analysis', *Computational and Structural Biotechnology Journal*. The Author(s), 18, pp. 1761–1773. doi: 10.1016/j.csbj.2020.06.039.

Kim, Eunkyung, Kang, Hyejin, Lee, Hyekyoung, Lee, Hyo Jeong, Suh, Myung Whan, Song, Jae Jin, Oh, Seung Ha and Lee, Dong Soo (2014) 'Morphological brain network assessed using graph theory and network filtration in deaf adults', *Hearing Research*. Elsevier B.V, 315, pp. 88–98. doi: 10.1016/j.heares.2014.06.007.

Kinney, Jefferson W., Bemiller, Shane M., Murtishaw, Andrew S., Leisgang, Amanda M., Salazar, Arnold M. and Lamb, Bruce T. (2018) 'Inflammation as a central mechanism in Alzheimer's disease', *Alzheimer's and Dementia: Translational Research*

and Clinical Interventions. Elsevier Inc., 4, pp. 575–590. doi: 10.1016/j.trci.2018.06.014.

Kitamura, S., Kiuchi, K., Taoka, T., Hashimoto, K., Ueda, S., Yasuno, F. and Kishimoto, T. (2013) 'Longitudinal white matter changes in Alzheimer's disease: A tractography-based analysis study.', *Brain Research*, 1515, pp. 12–18.

Klawiter, E. C., Schmidt, R. E., Trinkaus, K., Liang, H. F., Budde, M. D., Naismith, R. T., Song, S. K., Cross, A. H. and & Benzinger, T. L. (2011) 'Radial diffusivity predicts demyelination in ex vivomultiple sclerosis spinal cords.', *NeuroImage*, 55(4), pp. 1454–1460.

Kocagoncu, Ece, Quinn, Andrew, Firouzian, Azadeh, Cooper, Elisa, Greve, Andrea, Gunn, Roger, Green, Gary, Woolrich, Mark W., Henson, Richard N., Lovestone, Simon and Rowe, James B. (2020) 'Tau pathology in early Alzheimer's disease is linked to selective disruptions in neurophysiological network dynamics', *Neurobiology of Aging*. Elsevier Inc, 92, pp. 141–152. doi: 10.1016/j.neurobiolaging.2020.03.009.

Kocevar, Gabriel Stamile, Claudio, Hannoun, Salem, Cotton, François, Vukusic, Sandra, Durand-Dubief, Françoise and Sappey-Marinier, Dominique (2016) 'Graph Theory-Based Brain Connecitivity for Automatic Classification of Multiple Sclerosis Clincal Courses', *Frontiers in Neuroscience*.

Van Den Kommer, Tessa N., Comijs, Hannie C., Aartsen, Marja J., Huisman, Martijn, Deeg, Dorly J. H. and Beekman, Aartjan T. F. (2013) 'Depression and cognition: How do they interrelate in old age?', *American Journal of Geriatric Psychiatry*. Elsevier Inc, 21(4), pp. 398–410. doi: 10.1016/j.jagp.2012.12.015.

van der Kouwe, André J. W., Benner, Thomas, Salat, David H. and Fischl, Bruce (2008) 'Brain morphometry with multiecho MPRAGE', *NeuroImage*, 40(2), pp. 559–569. doi: 10.1016/j.neuroimage.2007.12.025.

Kruschke, John K. (2010) 'Bayesian data analysis', *Wiley Interdisciplinary Reviews: Cognitive Science*, 1(5), pp. 658–676. doi: 10.1002/wcs.72.

Kuang, Liqun, Gao, Yan, Chen, Zhongyu, Xing, Jiacheng, Xiong, Fengguang and Han, Xie (2020) 'White matter brain network research in Alzheimer's disease using persistent features', *Molecules*, 25(11), pp. 1–16. doi: 10.3390/molecules25112472.

Kulason, Sue, Xu, Eileen, Tward, Daniel J., Bakker, Arnold and Albert, Marilyn (2020) 'Entorhinal and Transentorhinal Atrophy in Preclinical Alzheimer ' s Disease', 14(August), pp. 1–12. doi: 10.3389/fnins.2020.00804.

Lachaud, Christian Michel and Renaud, Olivier (2011) 'A tutorial for analyzing human reaction times: How to filter data, manage missing values, and choose a statistical model', *Applied Psycholinguistics*, 32(2), pp. 389–416. doi: 10.1017/S0142716410000457.

de LaCoste, Marie Christine and White, Charles L. (1993) 'The role of cortical connectivity in Alzheimer's disease pathogenesis: A review and model system', *Neurobiology of Aging*, pp. 1–16. doi: 10.1016/0197-4580(93)90015-4.

Langbaum, J. B., Chen, K., Lee, W., Reschke, C., Bandy, D., Fleisher, A. S., Alexander, G. E., Foster, N. L., Weiner, M. W., Koeppe, R. A., Jagust, W. J. and Reiman, E. M. (2009) 'Categorical and correlational analyses of baseline fluorodeoxyglucose positron emission tomography images from the Alzheimer's Disease Neuroimaging Initiative (ADNI)', *NeuroImage*, 45, pp. 1107–1116.

Latora, Vito and Marchiori, Massimo (2001) 'Efficient behavior of small-world networks', *Physical Review Letters*, 87(19), pp. 198701-1-198701–4. doi: 10.1103/PhysRevLett.87.198701.

Lebel, C., Walker, L., Leemans, A., Phillips, L. and Beaulieu, C. (2008) 'Microstructural maturation of the human brain from childhood to adulthood', *NeuroImage*, 40(3), pp. 1044–1055.

Lee, Dong Hyuk, Lee, Peter, Seo, Sang Won, Roh, Jee Hoon, Oh, Minyoung, Oh, Jungsu S., Oh, Seung Jun, Kim, Jae Seung and Jeong, Yong (2019) 'Neural substrates of cognitive reserve in Alzheimer's disease spectrum and normal aging', *NeuroImage*. Elsevier Ltd, 186(November 2018), pp. 690–702. doi: 10.1016/j.neuroimage.2018.11.053.

Lee, Ji Han, Ryan, John, Andreescu, Carmen, Aizenstein, Howard and Limc, Hyun Kook (2015) 'Brainstem morphological changes in Alzheimer's disease', *NeuroReport*, 26(7), pp. 411–415. doi: 10.1097/WNR.0000000000000362.Brainstem.

Lee, Seung-Hwan, Coutua, Jean-Philippe, Wilkensa, Paul, Yendikia, Anastasia, Rosasa, H. Diana and Salata, David H. (2015) 'Tract-Based Analysis of White Matter Degeneration in Alzheimer's Disease', *Neuroscience*, 301, pp. 79–89. doi: 10.1016/j.neuroscience.2015.05.049.Tract-Based.

Leech, Robert and Sharp, David J. (2014) 'The role of the posterior cingulate cortex in cognition and disease', *Brain*, 137(1), pp. 12–32. doi: 10.1093/brain/awt162.

Leeds, Lesley, Meara, R. Jolyon, Woods, Robert and Hobson, J. Peter (2001) 'A comparison of the new executive functioning domains of the CAMCOG-R with existing tests of executive function in elderly stroke survivors', *Age and Ageing*, 30(3), pp. 251–254. doi: 10.1093/ageing/30.3.251.

Levinoff, J. Elis., Saumier, Daniel and Chertkow, Howard (2005) 'Focused attention deficits in patients with Alzheimer's disease and mild cognitive impairment', *Brain and Cognition*, 57(2), pp. 127–130.

Li, Xingfeng, Coyle, Damien, Maguire, Liam, Watson, DR and McGinnity, TM (2011) 'Gray matter concentration and effective connectivity changes in Alzheimer's disease : a longitudinal structural MRI study', *Neuroradiology*, 53, pp. 733–748. doi: 10.1007/s00234-010-0795-1.

Lima Portugal, Liana Catarina, Alves, Rita de Cássia Soares, Junior, Orlando Fernandes, Sanchez, Tiago Arruda, Mocaiber, Izabela, Volchan, Eliane, Smith Erthal, Fátima, David, Isabel Antunes, Kim, Jongwan, Oliveira, Leticia, Padmala, Srikanth, Chen, Gang, Pessoa, Luiz and Pereira, Mirtes Garcia (2020) 'Interactions between emotion and action in the brain', *NeuroImage*, 214(March). doi: 10.1016/j.neuroimage.2020.116728.

Limbachia, Chirag, Morrow, Kelly, Khibovska, Anastasiia, Meyer, Christian, Padmala, Srikanth and Pessoa, Luiz (2021) 'Controllability over stressor decreases responses in key threat-related brain areas', *Communications Biology*. Springer US, 4(1), pp. 1–11. doi: 10.1038/s42003-020-01537-5.

Lin, Feng, Ren, Ping, Lo, Raymond Y., Chapman, Benjamin P., Jacobs, Alanna, Baran, Timothy M., Porsteinsson, Anton P. and Foxe, John J. (2017) 'Insula and Inferior Frontal Gyrus' Activities Protect Memory Performance Against Alzheimer's Pathology in Old Age', *Journal of Alzheimer's Disease*, 55(3), pp. 669–678. doi: 10.3233/JAD-160715.Insula.

Liu, Hao, Hu, Haimeng, Wang, Huiying, Han, Jiahui, Li, Yunfei, Qi, Huihui, Wang, Meimei, Zhang, Sisi, He, Huijin and Zhao, Xiaohu (2020) 'A brain network constructed on an L1-norm regression model is more sensitive in detecting small world network changes in early AD', *Hindawi*.

Liu, Yawu, Spulber, Gabriela, Lehtimaki, Kimmo K., Kononen, Mervi, Hallikainen, Ilona, Grohn, Heidi, Kivipelto, Miia, Hallikainen, Merja, Vanninen, Ritva and Soininen, Hilkka (2011) 'Diffusion tensor imaging and Tract- Based Spatial Statistics in Alzheimer's disease and mild cognitive impairment', *Neurobiology of Aging*, pp. 1558–1571. doi: 10.1016/j.neurobiolaging.2009.10.006.

Lo, Chun Yi, Wang, Pei Ning, Chou, Kun Hsien, Wang, Jinhui, He, Yong and Lin, Ching Po (2010) 'Diffusion tensor tractography reveals abnormal topological organization in structural cortical networks in Alzheimer's disease', *Journal of Neuroscience*, 30(50), pp. 16876–16885. doi: 10.1523/JNEUROSCI.4136-10.2010.

López-Sanz, David, Garcés, Pilar, Álvarez, Blanca, Delgado-Losada, Mariá Luisa, López-Higes, Ramón and Maestú, Fernando (2017) 'Network Disruption in the Preclinical Stages of Alzheimer's Disease: From Subjective Cognitive Decline to Mild Cognitive Impairment', *International Journal of Neural Systems*, 27(8). doi: 10.1142/S0129065717500411.

Lord, Louis David, Stevner, Angus B., Deco, Gustavo and Kringelbach, Morten L. (2017) 'Understanding principles of integration and segregation using whole-brain computational connectomics: Implications for neuropsychiatric disorders', *Philosophical Transactions of the Royal Society A: Mathematical, Physical and Engineering Sciences*, 375(2096). doi: 10.1098/rsta.2016.0283.

Lövdén, Martin, Li, Shu Chen, Shing, Yee Lee and Lindenberger, Ulman (2007) 'Within-person trial-to-trial variability precedes and predicts cognitive decline in old and very old age: Longitudinal data from the Berlin Aging Study', *Neuropsychologia*, 45(12), pp. 2827–2838. doi: 10.1016/j.neuropsychologia.2007.05.005.

Lövdén, Martin, Schmiedek, Florian, Kennedy, Kristen M., Rodrigue, Karen M., Lindenberger, Ulman and Raz, Naftali (2013) 'Does variability in cognitive performance correlate with frontal brain volume?', *NeuroImage*, 64(1), pp. 209–215. doi: 10.1016/j.neuroimage.2012.09.039.

Lowe, Christine and Rabbitt, Patrick (1998) 'Test/re-test reliability of the CANTAB and ISPOCD neuropsychological batteries: Theoretical and practical issues', *Neuropsychologia*, 36(9), pp. 915–923. doi: 10.1016/S0028-3932(98)00036-0.

Luo, Wenjing, Greene, Abigail S. and Constable, R. Todd (2021) 'Within node connectivity changes, not simply edge changes, influence graph theory measures in functional connectivity studies of the brain', *NeuroImage*. Elsevier Inc., 240(May), p. 118332. doi: 10.1016/j.neuroimage.2021.118332.

Ma, Xiaofen, Jiang, Guihua, Fu, Shishun, Fang, Jin, Wu, Yunfan and Liu, Mengchen (2018) 'Enhanced Network Efficiency of Functional Brain Networks in Primary Insomnia Patients', 9(February), pp. 1–11. doi: 10.3389/fpsyt.2018.00046.

MacDonald, Stuart W. S., Hultsch, David F. and Dixon, Roger A. (2003) 'Performance variability is related to change in cognition: Evidence from the Victoria longitudinal study', *Psychology and Aging*, 18(3), pp. 510–523. doi: 10.1037/0882-7974.18.3.510.

MacDonald, Stuart W. S., Nyberg, Lars and Bäckman, Lars (2006) 'Intra-individual variability in behavior: links to brain structure, neurotransmission and neuronal activity', *Trends in Neurosciences*, 29(8), pp. 474–480. doi: 10.1016/j.tins.2006.06.011.

MacDonald, Stuart W. S., Nyberg, Lars, Sandblom, Johan, Fischer, Håkan and Bäckman, Lars (2008) 'Increased response-time variability is associated with reduced inferior parietal activation during episodic recognition in aging', *Journal of Cognitive Neuroscience*, 20(5), pp. 779–786. doi: 10.1162/jocn.2008.20502.

Machulda, M. M., Ward, H. A., Borowski, B., Gunter, J. L., Cha, R. H., O'Brien, P. C., Petersen, R. C., Boeve, B. F., Knopman, D., Tang-Wai, D. F., Ivnik, R. J., Smith, G. E., Tangalos, E. G. and Jr., C. R. Jack (2009) 'Comparison of memory fMRI response among Normal, MCI, and Alzheimer's patients', *Neurology*, 61(4), pp. 500–506.

Maruff, Paul, Falleti, Marina G., Collie, Alex, Darby, David and McStephen, Michael (2005) 'Fatigue-related impairment in the speed, accuracy and variability of psychomotor performance: Comparison with blood alcohol levels', *Journal of Sleep Research*, 14(1), pp. 21–27. doi: 10.1111/j.1365-2869.2004.00438.x.

McDonald, C. R., McEvoy, L. K., Gharapetian, L., Fennema-Notestine, C., Hagler, D. J., Holland, D., Koyama, A., Brewer, J. B.

and Dale, A. M. (2009) 'Regional rates of neocortical atrophy from normal aging to early Alzheimer disease', *Neurology*, 73(6), pp. 457–465. doi: 10.1212/WNL.0b013e3181b16431.

Mcevoy, Linda K., Fennema-notestine, Christine, Roddey, J. Cooper, Holland, Dominic, Pung, Christopher J., Brewer, James B. and Dale, Anders M. (2009) 'Alzheimer Disease : Quantitative Structural Neuroimaging for Detection and Prediction of Clinical and Purpose : Methods : Results : Conclusion ':, *Radiology*, 251(1), pp. 195–205.

McKhann, GM (2012) 'The diagnosis of dementia due to Alzheimer's disease', *Alzheimers Dement*, 7(3), pp. 263–269. doi: 10.1016/j.jalz.2011.03.005.The.

McKhann, Guy, Drachman, David, Folstein, Marshall, Katzman, Robert, Price, Donald and Stadlan, Emanuel M. (1984) 'Clinical diagnosis of alzheimer's disease: Report of the NINCDS-ADRDA work group⋆ under the auspices of department of health and human services task force on alzheimer's disease', *Neurology*, 34(7), pp. 939–944. doi: 10.1212/wnl.34.7.939.

McRobbie, D. W., Moore, E. A., Graves, Martin J. and Prince, Martin R. (2006) *MRI From Picture to Proton*. 2nd edn. Cambridge University Press.

McShane, Blakeley B., Gal, David, Gelman, Andrew, Robert, Christian and Tackett, Jennifer L. (2019) 'Abandon Statistical Significance', *American Statistician*, 73(sup1), pp. 235–245. doi: 10.1080/00031305.2018.1527253.

Mears, David and Pollard, Harvey B. (2016) 'Review Network Science and the Human Brain : Using Graph Theory to Understand the Brain and One of Its Hubs , the Amygdala , in Health and Disease', *Journal of Neuroscience Research*, 605(January), pp. 590–605. doi: 10.1002/jnr.23705.

Mella, Nathalie, De Ribaupierre, Sandrine, Eagleson, Roy and De Ribaupierre, Anik (2013) 'Cognitive intraindividual variability and white matter integrity in aging', *The Scientific World Journal*, 2013. doi: 10.1155/2013/350623.

Mesulam, MM (2000) 'A plasticity-based theory of the pathogenesis of Alz heimer's disease.', *Annals of Neurology*, 924, pp. 42–52.

Mielke, MM, Kozauer, NA, Chan, KC, George, M. and J, Toroney (2009) 'Regionally-specific diffusion tensor imaging in mild cognitive impairment and Alzheimer's disease', *NeuroImage*, 46, pp. 47–55.

Mijalkov, Mite, Kakaei, Ehsan, Pereira, Joana B., Westman, Eric and Volpe, Giovanni (2017) 'BRAPH: A graph theory software for the analysis of brain connectivity', *PLoS ONE*, 12(8).

Mito, Remika, Raffelt, David, Dhollander, Thijs, Vaughan, David N., Tournier, J. Donald, Salvado, Olivier, Brodtmann, Amy, Rowe, Christopher C., Villemagne, Victor L. and Connelly, Alan (2018) 'Fibre-specific white matter reductions in Alzheimer's disease and mild cognitive impairment', *Brain*, 141(3), pp. 888–902. doi: 10.1093/brain/awx355.

Mole, Jilu Princy, Subramanian, Leena, Bracht, Tobias, Morris, Huw, Metzler-baddeley, Claudia and Linden, David E. J. (2016) 'Increased fractional anisotropy in the motor tracts of Parkinson ' s disease suggests compensatory neuroplasticity or selective neurodegeneration', *European Radiology*. European Radiology, pp. 3327–3335. doi: 10.1007/s00330-015-4178-1.

Monte, S. M. de la (1989) 'Quantitation of cerebral atrophy in preclinical and end-stage Alzheimer's disease', *Annals of Neurology*, 25(5), pp. 450–459.

Mori, S. and Zhang, J. (2006) 'Principles of Diffusion Tensor Imaging and Its Applications to Basic Neuroscience Research', *Neuron*, 51(5), pp. 527–539. doi: https://doi.org/10.1016/j.neuron.2006.08.012.

Mori, Susumu and Van Zijl, Peter C. M. (2002) 'Fiber tracking: Principles and strategies - A technical review', *NMR in Biomedicine*, 15(7–8), pp. 468–480. doi: 10.1002/nbm.781.

Van De Mortel, Laurens Ansem, Thomas, Rajat Mani and Van Wingen, Guido Alexander (2021) 'Grey Matter Loss at Different Stages of Cognitive Decline: A Role for the Thalamus in Developing Alzheimer's Disease', *Journal of Alzheimer's Disease*, 83(2), pp. 705–720. doi: 10.3233/JAD-210173.

Moy, G., Millet, P., Haller, S., Baudois, S., de Bilbao, F., Weber, K., Lövblad, K., Lazeyras, F., Giannakopoulos, P. and Delaloye, C. (2011) 'Magnetic resonance imaging determinants of intraindividual variability in the elderly: Combined analysis of grey and white matter', *Neuroscience*. Elsevier Inc., 186, pp. 88–93. doi: 10.1016/j.neuroscience.2011.04.028.

Murphy, Andrew (2017) *Lingual gyrus*, *Radiopaedia*. Available at: https://radiopaedia.org/articles/lingual-gyrus.

Naggara, Olivier, Oppenheim, Catherine, Rieu, Dorothée, Raoux, Nadine, Rodrigo, Sebastian, Dalla Barba, Gianfranco and Meder, Jean François (2006) 'Diffusion tensor imaging in early Alzheimer's disease', *Psychiatry Research - Neuroimaging*, 146(3), pp. 243–249. doi: 10.1016/j.pscychresns.2006.01.005.

Nagy, Krisztina, Greenlee, Mark W. and Kovács, Gyula (2012) 'The lateral occipital cortex in the face perception network: an effective connectivity study', *Frontiers in Psychology*.

Najdenovska, Elena, Alemán-Gómez, Yasser, Battistella, Giovanni, Descoteaux, Maxime, Hagmann, Patric, Jacquemont, Sebastien, Maeder, Philippe, Thiran, Jean Philippe, Fornari, Eleonora and Cuadra, Meritxell Bach (2018) 'In-vivo probabilistic atlas of human thalamic nuclei based on diffusion-weighted magnetic resonance imaging', *Scientific Data*. The Author(s), 5(October), pp. 1–11. doi: 10.1038/sdata.2018.270.

Nesselroade, J. R. (1991) 'Interindividual differences in intraindividual change', in Collins, L. M. and Horn, J. L. (eds) *Best*

Methods for the Analysis of Change: Recent Advances, Unanswered Questions, Future Directions. Washington DC, pp. 92–105.

Nestor, Peter J., Fryer, Tim D. and Hodges, John R. (2006) 'Declarative memory impairments in Alzheimer's disease and semantic dementia', *NeuroImage*, 30(3), pp. 1010–1020. doi: 10.1016/j.neuroimage.2005.10.008.

Newman, M. E. J. and Girvan, M. (2004) 'Finding and evaluating community structure in networks', *Physical Review E - Statistical, Nonlinear, and Soft Matter Physics*, 69(22). doi: 10.1103/PhysRevE.69.026113.

Ng, Adeline Su Lyn, Wang, Juan, Ng, Kwun Kei, Su, Joanna Xian Chong, Qian, Xing, Kai, Joseph Wei Lim, Tan, Yi Jayne, Cui, Alisa Wen Yong, Chander, Russell Jude, Hameed, Shahul, Kang, Simon Seng Ting, Kandiah, Nagaendran and Zhou, Juan Helen (2021) 'Distinct network topology in Alzheimer ' s disease and behavioral variant frontotemporal dementia', *Alzheimer's Research & Therapy*. Alzheimer's Research & Therapy, 13(13), pp. 1–16.

Nie, Xiuling, Sun, Yu, Wan, Suiren, Zhao, Hui, Liu, Renyuan, Li, Xueping, Wu, Sichu, Nedelska, Zuzana, Hort, Jakub, Qing, Zhao, Xu, Yun and Zhang, Bing (2017) 'Subregional structural alterations in hippocampus and nucleus accumbens correlate with the clinical impairment in patients with Alzheimer's Disease clinical spectrum: Parallel combining volume and vertex-based approach', *Frontiers in Neurology*. doi: 10.3389/fneur.2017.00399.

Nir, Talia M., Jahanshad, Neda, Villalon-Reina, Julio E., Toga, Arthur W., Jack, Clifford R., Weiner, Michael W. and Thompson, Paul M. (2013) 'Effectiveness of regional DTI measures in distinguishing Alzheimer's disease, MCI, and normal aging', *NeuroImage: Clinical*. The Authors, 3, pp. 180–195. doi: 10.1016/j.nicl.2013.07.006.

Nowrangi, M. A., Lyketsos, C. G., Leoutsakos, J. S., Oishi, K., Albert, M., Mori, S. and Mielke, M. M. (2013) 'Longitudinal, region- specific course of diffusion tensor imaging measures in mild cognitive impairment and Alzheimer's disease', *Alzheimer's and Dementia*, 9(5), pp. 519–528.

Nulkar, Amit, Paralikar, Vasudeo and Juvekar, Sanjay (2019) 'Dementia in India - a call for action', *Journal of Global Health Reports*, 3. doi: doi:10.29392/joghr.3.e2019078.

O'Brien, Richard J. and Wong, Philip C. (2011) 'Amyloid precursor protein processing and alzheimer's disease', *Annual Review of Neuroscience*, 34, pp. 185–204. doi: 10.1146/annurev-neuro-061010-113613.

O'Donnell, L. J. and Westin, C. F. (2011) 'An Introduction to Diffusion Tensor Image Analysis', *Neurosurgery Clinics of North America*, 22(2), pp. 185–196.

Pate, Debra Sue, Margolin, David Ira, Friedrich, Frances J. and Bentley, Elizabeth Elia (1992) 'Decision-making and attentional processes in ageing and in dementia of the Alzheimer's type', *Cognitive Neuropsychology*, pp. 321–339.

Pennanen, C., Kivipelto, M., Tuomainen, S., Hartikainen, P., Hanninen, T., Laakso, MP, Hallikainen, M., Vanhanen, M., Nissinen, A., Helkala, EL, Vainio, P., Vanninen, R., Partanen, K. and Soininen, H. (2004) 'Hippocampus and entorhinal cortex in mild cognitive impairment and early AD', *Neurobiology of Aging*, 25, pp. 303–310.

Pereira, Joana B., Mijalkov, Mite, Kakaei, Ehsan, Mecocci, Patricia, Vellas, Bruno, Tsolaki, Magda, Kłoszewska, Iwona, Soininen, Hilka, Spenger, Christian, Lovestone, Simmon, Simmons, Andrew, Wahlund, Lars Olof, Volpe, Giovanni and Westman, Eric (2016) 'Disrupted Network Topology in Patients with Stable and Progressive Mild Cognitive Impairment and Alzheimer's Disease', *Cerebral Cortex*, 26(8), pp. 3476–3493. doi: 10.1093/cercor/bhw128.

Pereira, Joana B., Van Westen, Danielle, Stomrud, Erik, Strandberg, Tor Olof, Volpe, Giovanni, Westman, Eric and Hansson, Oskar (2018) 'Abnormal structural brain connectome in individuals with preclinical Alzheimer's disease', *Cerebral Cortex*, 28(10), pp. 3638–3649. doi: 10.1093/cercor/bhx236.

Phillips, Michelle, Rogers, Peter, Haworth, Judy, Bayer, Antony and Tales, Andrea (2013) 'Intra-Individual Reaction Time Variability in Mild Cognitive Impairment and Alzheimer's Disease: Gender, Processing Load and Speed Factors', *PLoS ONE*, 8(6). doi: 10.1371/journal.pone.0065712.

Phillips, OR, Joshi, SH, Piras, F., Orfei, MD, Iorio, M., Narr, KL, Shattuck, DW, Caltagirone, C., Spalletta, G. and Di Paola, M. (2016) 'The superficial white matter in Alzheimer's disease', *Human Brain Mapping*, 37, pp. 1321–1334.

Pierpaoli, C. and Basser, PJ (1996) 'Toward a quantitative assessment of diffusion anisotropy', *Magnetic Resonance in Medicine*, 36, pp. 893–906.

Pierpaoli, C. and Walker, L. (2010) 'TORTOISE: an integrated software package for processing of diffusion MRI data', *… Processing of Diffusion …*, 51(1), p. 2010. Available at: http://cds.ismrm.org/protected/10MProceedings/files/1597_6360.pdf.

Pievani, Michela, Agosta, Federica, Pagani, Elisabetta, Canu, Elisa, Sala, Stefania, Absinta, Martina, Geroldi, Cristina, Ganzola, Rossana, Frisoni, Giovanni B. and Filippi, Massimo (2010) 'Assessment of white matter tract damage in mild cognitive impairment and Alzheimer's disease', *Human Brain Mapping*, 31(12), pp. 1862–1875. doi: 10.1002/hbm.20978.

Pini, Lorenzo, Pievani, Michela, Bocchetta, Martina, Altomare, Daniele, Bosco, Paolo, Cavedo, Enrica, Galluzzi, Samantha, Marizzoni, Moira and Frisoni, Giovanni B. (2016) 'Brain atrophy in Alzheimer ' s Disease and aging', *Ageing Research Reviews*. Elsevier B.V., 30(2016), pp. 25–48. doi: 10.1016/j.arr.2016.01.002.

Prescott, Jeffrey W., Guidon, Arnaud, Dorsaiswamy, P. Mural., Choudhury, Kingshuk Roy, Liu, Chunlei and Petrella, Jeffrey R. (2014) 'Connectome : Changes in Cortical Network Topology with Increased', *Neuroradiology*, 273(1), pp. 175–184.

Price, J. L., Ko, A. I., Wade, M. J., Tsou, S. K., McKeel, D. W. and Morris, J. C. (2001) 'Neuron number in the entorhinal cortex and CA1 in preclinical Alzheimer disease', *Archives of Neurology*, 58(9), pp. 1395–1405.

Prince, JL and Morris, JC (1999) 'Tangles and plques in nondemented aging and "preclinical" Alzheimer's disease', *Annals of Neurology*, 45, pp. 358–368.

Prince, Martin, Wimo, Anders, Guerchet, Maëlenn, Gemma-Claire, Ali, Wu, Yu-Tzu and Prina, Matthew (2015) 'World Alzheimer Report 2015: The Global Impact of Dementia - An analysis of prevalence, incidence, cost and trends', *Alzheimer's Disease International*. doi: 10.1111/j.0963-7214.2004.00293.x.

Qiu, Anqi, Oishi, Kenichi, Miller, Michael I., Lyketsos, Constantine G., Mori, Susumu and Albert, Marilyn (2010) 'Surface-based analysis on shape and fractional anisotropy of white matter tracts in Alzheimer's disease', *PLoS ONE*, 5(3). doi: 10.1371/journal.pone.0009811.

Rabbitt, Patrick M. A., Osman, Paul, Moore, Belinda and Stollery, Brian (2001) 'There are stable individual differences in performance variability, both from moment to moment and from day to day', *Quarterly Journal of Experimental Psychology Section A: Human Experimental Psychology*, 54(4), pp. 981–1003. doi: 10.1080/713756013.

Raichle, M. E., MacLeod, A. M., Snyder, A. Z., Powers, W. J., Gusnard, D. A. and Shulman, G. L. (2002) 'A default mode of brain function', *Proceedings of the National Academy of Sciences*, 98(2), pp. 676–682. doi: 10.1073/pnas.98.2.676.

Raichle, ME (2015) 'The brain's default mode network.', *Annual Review of Neuroscience*, 38, pp. 433–447.

Ram, N., Conroy, D., Pincus, A., Hyde, A. and Molloy, L. (2012) 'Tethering theory to method: Using measures of intraindividual variability to operationalize individuals' dynamic characteristics', in Harring, Jeffrey R. and Hancock, Gregory R. (eds) *Advances in longitudinal methods in the social and behavioral sciences*. IAP Information Age Publishing, pp. 81–110.

Ramlall, S., Chipps, J., Pillay, B. J. and Bhigjee, A. I. (2013) 'Mild cognitive impairment and dementia in a heterogeneous elderly population: Prevalence and risk profile', *African Journal of Psychiatry (South Africa)*, 16(6), pp. 456–465. doi: 10.4314/ajpsy.v16i6.58.

Reijmer, Yael D., Leemans, Alexander, Caeyenberghs, Karen, Heringa, Sophie M., Koek, Huiberdina L. and Biessels, Geert Jan (2013) 'Disruption of cerebral networks and cognitive impairment in Alzheimer disease', *Neurology*, 80(15), pp. 1370–1377. doi: 10.1212/WNL.0b013e31828c2ee5.

Reisberg, B., Franssen, EH, Souren, LEM, Auer, SR and Akram, I. (2002) 'Evidence and mechanisms of retrogenesis in Alzheimer's and other dementias: management and treatment import', *Am J Alzheimer's Dis Other Demen*, 17, pp. 202–212.

Reisberg, Barry, Franssen, Emile H., Hasan, Syed Mahmood, Monteiro, Isabel, Boksay, Istvan, Souren, Liduim E. M., Kenowsky, Sunnie, Auer, Stefanie R., Elahi, Shahid and Kluger, Alan (1999) 'Retrogenesis: Clinical, physiologic, and pathologic mechanisms in brain aging, Alzheimer's and other dementing processes.pdf', *Eur Arch Psychiatry Clin Neuroscience*, 249(3), pp. 28–36.

Rombouts, Serge A. R. B., Barkhof, Frederik, Veltman, Dick J., Machielsen, Willem C. M., Witter, Menno P., Bierlaagh, Marije A., Lazeron, Richard H. C., Valk, Jaap and Scheltens, Philip (2000) 'Functional MR Imaging in Alzheimer ' s Disease during Memory Encoding', (December), pp. 1869–1875.

Rose, Stephen E., Janke, Andrew L. and Chalk, Jonathan B. (2008) 'Gray and white matter changes in Alzheimer's disease: A diffusion tensor imaging study', *Journal of Magnetic Resonance Imaging*, 27(1), pp. 20–26. doi: 10.1002/jmri.21231.

Rubinov, Mikail and Sporns, Olaf (2010) 'Complex network measures of brain connectivity: Uses and interpretations', *NeuroImage*, 52(3), pp. 1059–1069. doi: 10.1016/j.neuroimage.2009.10.003.

Ryan, Natalie S., Keihaninejad, Shiva, Shakespeare, Timothy J., Lehmann, Manja, Crutch, Sebastian J., Malone, Ian B., Thornton, John S., Mancini, Laura, Hyare, Harpreet, Yousry, Tarek, Ridgway, Gerard R., Zhang, Hui, Modat, Marc, Alexander, Daniel C., Rossor, Martin N., Ourselin, Sebastien and Fox, Nick C. (2013) 'Magnetic resonance imaging evidence for presymptomatic change in thalamus and caudate in familial Alzheimer's disease', *Brain*, 136(5), pp. 1399–1414. doi: 10.1093/brain/awt065.

Salat, David H., Greve, Douglad N., Pacheco, Jennifer L., Quinn, Brian T., Helmer, Karl G., Buckner, Randy L. and Fischl, Bruce (2009) 'Regional white matter volume differences in nondemented aging and Alzheimer's disease', *NeuroImage*, 44(4), pp. 1247–1258. doi: 10.1016/j.neuroimage.2008.10.030.

Salat, DH, Tucha, DS, Kouwea, AJW van der, Grevea, DN, Pappua, V., Lee, SY, Hevelonea, ND, Zaletaa, AK, Growdonb, JH, Corkina, S., Fischla, B. and Rosasa, HD (2010) 'White Matter Pathology Isolates the Hippocampal Formation in Alzheimer's Disease', *Neurobiology of Aging*, 31(2), pp. 244–256. doi: 10.1016/j.neurobiolaging.2008.03.013.White.

Sands, MJ and Levitin, A. (2004) 'Basics of magnetic resonance imaging', *Semin Vasc Surg*, 17(2), pp. 66–82.

Sano, Mary, Rosen, Wilma, Stern, Yaakov, Rosen, Jeffrey and Mayeux, Richard (1995) 'Simple reaction time as a measure of global attention in Alzheimer's disease', *Journal of the International Neuropsychological Society*, 1(1), pp. 56–61.

Sattler, Christine, Toro, Pablo, Schönknecht, Peter and Schröder, Johannes (2012) 'Cognitive activity, education and socioeconomic status as preventive factors for mild cognitive impairment and Alzheimer's disease', *Psychiatry Research*.

Elsevier Ltd, 196(1), pp. 90–95. doi: 10.1016/j.psychres.2011.11.012.

Schmitt, L. Ian, Wimmer, Ralf D., Nakajima, Miho, Happ, Michael, Mofakham, Sima and Halassa, Michael M. (2017) 'Thalamic amplification of cortical connecitivty sustains attentional control', *Nature*, 545(7653), pp. 219–223. doi: 10.1038/nature22073.Thalamic.

Sen, P. N. and Basser, P. J. (2005) 'A model for diffusion in white matter in the brain.', *Biophysical Journal*, 89, pp. 2927–2938.

Serra, Laura, Cercignani, Mara, Lenzi, Delia, Perri, Roberta, Fadda, Lucia, Caltagirone, Carlo, MacAluso, Emiliano and Bozzali, Marco (2010) 'Grey and white matter changes at different stages of Alzheimer's disease', *Journal of Alzheimer's Disease*, 19(1), pp. 147–159. doi: 10.3233/JAD-2010-1223.

Sexton, Claire. E., Kalu, Ukwuori G., Filippini, Nicola, Mackay, Clare E. and Ebmeier, Kalus P. (2011) 'A meta-analysis of diffusion tensor imaging in mild cognitive impairment and Alzheimer's disease', *Neurobiology of Aging*, 32(12), p. 2322.

Sheng, Xiaoning, Chen, Haifeng, Shao, Pengfei, Qin, Ruomeng, Zhao, Hui, Xu, Yun and Bai, Feng (2021) 'Brain Structural Network Compensation Is Associated With Cognitive Impairment and Alzheimer's Disease Pathology', *Frontiers in Neuroscience*, 15(February), pp. 1–13. doi: 10.3389/fnins.2021.630278.

Shu, Ni, Liang, Ying, Li, He, Zhang, Junying, Li, Xin, Wang, Liang, He, Yong, Wang, Yongyan and Zhang, Zhanjun (2012) 'Organization in White Matter Structural Networks in Amnestic Mild Cognitive Impairment ':, *Neuroradiology*, 265(2), pp. 518–527. doi: 10.1148/radiol.12112361/-/DC1.

Si, Shuaizong, Wang, Bin, Liu, Xiao, Yu, Chong, Ding, Chao and Zhao, Hai (2019) 'Brain Network Modeling Based on Mutual Information and Graph Theory for Predicting the Connection Mechanism in the Progression of Alzheimer ' s Disease'. doi: 10.3390/e21030300.

Simic, G., Stanic, G., Mladinov, M., Jovanov-Milosevic, N., Kostovic, I. and Hof, PR (2009) 'Does Alzheimer's disease begin in the brainstem?', *Neuropathology and Applied Neurobiology*, 35, pp. 532–554.

Sjöbeck, M., Elfgren, C., Larsson, E. M., Brockstedt, S., Lätt, J., Englund, E. and Passant, U. (2010) 'Alzheimer's disease (AD) and executive dysfunction. A case control study on the significance of frontal white matter changes detected by diffusion tensor imaging (DTI).', *Arch Gerontol Geriatr*, 50, pp. 260–266.

Soares, José M., Marques, Paulo, Alves, Victor and Sousa, Nuno (2013) 'A hitchhiker's guide to diffusion tensor imaging', *Frontiers in Neuroscience*, (7 MAR). doi: 10.3389/fnins.2013.00031.

Somers, David C. and Sheremata, Summer L. (2014) 'Attention maps in the brain', 4(4), pp. 327–340. doi: 10.1002/wcs.1230.Attention.

Song, S. K., Sun, S. W., Ramsbottom, M. J., Chang, C., Russell, J. and Cross, A. H. (2002) 'Dysmyelination revealed through MRI as increased radial (but unchanged axial) diffusion of water.', *NeuroImage*, 17(3), pp. 1429–1436.

Sonuga-Barke, Edmund J. S. and Castellanosa, F. Xavier (2007) 'Spontaneous attentional fluctuations in impaired states and pathological conditions: A neurobiological hypothesis', *Neuroscience & Biobehavioral Reviews*, 31(7), pp. 977–986.

Sorg, C., Riedl, V. and Muhlau, M. (2007) 'Selective changes of resting-state networks in individuals at risk for Alzheimer's disease', *Proceedings of the National Academy of Sciences of the United States of America*, 104(47), pp. 18760–18765.

Sowell, Elizabeth R., Peterson, Bradley S., Thompson, Paul M., Welcome, Suzanne E., Henkenius, Amy L. and Toga, Arthur W. (2003) 'Mapping cortical change across the human life span', *Nature Neuroscience*, 6(3), pp. 309–315. doi: 10.1038/nn1008.

Sporns, Olaf (2018) 'Graph theory methods: applications in brain networks', *Dialogues in clinical neuroscience*, pp. 111–121.

Spreng, R. Nathan (2012) 'The fallacy of a "task-negative" network', *Frontiers in Psychology*.

Squire, Larry R., Stark, Craig E. L. and Clark, Robert E. (2004) 'The medial temporal lobe', *Annual Review of Neuroscience*, 27, pp. 279–306.

Stahl, Robert, Dietrich, Olaf, Teipel, Stefan J., Hampel, Harald, Reiser, Maximilian F. and Schoenberg, Stefan O. (2007) 'White matter damage in Alzheimer disease and mild cognitive impairment: Assessment with diffusion-tensor MR imaging and parallel imaging techniques', *Radiology*, 243(2), pp. 483–492. doi: 10.1148/radiol.2432051714.

Stebbins, G. T. and Murphy, C. M. (2009) 'Diffusion tensor imaging in Alzheimer's disease and mild cognitive impairment.', *Behav. Neurol.*, 21(1), pp. 39–49.

Stevens, Alexander A., Tappon, Sarah C., Garg, Arun and Fair, Damien A. (2012) 'Functional brain network modularity captures inter- and intra-individual variation in working memory capacity', *PLoS ONE*, 7(1). doi: 10.1371/journal.pone.0030468.

Straube, Thomas, Schmidt, Stephanie, Weiss, Thomas, Mentzel, Hans Joachim and Miltner, Wolfgang H. R. (2009) 'Dynamic activation of the anterior cingulate cortex during anticipatory anxiety', *NeuroImage*, 44(3), pp. 975–981. doi: 10.1016/j.neuroimage.2008.10.022.

Stricker, N. H., Schweinsburg, B. C., Delano-Wood, L., Wierenga, C. E., Bangen, K. J., Haaland, K. Y., Frank, L. R., Salmon, D.

P. and Bondi, M. W. (2009) 'Decreased white matter integrity in late-myelinating fiber pathways in Alzheimer's disease supports retrogenesis', *NeuroImage*, 45(1), pp. 10–16. doi: 10.1016/j.neuroimage.2008.11.027.Decreased.

Stuss, Donald T., Murphy, Kelly J., Binns, Malcolm A. and Alexander, Michael P. (2003) 'Staying on the job: The frontal lobes control individual performance variability', *Brain*, 126(11), pp. 2363–2380. doi: 10.1093/brain/awg237.

Sugihara, S., Kinoshita, T., Matsusue, E., Fujii, S. and Ogawa, T. (2004) 'Usefulness of diffusion tensor imaging of white matter in Alzheimer disease and vascular dementia.', *Acta Neurologica Scandinavica*, 45(6), pp. 658–663.

Sullivan, E. V., Rohlfing, T. and Pfefferbaum, A. (2010) 'Quantitative fiber tracking of lateral and interhemispheric white matter systems in normal aging: relations to timed performance.', *Neurobiology of Aging*, 31(3), pp. 464–481.

Sun, Yu, Bi, Qiuhui, Wang, Xiaoni, Hu, Xiaochen, Li, Huijie, Li, Xiaobo, Ma, Ting, Lu, Jie, Chan, Piu, Shu, Ni and Han, Ying (2019) 'Prediction of conversion from amnestic mild cognitive impairment to Alzheimer's disease based on the brain structural connectome', *Frontiers in Neurology*, 10(JAN), p. 1178. doi: 10.3389/fneur.2018.01178.

Supekar, Kaustubh, Menon, Vinod, Rubin, Daniel, Musen, Mark and Greicius, Michael D. (2008) 'Network analysis of intrinsic functional brain connectivity in Alzheimer's disease', *PLoS Computational Biology*, 4(6). doi: 10.1371/journal.pcbi.1000100.

Swan, Gary E. and Lessov-Schlaggar, Christina N. (2007) 'The effects of tobacco smoke and nicotine on cognition and the brain', *Neuropsychology Review*, 17(3), pp. 259–273. doi: 10.1007/s11065-007-9035-9.

Tan, Rachel H., Wong, Stephanie, Hodges, John R., Halliday, Glenda M. and Hornberger, Michael (2013) 'Retrosplenial cortex (BA 29) volumes in behavioral variant frontotemporal dementia and Alzheimer's disease', *Dementia Geriatric Cognitive Disorders*, 35(3–4), pp. 177–182.

Taylor, Paul A., Chen, Gang, Cox, Robert W. and Saad, Ziad S. (2015) 'Open Environment for Multimodal Interactive Connectivity Visualization and Analysis', *Brain Connectivity*, 6(2), pp. 109–121. doi: 10.1089/brain.2015.0363.

Taylor, Paul A., Cho, Kuan Hung, Lin, Ching Po and Biswal, Bharat B. (2012) 'Improving DTI Tractography by including Diagonal Tract Propagation', *PLoS ONE*, 7(9). doi: 10.1371/journal.pone.0043415.

Taylor, Paul A. and Saad, Ziad S. (2013) 'FATCAT: (An Efficient) functional and tractographic connectivity analysis toolbox', *Brain Connectivity*, 3(5), pp. 523–535. doi: 10.1089/brain.2013.0154.

Teipel, Stefan J., Grothe, Michel J., Filippi, Massimo, Fellgiebel, Andreas, Dyrba, Martin, Frisoni, Giovanni B., Meindl, Thomas, Bokde, Arun L. W., Hampel, Harald, Klöppel, Stefan and Hauenstein, Karlheinz (2014) 'Fractional anisotropy changes in Alzheimer's disease depend on the underlying fiber tract architecture: A multiparametric DTI study using joint independent component analysis', *Journal of Alzheimer's Disease*, 41(1), pp. 69–83. doi: 10.3233/JAD-131829.

Teipel, Stefan J., Stahl, Robert, Dietrich, Olaf, Schoenberg, Stefan O., Perneczky, Robert, Bokde, Arun L. W., Reiser, Maximilian F., Möller, Hans Jürgen and Hampel, Harald (2007) 'Multivariate network analysis of fiber tract integrity in Alzheimer's disease', *NeuroImage*, 34(3), pp. 985–995. doi: 10.1016/j.neuroimage.2006.07.047.

Thompson, Paul M., Hayashi, Kiralee M., Zubicaray, Greig De, Janke, Andrew L., Rose, Stephen E., Semple, James, Herman, David, Hong, Michael S., Dittmer, Stephanie S., Doddrell, David M. and Toga, Arthur W. (2003) 'Dynamics of Gray Matter Loss in Alzheimer ' s Disease', *Journal of Neuroscience*, 23(3), pp. 994–1005.

Thorpe, Simon, Fize, Denis and Marlot, Catherine (1996) 'Speed of processing in the human visual system.pdf'.

Tinaz, Sule, Lauro, Peter M., Ghosh, Pritha, Lungu, Codrin and Horovitz, Silvina G. (2017) 'Changes in functional organization and white matter integrity in the connectome in Parkinson's disease', *NeuroImage: Clinical*. The Author(s), 13, pp. 395–404. doi: 10.1016/j.nicl.2016.12.019.

Tromp, Do (2016) 'Diffusion Imaging - DTI Scalars (FA, MD, AD, RD) - How do they relate to brain structure?', pp. 1–3. doi: 10.15200/winn.146119.94778.

Tuch, David S., Salat, David H., Wisco, Jonathan J., Zaleta, Alexandra K., Hevelone, Nathanael D. and Rosas, H. Diana (2005) 'Choice reaction time performance correlates with diffusion anisotropy in white matter pathways supporting visuospatial attention', *Proceedings of the National Academy of Sciences of the United States of America*, 102(34), pp. 12212–12217. doi: 10.1073/pnas.0407259102.

Tuladhar, Anil M., Van Uden, Ingeborg W. M., Rutten-Jacobs, Loes C. A., Lawrence, Andrew, Van Der Holst, Helena, Van Norden, Anouk, De Laat, Karlijn, Van Dijk, Ewoud, Claassen, Jurgen A. H. R., Kessels, Roy P. C., Markus, Hugh S., Norris, David G. and De Leeuw, Frank Erik (2016) 'Structural network efficiency predicts conversion to dementia', *Neurology*, 86(12), pp. 1112–1119. doi: 10.1212/WNL.0000000000002502.

Ullén, Fredrik, Forsman, Lea, Blom, Örjan, Karabanov, Anke and Madison, Guy (2008) 'Intelligence and variability in a simple timing task share neural substrates in the prefrontal white matter', *Journal of Neuroscience*, 28(16), pp. 4238–4243. doi: 10.1523/JNEUROSCI.0825-08.2008.

Vasquez, Brandon P., Binns, Malcolm A. and Anderson, Nicole D. (2018) 'Response Time Consistency Is an Indicator of Executive Control Rather than Global Cognitive Ability', *Journal of the International Neuropsychological Society*, 24, pp. 456–465. doi: 10.1017/S1355617717001266.

Veronese, Mattia, Moro, Lucia, Arcolin, Marco, Dipasquale, Ottavia, Rizzo, Gaia, Expert, Paul, Khan, Wasim, Fisher, Patrick M., Svarer, Claus, Bertoldo, Alessandra, Howes, Oliver and Turkheimer, Federico E. (2019) 'Covariance statistics and network analysis of brain PET imaging studies', *Scientific Reports*. Springer US, 9(1), pp. 1–15. doi: 10.1038/s41598-019-39005-8.

Walhovd, Kristine B. and Fjell, Anders M. (2007) 'White matter volume predicts reaction time instability', *Neuropsychologia*, 45(10), pp. 2277–2284. doi: 10.1016/j.neuropsychologia.2007.02.022.

Wang, Changsheng, Stebbins, Glenn T., Medina, David A., Shah, Raj C., Bammer, Roland, Moseley, Michael E. and Toledo-Morrell, Leyla de (2012) 'Atrophy and dysfunction of parahippocampal white matter in mild Alzheimer's disease', *Neurobiology of Aging*, 33(1), pp. 43–52. doi: 10.1016/j.neurobiolaging.2010.01.020.Atrophy.

Wang, Jinhui, Zuo, Xinian, Dai, Zhengjia, Xia, Mingrui, Zhao, Zhilian, Zhao, Xiaoling, Jia, Jianping, Han, Ying and He, Yong (2013) 'Disrupted functional brain connectome in individuals at risk for Alzheimer's disease', *Biological Psychiatry*. Elsevier, 73(5), pp. 472–481. doi: 10.1016/j.biopsych.2012.03.026.

Wang, Tao, Shi, Feng, Jin, Yan, Yap, Pew Thian, Wee, Chong Yaw, Zhang, Jianye, Yang, Cece, Li, Xia, Xiao, Shifu and Shen, Dinggang (2016) 'Multilevel Deficiency of White Matter Connectivity Networks in Alzheimer's Disease: A Diffusion MRI Study with DTI and HARDI Models', *Neural Plasticity*, 2016. doi: 10.1155/2016/2947136.

Wang, Xiao Ni, Zeng, Yang, Chen, Guan Qun, Zhang, Yi He, Li, Xuan Yu, Hao, Xu Yang, Yu, Yang, Zhang, Meng, Sheng, Can, Li, Yu Xia, Sun, Yu, Li, Hong Yan, Song, Yang, Li, Kun Cheng, Yan, Tian Yi, Tang, Xiao Ying and Han, Ying (2016) 'Abnormal organization of white matter networks in patients with subjective cognitive decline and mild cognitive impairment', *Oncotarget*, 7(31), pp. 48953–48962. doi: 10.18632/oncotarget.10601.

Wang, Zhiqun, Jia, Xiuqin, Liang, Peipeng, Qi, Zhigang and Yang, Yanhui (2011) 'Changes in thalamus connectivity in mild cognitive impairment : Evidence from resting state fMRI Changes in thalamus connectivity in mild cognitive impairment : Evidence from resting state fMRI', *European Journal of Radiology*. Elsevier Ireland Ltd, 81(2), pp. 277–285. doi: 10.1016/j.ejrad.2010.12.044.

Watts, Duncan J. and Strogatz, Steven H. (1998) 'Collective dynamics of "small-world" networks', in *The Structure and Dynamics of Networks*, pp. 301–303. doi: 10.1515/9781400841356.301.

Wehrli, FW and Kanal, E. (1987) 'Orbital imaging: factors determining magnetic resonance imaging appearance', *Radio; Clin North Am*, 25(3), pp. 419–427.

Weiler, Marina, Casseb, Raphael Fernandes, de Campos, Brunno Machado, Teixeira, Camila Vieira de Ligo, Carletti-Cassani, Ana Flávia Mac Knight, Vicentini, Jéssica Elias, Magalhães, Thamires Naela Cardoso, de Almeira, Débora Queiroz, Talib, Leda Leme, Forlenza, Orestes Vicente, Balthazar, Marcio Luiz Figueredo and Castellano, Gabriela (2018) 'Cognitive reserve relates to functional network efficiency in Alzheimer's disease', *Frontiers in Aging Neuroscience*, 10(AUG), pp. 1–14. doi: 10.3389/fnagi.2018.00255.

Weissman, D. H., Roberts, K. C., Visscher, K. M. and Woldorff, M. G. (2006) 'The neural bases of momentary lapses in attention', *Nature Neuroscience*, 9(7), pp. 971–978. doi: 10.1038/nn1727.

Werf, Ysbrand D. Van der, Jolles, Jelle, Witter, Menno P. and Uylings, Harry B. M. (2003) 'Contributions of thalamic nuclei to declarative memory functioning', *Cortex*, 39(4–5), pp. 1047–1062.

Van Der Werf, Ysbrand D., Tisserand, Danielle J., Visser, Pieter Jelle, Hofman, Paul A. M., Vuurman, Eric, Uylings, Harry B. M. and Jolles, Jelle (2001) 'Thalamic volume predicts performance on tests of cognitive speed and decreases in healthy aging: A magnetic resonance imaging-based volumetric analysis', *Cognitive Brain Research*, 11(3), pp. 377–385. doi: 10.1016/S0926-6410(01)00010-6.

West, Elizabeth A., Moschak, Travis M. and Carelli, Regina M. (2018) 'Distinct Functional Microcircuits in the Nucleus Accumbens Underlying Goal-Directed Decision-Making', *Computations and Neural Circuits*, pp. 199–219.

West, Robert, Murphy, Kelly J., Armilio, Maria L., Craik, Fergus I. M. and Stuss, Donald T. (2002) 'Lapses of intention and performance variability reveal age-related increases in fluctuations of executive control', *Brain and Cognition*, 49(3), pp. 402–419. doi: 10.1006/brcg.2001.1507.

Woo, Young Jae, Roussos, Panos, Haroutunian, Vahram, Katsel, Pavel, Gandy, Samuel, Schadt, Eric E. and Zhu, Jun (2020) 'Comparison of brain connectomes by MRI and genomics and its implication in Alzheimer's disease', *BMC Medicine*. BMC Medicine, 18(1), pp. 1–17. doi: 10.1186/s12916-019-1488-1.

World Health Organisation (2015) *The Epidemiology and Impact of Dementia: Current State and Future Trends*, *The Epidemiology and Impact of Dementia: Current State and Future Trends*. Available at: http://www.who.int/mental_health/neurology/dementia/thematic_briefs_dementia/en/.

'World Medical Association Declaration of Helsinki: ethical principles for medical research involving human subjects' (2013) *The Journal of the American College of Dentists*, 81(3), pp. 14–18. doi: 10.1093/acprof:oso/9780199241323.003.0025.

Wright, Laura M., Marco, Matteo De, Venneri, Annalena, Wright, Laura M. and Marco, Matteo De (2021) 'A Graph Theory Approach to Clarifying Aging and Disease Related Changes in Cognitive Networks', 13(July), pp. 1–19. doi: 10.3389/fnagi.2021.676618.

Wu, Zhanxiong, Xu, Dong, Potter, Thomas and Zhang, Yingchun (2019) 'Effects of brain parcellation on the characterization of topological deterioration in Alzheimer's disease', *Frontiers in Aging Neuroscience*, 11(MAY). doi: 10.3389/fnagi.2019.00113.

Xie, S., Xiao, JX, Gong, GL, Zang, YF, Wang, YH, Wu, HK and Jiang, XX (2006) 'Voxel-based detection of white matter abnormalities in mild Alzheimer disease.', *Neurology*, 66, pp. 1845–1849.

Xie, Sheng, Xiao, Jiang Xi, Wang, Yin Hua, Wu, Hong Kun, Gong, Gao Lang and Jiang, Xue Xiang (2005) 'Evaluation of bilateral cingulum with tractography in patients with Alzheimer's disease', *NeuroReport*, 16(12), pp. 1275–1278. doi: 10.1097/01.wnr.0000174061.41897.ee.

Yang, Huanqing, Xu, Hua, Li, Qingfeng, Jin, Yan, Jiang, Weixiong, Wang, Jinghua, Wu, Yina, Li, Wei, Yang, Cece, Li, Xia, Xiao, Shifu, Shi, Feng and Wang, Tao (2019) 'Study of brain morphology change in Alzheimer's disease and amnestic mild cognitive impairment compared with normal controls', *General Psychiatry*, 32(2), pp. 1–9. doi: 10.1136/gpsych-2018-100005.

Yesavage, Jerome A., Brink, T. L., Rose, Terence L., Lum, Owen, Huang, Virginia, Adey, Michael and Leirer, Von Otto (1982) 'Development and validation of a geriatric depression screening scale: A preliminary report', *Journal of Psychiatric Research*, 17(1), pp. 37–49. doi: 10.1016/0022-3956(82)90033-4.

Zajac, Lauren, Koo, Bang Bon, Bauer, Corinna M. and Killiany, Ron (2017) 'Seed location impacts whole-brain structural network comparisons between healthy elderly and individuals with alzheimer's disease', *Brain Sciences*, 7(4). doi: 10.3390/brainsci7040037.

Zarei, Mojtaba, Patenaude, Brian, Damoiseaux, Jessica, Morgese, Ciro, Smith, Steve, Matthews, Paul M., Barkhof, Frederik, Rombouts, Serge, Sanz-Arigita, Ernesto and Jenkinson, Mark (2010) 'Combining shape and connectivity analysis: An MRI study of thalamic degeneration in Alzheimer's disease', *NeuroImage*, 49(1), pp. 1–8. doi: 10.1016/j.neuroimage.2009.09.001.

Zhang, Y., Schuff, N., Jahng, G. H., Bayne, W., Mori, S., Schad, L., Mueller, S., Du, A. T., Kramer, J. H., Yaffe, K., Chui, H., Jagust, W. J., Miller, B. L. and Weiner, M. W. (2007) 'Diffusion tensor imaging of cingulum fibers in mild cognitive impairment and Alzheimer disease', *Neurology*, 68(1), pp. 13–19. Available at: https://www.ncbi.nlm.nih.gov/pmc/articles/PMC3624763/pdf/nihms412728.pdf.

Zhang, Yu, Schuff, Norbert, Camacho, Monica, Chao, Linda L., Fletcher, Thomas P., Yaffe, Kristine, Woolley, Susan C., Madison, Catherine, Rosen, Howard J., Miller, Bruce L. and Weiner, Michael W. (2013) 'MRI Markers for Mild Cognitive Impairment: Comparisons between White Matter Integrity and Gray Matter Volume Measurements', *PLoS ONE*, 8(6), pp. 29–32. doi: 10.1371/journal.pone.0066367.

Zhao, Sinan, Rangaprakash, D., Liang, Peipeng and Deshpande, Gopikrishna (2019) 'Deterioration from healthy to mild cognitive impairment and Alzheimer ' s disease mirrored in corresponding loss of centrality in directed brain networks', *Brain Informatics*. Springer Berlin Heidelberg, pp. 0–10. doi: 10.1186/s40708-019-0101-x.

Zhao, Tengda, Sheng, Can, Bi, Qiuhui, Niu, Weili, Shu, Ni and Han, Ying (2017) 'Age-related differences in the topological efficiency of the brain structural connectome in amnestic mild cognitive impairment', *Neurobiology of Aging*. Elsevier Inc, 59, pp. 144–155. doi: 10.1016/j.neurobiolaging.2017.08.005.

Zhao, Xiaohu, Liu, Yong, Wang, Xiangbin, Liu, Bing, Xi, Qian, Guo, Qihao, Jiang, Hong, Jiang, Tianzi and Wang, Peijun (2012) 'Disrupted small-world brain networks in moderate Alzheimer's disease: A resting-state fMRI study', *PLoS ONE*, 7(3). doi: 10.1371/journal.pone.0033540.

Supplementary material

Section A

RBA script for DTI measures

```
#!/bin/bash

#adjust the path and file name

input_path=/home/stephanie/rba/RBA_AllCovariates

cd $input_path

#=========================================================================

#MVM file contains columns of data containing subjects, region of interest, response variable (Y) and explanatory variables. All subjects' connections in a grid file and connections are picked if connection is present in all subjects (intersect).

#=========================================================================

MVM_file = intersect_scale1_cmp_MVM_000_v3_MVMtbl.txt

MVM=$input_path/$MVM_file

#########################################################################

Var='FA'

#Var stands for variable and is the DTI measure of interest, such as FA, MD, AxD, RD, BL, fNT, fNV, NT, NV or PV.

grep -n  ${Var}  $MVM_file | awk -F  ":" '{print $2}'   > a

sed -e 's/FA//g' a > b

#Edit the above with variable of interest, such as FA, MD, AxD, RD, BL, fNT, fNV, NT, NV or PV.

sed -i '/ s /d' b

awk  '{$1=$1};1' b > c

cat c | awk -F '[ ]' '{print $1" "$2" "$3" "$4" "$5" "$6" "$7}' > ${Var}_MVM.txt

echo -e "subject group sex age education household_income region ${Var}\n$(cat $input_path/${Var}_MVM.txt)" > $input_path/${Var}_MVM.txt

MVM_var=$input_path/${Var}_MVM.txt

output=${Var}_out

#rm $output.*

#=========================================================================

#-ridgePlot show ridge plots of the posterior distribution among the regions for each effect of interest specified through -EOI. In this script, the two numbers 8 and 6 specifies the figure window size with 8 inches wide and 6 inches high.

#-prefix: specify output file names.
```

#-Subj: Specifies the column name that is selected as the measuring unit variable.

#-ROI: Specifies the column name that is selected as the region variable.

#-Y: Specifies the column names selected as the response variable.

#-chains: Specifies the number of Markov chains.

#-WCP is a speed up runtime feature that can adopted through within-chain parallelisation if a computer is equipped with as many CPUs as a factor 4 (e.g., 8, 16, 24, ...). For example, this script has 8 CPUs per chain.

#-iterations: Number of iterations per Markov chain.

#-model: Specifics the effects associated with explanatory variables.

#-cVars: List of categorical variables

#-qVars: Lists numerical variables.

#-EOI: Effects of interest in the output.

#-MD: Missing data in input.

#-distROI: Distribution of ROIs.

#-distSubj: Distribution of subjects.

#-distY: Distribution of response variable. If the data are skewed or have outliers, use Student's t-distribution ('student').

#-dataTable: List the data structure in a table of long format (cf. wide format) in R with a header as the first line.

```
#=========================================================================

time RBA -ridgePlot 8 6 -prefix $output -Subj subject -ROI region -Y ${Var}\

            -chains 16 -WCP 8 -iterations 6000 -model
 '1+Group+Sex+Age+Education+Household_Income' \

             -cVars 'Group,Sex,Household_Income' -qVars 'Age,Education' -EOI
'Intercept,Group,Sex,Age,Education,Household_Income' -MD \

           -StanPath /home/jankiemm/.cmdstanr/cmdstan-2.26.1  -distROI 'student' -distSubj
'student' -distY 'student' \

             -dataTable $MVM_var

#=========================================================================
```

RBA script for graph theory measure

```
#!/bin/bash

#adjust the path and file name

input_path=/home/stephanie/rba/Graph_Theory

cd $input_path

#=========================================================================
```

#MVM file contains columns of data containing subjects, region of interest, response variable (Y) and explanatory variables. All subjects' connections in a grid file and connections are picked if connection is present in all subjects (intersect).

#==

MVM_file=intersect_scale1_cmp_MVM_000_v3_MVMtbl.txt

MVM=$input_path/$MVM_file

##

Var='nodal_efficiency'

#Var stands for variable and is the graph measure of interest, such as nodal efficiency, local efficiency, nodal strength or transitivity.

MVM_var=$input_path/RBA_${Var}_matrix.txt

output=RBA_${Var}_out

#rm $output.*

#==

#-ridgePlot show ridge plots of the posterior distribution among the regions for each effect of interest specified through -EOI. In this script, the two numbers 8 and 6 specifies the figure window size with 8 inches wide and 6 inches high.

#-prefix: specify output file names.

#-Subj: Specifies the column name that is selected as the measuring unit variable.

#-ROI: Specifies the column name that is selected as the region variable.

#-Y: Specifies the column names selected as the response variable.

#-chains: specifies the number of Markov chains.

#-WCP is a speed up runtime feature that can adopted through within-chain parallelisation if a computer is equipped with as many CPUs as a factor 4 (e.g., 8, 16, 24, ...). For example, this script has 8 CPUs per chain.

#-iterations: Number of iterations per Markov chain.

#-model: Specifics the effects associated with explanatory variables.

#-cVars: List of categorical variables

#-qVars: Lists numerical variables.

#-EOI: Effects of interest in the output.

#-MD: Missing data in input.

#-distROI: Distribution of ROIs.

#-distSubj: Distribution of subjects.

#-distY: Distribution of response variable. If the data are skewed or have outliers, use Student's t-distribution ('student').

#-dataTable: List the data structure in a table of long format (cf. wide format) in R with a header as the first line.

#==

```
time RBA -ridgePlot 8 6 -prefix $output -Subj subject -ROI region -Y ${Var}_matrix_df\
        -chains 16 -WCP 8 -iterations 6000 -model
'1+Group+Sex+Age+Education+Household_Income' \
        -qVars ' Age,Education' -cVars 'Group,Sex,Household_Income' -EOI
'Intercept,Group,Sex,Age,Education,Household_Income' -MD \
        -StanPath /home/jankiemm/.cmdstanr/cmdstan-2.26.1  -distROI 'student' -distSubj
'student' -distY 'student' \
         -dataTable $MVM_var
```

#==

Section B

Supplementary Table 1: Chosen interval, corresponding sessions, and test order for each participant.

Participant ID	Chosen interval	Sessions	Test order		
Controls					
AS001	T3	7, 8, 9	2	3	1
AX001	T1	1, 2, 3	2	3	1
BH001	T2	4, 5, 6	2	3	1
CG001	T2	4, 5, 6	2	1	3
DE001	T1	1, 2, 3	2	1	3
DZ001	T2	4, 5, 6	1	2	3
EE002	T3	7, 8, 9	1	3	2
EL001	T2	4, 5, 6	3	2	1
FS001	T2	4, 5, 6	3	2	1
HE001	T3	7, 8, 9	2	1	3
JH001	T2	4, 5, 6	1	2	3
JS002	T3	7, 8, 9	2	3	1
JS003	T3	7, 8, 9	1	2	3
NS001	T3	7, 8, 9	1	2	3
PD001	T3	7, 8, 9	3	2	1
PL001	T3	7, 8, 9	2	1	3
RF001	T1	1, 2, 3	1	2	3
SS001	T2	4, 5, 6	1	2	3
TY001	T3	7, 8, 9	2	1	3
YM001	T2	4, 5, 6	2	3	1
AD					
AS002	T2	4, 5, 6	1	2	3
AY001	T3	7, 8, 9	1	2	3

CA001	T2	4, 5, 6	3	2	1
CN003	T2	4, 5, 6	2	3	1
CT001	T2	4, 5, 6	3	1	2
EE003	T1	1, 2, 3	1	3	2
ES001	T3	7, 8, 9	3	1	2
FY001	T3	7, 8, 9	2	1	3
GB001	T3	7, 8, 9	2	3	1
HZ001	T1	1, 2, 3	1	2	3
JA001	T2	4, 5, 6	3	2	1
JY001	T3	7, 8, 9	1	2	3
MA001	T3	7, 8, 9	3	1	2
MK002	T1	1, 2, 3	1	2	3
MR001	T3	7, 8, 9	1	3	2
RA001	T3	7, 8, 9	3	1	2

301 connections

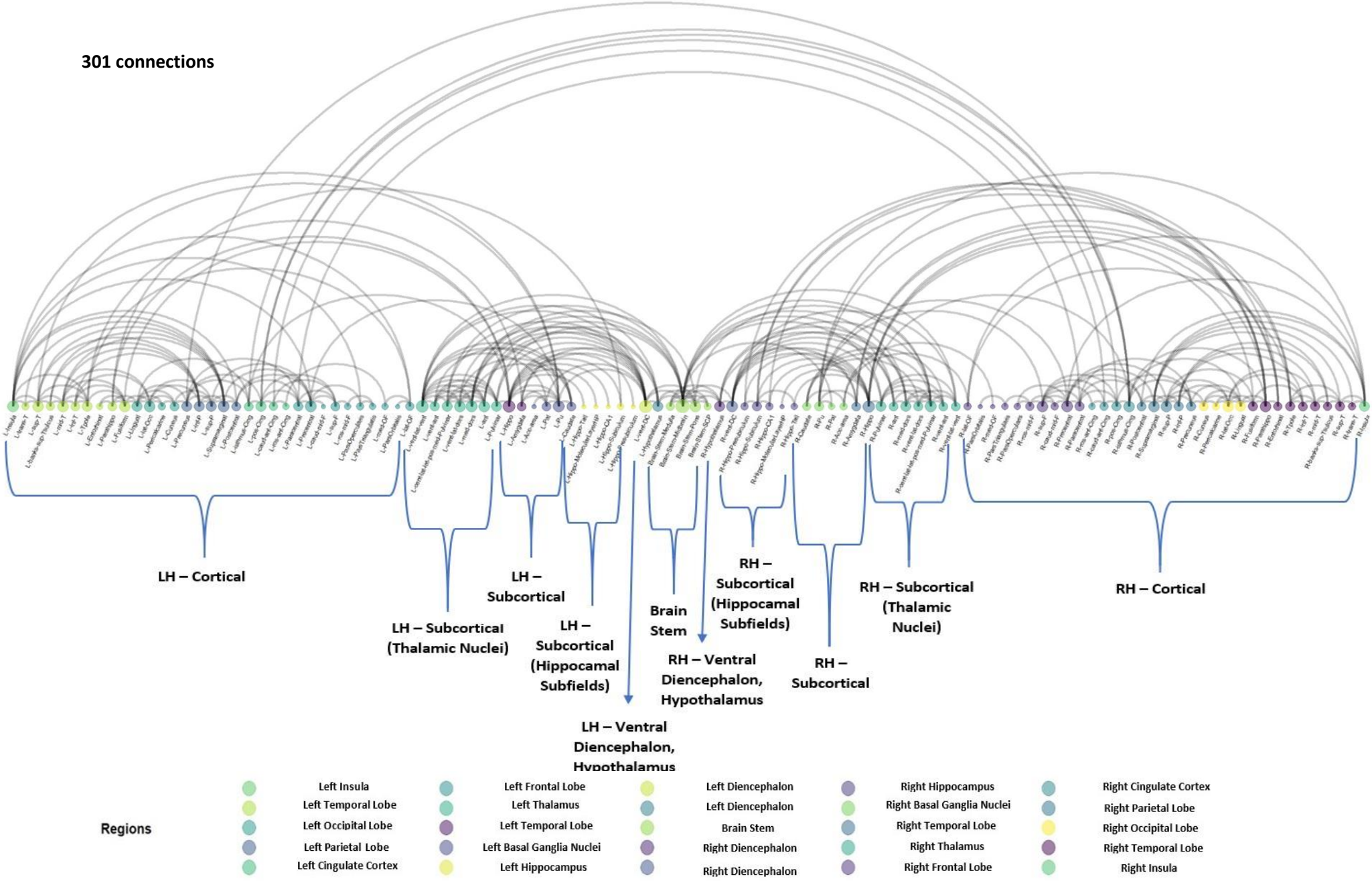

Supplementary Figure 1: Common connections (301) across all participants in the sample after tractography. RH, Right Hemisphere; LH, Left Hemisphere

Supplementary Table 2: 126 grey matter regions from the Connectome Mapper (scale 1).

Right Hemisphere – Cortical Structures	**Right Hemisphere – Subcortical Structures (Thalamic Nuclei)**	**Left Hemisphere – Cortical Structures**	**Left Hemisphere – Subcortical Structures (Thalamic Nuclei)**
1. Right Lateral Orbitofrontal Cortex	35. Right Pulvinar	62. Left Lateral Orbitofrontal Cortex	96. Left Pulvinar
2. Right Pars Orbitalis	36. Right Anterior Thalamus	63. Left Pars Orbitalis	97. Left Anterior Thalamus
3. Right Frontal Pole	37. Right Mediodorsal Thalamus	64. Left Frontal Pole	98. Left Mediodorsal Thalamus
4. Right Medial Orbitofrontal Cortex	38. Right Ventral Latero-Dorsal Nucleus Thalamus	65. Left Medial Orbitofrontal Cortex	99. Left Ventral Latero-Dorsal Thalamus
5. Right Pars Triangularis	39. Right Central Lateral-Lateral Posterior-Medial Pulvinar	66. Left Pars Triangularis	100. Left Central Lateral-Lateral Posterior-Medial Pulvinar
6. Right Pars Opercularis	40. Right Ventral Anterior Thalamus	67. Left Pars Opercularis	101. Left Ventral Anterior Thalamus
7. Right Rostral Middle Frontal Gyrus	41. Right Ventral Latero-Ventral Thalamus	68. Left Rostral Middle Frontal Gyrus	102. Left Ventral Latero-Ventral Thalamus
8. Right Superior Frontal Gyrus	**Right Hemisphere – Subcortical Structures**	69. Left Superior Frontal Gyrus	**Left Hemisphere – Subcortical Structures**
9. Right Caudal Middle Frontal Gyrus	42. Right Caudate Nucleus	70. Left Caudal Middle Frontal Gyrus	103. Left Caudate Nucleus
10. Right Precentral Gyrus	43. Right Putamen	71. Left Precentral Gyrus	104. Left Putamen
11. Right Paracentral Lobule	44. Right Pallidum	72. Left Paracentral Lobule	105. Left Pallidum
12. Right Rostral Anterior Cingulate Cortex	45. Right Nucleus Accumbens area	73. Left Rostral Anterior Cingulate Cortex	106. Left Nucleus Accumbens area
13. Right Caudal Anterior Cingulate Cortex	46. Right Amygdala	74. Left Caudal Anterior Cingulate Cortex	107. Left Amygdala
14. Right Posterior Cingulate Cortex	47. Right Hippocampus	75. Left Posterior Cingulate Cortex	108. Left Hippocampus
15. Right Isthmus Cingulate Cortex	**Right Hemisphere – Subcortical Structures (Hippocampal Subfields)**	76. Left Isthmus Cingulate Cortex	**Left Hemisphere – Subcortical Structures (Hippocampal Subfields)**
16. Right Postcentral Gyrus	48. Right Hippocampus: Parasubiculum	77. Left Postcentral Gyrus	109. Left Hippocampus: Parasubiculum
17. Right Supramarginal Gyrus	49. Right Hippocampus: Presubiculum	78. Left Supramarginal Gyrus	110. Left Hippocampus: Presubiculum
18. Right Superior Parietal Lobule	50. Right Hippocampus: Subiculum	79. Left Superior Parietal Lobule	111. Left Hippocampus: Subiculum
19. Right Inferior Parietal Lobule	51. Right Hippocampus: CA1	80. Left Inferior Parietal Lobule	112. Left Hippocampus: CA1
20. Right Precuneus Cortex	52. Right Hippocampus: CA3	81. Left Precuneus Cortex	113. Left Hippocampus: CA3
21. Right Cuneus Cortex	53. Right Hippocampus: CA4	82. Left Cuneus Cortex	114. Left Hippocampus: CA4
22. Right Pericalcarine Cortex	54. Right Hippocampus: GCDG	83. Left Pericalcarine Cortex	115. Left Hippocampus: GCDG

23. Right Lateral Occipital Gyrus	55. Right Hippocampus: HATA	84. Left Lateral Occipital Gyrus	116. Left Hippocampus: HATA
24. Right Lingual Gyrus	56. Right Hippocampus: Fimbria	85. Left Lingual Gyrus	117. Left Hippocampus: Fimbria
25. Right Fusiform Gyrus	57. Right Hippocampus: Molecular-Layer HP Dentate Gyrus	86. Left Fusiform Gyrus	118. Left Hippocampus: Molecular-Layer HP Dentate Gyrus
26. Right Parahippocampal Gyrus	58. Right Hippocampus: Hippocampal Fissure	87. Left Parahippocampal Gyrus	119. Left Hippocampus: Hippocampal Fissure
27. Right Entorhinal Cortex	59. Right Hippocampus: Tail	88. Left Entorhinal Cortex	120. Left Hippocampus: Tail
28. Right Temporal Pole	**Right Hemisphere – Ventral Diencephalon**	89. Left Temporal Pole	**Left Hemisphere – Ventral Diencephalon**
29. Right Inferior Temporal Gyrus	60. Right Ventral Diencephalon	90. Left Inferior Temporal Gyrus	121. Left Ventral Diencephalon
30. Right Middle Temporal Gyrus	**Right Hemisphere - Hypothalamus**	91. Left Middle Temporal Gyrus	**Left Hemisphere - Hypothalamus**
31. Right Banks of the Superior Temporal Sulcus (Bankssts)	61. Right Hypothalamus	92. Left Banks of the Superior Temporal Sulcus (Bankssts)	122. Left Hypothalamus
32. Right Superior Temporal Gyrus		93. Left Superior Temporal Gyrus	**Brainstem Structures**
33. Right Transverse Temporal Gyrus		94. Left Transverse Temporal Gyrus	123. Brainstem Midbrain
34. Right Insula		95. Left Insula	124. Brainstem Pons
			125. Brainstem Medulla
			126. Brainstem SCP

Supplementary Table 3: Connections with either very low or very high P+ values, where low P+ means Controls > AD and high P+ means Controls < AD, of FA with their corresponding values of AxD and RD for that connection.

Region 1	Region 2	FA								AxD								RD							
		Mean (SD)	P+	Quantile Intervals					Mean (SD)	P+	Quantile Intervals					Mean (SD)	P+	Quantile Intervals							
				2.5 %	5%	50%	95%	97.5 %			2.5 %	5%	50%	95%	97.5 %			2.5 %	5%	50%	95%	97.5 %			
Cortical Temporal Lobe to Cortical Temporal Lobe																									
L-Parahippo	L-Entorhinal	-1.46×10^{-2} (7.81×10^{-3})	**0.03***	-3.02×10^{-2}	-2.76×10^{-2}	-1.46×10^{-2}	-1.82×10^{-3}	6.70×10^{-4}	1.64×10^{-2} (1.40×10^{-2})	0.88	-1.16×10^{-2}	-6.88×10^{-3}	1.66×10^{-2}	3.96×10^{-2}	4.38×10^{-2}	1.87×10^{-2} (1.20×10^{-2})	**0.95***	-4.62×10^{-3}	-5.05×10^{-4}	1.86×10^{-2}	3.86×10^{-2}	4.29×10^{-2}			
Cortical Temporal Lobe to Subcortical Hippocampus Subregions (Subcortical Temporal Lobe)																									
R-Parahippo	R-Hippo-Subiculum	-1.35×10^{-2} (8.14×10^{-3})	**0.05***	-3.01×10^{-2}	-2.72×10^{-2}	-1.35×10^{-2}	-2.83×10^{-4}	2.12×10^{-3}	1.57×10^{-2} (1.33×10^{-2})	0.88	-1.09×10^{-2}	-6.27×10^{-3}	1.58×10^{-2}	3.72×10^{-2}	4.14×10^{-2}	1.64×10^{-2} (1.18×10^{-2})	0.92	-6.68×10^{-3}	-2.70×10^{-3}	1.61×10^{-2}	3.62×10^{-2}	4.01×10^{-2}			
Subcortical Thalamus to Subcortical Thalamus																									
R-cent-lat-lat-pos-med-Pulvinar	R-vent-lat-vent	-1.41×10^{-2} (8.68×10^{-3})	**0.05***	-3.12×10^{-2}	-2.82×10^{-2}	-1.40×10^{-2}	-4.42×10^{-5}	2.87×10^{-3}	1.49×10^{-2} (1.41×10^{-2})	0.86	-1.28×10^{-2}	-8.15×10^{-3}	1.48×10^{-2}	3.79×10^{-2}	4.32×10^{-2}	1.20×10^{-2} (1.13×10^{-2})	0.86	-9.99×10^{-3}	-6.34×10^{-3}	1.19×10^{-2}	3.06×10^{-2}	3.45×10^{-2}			
L-Pulvinar	L-vent-lat-vent	3.27×10^{-2} (1.28×10^{-2})	**0.99****	7.01×10^{-3}	1.16×10^{-2}	3.27×10^{-2}	5.39×10^{-2}	5.77×10^{-2}	2.06×10^{-2} (1.91×10^{-2})	0.87	-1.43×10^{-2}	-9.08×10^{-3}	1.95×10^{-2}	5.35×10^{-2}	6.09×10^{-2}	6.68×10^{-3} (1.12×10^{-2})	0.73	-1.54×10^{-2}	-1.15×10^{-2}	6.54×10^{-3}	2.52×10^{-2}	2.91×10^{-2}			
L-ant	L-cent-lat-lat-pos-med-Pulvinar	-1.27×10^{-2} (7.94×10^{-3})	**0.05***	-2.83×10^{-2}	-2.57×10^{-2}	-1.27×10^{-2}	3.09×10^{-4}	2.67×10^{-3}	1.33×10^{-2} (1.31×10^{-2})	0.85	-1.21×10^{-2}	-7.97×10^{-3}	1.32×10^{-2}	3.49×10^{-2}	3.94×10^{-2}	1.61×10^{-2} (1.14×10^{-2})	0.92	-5.89×10^{-3}	-2.35×10^{-3}	1.60×10^{-2}	3.52×10^{-2}	3.88×10^{-2}			
Subcortical Thalamus to Brainstem																									
R-Pulvinar	Brain-Stem-Midbrain	1.41×10^{-2} (8.99×10^{-3})	**0.95***	-3.12×10^{-3}	-2.89×10^{-4}	1.38×10^{-2}	2.93×10^{-2}	3.24×10^{-2}	1.77×10^{-2} (1.39×10^{-2})	0.90	-9.06×10^{-3}	-4.38×10^{-3}	1.77×10^{-2}	4.07×10^{-2}	4.56×10^{-2}	4.00×10^{-3} (1.15×10^{-2})	0.64	-1.81×10^{-2}	-1.45×10^{-2}	3.81×10^{-3}	2.31×10^{-2}	2.69×10^{-2}			

L-Pulvinar	Brain-Stem-Midbrain	1.59×10^{-2} (9.28×10^{-3})	**0.96***	-1.46×10^{-3}	1.25×10^{-3}	1.56×10^{-2}	3.19×10^{-2}	3.53×10^{-2}	3.44×10^{-2} (1.75×10^{-2})	**0.99** **	2.98×10^{-3}	7.50×10^{-3}	3.32×10^{-2}	6.52×10^{-2}	7.24×10^{-2}	5.92×10^{-3} (1.13×10^{-2})	0.70	-1.61×10^{-2}	-1.27×10^{-2}	5.91×10^{-3}	2.45×10^{-2}	2.84×10^{-2}
L-cent-lat-lat-pos-med-Pulvinar	Brain-Stem-Midbrain	1.50×10^{-2} (9.28×10^{-3})	**0.96***	-2.28×10^{-3}	5.75×10^{-4}	1.47×10^{-2}	3.10×10^{-2}	3.46×10^{-2}	3.37×10^{-2} (1.67×10^{-2})	**0.99** **	3.69×10^{-3}	8.05×10^{-3}	3.29×10^{-2}	6.22×10^{-2}	6.93×10^{-2}	6.14×10^{-3} (1.14×10^{-2})	0.71	-1.61×10^{-2}	-1.23×10^{-2}	6.01×10^{-3}	2.50×10^{-2}	2.88×10^{-2}
Subcortical Temporal Lobe to Subcortical Hippocampus Subregions (Subcortical Temporal Lobe)																					
L-Hippo	L-Hippo-CA1	-1.41×10^{-2} (8.25×10^{-3})	**0.04***	-3.07×10^{-2}	-2.79×10^{-2}	-1.40×10^{-2}	-7.1×10^{-4}	1.91×10^{-3}	3.74×10^{-3} (1.90×10^{-2})	0.62	-3.89×10^{-2}	-2.97×10^{-2}	5.40×10^{-3}	3.15×10^{-2}	3.65×10^{-2}	9.80×10^{-3} (1.27×10^{-2})	0.79	-1.59×10^{-2}	-1.14×10^{-2}	9.84×10^{-3}	3.07×10^{-2}	3.45×10^{-2}
Subcortical Hippocampus Subregions (Subcortical Temporal Lobe) to Subcortical Hippocampus Subregions (Subcortical Temporal Lobe)																					
R-Hippo-Subiculum	R-Hippo-CA1	-1.43×10^{-2} (7.95×10^{-3})	**0.04***	-3.01×10^{-2}	-2.72×10^{-2}	-1.43×10^{-2}	-1.09×10^{-3}	1.52×10^{-3}	1.82×10^{-2} (1.40×10^{-2})	0.91	-8.71×10^{-3}	-4.37×10^{-3}	1.80×10^{-2}	4.15×10^{-2}	4.68×10^{-2}	1.50×10^{-2} (1.16×10^{-2})	0.90	-7.91×10^{-3}	-3.88×10^{-3}	1.50×10^{-2}	3.38×10^{-2}	3.81×10^{-2}

Key: SD, Standard Deviation; FA, Fractional Anisotropy; AxD, Axial Diffusivity; RD, Radial Diffusivity; R, Right; L, Left

Note: Data presented are group difference means with standard deviations in parentheses.

*Strong evidence, **Very strong evidence

P+ ≤ 0.05: Controls > AD, P+ ≥ 0.95: Controls < AD

Supplementary Table 4: Connections with either very low or very high P+ values of MD, where low P+ means Controls > AD and high P+ means Controls < AD, with their corresponding P+ values of AxD and RD for that connection.

Region 1	Region 2	MD							AxD							RD						
		Mean (SD)	P+	Quantile Intervals					Mean (SD)	P+	Quantile Intervals					Mean (SD)	P+	Quantile Intervals				
				2.5 %	5%	50%	95%	97.5 %			2.5 %	5%	50%	95%	97.5 %			2.5 %	5%	50%	95%	97.5 %
Cortical Cingulate Cortex to Cortical Occipital Lobe																						
L-isthmus-Cing	L-Lingual	1.88×10^{-2} (1.14×10^{-2})	**0.96***	-2.96×10^{-3}	6.79×10^{-4}	1.86×10^{-2}	3.80×10^{-2}	4.18×10^{-2}	2.75×10^{-2} (1.75×10^{-2})	**0.96***	-3.20×10^{-3}	1.44×10^{-3}	2.63×10^{-2}	5.84×10^{-2}	6.63×10^{-2}	1.28×10^{-2} (1.13×10^{-2})	0.87	-9.07×10^{-3}	-5.42×10^{-3}	1.26×10^{-2}	3.13×10^{-2}	3.54×10^{-2}
Cortical Cingulate Cortex to Cortical Temporal Lobe																						
R-isthmus-Cing	R-Parahippo	1.75×10^{-2} (1.06×10^{-2})	**0.95***	-3.00×10^{-3}	3.12×10^{-4}	1.74×10^{-2}	3.52×10^{-2}	3.86×10^{-2}	1.65×10^{-2} (1.32×10^{-2})	0.90	-9.53×10^{-3}	-5.29×10^{-3}	1.65×10^{-2}	3.80×10^{-2}	4.24×10^{-2}	1.73×10^{-2} (1.18×10^{-2})	0.93	-5.33×10^{-3}	-1.68×10^{-3}	1.71×10^{-2}	3.70×10^{-2}	4.10×10^{-2}
Cortical Temporal Lobe to Subcortical Temporal Lobe																						
R-Entorhinal	R-Hippo	1.75×10^{-2} (1.06×10^{-2})	**0.95***	-3.00×10^{-3}	3.12×10^{-4}	1.74×10^{-2}	3.52×10^{-2}	3.86×10^{-2}	1.65×10^{-2} (1.32×10^{-2})	0.90	-9.53×10^{-3}	-5.29×10^{-3}	1.65×10^{-2}	3.80×10^{-2}	4.24×10^{-2}	1.73×10^{-2} (1.18×10^{-2})	0.93	-5.33×10^{-3}	-1.68×10^{-3}	1.71×10^{-2}	3.70×10^{-2}	4.90×10^{-2}
Cortical Temporal Lobe to Subcortical Hippocampus Subregions (Subcortical Temporal Lobe)																						
R-Parahippo	R-Hippo-Presubiculum	2.22×10^{-2} (1.18×10^{-2})	**0.97***	-7.59×10^{-5}	3.43×10^{-3}	2.18×10^{-2}	4.21×10^{-2}	4.64×10^{-2}	1.71×10^{-2} (1.40×10^{-2})	0.89	-1.02×10^{-2}	-5.88×10^{-3}	1.72×10^{-2}	4.01×10^{-2}	4.45×10^{-2}	3.17×10^{-2} (1.48×10^{-2})	**0.99****	3.81×10^{-3}	7.90×10^{-3}	3.13×10^{-2}	5.65×10^{-2}	6.15×10^{-2}
Subcortical Temporal Lobe to Subcortical Hippocampus Subregions (Subcortical Temporal Lobe)																						
R-Hippo	R-Hippo-Presubiculum	1.72×10^{-2} (1.07×10^{-2})	**0.95***	-3.62×10^{-3}	-2.88×10^{-4}	1.71×10^{-2}	3.50×10^{-2}	3.85×10^{-2}	1.49×10^{-2} (1.37×10^{-2})	0.87	-1.15×10^{-2}	-7.24×10^{-3}	1.48×10^{-2}	3.74×10^{-2}	4.17×10^{-2}	2.16×10^{-2} (1.26×10^{-2})	**0.96***	-2.24×10^{-3}	1.34×10^{-3}	2.14×10^{-2}	4.27×10^{-2}	4.70×10^{-2}

L-Hippo	L-Hippo-Presubiculum	2.14×10^{-2} (1.23×10^{-2})	**0.97***	-1.16×10^{-3}	2.31×10^{-3}	2.08×10^{-2}	4.25×10^{-2}	4.69×10^{-2}	1.90×10^{-2} (1.55×10^{-2})	0.89	-1.17×10^{-2}	-6.52×10^{-3}	1.88×10^{-2}	4.46×10^{-2}	4.94×10^{-2}	2.73×10^{-2} (1.47×10^{-2})	**0.97***	-4.45×10^{-4}	4.13×10^{-3}	2.68×10^{-2}	5.21×10^{-2}	5.72×10^{-2}
Subcortical Hippocampus Subregions (Subcortical Temporal Lobe) to Subcortical Hippocampus Subregions (Subcortical Temporal Lobe)																					
R-Hippo-Presubiculum	R-Hippo-Subiculum	1.91×10^{-2} (1.10×10^{-2})	**0.96***	-2.30×10^{-3}	1.37×10^{-3}	1.88×10^{-2}	3.72×10^{-2}	4.13×10^{-2}	1.91×10^{-2} (1.43×10^{-2})	0.91	-8.15×10^{-3}	-4.08×10^{-3}	1.89×10^{-2}	4.28×10^{-2}	4.82×10^{-2}	1.10×10^{-2} (1.17×10^{-2})	**0.97***	-1.20×10^{-2}	-7.97×10^{-3}	1.09×10^{-2}	3.05×10^{-2}	3.40×10^{-2}

Key: SD, Standard Deviation; MD, Mean Diffusivity; AxD, Axial Diffusivity; RD, Radial Diffusivity; R, Right; L, Left

Note: Data presented are group difference means with standard deviations in parentheses.

*Strong evidence, **Very strong evidence

P+ ≤ 0.05: Controls > AD, P+ ≥ 0.95: Controls < AD

Other DTI measures

In the current analyses, we also looked at other measures listed below with a description of each:

(1) Number of tracks in that white matter region-of-interest (WM-ROI) (NT) – The number of fibres/tracks/streamlines extracted within a particular bundle. Gao et al. (2011) reported less NT from the genu of the corpus callosum in the healthy controls group compared to the AD group.

(2) Fractional number of tracks in that WM-ROI (fNT) – Fractional number of tracks in a particular WM-ROI, defined as NT divided by the total number of tracts found.

(3) BL – Average length, in mm, of the fibre tracts in each bundle and calculated as

$$\overline{BL} = \frac{1}{N} \sum_{i} BL_i$$

Where N is the number of fibre tracts in each bundle and BL_I is the length of the i-th track (Barrio-Arranz *et al.*, 2015).

Significant changes in BL have been discovered in older adults (Baker *et al.*, 2014; Behrman-Lay *et al.*, 2015). Behram-Lay et al. (2015) reported that a decrease in BL across numerous lobes in healthy older individuals was associated with lower cognitive performance in both executive and cognitive processing speed tests.

(4) Physical volume of tracts (PV) – The total volume, in mm^3, of each bundle is measured as:

$$PV = N \times |V|$$

Where $|V|$ is volume's voxel size and N is the number of voxels occupied by the fibres in the bundle (Barrio-Arranz *et al.*, 2015).

(5) Number of voxels in that WM-ROI (NV)

(6) Fractional volume of tracks compared to masked total volume (fNV)

Woo et al. (2020) characterised diffusion measures, e.g., volume, average length, FA, MD, AxD and RD, of 18 tracts. They reported that volumes had a positive relationship with MD and RD in all tracts, while the average length of tracts had a negative relationship with MD and RD.

Supplementary Table 5 and *Supplementary Table 6* below shows group difference means with standard deviations, P+ values as well as quantile intervals of BL, fNT, fNV, NT, NV and PV corresponding to the FA connections identified in *Figure 14* and Supplementary *Table 3* (FA connections with either very low or very high P+ values, where low P+ means Controls > AD and high P+ means Controls < AD). *Supplementary Table 7* and *Supplementary Table 8* below shows group difference means with standard deviations, P+ values as well as quantile intervals of BL, fNT, fNV, NT, NV and PV corresponding to the MD connections identified in *Figure 19* and Supplementary *Table 4* (MD connections with either very low or very high P+ values, where low P+ means Controls > AD and high P+ means Controls < AD).

Supplementary Table 5: FA connections identified with either very low or high P+ values with their corresponding values of BL, fNT and fNV for each connection.

Region 1	Region 2	BL							fNT						fNV					
		Mean (SD)	P+	Quantile Intervals					Mean (SD)	P+	Quantile Intervals				Mean (SD)	P+	Quantile Intervals			
				2.5 %	5%	50%	95%	97.5 %			2.5 %	5%	50%	95%	97.5 %		2.5 %	5%	50%	95%	97.5 %
Cortical Temporal Lobe to Cortical Temporal Lobe																					
L-Parahippo	L-Entorhinal	-0.31 (0.63)	0.29	-1.55	-1.32	-0.32	0.77	1.02	1.15×10^{-5} (7.62×10^{-5})	0.54	-1.33×10^{-4}	-1.04×10^{-4}	6.56×10^{-6}	1.44×10^{-4}	1.81×10^{-4}	-1.43×10^{-4} (1.61×10^{-4})	0.18	-4.70×10^{-4}	-4.09×10^{-4}	-1.40×10^{-4}	1.16×10^{-4}	1.63×10^{-4}
Cortical Temporal Lobe to Subcortical Hippocampus Subregions (Subcortical Temporal Lobe)																					
R-Parahippo	R-Hippo-Subiculum	-0.50 (0.69)	0.22	-1.91	-1.61	-0.48	0.58	0.83	4.08×10^{-6} (2.94×10^{-5})	0.55	-5.23×10^{-5}	-4.32×10^{-5}	3.61×10^{-6}	5.36×10^{-5}	6.37×10^{-5}	-8.40×10^{-5} (1.68×10^{-4})	0.30	-4.16×10^{-4}	-3.57×10^{-4}	-8.42×10^{-5}	1.90×10^{-4}	2.48×10^{-4}
Subcortical Thalamus to Subcortical Thalamus																					
R-cent-lat-lat-pos-med-Pulvinar	R-vent-lat-vent	-0.28 (0.65)	0.33	-1.60	-1.36	-0.26	0.75	0.95	-8.32×10^{-5} (8.09×10^{-5})	0.13	-2.63×10^{-4}	-2.24×10^{-4}	-7.52×10^{-5}	3.11×10^{-5}	5.38×10^{-5}	-1.20×10^{-4} (1.67×10^{-4})	0.23	-4.57×10^{-4}	-3.97×10^{-4}	-1.19×10^{-4}	1.51×10^{-4}	2.14×10^{-4}
L-Pulvinar	L-vent-lat-vent	-0.41 (0.60)	0.24	-1.66	-1.42	-0.40	0.54	0.74	-2.99×10^{-5} (1.97×10^{-4})	0.42	-3.76×10^{-4}	-3.26×10^{-4}	-4.63×10^{-5}	3.07×10^{-4}	3.78×10^{-4}	-4.19×10^{-5} (1.97×10^{-4})	0.39	-4.05×10^{-4}	-3.48×10^{-4}	-5.28×10^{-5}	2.93×10^{-4}	3.74×10^{-4}
L-ant	L-cent-lat-lat-pos-med-Pulvinar	-0.61 (0.78)	0.20	-2.10	-1.84	-0.64	0.73	1.04	-5.22×10^{-6} (3.15×10^{-5})	0.43	-6.81×10^{-5}	-5.55×10^{-5}	-5.45×10^{-6}	4.63×10^{-5}	5.81×10^{-5}	-1.46×10^{-4} (1.64×10^{-4})	0.18	-4.80×10^{-4}	-4.22×10^{-4}	-1.40×10^{-4}	1.14×10^{-4}	1.62×10^{-4}
Subcortical Thalamus to Brainstem																					
R-Pulvinar	Brain-Stem-Midbrain	-0.38 (0.97)	0.27	-1.93	-1.67	-0.51	1.36	2.13	-2.40×10^{-5} (4.01×10^{-5})	0.27	-1.14×10^{-4}	-9.36×10^{-5}	-2.09×10^{-5}	3.49×10^{-5}	4.70×10^{-5}	1.73×10^{-3} (1.24×10^{-3})	0.90	-8.82×10^{-4}	-4.76×10^{-4}	1.80×10^{-3}	3.71×10^{-3}	4.05×10^{-3}

L-Pulvinar	Brain-Stem-Midbrain	-1.01 (0.95)	0.12	-2.95	-2.53	-1.00	0.49	0.88	-2.63×10^{-4} (1.11×10^{-4})	**0.01****	-4.90×10^{-4}	-4.47×10^{-4}	-2.60×10^{-4}	-8.45×10^{-5}	-5.22×10^{-5}	1.60×10^{-3} (7.85×10^{-4})	**0.96***	-1.59×10^{-4}	1.40×10^{-4}	1.67×10^{-3}	2.78×10^{-3}	2.97×10^{-3}
L-cent-lat-lat-pos-med-Pulvinar	Brain-Stem-Midbrain	-1.04 (0.99)	0.11	-3.26	-2.82	-0.93	0.36	0.66	-2.09×10^{-5} (3.73×10^{-5})	0.29	-1.05×10^{-4}	-8.73×10^{-5}	-1.82×10^{-5}	3.49×10^{-5}	4.61×10^{-5}	9.66×10^{-4} (6.87×10^{-4})	0.92	-2.78×10^{-4}	-1.16×10^{-4}	9.46×10^{-4}	2.15×10^{-3}	2.36×10^{-3}
Subcortical Temporal Lobe to Subcortical Hippocampus Subregions (Subcortical Temporal Lobe)																					
L-Hippo	L-Hippo-CA1	0.05 (0.66)	0.53	-1.26	-1.03	0.05	1.12	1.35	-9.63×10^{-6} (3.10×10^{-5})	0.38	-7.29×10^{-5}	-6.08×10^{-5}	-9.29×10^{-6}	4.01×10^{-5}	5.12×10^{-5}	-1.56×10^{-4} (1.75×10^{-4})	0.18	-5.09×10^{-4}	-4.46×10^{-4}	-1.53×10^{-4}	1.23×10^{-4}	1.74×10^{-4}
Subcortical Hippocampus Subregions (Subcortical Temporal Lobe) to Subcortical Hippocampus Subregions (Subcortical Temporal Lobe)																					
R-Hippo-Subiculum	R-Hippo-CA1	0.01 (0.68)	0.50	-1.29	-1.08	0.00	1.14	1.40	-1.07×10^{-6} (3.01×10^{-5})	0.49	-5.98×10^{-5}	-4.95×10^{-5}	-1.01×10^{-6}	4.77×10^{-5}	5.87×10^{-5}	-9.05×10^{-5} (1.74×10^{-4})	0.29	-4.29×10^{-4}	-3.75×10^{-4}	-8.92×10^{-5}	1.96×10^{-4}	2.56×10^{-4}

Key: SD, Standard Deviation; BL, average length in mm; fNT, Fractional number of tracks in that white matter region-of-interest (WM-ROI); fNV, Fractional volume of tracks compared to masked total volume; R, Right; L, Left

Note: Data presented are group difference means with standard deviations in parentheses.

*Strong evidence, **Very strong evidence

P+ ≤ 0.05: Controls > AD, P+ ≥ 0.95: Controls < AD

Supplementary Table 6: FA connections identified with either very low or high P+ values with their corresponding values of NT, NV and PV for each connection.

Region 1	Region 2	NT							NV						PV					
		Mean (SD)	P+	Quantile Intervals					Mean (SD)	P+	Quantile Intervals				Mean (SD)	P+	Quantile Intervals			
				2.5 %	5%	50%	95%	97.5 %			2.5%	5%	50%	95%	97.5%		2.5 %	5%	50%	95%	97.5 %
Cortical Temporal Lobe to Cortical Temporal Lobe																					
L-Parahippo	L-Entorhinal	-3.33×10^4 (3.49×10^4)	0.15	-1.0×10^5	-8.86×10^4	-3.40×10^4	2.50×10^4	4.22×10^4	-99.62 (70.21)	0.07	-240.96	-217.45	-98.24	12.86	36.80	-340.30 (241.48)	0.07	-823.11	-742.00	-333.93	44.83	123.07
Cortical Temporal Lobe to Subcortical Hippocampus Subregions (Subcortical Temporal Lobe)																					
R-Parahippo	R-Hippo-Subiculum	1.49×10^2 (1.62×10^4)	0.50	-3.15×10^4	-2.62×10^4	-2.05×10^1	2.72×10^4	3.26×10^4	-50.24 (71.49)	0.24	-189.96	-167.58	-50.87	67.60	93.47	-167.10 (247.30)	0.25	-644.82	-572.42	-168.90	240.87	323.95
Subcortical Thalamus to Subcortical Thalamus																					
R-cent-lat-lat-pos-med-Pulvinar	R-vent-lat-vent	-1.06×10^5 (4.67×10^4)	**<0.01****	-2.10×10^5	-1.87×10^5	-1.01×10^5	-3.86×10^4	-2.73×10^4	-73.42 (72.62)	0.15	-216.39	-191.21	-74.38	46.69	71.63	-248.07 (248.03)	0.15	-740.04	-655.94	-243.57	151.27	239.06
L-Pulvinar	L-vent-lat-vent	-1.06×10^5 (7.05×10^4)	0.07	-2.41×10^5	-2.18×10^5	-1.07×10^5	1.30×10^4	3.63×10^4	-39.89 (85.25)	0.30	-195.31	-168.93	-44.14	106.16	143.63	-134.60 (292.51)	0.30	-666.38	-590.77	-147.33	365.81	491.07
L-ant	L-cent-lat-lat-pos-med-Pulvinar	-1.15×10^4 (1.72×10^4)	0.24	-4.61×10^4	-3.96×10^4	-1.15×10^4	1.64×10^4	2.19×10^4	-105.62 (71.93)	0.07	-251.11	-224.30	-104.94	9.80	31.84	-356.32 (247.80)	0.07	-861.63	-772.15	-348.43	42.56	112.82
Subcortical Thalamus to Brainstem																					

R-Pulvinar	Brain-Stem-Midbrain	-2.51×10^4 (1.93×10^4)	0.08	-6.64×10^4	-5.74×10^4	-2.40×10^4	4.24×10^3	9.95×10^3	714.03 (357.41)	**0.97***	-56.37	92.66	728.66	1277.17	1375.74	2433.89 (1248.64)	**0.96***	-288.26	243.24	2500.00	4405.82	4774.19
L-Pulvinar	Brain-Stem-Midbrain	-1.55×10^5 (7.89×10^4)	**0.02****	-3.25×10^5	-2.94×10^5	-1.49×10^5	-3.37×10^4	-1.27×10^4	455.08 (274.40)	**0.95***	-109.69	-12.10	463.54	891.11	967.68	1563.55 (932.79)	**0.95***	-337.44	-36.49	1596.07	3055.42	3322.11
L-cent-lat-lat-pos-med-Pulvinar	Brain-Stem-Midbrain	-1.53×10^4 (1.94×10^4)	0.20	-5.56×10^4	-4.77×10^4	-1.46×10^4	1.49×10^4	2.06×10^4	238.28 (268.89)	0.79	-238.62	-182.81	238.50	677.54	768.94	810.02 (920.10)	0.78	-815.27	-632.24	821.49	2318.03	2612.02
Subcortical Temporal Lobe to Subcortical Hippocampus Subregions (Subcortical Temporal Lobe)																				
L-Hippo	L-Hippo-CA1	-8.42×10^3 (1.65×10^4)	0.29	-4.18×10^4	-3.55×10^4	-8.45×10^3	1.85×10^4	2.45×10^4	-79.76 (74.54)	0.14	-229.31	-203.32	-79.56	40.87	66.09	-270.11 (254.32)	0.14	-776.75	-692.12	-266.67	140.96	226.60
Subcortical Hippocampus Subregions (Subcortical Temporal Lobe) to Subcortical Hippocampus Subregions (Subcortical Temporal Lobe)																				
R-Hippo-Subiculum	R-Hippo-CA1	-3.85×10^2 (1.61×10^4)	0.49	-3.20×10^4	-2.67×10^4	-5.55×10^2	2.59×10^4	3.15×10^4	-42.87 (74.65)	0.28	-188.09	-165.49	-43.54	80.85	105.90	-145.29 (255.07)	0.28	-655.20	-567.36	-149.83	278.74	357.30

Key: SD, Standard Deviation; NT, Number of tracks in that WM-ROI; NV, Number of voxels in that WM-ROI; PV, Physical volume of tracts; R, Right; L, Left

Note: Data presented are group difference means with standard deviations in parentheses.

*Strong evidence, **Very strong evidence

P+ ≤ 0.05: Controls > AD, P+ ≥ 0.95: Controls < AD

Supplementary Table 7: MD connections identified with either very low or high P+ values with their corresponding values of BL, fNT and fNV for each connection.

Region 1	Region 2	BL							fNT							fNV					
		Mean (SD)	P+	Quantile Intervals					Mean (SD)	P+	Quantile Intervals					Mean (SD)	P+	Quantile Intervals			
				2.5 %	5%	50%	95%	97.5 %			2.5 %	5%	50%	95%	97.5 %			2.5 %	5%	50%	95%	97.5 %
Cortical Cingulate Cortex to Cortical Occipital Lobe																					
L-isthmus-Cing	L-Lingual	0.19 (0.69)	0.60	-1.09	-0.88	0.15	1.38	1.66	6.12×10^{-6} (2.95×10^{-5})	0.58	-4.94×10^{-5}	-4.06×10^{-5}	5.27×10^{-6}	5.63×10^{-5}	6.80×10^{-5}	-3.50×10^{-7} (1.83×10^{-4})	0.48	-3.39×10^{-4}	-2.89×10^{-4}	-7.38×10^{-6}	3.11×10^{-4}	3.83×10^{-4}
Cortical Cingulate Cortex to Cortical Temporal Lobe																					
R-isthmus-Cing	R-Parahippo	-1.99 (1.18)	**0.03***	-4.64	-4.10	-1.88	-0.28	0.04	-1.68×10^{-5} (3.31×10^{-5})	0.31	-8.85×10^{-5}	-7.29×10^{-5}	-1.50×10^{-5}	3.38×10^{-5}	4.38×10^{-5}	-1.27×10^{-4} (1.66×10^{-4})	0.21	-4.61×10^{-4}	-3.94×10^{-4}	-1.24×10^{-4}	1.41×10^{-4}	1.97×10^{-4}
Cortical Temporal Lobe to Subcortical Temporal Lobe																					
R-Entorhinal	R-Hippo	-1.42 (0.93)	**0.05***	-3.46	-3.05	-1.36	0.01	0.30	-4.63×10^{-5} (4.67×10^{-5})	0.15	-1.55×10^{-4}	-1.33×10^{-4}	-4.05×10^{-5}	1.96×10^{-5}	3.04×10^{-5}	-1.62×10^{-4} (1.70×10^{-4})	0.17	-5.13×10^{-4}	-4.52×10^{-4}	-1.60×10^{-4}	1.07×10^{-4}	1.60×10^{-4}
Cortical Temporal Lobe to Subcortical Hippocampus Subregions (Subcortical Temporal Lobe)																					
R-Parahippo	R-Hippo-Presubiculum	-1.06 (0.93)	0.08	-3.45	-2.84	-0.91	0.15	0.34	-3.46×10^{-6} (2.95×10^{-5})	0.45	-6.15×10^{-5}	-5.21×10^{-5}	-3.44×10^{-6}	4.58×10^{-5}	5.51×10^{-5}	-8.68×10^{-5} (1.73×10^{-4})	0.30	-4.20×10^{-4}	-3.68×10^{-4}	-8.73×10^{-5}	1.98×10^{-4}	2.59×10^{-4}
Subcortical Temporal Lobe to Subcortical Hippocampus Subregions (Subcortical Temporal Lobe)																					
R-Hippo	R-Hippo-Presubiculum	0.22 (0.68)	0.63	-1.08	-0.86	0.20	1.35	1.59	-5.22×10^{-6} (2.88×10^{-5})	0.43	-6.26×10^{-5}	-5.20×10^{-5}	-4.92×10^{-6}	4.13×10^{-5}	5.14×10^{-5}	-9.19×10^{-5} (1.66×10^{-4})	0.29	-4.20×10^{-4}	-3.61×10^{-4}	-9.32×10^{-5}	1.82×10^{-4}	2.41×10^{-4}

L-Hippo	L-Hippo-Presubiculum	0.26 (0.66)	0.65	-0.96	-0.76	0.24	1.39	1.67	-7.46×10^{-6} (2.98×10^{-5})	0.40	-6.68×10^{-5}	-5.60×10^{-5}	-7.47×10^{-6}	4.04×10^{-5}	5.07×10^{-5}	-9.89×10^{-5} (1.66×10^{-4})	0.27	-4.23×10^{-4}	-3.71×10^{-4}	-9.90×10^{-5}	1.78×10^{-4}	2.30×10^{-4}
Subcortical Hippocampus Subregions (Subcortical Temporal Lobe) to Subcortical Hippocampus Subregions (Subcortical Temporal Lobe)																					
R-Hippo-Presubiculum	R-Hippo-Subiculum	0.44 (0.72)	0.73	-0.85	-0.66	0.40	1.68	1.99	-1.66×10^{-6} (2.86×10^{-5})	0.48	-5.8×10^{-5}	-4.82×10^{-5}	-1.83×10^{-6}	4.59×10^{-5}	5.64×10^{-5}	-7.00×10^{-5} (1.74×10^{-4})	0.34	-4.09×10^{-4}	-3.51×10^{-4}	-7.19×10^{-5}	2.16×10^{-4}	2.78×10^{-4}

Key: SD, Standard Deviation; BL, average length in mm; fNT, Fractional number of tracks in that white matter region-of-interest (WM-ROI); fNV, Fractional volume of tracks compared to masked total volume; R, Right; L, Left

Note: Data presented are group difference means with standard deviations in parentheses.

*Strong evidence, **Very strong evidence

P+ ≤ 0.05: Controls > AD, P+ ≥ 0.95: Controls < AD

Supplementary Table 8: MD connections identified with either very low or high P+ values with their corresponding values of NT, NV and PV for each connection.

Region 1	Region 2	NT							NV							PV					
		Mean (SD)	P+	Quantile Intervals					Mean (SD)	P+	Quantile Intervals					Mean (SD)	P+	Quantile Intervals			
				2.5 %	5%	50%	95%	97.5 %			2.5%	5%	50%	95%	97.5%			2.5 %	5%	50%	95%	97.5 %
Cortical Cingulate Cortex to Cortical Occipital Lobe																					
L-isthmus-Cing	L-Lingual	-3.89×10^{3} (1.57×10^{4})	0.39	-3.36×10^{4}	-2.88×10^{4}	-4.12×10^{3}	2.24×10^{4}	2.83×10^{4}	-26.64 (76.23)	0.34	-169.03	-144.82	-29.32	102.44	134.59	-91.43 (265.72)	0.35	-592.97	-512.64	-99.88	357.47	457.52
Cortical Cingulate Cortex to Cortical Temporal Lobe																					
R-isthmus-Cing	R-Parahippo	-1.77×10^{4} (1.80×10^{4})	0.15	-5.63×10^{4}	-4.85×10^{4}	-1.67×10^{4}	9.93×10^{3}	1.55×10^{4}	-80.12 (70.65)	0.12	-222.51	-197.26	-80.31	35.04	59.31	-270.99 (242.18)	0.13	-748.70	-670.58	-268.45	123.20	201.51

Cortical Temporal Lobe to Subcortical Temporal Lobe																				
R-Entorhinal	R-Hippo	-3.89×10^4 (2.48×10^4)	**0.03***	-9.71×10^4	-8.52×10^4	-3.55×10^4	-3.77×10^3	1.44×10^3	-100.87 (72.65)	0.08	-247.70	-221.14	-100.00	15.79	39.66	-343.22 (249.30)	0.08	-851.03	-763.87	-338.82	54.04	119.02
Cortical Temporal Lobe to Subcortical Hippocampus Subregions (Subcortical Temporal Lobe)																				
R-Parahippo	R-Hippo-Presubiculum	-3.32×10^3 (1.59×10^4)	0.41	-3.47×10^4	-2.88×10^4	-3.59×10^3	2.27×10^4	2.85×10^4	-41.56 (73.69)	0.28	-185.51	-161.06	-41.93	79.59	103.48	-140.76 (253.80)	0.28	-633.41	-556.84	-142.80	283.96	368.52
Subcortical Temporal Lobe to Subcortical Hippocampus Subregions (Subcortical Temporal Lobe)																				
R-Hippo	R-Hippo-Presubiculum	-1.77×10^4 (1.60×10^4)	0.13	-4.90×10^4	-4.38×10^4	-1.77×10^4	8.75×10^3	1.41×10^4	-54.08 (71.52)	0.22	-192.78	-170.39	-54.39	63.62	85.14	-181.49 (246.29)	0.23	-668.41	-583.16	-181.25	223.00	297.83
L-Hippo	L-Hippo-Presubiculum	-1.69×10^4 (1.61×10^4)	0.14	-4.89×10^4	-4.33×10^4	-1.67×10^4	9.30×10^3	1.48×10^4	-54.68 (71.91)	0.22	-195.44	-171.59	-55.09	63.47	88.27	-182.13 (248.78)	0.23	-680.28	-591.69	-182.34	223.22	304.85
Subcortical Hippocampus Subregions (Subcortical Temporal Lobe) to Subcortical Hippocampus Subregions (Subcortical Temporal Lobe)																				
R-Hippo-Presubiculum	R-Hippo-Subiculum	-4.49×10^3 (1.58×10^4)	0.38	-3.56×10^4	-3.04×10^4	-4.67×10^3	2.15×10^4	2.72×10^4	-35.03 (74.17)	0.31	-178.52	-153.96	-35.72	88.42	112.99	-118.99 (255.90)	0.32	-619.87	-541.56	-118.70	301.79	383.63

Key: SD, Standard Deviation; NT, Number of tracks in that WM-ROI; NV, Number of voxels in that WM-ROI; PV, Physical volume of tracts; R, Right; L, Left

Note: Data presented are group difference means with standard deviations in parentheses.

*Strong evidence, **Very strong evidence

P+ ≤ 0.05: Controls > AD, P+ ≥ 0.95: Controls < AD

AD

Controls

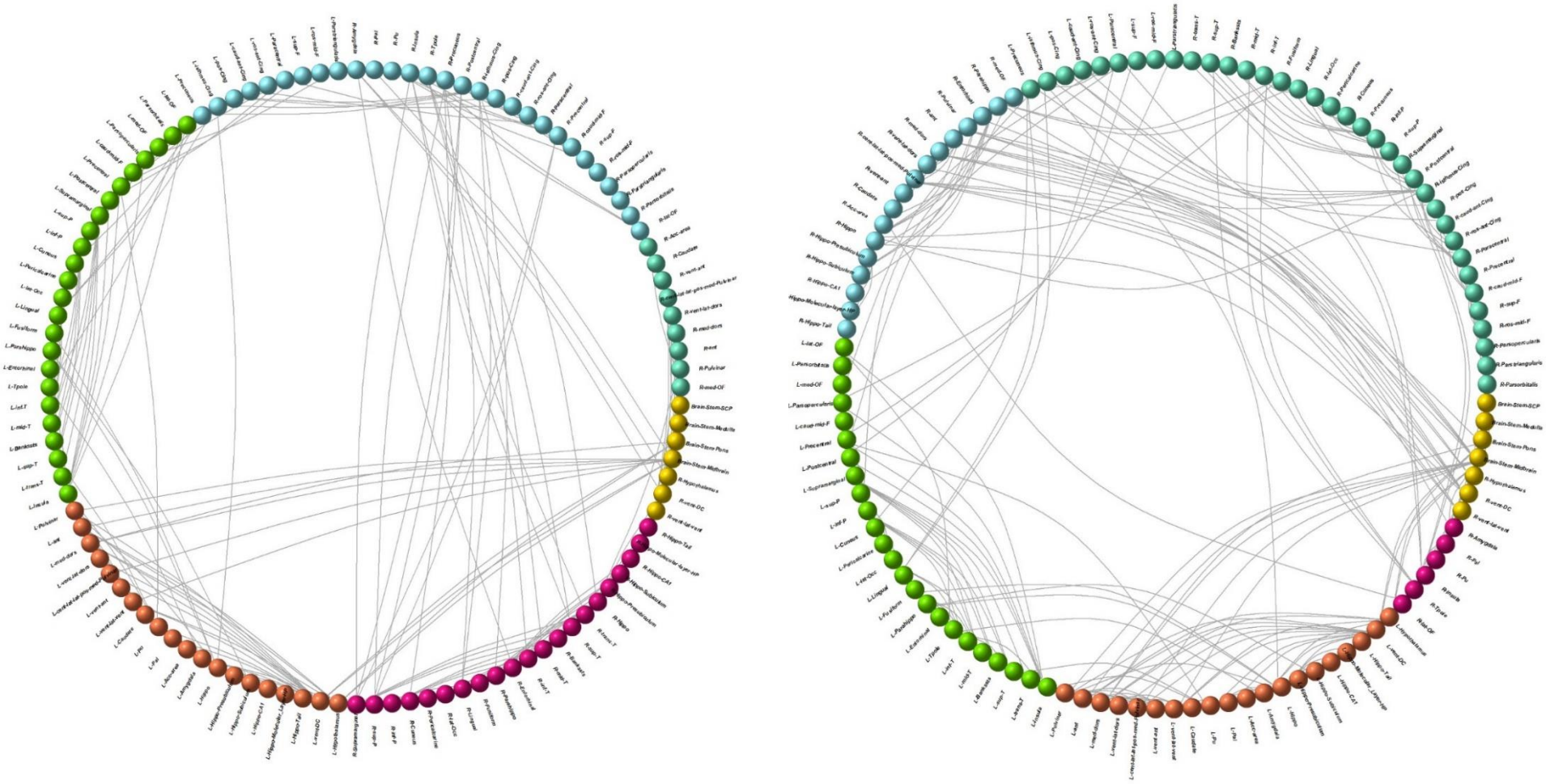

Supplementary Figure 2: Both controls and AD had the same number of clusters. Modularity showed no significant between-group differences.

Supplementary Table 9: Multiple linear regression analysis with modularity as the dependent variable.

Effect	Coefficient Estimate (Standard Error)	*t*	95% Confidence Interval	*p*
Intercept	0.56 (0.01)	52.81	0.54; 0.58	**< 0.001*** **
Group[a]				
Controls	(reference)		(reference)	(reference)
AD	-0.01 (0.01)	-1.01	-0.03; 0.01	**0.32**
Sex[b]				
Female	(reference)		(reference)	(reference)
Male	0.02 (0.01)	1.99	0.0003; 0.04	0.06
Age in years[c]	-0.005 (0.005)	-1.13	-0.01; 0.004	0.27
Education in years[c]	-0.002 (0.005)	-0.36	-0.01; 0.008	0.72
Monthly Household Income[d]				
Level 2	0.05 (0.03)	2.02	0.002; 0.11	0.05
Level 3	0.02 (0.02)	1.42	-0.01; 0.06	0.17
Level 4	(reference)		(reference)	(reference)
Level 5	-0.001 (0.01)	-0.08	-0.03; 0.02	0.94
Level 6	0.004 (0.01)	0.34	-0.02; 0.03	0.73

Key: AD, Alzheimer's Disease

[a]Group is represented as 1 dummy variable with "Controls" serving as the reference group.

[b]Sex is represented as 1 dummy variable with "Female" serving as the reference group.

[c]Variable was standardised.

[d]Monthly Household Income is represented as 4 dummy variables with "Level 4" serving as the reference group.

*p ≤ 0.05, **p < 0.01, ***p < 0.001

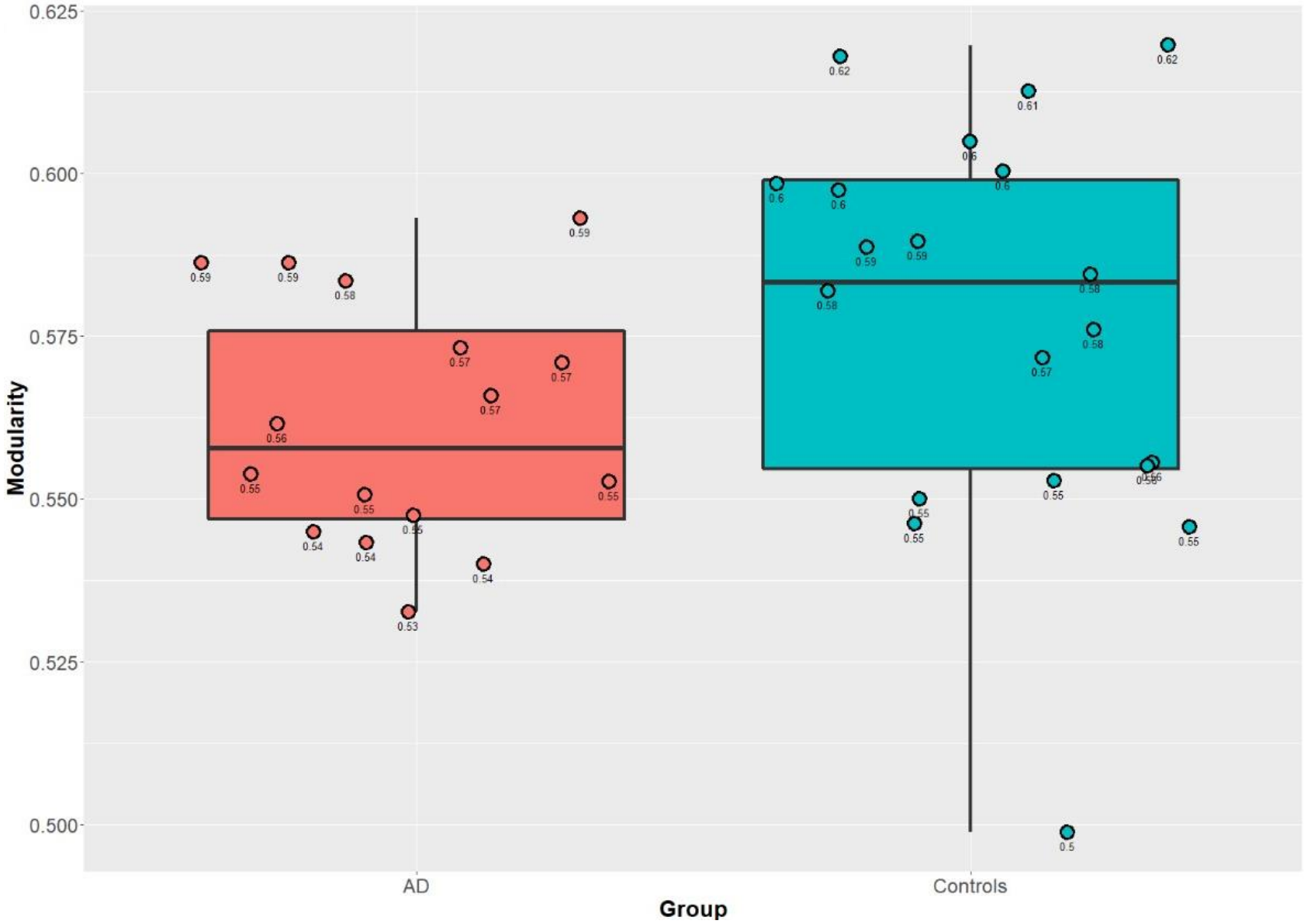

Supplementary Figure 3: Box-and-whiskers plots showing modularity in each group. Points represent the modularity of each individual in each group.